PB90-235797

Laboratory Investigation of Residual Liquid Organics from Spills, Leaks, and the Disposal of Hazardous Wastes in Groundwater

New Mexico Inst. of Mining and Technology, Socorro

Prepared for:

Robert S. Kerr Environmental Research Lab., Ada, OK

Aug 89

U.S. Department of Commerce
National Technical Information Service
NTIS

PB90-235797

Project Summary EPA/600/6-90/004
(RSKERL-Ada-9021)

LABORATORY INVESTIGATION
OF RESIDUAL LIQUID ORGANICS
from spills, leaks, and the disposal of hazardous wastes
in groundwater

by
John L. Wilson, Stephen H. Conrad, William R. Mason
William Peplinski, and Edward Hagan

Department of Geoscience
& Geophysical Research Center
New Mexico Institute of Mining and Technology
Socorro, New Mexico 87801

Cooperative Agreement: EPA CR-813571
Project Officer: Jerry Jones
Robert S. Kerr Environmental Research Laboratory
Office of Research And Development
U.S. Environmental Protection Agency
Ada, Oklahoma 74820

This study was conducted in cooperation with
the New Mexico Water Resources Research Institute,
Las Cruces, New Mexico, under Grant NMWRRI 1345648

ROBERT S. KERR ENVIRONMENTAL RESEARCH LABORATORY
OFFICE OF RESEARCH AND DEVELOPMENT
U.S. ENVIRONMENTAL PROTECTION AGENCY
ADA, OKLAHOMA 74820

REPRODUCED BY
U.S. DEPARTMENT OF COMMERCE
NATIONAL TECHNICAL INFORMATION SERVICE
SPRINGFIELD, VA. 22161

TECHNICAL REPORT DATA

(Please read Instructions on the reverse before completing)

1. REPORT NO. EPA/600/6-90/004

2.

3. RECIPIENT'S ACCESSION NO. PB90 235797/AS

4. TITLE AND SUBTITLE
LABORATORY INVESTIGATION OF RESIDUAL LIQUID ORGANICS FROM SPILLS, LEAKS, AND THE DISPOSAL OF HAZARDOUS WASTES IN GROUNDWATER

5. REPORT DATE Aug. 89

6. PERFORMING ORGANIZATION CODE

7. AUTHOR(S)
John L. Wilson, Stephen H. Conrad, William R. Mason, William Peplinski, and Edward Hagan

8. PERFORMING ORGANIZATION REPORT NO.

9. PERFORMING ORGANIZATION NAME AND ADDRESS
Department of Geoscience & Geophysical Research Center
New Mexico Institute of Mining and Technology
Socorro, NM 87801

10. PROGRAM ELEMENT NO. CBWD1A

11. CONTRACT/GRANT NO. CR-813571

12. SPONSORING AGENCY NAME AND ADDRESS
Robert S. Kerr Environmental Research Laboratory
U.S. Environmental Protection Agency
P.O. Box 1198
Ada, OK 74820

13. TYPE OF REPORT AND PERIOD COVERED Final Proj. Rpt. (04/86-08/89)

14. SPONSORING AGENCY CODE

15. SUPPLEMENTARY NOTES

Project Officer: Jerry N. Jones, FTS: 743-2251

16. ABSTRACT

Organic liquids that are essentially immiscible with water migrate through the subsurface through the influence of capillary, viscous and buoyancy forces. Four experimental methods were employed. First, quantitative displacement experiments using short soil columns; second, additional quantitative displacement experiments using long soil columns; third, pore and blob casts; and fourth, etched glass micromodels were used to visually observe dynamic multi-phase displacement processes in pore networks. It was found that the spatial distribution and saturation of organic liquid within the porous media depends on a variety of factors, including: (1) the fluid properties of interfacial tension, viscosity, and density; (2) soil structure and heterogeneity; (3) the number of fluid phases present; and (4) the fluid flow rates. Photomicrographs on a pore scale show that the residual organic liquid appears as blobs, films, rings, and wedges of microscopic size. The size, shape, and spatial distribution of these blobs, films, rings, and wedges affects the dissolution of organic liquid into the water phase, volatilization into the air phase, and the adsorption and biodegradation of organic components. These four processes are of concern in the prediction of pollution migration and the design of aquifer remediation schemes.

17. KEY WORDS AND DOCUMENT ANALYSIS

a. DESCRIPTORS	b. IDENTIFIERS/OPEN ENDED TERMS	c. COSATI Field/Group

18. DISTRIBUTION STATEMENT
RELEASE TO PUBLIC

19. SECURITY CLASS *(This Report)* UNCLASSIFIED

20. SECURITY CLASS *(This page)* UNCLASSIFIED

21. NO. OF PAGES 285

22. PRICE

EPA Form 2220-1 (Rev. 4-77) PREVIOUS EDITION IS OBSOLETE

NOTICE

This document has been reviewed in accordance with U.S. Environmental Protection Agency policy and approved for publication. Mention of trade names or commercial products does not constitute endorsement or recommendation for use.

ACKNOWLEDGMENTS

This work described in this report was sponsored by the R. S. Kerr Laboratory, Office of Research And Development, U.S. Environmental Protection Agency, Ada, Oklahoma, under Grant Number EPA CR-813571-01-0, and the New Mexico Water Resources Research Institute, Las Cruces, New Mexico, under Grant Number NMWRRI 1345648. Additional financial support was provided by the Research Branch, Water Resources Division, U.S. Geological Survey, Menlo Park, California.

The authors would like to acknowledge the assistance of: Mary Graham, who introduced us to the techniques of manufacturing etched glass micromodels; Robert Mace, who ran the short column Llano soil experiments; and Jamine Wan, who took some of the photomicrographs. Dr. Norman Morrow of New Mexico Tech's Petroleum Research Recovery Center freely shared his understanding of similar problems encountered in both petroleum reservoir engineering and soil physics. Many of the experiments described in this report are progeny of earlier experiments performed by Dr. Morrow and others in petroleum research laboratories.

The authors would also like to acknowledge the comments of our various reviewers for the Environmental Protection Agency, the New Mexico Water Resources Research Institute, and Steve Conrad's Ph.D. Committee. These reviewers include Fred Phillips, Dan Stephens, Norm Morrow, Jack Parker, Danny Reible and Robert Bowman.

S^*_{or}	maximum, low capillary and Bond number, two-phase organic liquid saturation
S_w	water or wetting phase saturation
S_{wr}	residual water or wetting phase saturation
S_{wi}	irreducible water saturation = S_{wr}
V	volume
V_p	pore volume
V_s	soil volume
V_t	total volume
V_v	void volume
γ	surface tension between air and water
θ	contact angle
μ_o	dynamic viscosity in the organic liquid
μ_w	dynamic viscosity in the water phase
ϱ_b	soil bulk density
ϱ_o	organic liquid density
ϱ_s	particle density
ϱ_w	water density
σ	interfacial tension between two fluid phases
$\sigma_{aw} = \sigma_{wa}$	air-water interfacial tension = surface tension, γ
σ_{ao}	air-organic liquid interfacial tension
$\sigma_{ow} = \sigma_{wo}$	organic liquid-water interfacial tension
$\Delta\varrho$	density difference between two fluids
ΔP	a pressure drop
Σ	spreading coefficient

LIST OF ABBREVIATIONS AND SYMBOLS

g or g	gravitational constant
k	intrinsic permeability of the porous media
k_{ro}	relative permeability for the organic liquid phase
k_{rw}	relative permeability for the water or wetting phase
n	porosity
q_w	specific discharge in the water phase
r_t	radius of a capillary tube
z	elevation
A	gross cross-sectional area of, eg, a column
H_c	capillary head (= P_c /ϱg)
IFT	interfacial tension between two fluid phases = σ
J_w	hydraulic gradient in the water phase
K_w	saturated hydraulic conductivity for water
M_s	mass of soil
M_w	mass of water
N_B	Bond number; represents the ratio of gravitational forces to viscous forces for a multi-phase flow situation
N_c	capillary number; represents the ratio of capillary forces to viscous forces for a multi-phase flow situation
P_c	capillary pressure
P_{nw}	non-wetting phase pressure
P_o	organic liquid phase pressure
P_w	water or wetting phase pressure
Q	total discharge
R	radius of curvature
S_a	air saturation
S_o	organic liquid saturation
S_{or}	residual organic liquid saturation

LIST OF TABLES

TABLE	TITLE	PAGE
1-1.	Migration pattern for an organic liquid more dense than water (left), and less dense than water (right)	2
4-1.	Measured properties of fluids used in experiments.	28
4-2.	Relationship between wettability measurement methods.	34
7-1.	Properties of fluids used in pore and blob cast visualization experiments.	80
7-2.	Absolute viscosities of selected organic liquids.	85
9-1.	Soltrol residual saturation and other measurements in Sevilleta sand, for three temperature dependent categories	132
9-2.	Summary of Soltrol / Sevilleta sand saturated zone results.	133
9-3.	Summary of kerosene / Sevilleta sand saturated zone results.	144
9-4.	Summary of gasoline / Sevilleta sand saturated zone results.	144
9-5.	Summary of n-decane / Sevilleta sand saturated zone results.	145
9-6.	Summary of p-xylene / Sevilleta sand saturated zone results.	145
9-7.	Summary of PCE / Sevilleta sand saturated zone results.	146
9-8.	Average values for different organic liquids in the Sevilleta sand saturated zone experiments.	146
9-9	The interfacial tension of some priority pollutants with water.	151
9-10	Summary of Soltrol / Traverse City soil saturated zone results.	154
9-11.	Summary of Soltrol / Llano soil saturated zone results.	154
9-12.	Average values of measured properties and saturations for different sandy soils, in the saturated zone experiments run with Soltrol.	156
9-13.	Long column data for two different sandy soils run with Soltrol.	163
9-14.	Measurements of bulk residual organic saturations in two heterogeneous packings of the Sevilleta sand. The sand was divided into a coarse and a fine fraction, and the coarse fraction was packed into the column as cylindrical lenses within a matrix of the fine fraction.	184
10-1.	Results from the vadose zone column experiments. Soltrol-130 was used as the organic liquid and Sevilleta sand served as the soil.	209
10-2.	Relative density differences and interfacial tensions in the vadose zone and saturated zone.	211
10-3.	Results from vadose zone column experiments performed to examine the saturation distributions in the transition zone between the saturated zone and the vadose zone. The media was Sevilleta sand and the organic liquid was Soltrol.	215
A-1.	Two-phase TFE column residual saturation results; styrene was used unless otherwise noted.	237
C-1.	Numerical values of measured saturations, pressures, and temperatures. (continued on next four pages)	256

FIGURE	TITLE	PAGE
C-1.	Soltrol-water saturation curve for SW trial 7.	241
C-2.	Soltrol-water saturation curve for SW trial 8.	242
C-3.	Soltrol-water saturation curve for SW trial 9.	243
C-4.	Soltrol-water saturation curve for SW trial 10.	244
C-5.	Soltrol-water saturation curve for SW trial 11.	245
C-6.	Soltrol-water saturation curve for SW trial 12.	246
C-7.	Soltrol-water saturation curve for SW trial 13.	247
C-8.	Soltrol-water primary drainage curves for SW trials 7-13, minus trial 8.	248
C-9.	Soltrol-air saturation curve for SA trial 1.	249
C-10.	Soltrol-air saturation curve for SA trial 2.	250
C-11.	Comparison of Soltrol-air primary drainage curves for SA trials 1 & 2.	251
C-12.	Air-water saturation curve for AW trial 1.	252
C-13.	Air-water saturation curve for AW trial 2.	253
C-14.	Air-water saturation curve for AW trial 3.	254
C-15.	Comparison of air-water primary drainage curves for SA trials 1-3.	255

FIGURE TITLE PAGE

10-6. Detail of steady state conditions after the Soltrol invasion into the vadose zone model. 201

10-7. Steady state conditions after the Soltrol invasion into the vadose zone model. 203

10-8. Detail of steady state conditions after the Soltrol has been drained by air from the vadose zone model. 204

10-9. Steady state conditions after the Soltrol has been drained by air from the vadose zone model. 205

10-10. Steady state conditions in a micromodel after a) Soltrol has been drained by air from a vadose zone model, and b) Soltrol has been displaced by water in a saturated zone model. 206

10-11. Detail a thin organic liquid film located between the gas and water. The photo represents steady state conditions after the Soltrol has been drained by air from the vadose zone model. 207

10-12. A photomicrograph of a pore cast thin section from the simulated three-phase system in the Sevilleta sand. The middle of the photo depicts a pore body filled with non-wetting phase (blue or dark grey). Above it is thick 'film' of intermediate wetting phase (white or light grey), that is 'smiling' into a pore throat. The pore throat is otherwise filled with wetting fluid (red or light grey). Shown at 100X magnification. ... 212

10-13. A photomicrograph of a pore cast thin section from the simulated three-phase system in the Sevilleta sand. The middle of the photo depicts a pore body filled with non-wetting phase (blue or dark grey). It is surrounded by an intermediate wetting film (white or light grey), that is 'smiling' into the pore throat on the right, and filling most of the pore throat to the left. Shown at 100X magnification. 213

10-14. A photomicrograph of a pore cast thin section from the simulated three-phase system in the Sevilleta sand. The middle of the photo depicts a small pore body filled with non-wetting phase (blue or dark grey). It is surrounded by an intermediate wetting film (white or light grey), that is 'smiling' into the pore throats on the right, left and below. The pore throats are filled with the wetting fluid (red or black in this photo). Shown at 100X magnification. 214

10-15. Inferred distribution of fluids in the vadose zone for the Sevilleta sand, using Soltrol-130 as the organic liquid in individual short column experiments. The dry zone data is taken from Table 10-1, while the transition zone data is taken from Table 10-3. Results from experimental trials 5 and 6 are suspect for reasons discussed in the text. 216

10-16. A photomicrograph of non-spreading PCE in a micromodel. 220

10-17. A photomicrograph of non-spreading PCE in a micromodel. This is a close-up to the photo shown in Figure 10-16. 221

10-18. A photomicrograph of Soltrol in a micromodel. The geometry is similar to that depicted for PCE in Figure 10-16. 222

FIGURE TITLE PAGE

9-45. Soltrol draining a horizontally-aligned 'coarse lens' micromodel from the left. The photos show fluid distributions as a) the Soltrol was part way through the model, and b) once the Soltrol had advanced completely through the model. 178

9-46. Water imbibing into the horizontally-aligned 'coarse lens' micromodel from the right. The photos show fluid distributions as a) the water was part way through the model, and b) once the water had advanced completely through the model. 180

9-47. Water imbibing into the vertical 'coarse lens' micromodel from the right (the bottom of the model). The photos show fluid distributions after the water had advanced completely through the model. 182

9-48. Photograph of residual organic liquid saturation (shaded light) in a heterogeneous sand pack. Water was flooded from right to left at a low rate. Notice the high organic liquid saturation in the coarse lenses. ... 183

9-49. Photograph of residual organic liquid saturation (shaded light) in another heterogeneous sand pack. Water was flooded from right to left. A high rate of flow produced sufficient force to displace some organic liquid from the coarse lenses. 183

9-50 Random lenses of permeability k_2 in a matrix of permeability k_1. 186

9-51 Uniform, parallel lenses of permeability k_2 in a matrix of permeability k_1: a) side view of several lenses, and b) cut-away view of one lense. ... 187

9-52 Pressure profiles in soil i for fluids A and B, with fluid A as a) the wetting fluid, and b) the non-wetting fluid. i =1,2 coarse or fine. 189

9-53. Pressure profiles for fluids A and B, with fluid A as the wetting fluid, for a) the fine matrix and b) the more coarse lense. 189

9-54. Critical flow rates needed to displace organic liquid from coarse lenses as a function of permeability in the coarse lens (top), and in the fine matrix (bottom). 191

10-1. Schematic of residual organic liquid trapped in the vadose zone. 194

10-2. Diagram of spreading potential for a drop of organic liquid floating on the air (gas)-water interface (after Adamson, 1982, and others). The water is wetting, the air is non-wetting, and the organic liquid is intermediate wetting. 197

10-3. A conceptual plot of residual saturation for the wetting fluid (solid line) and the non-wetting fluid (dashed line), as a function of the ratio of the sum of viscous and buoyancy forces, to capillary forces. 198

10-4. Initial vadose zone condition, with water drained by air to residual (irreducible) water saturation. 200

10-5. Detail of Soltrol invasion into a different vadose zone model. The Soltrol was advancing by filling pores and by film flow. 201

FIGURE TITLE PAGE

9-34. Homogeneous model. In the upper photo (a) Soltrol displaced water from the left (the top of the model) to the right (the bottom of the model), at 1.5 ml/min yielding a residual (irreducible) wetting phase saturation. In the lower photo (b) Soltrol was displaced by water from the right (the bottom of the model) to the left (the top), also at 1.5 ml/min, yielding a residual non-wetting residual saturation. 160

9-35. Residual organic saturation, in short and long columns, for Soltrol in the tested soils. The error bars represent sample standard deviations for the short column experiments. 163

9-36 Relationship between Soltrol residual saturation and capillary number, for Sevilleta sand and Llano sand. .... , 164

9-37. Relationship between Soltrol residual saturation and capillary number, for Sevilleta sand and Llano sand. .... , 164

9-38. Hydraulic gradients required to initiate blob mobilization in porous media of various permeabilities, for organic liquids of various interfacial tensions. 166

9-39. Recovery of residual saturation as a function of permeability and hydraulic gradient for an interfacial tension of 10 dyne/cm. 167

9-40. Non-wetting fluid near a material boundary: a) moving from coarse to fine and encountering a capillary barrier; and b) moving from fine to coarse and encountering a 'capillary end effect' resulting in rivulets of non-wetting flow across the boundary 170

9-41. Aggregated model. In the upper photo (a) Soltrol displaced water at a rate of 0.075 ml/min, from the left (the top of the model) to the right (the bottom of the model), yielding a residual (irreducible) wetting phase saturation. In the lower photo (b) Soltrol was displaced by water at the same rate, from the right (the bottom of the model) to the left (the top) yielding a residual non-wetting residual saturation. 172

9-42. Aggregated model detail from Figure 9-11, showing conditions following the displacement of the water by Soltrol (a. upper photo), and at residual non-wetting phase saturation (b. lower photo). The area is located just below the very center of the model. 173

9-43. Aggregated model detail from Figure 9-11, showing conditions following the displacement of the water by Soltrol (a. upper photo), and at residual non-wetting phase saturation (b. lower photo). The area is located near the top of the model, just to the right of the centerline. . 174

9-44. Aggregated model. In the upper photo (a) Soltrol displaced water from the left (the top of the model) to the right (the bottom of the model), at 1.5 ml/min yielding a residual (irreducible) wetting phase saturation. In the lower photo (b) Soltrol was displaced by water from the right (the bottom of the model) to the left (the top), also at 1.5 ml/min, yielding a residual non-wetting residual saturation. 175

FIGURE	TITLE	PAGE
9-16.	Photomicrograph of a complex blob as observed in the micromodel. ..	130
9-17.	Correlation of maximum Soltrol saturation (triangles), and residual Soltrol saturation (squares), to porosity in the Sevilleta sand.	134
9-18.	Sevilleta sand pore cast photomicrographs of (a) a singlet blob occupying one pore body, in the upper photo, and (b)a doublet blob occupying two pore bodies and a pore throat, in the lower photo.	135
9-19.	Sevilleta sand pore cast photomicrograph of a variety of blobs including some that are complex and branching.	136
9-20.	Sevilleta sand blob cast photomicrographs of (a) non-branching blobs, and (b) branching blobs.	137
9-21.	Photomicrograph of Sevilleta sand pore cast covering many pores. ...	139
9-22.	SEM photomicrograph of many blob casts from the Sevilleta sand. ...	139
9-23.	The spatial distribution of a single-component residual organic liquid undergoing dissolution as a function of time when the local equilibrium assumption is invoked.	142
9-24.	The spatial distribution of a single-component residual organic liquid undergoing dissolution as a function of time when a local equilibrium between the fluid phases is not reached. A dispersed zone forms and grows until a steady state is reached.	142
9-25.	Residual organic liquid saturation as a function of the maximum organic liquid saturation.	147
9-26.	Residual organic saturation for tested organic liquids in the Sevilleta sand.	148
9-27.	Residual organic saturation as a function of interfacial tension (IFT). ..	149
9-28.	Residual organic saturation as a function of non-wetting phase viscosity.	152
9-29.	Residual organic saturation as a function of non-wetting phase density.	152
9-30.	Residual organic saturation for Soltrol in tested soils.	156
9-31.	Residual organic saturation for Soltrol, as a function of organic carbon content in different soils.	157
9-32.	Residual organic saturation for Soltrol, as a function of porosity in different soils.	158
9-33.	Residual organic saturation for Soltrol, as a function of water saturated hydraulic conductivity in different soils.	158

FIGURE	TITLE	PAGE
9-2.	Two sketches illustrating fundamentals: a) cohesive forces acting on a molecule inside a fluid and at its interface with another, immiscible fluid; and b) hydrostatic equilibrium of two fluid phases in contact with a solid phase.	112
9-3.	Capillary rise in a slim tube.	113
9-4.	Effect of pore aspect ratio on organic liquid trapping in a tube of non-uniform diameter (after Chatzis et al., 1983).	114
9-5.	Wetting fluid displacing a non-wetting fluid from a circular, high aspect ratio pore under strongly wet conditions (after Wardlaw, 1982).	115
9-6.	One fluid displacing another from a circular, high aspect ratio pore, under intermediate wetting conditions (after Wardlaw, 1982).	115
9-7.	Final condition after an advancing fluid displaced a retreating fluid from a rough-walled pore under intermediate wetting conditions (after Wardlaw, 1982).	116
9-8.	Sketches illustrating trapping mechanisms using the pore doublet model (after Chatzis et al., 1983)	117
9-9.	Relationship between residual saturation and capillary number for sandstones and glass beads.	122
9-10.	Residual saturation in uniform glass beads due to variable capillary number entrapment of the continuous non-wetting phase (dashed line), and due to mobilization of non-wetting phase originally trapped at a low capillary capillary number (solid line).	123
9-11.	Micromodel study. In the upper photo (a) Soltrol displaced water from the left (the top of the model) to the right (the bottom of the model), yielding a residual (irreducible) wetting phase saturation. In the lower photo (b) Soltrol was displaced by water from the right (the bottom of the model) to the left (the top) yielding a residual non-wetting residual saturation.	125
9-12.	Detail from Figure 9-11 showing conditions following the displacement of the water by Soltrol (a. upper photo), and at residual non-wetting phase saturation (b. lower photo). The area is located just below the very center of the model.	126
9-13.	Detail from Figure 9-11 showing conditions following the displacement of the water by Soltrol (a. upper photo), and at residual non-wetting phase saturation (b. lower photo). The area is located near the top of the model, just to the right of the centerline.	127
9-14.	A second experiment in the homogeneous micromodel, depicting conditions at the end of the organic liquid invasion–compare to Figure 9-11a	128
9-15.	Photomicrographs of (a) a singlet blob occupying one pore body in the upper photo, and (b)a doublet blob occupying two pore bodies and a pore throat in the lower photo.	129

FIGURE TITLE PAGE

5-7. Vadose Zone Test Step 3: Organic liquid drained by air. 58

5-8. Temperature range and its effect on the accuracy of results. 60

6-1. Long column experimental setup. 65

6-2. Long column construction details. 67

7-1. Exploded view of the TFE Short Column. 78

7-2. Viscosity of initiated styrene vs. time. 79

7-3. Experimental setup of a styrene flood. 84

7-4. Intermediate-wetting phase flood. 90

7-5. Cross-section of styrene flooding into a water-saturated column with organic wet walls: a) early time; b) late time. 94

8-1. Pore-network pattern for the homogeneous model. 98

8-2. Mirror construction. 99

8-3. Mirror with enamel removed to reveal copper surface. 100

8-4. Copper surface coated with Kodak Thin Film Resist (KTFR). 100

8-5. Pore-network pattern exposed with UV light onto coated copper surface. 101

8-6. Pore-network pattern exposed on the resin coating. 102

8-7. Copper and silver layers under the pore network pattern removed to reveal the underlying glass plate. 102

8-8. SEM photomicrograph of the cross-section through a typical pore within a micromodel. 103

8-9. Photograph of network pattern showing the capillary barrier built into one end of a micromodel. 104

8-10. Two-phase micromodel experimental set-up. 105

8-11. Three-phase micromodel experimental set-up. 106

8-12. Pore-network pattern for the 'aggregated' model. 107

8-13. Pore-network pattern for the heterogeneous 'stringer' model. 107

9-1. Schematic of residual organic liquid trapped in the saturated zone 108

LIST OF FIGURES

FIGURE	TITLE	PAGE
1-1.	Migration pattern for an organic liquid more dense than water (left), and less dense than water (right)	2
4-1.	A simple experiment illustrating the relatively low volatility of Soltrol, compared to water.	29
4-2.	Setup for the organic liquid and water capillary pressure – saturation relationship.	31
4-3.	Contact angle measurement on a clean, smooth solid surface.	33
4-4.	Generic representation of relative permeabilities versus saturation for the long column experiments.	35
4-6.	SEM photomicrographs of Sevilleta sand.	37
4-5.	Particle size analysis for three of the soils used in this study.	37
4-8.	A typical organic liquid-water capillary pressure-saturation curve used to determine wettability, in this case for Soltrol-130 in Sevilleta sand.	39
4-7.	Typical Sevilleta sand capillary pressure-saturation curves.	39
4-9.	Relative permeability vs water saturation for water and Soltrol in the Sevilleta soil..	40
4-10.	Relative permeability vs water saturation for water and Soltrol in the Llano soil.	41
4-11.	Water saturation versus capillary pressure for Soltrol draining water from Palouse loam.	42
5-1.	The short column apparatus.	45
5-2.	Air entry test for bottom end cap filter and seal.	47
5-3.	Saturated Zone Test Step 1: Organic liquid flood into a water saturated column.	52
5-4.	Saturated Zone Test Step 2: Waterflooding at low velocity to reduce the organic liquid to its residual saturation.	53
5-5.	Vadose Zone Test Step 1: Water being drained with air under an applied suction.	55
5-6.	Vadose Zone Test Step 2: Organic liquid flood in a column already drained by air.	56

Section 10 VADOSE ZONE RESULTS AND DISCUSSION 194
Review Of Capillary Trapping Phenomena In Porous Media 195
Micromodel Flow Visualization Of Three Phase Displacement And Capillary Trapping 198
Capillary Trapping And Residual Saturation In An Unconsolidated Soil: The Sevilleta Sand 208
Micromodel Visualization Of Capillary Trapping Of A Non-spreading Organic Liquid 218

REFERENCES 224

APPENDIX A:
Quantitative Two-phase Residual Saturation Results, With Styrene As The Organic Phase 236

APPENDIX B
Videotapes Of Micromodel Experiments 239

APPENDIX C
Saturation Curves And Processed Data For The Short Column Sevilleta Sand Experiments 240

APPENDIX D
Raw Data From The Short Column Experiments 261

Soil Packing 49
Dearing 50
Saturated Zone Experiments 51
Vadose Zone Experiments 54
Possible Sources Of Error 58
Limitations Of The Apparatus And Technique 63

Section 6 LONG COLUMN EXPERIMENTAL METHODS 64
Long Column Apparatus 64
Fluids And Soils 68
Column Packing And Degassing 68
Measuring Absolute Permeability, Relative Permeability And Saturation 70
Possible Sources Of Error 73
Limitations Of The Technique 75

Section 7 PORE AND BLOB CAST EXPERIMENTAL METHODS 76
Column Design 76
Fluid And Soil Characterization 77
Saturated Zone Experimental Procedure 81
Vadose Zone Experimental Procedures 87
Possible Sources Of Error 91
Limitations Of The Technique 95

Section 8 MICROMODEL EXPERIMENTAL METHODS 97
Micromodel Construction 97
Micromodel Experimental Procedure 103
Limitations Of The Technique 106

Section 9 SATURATED ZONE RESULTS AND DISCUSSION 108
Review Of Capillary Trapping Phenomena In Porous Media 110
Micromodel Flow Visualization Of Two Phase Displacement And Capillary Trapping 124
Capillary Trapping And Residual Saturation In An Unconsolidated Soil: The Sevilleta Sand 130
Residual Saturations For Various Organic Liquids 143
Residual Saturation For Different Soils 153
Influence Of The Initial Rate Of Organic Liquid Invasion 159
Influence Of Water Flow Rate On Residual Organic Mobilization 162
Organic Liquid Movement And Capillary Trapping In A Heterogeneous Porous Media 168

ABSTRACT

Organic liquids that are essentially immiscible with water migrate through the subsurface under the influence of capillary, viscous, and buoyancy forces. These liquids originate from the improper disposal of hazardous wastes, and the spills and leaks of petroleum hydrocarbons and solvents. The laboratory studies described in this report examined this migration, with a primary focus on the behavior of the residual organic liquid saturation, referring to that portion of the organic liquid that is 'trapped' by capillary forces in the soil matrix. Residual organic saturation often constitutes the major volume of the organic liquid pollution, and acts as a continual source of dissolved or vapor phase organics.

Four experimental methods were employed. First, quantitative displacement experiments using short soil columns were performed to relate the magnitude of residual organic liquid saturation to fluid properties, the soil, and the number of fluid phases present. Second, additional quantitative displacement experiments using a long soil column were performed to relate the mobilization of residual organic liquid saturation in the saturated zone to wetting fluid flow rates. Third, pore and blob casts were produced by a technique in which an organic liquid was solidified in place within a soil column at the conclusion of a displacement experiment, allowing the distribution of fluid phases within the pore space to be observed. The columns were sectioned and examined under optical and scanning electron microscopes. Photomicrographs of these sections show the location of the organic phase within the porous soil matrix under a variety of conditions. Fourth, etched glass micromodels were used to visually observe dynamic multi-phase displacement processes in pore networks. Fluid movement was recorded on film and video tape.

We found that the spatial distribution and saturation of organic liquid within the porous media depends on a variety of factors, including: (1) the fluid properties of interfacial tension, viscosity, and density; (2) the soil structure and heterogeneity; (3) the number of fluid phases present; and (4) the fluid flow rates. Photomicrographs on a pore scale show that the residual organic liquid appears as blobs, films, rings, and wedges of microscopic size, depending on these factors. The size, shape, and spatial distribution of these blobs, films, rings and wedges affects the dissolution of organic liquid into the water phase, volatilization into the air phase, and the adsorption and biodegradation of organic components. These four processes are of concern in the prediction of pollution migration and the design of aquifer remediation schemes.

Large amounts of residual organic are trapped as isolated blobs in the saturated zone. Smaller amounts are 'trapped' as interconnected films, rings and wedges in the vadose zone, where the movement and distribution of organic liquids is much more complex. Residual saturations are very sensitive to soil textural heterogeneities. Even minor amounts of clay in an otherwise sandy soil may play a significant role. In the saturated zone residual saturations are largely independent of fluid properties. The rate of initial invasion of a non-wetting organic liquid may influence 'irreducible water saturations', and subsequent residual organic liquid saturations.The term 'irreducible saturation' is misleading, because the water phase is still interconnected by a water film and can be drained. In the vadose zone, the residual organic liquid saturation, which is interconnected by a similar film, may also be drained and is probably sensitive to the air flow rates in vacuum extraction and similar remedial schemes. The organic liquid film becomes a population of non-connected coalesced lenses floating at the water-air interface, when non-spreading organic liquids are involved. Residual saturation in the saturated zone can by mobilized by increasing groundwater velocities or reducing interfacial tensions with surfactants. The former is impractical while the later is potentially feasible, at least for partial mobilization.

TABLE OF CONTENTS

PAGE

ABSTRACT iv

TABLE OF CONTENTS v

LIST OF FIGURES viii

LIST OF TABLES xvi

LIST OF ABBREVIATIONS AND SYMBOLS xvii

ACKNOWLEDGMENTS xix

Section 1 INTRODUCTION 1
- Nature Of The Problem 1
- Scope Of Previous Work 3
- Motivation For This Study 4
- Objectives 5
- Experimental Approach 6
- Organization Of This Report 7

Section 2 CONCLUSIONS 8
- The Saturated Zone 8
- The Vadose Zone 14
- Experimental Approach 15

Section 3 RECOMMENDATIONS 17
- Issues For Future Research 17
- Improvements In Experimental Equipment & Procedure 23

Section 4 CHARACTERIZING EXPERIMENTAL FLUIDS AND SOILS 27
- Fluid Characterization 27
- Soil Characterization 30

Section 5 SHORT COLUMN EXPERIMENTAL METHODS 43
- Fluids And Soils 44
- Experimental Apparatus 44

SECTION 1

INTRODUCTION

NATURE OF THE PROBLEM

Many hazardous waste sites, and most leaking underground storage tanks, involve non-aqueous phase organic liquids (e.g., Burmaster and Harris, 1982; Chaffee and Weimar, 1983; Convery, 1979; EPA, 1980,1982,1983; Feenstra and Coburn, 1986; J.R.Roberts *et al.*, 1982; Jercinovic, 1984; Maugh, 1979 ; McKee et al., 1972; Villaume, 1988; Williams and Wilder, 1971). Usually released at or near the surface, these organic liquid contaminants move downward through the vadose zone toward the water table. Migrating as a liquid phase separate from the air and water already present in the vadose zone, some of the organic liquid is immobilized within the pore space by capillary forces. The remainder passes on, and if the volume of organic liquid is large enough it eventually reaches the water table. If it is less dense than water the organic liquid spreads laterally along the water table (see right side of Figure 1-1). If the organic liquid is more dense than water, it continues to move downward into the saturated zone (the left side of Figure 1-1). In both cases the organic liquid usually migrates down-gradient with the ambient groundwater flow, although dense organic liquids may migrate in other directions as they encounter dipping barriers. In the saturated zone, which is mostly below the water table and includes the capillary fringe, more organic liquid is immobilized by capillary forces (Schwille, 1967, 1981, 1984, 1988; van Dam, 1967; de Pastrovich *et al.*, 1979; Schiegg, 1980; Wilson and Conrad, 1984; Albertson *et al.*, 1986; Schiegg and McBride, 1987). Here the immobilized organics remain as small, disconnected pockets of liquid, sometimes called 'blobs', no longer connected to the main body of organic liquid.

The immobilized volume is called the 'residual oil saturation' in petroleum reservoir engineering (Taber, 1969; Morrow, 1979; Chatzis *et al.*, 1983; Anderson,1987b), and is measured as the volume of organic liquid trapped in the pores relative to the volume of the pores. Organic liquid at residual saturation can occupy from 15% to 50% of the pore space in petroleum reservoir rocks under conditions that are equivalent to those in the groundwater saturated zone (Melrose and Brandner, 1974). At a spill or hazardous waste site the entire volume of organic liquid can be exhausted by this immobilization, although if the volume of organic liquid is large enough, it continues to migrate down-gradient where it becomes a threat to the safety of drinking water or agricultural water supplies (Schwille,1967,1981; de Pastrovich *et al.*, 1979). This report refers to the immobilized organic liquid as 'residual organic liquid'. As described in detail in sections 9 & 10 of this report, the actual spatial distribution of the residual saturation within the pore space is completely different in the vadose and saturated zones.

The organic liquid phase is sometimes referred to as being immiscible with water and air. Although that expression is used here, it is important to realize that small concentrations of the various components of the organic phase volatilize into the air phase and dissolve into the water phase. A 'halo' of dissolved organic components precedes the immiscible phase in its migration (Figure 1-1). Even when the so-called immiscible organic liquid has been immobilized by capillary trapping, the passing groundwater dissolves some of the residual. In effect, the organic liquid phase acts as a continuing

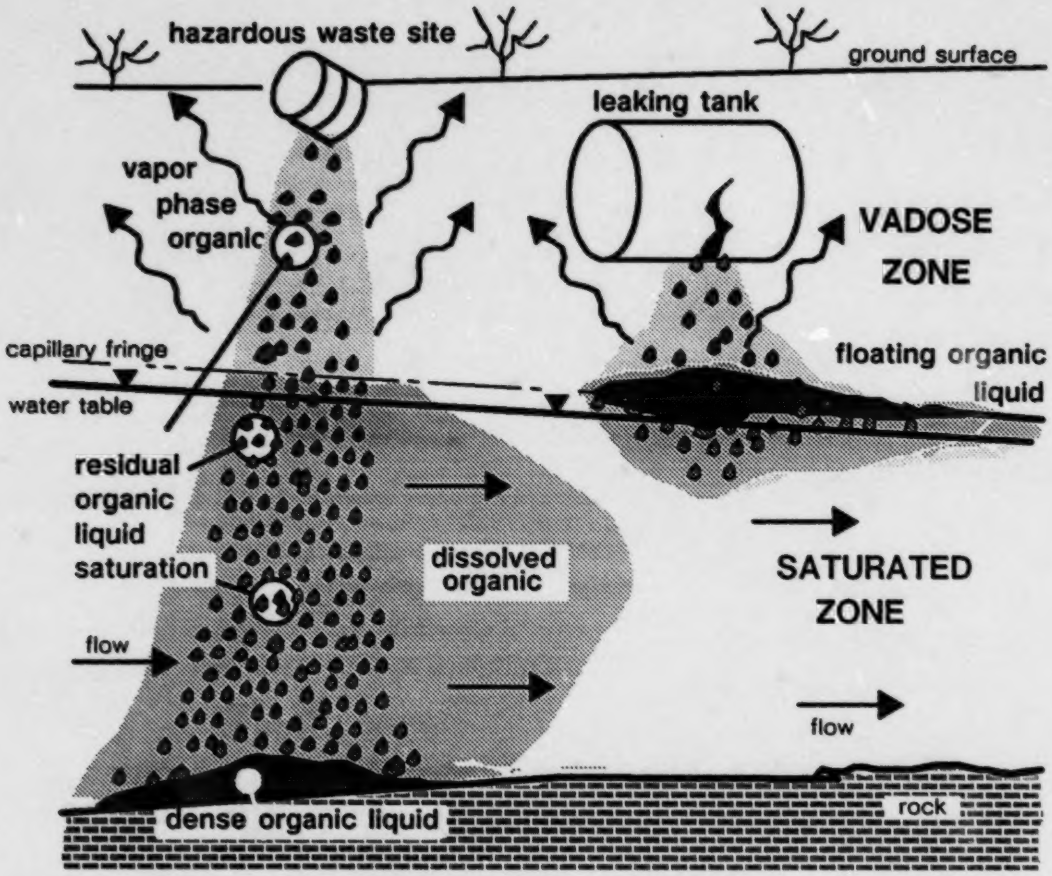
hazardous waste site
ground surface
leaking tank
vapor phase organic
VADOSE ZONE
capillary fringe
water table
floating organic liquid
residual organic liquid saturation
dissolved organic
SATURATED ZONE
flow
flow
dense organic liquid
rock

FIGURE 1-1. Migration pattern for an organic liquid more dense than water (left), and less dense water (right).

source of dissolved organic pollutants (eg, Tuck *et al.*, 1988). Similarly, in the vadose zone, the residual organic liquid that volatilizes into the air phase migrates by gaseous diffusion and advection, becoming a source of organic components to air or water pollution, and a possible explosion hazard. In large spills and leaks it is apparent that most of the liquid organic remains as a liquid, some is volatilized, and a little is dissolved. However small in volume, the volatilized or dissolved components are usually the ones that cause problems. The liquid organic phase acts as a reservoir of additional organic to replenish the air and water phases with dangerous and/or toxic material. Clearly, the source of the dissolved or gaseous organic constituents — the liquid organic phase — must be removed or isolated in order to restore a polluted aquifer.

There is no wholly effective mechanism to remove the residual organic liquid. Waiting for the residual to dissolve can take several decades. In the vadose zone, induced volatilization may help reduce the residual volume for lighter organics, but is not effective for heavier ones (Burris et al., 1986). Engineered removal is usually attempted hydraulically, by sweeping the organic liquid out with water, or biologically, by encouraging the consumption of the organic constituents by the soil microbial community. This last process, biodegradation, is the focus of current research and several recent restoration efforts. It is seldom tried alone, for the microbes generally consume only the dissolved organics. Moreover, some organic chemicals are extremely resistant to biodegradation. PCB's, for example, may biodegrade very slowly, or not at all in the subsurface (J.R.Roberts *et al.*, 1982). Hydraulic sweeps remain a major component of any attempt to remove organic liquids although, commonly, hydraulic sweeps fail to remove all the liquid organic phase, often leaving a significant quantity of residual organic liquids behind (Wilson and Conrad, 1984). There is, of course, another removal option often used for small pollution events: excavate the site and dispose of or treat the contaminated soil. For large sites this alternative is unfeasible. Since there is no panacea for the removal of organic liquids, containment is often adopted as part of a restoration strategy. Hydraulic containment (e.g., Wilson, 1984), often in combination with structural barriers such as a slurry wall, is becoming standard practice.

SCOPE OF PREVIOUS WORK

Development of improved technologies to clean up organic pollutants depends in large part on developing an ability to understand and predict the migration of liquid, vapor, and dissolved organics. Liquid organics move through a water and sometimes air filled porous soil, as a separate phase, under the influence of viscous, gravity, and capillary forces. Dissolved organics move in the water phase and are subject to advection, dispersion, biodegradation, and adsorption onto soil particles. Organic vapors in the air phase are subject to similar mechanisms. A few of these major transport mechanisms are fairly well understood today, principally those associated with the behavior of dissolved organics. McCarty et al. (1981) and P. V. Roberts et al. (1982) have reviewed the progress of this research.

In contrast, the organic liquid phase transport mechanism has been virtually ignored by the research community in the United States, although it has been the subject of empirical studies in Europe (e.g., Albertson *et al.*, 1986; Schwille, 1967, 1981, 1984, and 1988; van Dam, 1967; Schiegg, 1980). Recently, however, American researchers have obtained some laboratory results. Convery (1979) ran gravity drainage experiments on a long column to relate organic liquid retention in the vadose zone with grain size and sorting. Eames (1981) used a short soil core centrifuging method to measure residuals in the vadose zone. Eckberg and Sunada (1984), and Ferrand *et al.* (1986) used gamma radiation attenuation and bulk soil electrical resistivity to measure three-phase fluid saturations at various times and at various elevations above a water table following a simulated petroleum spill. The experimental procedure allowed a petroleum 'spill' to be tracked as it moved through the vadose zone to the water table. Cary *et al.* (1989) performed experiments to test the ability of multiphase flow theory to predict the infiltration and redistribution of wetting and non-wetting fluids. They met with limited success. Lenhard and Parker (1988b) used theoretical three-phase saturation-pressure relationships to estimate the volume of oil in soils given observed fluid levels in monitoring wells.

Some simple numerical simulations of multi-phase transport have been developed. These focus on immiscible transport of continuous phases. Residual organic liquids, trapped by capillary forces, are often ignored, although they are sometimes treated as a source of dissolved contamination. This research effort mirrors the state of the art of petroleum engineering's 'black oil' models. A few researchers (notably Baehr and Corapciaglu, 1984 and 1987; Corapciaglu and Baehr, 1987; Abriola and Pinder, 1985a,b; and Pinder and Abriola, 1986) have looked into interphase transfer, including the volatilization and solution of organic components, using computer simulations. This again reflects the state of the art in petroleum engineering, where so-called compositional models are used to examine enhanced recovery techniques.

Parker *et al.* (1987) have proposed a model to estimate the functional relationships between fluid pressures, saturations, and permeabilities of two- or three-phase porous media systems, and these functional relationships have been implemented in a multi-phase numerical flow model (Kuppusamy *et al.*, 1987). The model has since been extended to include the effects of hysteresis and non-wetting phase trapping (Parker and Lenhard, 1987; and Lenhard and Parker, 1987a). The results of concurrent laboratory work were used to validate the model (Lenhard and Parker, 1987b,1988a,1989; and Lenhard *et al.*, 1988).

Petroleum engineering's long history of research into improving recovery from petroleum reservoirs may be applied to rehabilitating fresh-water aquifers polluted by organic liquids. Through over forty years of experimentation, petroleum engineering has amassed considerable expertise in multi-phase transport, the mechanics of oil phase capillary trapping, and oil recovery. To date, relatively little of this technology has been applied to recovering organic hazardous wastes and petroleum hydrocarbons released in the near-surface environment. The petroleum literature on residual oil saturation is reviewed in papers by Anderson (1988), Chatzis et al. (1983), Melrose and Brandner (1974), and Taber (1969). In groundwater hydrology we too are concerned with the capillary trapping of residual saturation, and with its removal. However, unlike petroleum engineers, we are also concerned with the mechanisms that initially brought the 'oil' into the aquifer in the first place. In the 'oil patch' that is the province of petroleum geologists, and it involves issues that are quite different than ours. Consequently, we can expect little help from the oil patch on these mechanisms.

MOTIVATION FOR THIS STUDY

Residual organic liquid saturation often constitutes the major volume of the organic pollution, and acts as a continual source of dissolved or vapor phase organics (Wilson and Conrad, 1984). In particular, there is a need to understand how the residual organic liquid is trapped and how it can be hydraulically mobilized or otherwise removed. As shown in Sections 9 and 10 of this report, the residual organic liquid appears to form blobs, films, wedges and rings of microscopic size, depending on the presence of other fluids, the pore geometry, the surface wetting of the solids, and soil heterogeneity. The term wetting refers to the relative affinity of the solid surface for the available fluids. Water is normally the wetting fluid in most soils. Organic liquid is normally non-wetting relative to water, and wetting relative to soil gas. The size, shape, and spatial distribution of these blobs, films, wedges and rings affects the dissolution of organic liquid into the water phase, volatilization into the air phase, and the adsorption and biodegradation of organic components. The presence of residual organic liquid also affects the relative permeability versus saturation curves used in numerical simulation codes of fluid movement and pollution migration. A paucity of experimental results regarding these issues makes site characterization conjectural, predictive modelling unreliable, and remediation design of organic liquid leak or waste sites less effective than might be possible.

OBJECTIVES

The goal of this study was to better understand the basic physical mechanisms controlling the movement, and especially the capillary trapping, of organic liquids in soils and groundwater. Emphasis was on relating the various mechanisms to the issues of contaminant movement, characterization, and remediation. This broad goal was broken down into two sets of specific research objectives, addressing issues relevant to the saturated and vadose zones, respectively:

The Saturated Zone

Assuming that water is wetting and the organic liquid is non-wetting, our research objectives for saturated zone conditions were to:

•$_1$ conduct a literature review of basic concepts, including non-wetting phase capillary trapping and mobilization mechanisms, and petroleum experience;

•$_2$ conduct experiments that permit the visualization of two-phase fluid flow and capillary trapping, and record the visualizations on film and videotape;

•$_3$ perform a detailed study of two phase flow capillary trapping and non-wetting phase residual saturation in a typical unconsolidated soil, testing the hypothesis that its behavior can be predicted from previously published results from the petroleum engineering literature;

•$_4$ compare non-wetting phase residual saturations for various organic liquids, testing the hypothesis that residual saturation is largely independent of organic liquid composition for expected conditions in hydrology;

•$_5$ compare non-wetting phase residual saturations for various soils, testing the hypothesis that residual saturations should be similar in soils that have a similar grain size distribution;

•$_6$ investigate how the rate of initial invasion of a non-wetting organic liquid may influence irreducible water saturations and, later, organic residual saturations;

•$_7$ investigate the possible hydraulic mobilization of non-wetting phase residual organic liquid, by increasing groundwater velocities, testing Wilson and Conrad's (1984) conclusion that this is largely an unrealistic aquifer remediation alternative unless interfacial tensions are reduced significantly; and

•$_8$ test the hypothesis that porous media heterogeneity can dominate displacement and trapping mechanisms.

The Vadose Zone

Our research objectives for vadose zone conditions were to:

$\bullet_1$ conduct a literature review of basic concepts, including capillary trapping mechanisms, mobilization issues, and petroleum experience;

$\bullet_2$ conduct experiments that permit the visualization of multi-phase fluid flow and capillary trapping, testing the hypothesis that spreading organic liquids typically form a film between the water and air phases;

$\bullet_3$ perform a detailed study of capillary trapping and residual saturation in a typical unconsolidated soil, testing the hypothesis that organic liquid residual saturations are significantly lower in the vadose zone, than they are in the saturated zone; and

$\bullet_4$ conduct experiments that permit the visualization of capillary trapping for non-spreading organic liquids, testing the hypothesis that non-spreading organic liquids behave differently than non-spreading organic liquids.

EXPERIMENTAL APPROACH

The problem was approached experimentally in four ways:

1. **Quantitative displacement experiments using short columns** were performed to relate the magnitude of residual organic liquid saturation to fluid and soil properties, and to the number of fluid phases present (i.e., both saturated and vadose zone conditions).

2. **Quantitative displacement experiments using long columns** were performed under two-phase saturated zone conditions, yielding water and organic liquid relative permeabilities. In these experiments, reductions of residual organic saturation were correlated to the pressure gradient applied in hydraulic sweeps, and the potential for hydraulic mobilization of residual 'blobs' was investigated.

3. **Pore and blob casts** were produced for saturated zone conditions by a technique in which the organic liquid was solidified in place within a soil column at the conclusion of a displacement experiment, allowing the distribution of organic liquid to be observed. The polymerized organic phase was rigid and chemically resistant. Following polymerization, the water phase was removed and replaced by an epoxy resin. The solid core, composed of soil, solidified styrene (the organic phase), and epoxy resin (the water phase), was cut into sections to show the organic liquid phase in relation to the soil and the water phase. The sections were photographed under an optical microscope. Although polymerization only gave a 'snapshot' of the displacement process,

it offered the advantage of seeing organic liquid in its 'natural habitat' (i.e. within a soil) as compared to that observed in etched glass micromodels. Sometimes, instead of replacing the water with epoxy resin, the solid matrix of the soil column was dissolved with hydrofluoric acid, leaving only the hardened organic liquid. The solidified organic phase was then observed under a scanning electron microscope (SEM) and photographed. For vadose zone conditions, styrene and epoxy liquids were sequentially applied, drained and hardened in an attempt to simulate proper fluid distributions above the water table. The resulting pore casts were photographed under an optical microscope.

4. **Etched glass micromodels** were used to observe dynamic multi-phase displacement processes. Micromodels provide two-dimensional networks of three-dimensional pores. They offer the ability to actually see fluids displace one another in both a bulk sense and also within individual pores. Although displacements are known to be dependent upon a variety of factors, this report describes micromodel experiments that focused on only three: (1) the fluid flow rate, (2) the presence of heterogeneities, and (3) the number of fluid phases present. The experiments were photographed and videotaped.

To interpret the experiments in heterogeneous material, we also developed a new but simple theoretical model of multiphase flow and capillary trapping. The model is based on the interplay between viscous and capillary forces.

ORGANIZATION OF THIS REPORT

Following this introduction are two sections (2 & 3) that summarize the report conclusions and recommendations. The next five sections (4 through 8) detail fluid and soil characteristics, and the experimental methodology, used for each of the experimental approaches outlined above. These sections contain detailed information that may be used by future investigators wishing to verify or extend the results of this study. The reader more concerned with results than methods can probably skip them. The last two sections (9 & 10) describe experimental results for saturated zone and vadose zone conditions, respectively. These sections contain a large number of photomicrographs that visualize multiphase flow and residual saturation.

SECTION 2

CONCLUSIONS

The intent of this study has been to better understand the basic physical mechanisms controlling the movement, and especially the capillary trapping, of organic liquid pollutants in soils and groundwater. This goal was pursued by observing organic liquid behavior in laboratory soil columns and etched glass micromodels, built to represent various conditions in the subsurface. Fluid movement observed in these studies is explained in terms of three basic forces acting on the fluid phases: capillary forces, viscous forces associated with flow, and the effect of gravity.

Below we review our conclusions for the saturated and vadose zone experiments. The most interesting series of observations has illustrated how the interplay between capillarity and soil heterogeneities profoundly influence the migration and trapping of an organic phase in a multi-phase system. We end with several conclusions concerning experimental procedures.

We strongly recommend that the reader peruse the photographs in Sections 9 and 10, in order to appreciate these conclusions

THE SATURATED ZONE

- **As organic liquid moves through the saturated zone, a significant portion is left behind, trapped by capillary forces. In water wet soils this residual organic liquid saturation is trapped as discontinuous 'blobs'.** Photomicrographs taken of micromodel pores, blob casts and pore casts indicate that trapped blobs form a variety of shapes: from spherical shaped singlets occupying one pore, to complex, branching multi-pore blobs.

- **Capillary trapped blobs are trapped by two different mechanisms.** 'Snap-off' creates singlets, while by-passing creates doublets and much more complex, branched shapes. By-passing is also the major mechanism when soil heterogeneities are involved.

- **Large amounts of residual organic are trapped by capillary forces.** We observed residual saturations that ranged from 14% to 30% in unconsolidated sands, and possibly higher in heterogeneous sand packs. If these estimates are typical for most organic liquids and sandy soils, then there is a tremendous storage capacity for organic liquid pollutants in the saturated zone. For example, expressed in terms of volumetric retention (Equation 9-5), the Sevilleta sand has the capacity to store over 90 liters of organic liquid per cubic meter of soil, in the saturated zone. A single 10,000 gallon spill of an organic liquid could be absorbed in about 420 m^3 of the saturated soil. This volume corresponds to a cube of soil with sides only 7.5 meters in length. Even for soil residual saturations of only a third of this, the capacity is still large.

- **The size and shape distribution of the trapped blobs can influence interphase transfer.** For large, branched blobs, in which perhaps only the ends of the ganglia are exposed to the bulk flow of water, dissolution of soluble components may be limited by diffusion through thin films of water lining pore walls. From our review of photomicrographs we've concluded that:

  - o Mass transfer coefficients used in the mathematical models of partitioning often employ the analogy of an equivalent spherical blob (e.g., Pfannkuch, 1984). Certainly singlets fit this model, but an appropriate definition of equivalent sphere size has yet to be proposed for the population of more complex and branched blobs.

  - o The position of a blob within the pore space has a strong influence on mass transfer between phases. If a large portion of the blob surface is in contact with only a thin film of water, as certainly seen in our pore casts and micromodels, then the transfer rate may be limited by advection or diffusion in the film. Videotaped micromodel observations indicate that the flowing water moves around the blobs, through the unoccupied pores, with little water movement in the films to help advect organic components away.

  - o As components of the organic phase partition from it, a blob gets smaller, and the residual organic saturation is reduced over time. Water phase relative permeability increases.

  - o Mass transfer may or may not be governed by local equilibrium. When groundwater velocities are high enough or the dissolution kinetics are slow enough, the local equilibrium assumption no longer holds. In this sense the rate of mass transfer between phases strongly depends upon the distribution of the residual saturation. For large, single component, branched blobs mass transfer can be limited by a diffusional process. Substantial portions of these blobs are only in contact with thin water films along the walls of pores. Diffusion through the films to the main body of passing groundwater can be the rate-limiting step in solubilizing organic liquid into the water phase. If the flowing water-phase dispersed zone is large enough, or the zone of trapped organics is relatively small, the solubility limit of the organic liquid in water may never be reached.

  - o Dissolution from a multi-component organic phase is more complex. For large branched blobs or by-passed regions of multi-component liquids, the mass transfer rate for a given component can become limited by rate of diffusion of that component within the organic phase to the organic/water interface. Since the major portion of the transfer may be occuring at the ends of these tortuous blobs, intra-blob diffusion may be small.

- **The size and shape distribution of the trapped blobs can influence microorganisms.** Our review of photomicrographs has lead us to conclude that:

    - ○ Microorganisms attached to the pore wall, at the water-solid interface, experience an environment that depends on their location. In blob-filled pore throats, the organisms have ready access to organic components that partition into the aqueous phase from the nearby blob surface. However, these organisms may not have a ready supply of other substrates, which can only diffuse (or flow) slowly through the thin water film that lines the pore throat. In blob-filled pore bodies that have a surrounding water film, the same situation applies, as it does for microorganisms attached to the blob surface in these regions of thin aqueous films. In the other pores, occupied by flowing water, wall-attached microorganisms are readily exposed to available dissolved substrates, subject only to upstream substrate re-supply.

    - ○ Migration of microorganisms is also probably influenced by the spatial distribution of blobs. It should be difficult for a seed population to find its way into regions with thin aqueous films because of their low flow rates and tortuous diffusion paths. In any event, most organisms would probably not thrive in these stagnant regions because of the substrate re-supply problem and the possibility of toxicity due to locally high concentrations of dissolved organics.

- **Prediction of residual saturation levels in a given soil is uncertain.** A wide variety of residual organic liquid saturation measurements were made on the Sevilleta sand, an unconsolidated, aeolian sand. Its texture is much more like glass beads than sandstone, both of which had been previously investigated by petroleum engineers. We examined the hypothesis that, because of its similar texture, the Sevilleta sand should behave more like the glass beads. Uniform glass beads exhibit a residual saturation of 14-16%. The Sevilleta mean residual saturation was 27.1%, almost 10% greater than expected. Singlet blobs are common in glass beads. Photomicrographs of Sevilleta blob and pore casts revealed a much larger population of complex, branching blobs. Residual saturations in the Sevilleta sand did not behave as expected.

- **Residual saturations should, but may not be similar in soils that have a similar texture and grain size distribution.** We examined residual saturations in a variety of sandy soils. Two soils of very similar texture and grain size (the Sevilleta sand and the Traverse City sand) yielded significantly different residual saturations (27.1% and 17.6%, respectively). Two soils with somewhat different textures and grain sizes (the Traverse City sand and the coarser, less uniform Llano sand) had very similar residual saturations (17.6% and 15.8%, respectively).

- **Even minor amounts of clay or silt in a soil may play a significant role in the observed residual saturation.** The Sevilleta sand may had 2% clay and silt, by weight. The Traverse City and Llano sands were essentially clay and silt free. We hypothesize that the clay and silt content of the Sevilleta was responsible for the high residual saturation and complex, branching blobs that we observed. One possible mechanism is clay swelling in the pore throats, leading to increased by-passing. Another explanation is that the fine material may have settled into microlayers during the wet column packing procedure. This type of heterogeneity could lead to increased water by-passing of the coarser material. If this latter explanation is true, then this experiment demonstrates that even minimal soil structure and heterogeneity can have a dramatic influence on behavior.

- Models of organic liquid movement employ prescribed values of residual organic liquid saturation as a soil property. It would be convenient to be able to estimate residual saturations from more primitive soil properties, such as grain size distribution (see, eg, Soll and Celia, 1988). **These experiments indicate that textural considerations alone may lead to unreliable estimates and erroneous models of residual saturation.**

- **Fine-grained, water-wet soils (which do not shrink in the presence of organics) can serve as an effective barrier to organic liquid movement in the subsurface.** This was indirectly demonstrated by our inability to inject an organic phase into the Palouse loam.

- **Under low capillary and Bond number conditions residual saturation in a given soil is largely independent of organic liquid composition.** We measured residual saturations for a variety of multi-component and single component organic liquids: Soltrol-130, gasoline, kerosene, p-xylene, n-decane, and tetrachloroethylene (PCE). In repeated quantitative short column experiments we found no correlation between residual saturation, and viscosity, density, or interfacial tension for the six organic liquids tested. The residual saturation was virtually identical for all of the organic liquids.

- **Residual saturations appear to be relatively insensitive to fluid properties and very sensitive to soil properties (and heterogeneities).** This is true only under low capillary and Bond number conditions.

- **At a particular contamination site** it may seem reasonable to directly measure residual saturation of whatever organic liquid was spilled. **We recommend that tests be conducted with an ideal fluid, using uncontaminated soil from the site.** Unless some odd wetting behavior is anticipated, or unless some interaction between fluids, or between fluids and the solid is expected, it is probably preferable to chose a fluid which has:

  1. a sufficient density difference with water;
  2. low solubility;
  3. low volatility; and,
  4. low toxicity.

The easiest fluids for us to use were Soltrol and decane.

- **The rate of initial invasion of a non-wetting organic liquid may influence 'irreducible water saturations' and, later, organic residual saturations.** The amount of organic liquid that is ultimately trapped is strongly dependent on the nature of original emplacement.

- **The term 'irreducible water saturation' is misleading.** The term is often used to represent the wetting phase residual saturation. However, even at residual saturation the wetting phase is continuous, and is composed of an interconnected network of films, pendular rings, and wedges. This is a considerably different situation than the discontinuous 'blobs' pictured in this report for the non-wetting phase residual. The wetting phase liquid can move through its interconnected network, draining the films and rings, and reducing the residual wetting phase saturation. If there is no barrier to organic phase migration, and the organic phase pressures cannot build-up, then by-passed pockets of water, constituting a major portion of the residual water saturation, may not drain. The residual water saturation is not a single 'irreducible' value, but depends on boundary conditions.

- **Residual organic liquid can be mobilized by increasing groundwater velocities.** Residual organic liquid blobs are easier to mobilize for lower interfacial tensions, higher permeability soils, and in the lab. They are harder to mobilize for higher interfacial tensions, lower permeabilities, and in the field where there are severe practical constraints on the hydraulic gradient. Although it may be possible, intentionally or by accident, to mobilize some of the residual, it is difficult to get it all.

- **The groundwater velocities and capillary numbers needed for mobilization make hydraulic remediation of contamination unrealistic in the saturated zone.** Several schemes have been published in the literature and implemented in the field for hydraulically sweeping organic liquids from polluted aquifers. These schemes are presumably meant to sweep out the continuous organic liquid, knowingly leaving behind the residual. More often it seems that naivete prevails, and many designers assume that as long as ground water is flowing toward a collection system, eventually all of the organic liquid will make it. No matter how long one waits, unless gradients are increased above the critical level, none of the residual will be hydraulically removed (Wilson and Conrad, 1984). The critical velocity and capillary number(see Equation 9-6) needed to initiate mobilization is much higher than the sandstone values used by Wilson and Conrad (1984) in their study of hydraulic remediation. Despite their low estimate they concluded that hydraulic floods are unrealistic remediation alternatives. We amplify that conclusion.

- **The interfacial tension (IFT) must be reduced significantly to allow hydraulic schemes to perform adequately.** Surfactant floods hold promise of reducing the IFT sufficiently to allow some mobilization of the residual. However, unless the IFT is reduced to the point of emulsification of the organic liquid, it is doubtful that more than a small proportion of the organic liquid can be mobilized under field conditions.

- **Porous media heterogeneities dominate displacement and trapping mechanisms.** We presented flow visualization results from micromodels representing 1) an aggregated soil (strings of interconnected macropores or fractures, separating clumps of micropores), and 2) a soil with discontinuous lenses (lenses of coarse pores within an otherwise homogeneous model). The character of these displacements were contrasted with homogeneous displacements. The discontinuous stringers experiments were duplicated in short column studies, yielding both pore casts and quantitative measurements of trapping in a heterogeneously packed sand column. These experiments demonstrate that:
  - **The saturation and spatial distribution of organic liquid found behind an advancing front of organic liquid depends upon the combined effects of soil heterogeneity and capillarity.**
  - **Organic liquid selectively travels through the coarser and more permeable portions of heterogeneous aquifers, by-passing finer-grained regions.** Organic liquids can be expected to move quickly through aquifers which have interconnected coarse layers or fractures. In New England groundwater consultants commonly distinguish between gasoline leaking from underground tanks in unconsolidated, glacial deposits, and leaks in ledge or bedrock. In the unconsolidated deposits anecdotal evidence suggests that much of the gasoline is trapped by capillary forces, with very limited and slow migration of the liquid gasoline. The gasoline tends to appear in nearby brooks dissolved in the groundwater discharge. In crystalline rock terrain the gasoline moves quickly and far, with observable liquid gasoline discharges to nearby brooks.
  - **Following the recovery of free liquid organic, the residual saturations left behind in interconnected fractures or macropores tend to be *smaller* than in a homogeneous porous material, but can be expected to extend over a *larger* portion of aquifer.**
  - **At typical aquifer flow velocities, capillary forces can relegate the flow of water to finer-grained regions, by-passing the coarser organic liquid-filled regions.** Corroborating results were obtained from micromodels, column experiments and a simple mathematical model.
  - **Following the recovery of free liquid organic, the residual saturation left behind in a heterogeneous aquifer, that is composed of disconnected coarse lenses, tends to be *larger* than in a homogeneous aquifer, but can be expected to extend over a *smaller* portion of aquifer.**
- **Increased recovery of organic liquids from coarse lenses may be attained by increasing the pumping rate.** This principle was demonstrated in the micromodel, soil columns, and mathematical theory. However, the theory predicts that should velocities get high enough, water will prefer to move through the coarse lenses and by-pass organic liquid in the fine matrix. This suggests that varying the pumping rate, over long periods of time, may have a beneficial effect.

- **The effects of the lens pattern of heterogeneity were incorporated into a simple mathematical model.** The model was qualitatively validated by the column and micromodel experiments. The model represents a balance of viscous and capillary forces on a large spatial scale, and can be expressed in terms of an effective capillary number.

- **This simple model suggests that it is feasible to develop effective properties or equivalent homogeneous models of behavior in heterogeneous materials.** Computer simulation codes into which these equivalent homogeneous properties are inserted may not be conventional codes. They will need to account for the partial desaturation of lenses, and the effect that has on effective relative permeabilities and saturations. For example, the effective permeabilities and residual saturations will certainly depend on the rate and direction of flow. We believe that this is a typical consequence of dealing with effective properties in non-linear systems. Certainly Yeh et al. (1985a,b,c), Mantoglou and Gelhar (1987), and McCord et al. (1988a,b) encountered the same issue in their work on the Richard's equation approach to water flow in the vadose zone.

THE VADOSE ZONE

- **The movement of organic liquid through the vadose zone is more complex than organic liquid movement in the saturated zone, especially because of the tendency for many organics to spread.** The organic liquid is of intermediate wettability between water, the wetting phase, and the non-wetting gas phase (at least for the conditions examined here). The propensity for a given organic liquid to spread between water and gas can be predicted from the spreading coefficient, $\Sigma = \sigma_{aw} - (\sigma_{ow} + \sigma_{ao})$, where the σ's represent IFT's. Positive spreading coefficients lead to organic liquid films along the water-gas interface.

- **A spreading organic liquid forms (1) a film between the gas and water phases, as well as (2) pockets of organic liquid that replace gas in the pore bodies, and gas or water in the pore throats.**

- **Films appear to be an important mechanism of organic liquid invasion into the vadose zone.** The organic liquid usually advances by displacing gas, and sometimes water, from pore throats and bodies. It also advances through film flow, most easily seen in our experiments when pockets of organic liquid began to accumulate deeper in a micromodel, with no obvious connection to sources of organic liquid above. Some water is by-passed, mostly in pore throats, as is some air, mostly in pore bodies. The resulting entrapped air bubbles are essentially identical to the non-wetting phase blobs seen in the two-phase saturated zone experiments.

- **In the vadose zone the residual saturation of a spreading organic liquid consists of films, pendular rings, wedges surrounding aqueous pendular rings, and filled pore throats.** There are a few isolated organic liquid blobs trapped in otherwise water filled pore bodies, and the occasional gas bubble trapped inside an organic liquid blob.

- **Films of a spreading organic liquid maintain continuity of the organic phase.** The pockets of residual organic liquid trapped in vadose zone pore bodies or pore throats communicate; they are not isolated blobs.

- **Residual saturations are much lower in the vadose zone than they are in the saturated zone.** In the Sevilleta soil the vadose zone residual saturation is 9.1%, compared to 27.1% for saturated zone conditions. The lower residual is explained by:

    - continuity of the films during drainage;
    - presence of a third, non-wetting gas phase;
    - additional buoyancy forces due to the greater density contrast of the organic liquid to air, than to water; and
    - less capillarity due to the lower IFT between the organic liquid and gas, than between the organic liquid and water.

- **The capacity for storing or retaining organic liquids is much smaller in the vadose zone than in the saturated zone.**

- **The films expose a large organic liquid surface area to the gas phase, making soil venting of organics in the vadose zone an attractive remediation strategy.** The rate of mass transfer may be limited by diffusion within the film portion of a multi-component organic liquid. The controlling variables are film thickness and tortuosity, and the geometry of its connection to larger pockets of organic liquid.

- **The formation of films also exposes a large organic liquid surface area to the water phase, increasing the effective solubility of the organic.** The effectiveness of this transfer is severely limited by the water flow rate.

- **The distribution of the films and pockets of organic liquid can influence microorganisms.** Our review of photomicrographs has lead us to conclude that:

    - There are largely air filled pores, with a ready access to oxygen, but with only a very thin double film of water and organic liquid. At residual saturation these films would have a very limited ability to resupply needed nutrients to microorganisms.
    - The environment of water filled pore throats and pendular rings may be controlled by the lack of oxygen. The film of organic liquid should suppress oxygen transfer to the water phase.
    - We speculate that transient changes in fluid saturations would improve the environmental conditions for aerobic bacteria.

- **Biosurfactants are a by-product of biological activity, especially for organisms that attach at the organic liquid-water interface.** We hypothesize that these natural surfactants could change interfacial tensions enough to reduce organic liquid saturations by drainage (see Figure 10-3).

- **Non-spreading organic liquids do not form films, but rather coalesce into small lenses that float at the water-gas interface.** Non-spreading organics,e.g., halogenated organic solvents, have a negative spreading coefficient.

- **The residual saturation of a non-spreading organic liquid consists of floating lenses at the water-gas interface, pendular rings, wedges surrounding aqueous pendular rings, and filled pore throats.** There is no interconnecting film.

- **The soil venting of non-spreading organics in the vadose zone may not be nearly so attractive a remediation strategy.** The organic liquid surface area exposed to the gas phase is severely reduced by the coalescence of the organic into lenses. The mass transfer coefficient should be much lower.

- **Biosurfactants that are a by-product of biological activity could change interfacial tensions enough to alter a non-spreading organic liquid to become a spreading organic liquid. This should improve mass transfer coefficients.**

EXPERIMENTAL APPROACH

- **Flow visualization techniques employing micromodels and styrene polymerization provide useful tools with which to examine multi-phase displacement processes on both pore and bulk scales.**

- **The similarity of the blobs trapped in micromodel experiments to those trapped in two-phase pore casts and blob casts provide some confidence that the micromodels provide a reasonable analogy to multi-phase flow in soils.**

- **We believe that micromodel results can be generalized to aquifer scales, as illustrated by the heterogeneous aquifer with stringers (Section 9).**

- **Flow visualization approaches can be applied to other related pollutant transport problems, for example: *diffusion, hydrodynamic dispersion, and 'small-scale' macro-dispersion; bacteria and colloid adhesion and migration; biotransformation of organic pollutants; adsorption of dissolved organic pollutants and the possible alteration of soil wetting properties.***

- **New equipment must be designed and constructed in order to examine the movement and trapping of organic liquids in low permeability soils.**

SECTION 3

RECOMMENDATIONS

Recommendations are divided into two groups. The first group deals more with the science of multi-phase flow and recommends additional research. The second group looks at the experimental procedure and equipment, and recommends improvements.

RECOMMENDED ISSUES FOR FUTURE RESEARCH

Saturated Zone Research

- **Observe blob size distribution via imaging, Scanning Electron Microscope (SEM), and Coulter counter.** We had hoped to conduct a statistical analysis of size and shape blob casts. However, two of the problems that we encountered led us to reconsider. First, the preferential wetting of the TFE (Teflon™) column walls may have led to a final non-uniform distribution of residual saturation over the column cross-section (see Section 7). Blob populations taken from this sample might not be representative. Second, the samples of blob casts we examined showed many broken casts (see photomicrographs in Section 9). We believe that these problems can be overcome, and recommend that future research efforts collect this statistical data. In particular we recommend the use of image analysis on pore cast fat sections, that are sequentially polished to provide parallel sections into the sample. These sections can be reconstructed on a computer into a three dimensional model of the space that shows the relative locations of minerals and fluids. The fat sections may prove too transparent to allow adequate discrimination of the phases. If so, parallel thin sections can be prepared, but with a loss of material between the sections.

- **Observe fluid distributions with pore and 'blob' casts for other saturations.** The *in situ* visualization work with pore and blob casts focused on residual non-wetting phase saturations. These techniques should be applied to the visualization of fluid distributions at other saturations.

- **Investigate residual organic liquid saturations of other soils, with an emphasis on correlation with texture & porosity.** A combination of quantitative experiments, pore casts, and blob casts should be employed to develop a detailed morphology of this issue, which the experiments reported herein barely begin to address. We've observed two very similar soils with dissimilar residual saturations, while other, dissimilar soils have almost identical residual saturations. This is a disturbing result which requires additional explanation.

- **Determine the role of clay minerals on residual organic liquid saturations.** We found our highest residual saturations, and most complex blobs, in the Sevilleta soil. Of the sandy soils we investigated, this was the only soil with any significant amount of clay and silt in it (perhaps 2%). It is possible that the clay's swelling properties played a role in the high residual saturation, although it may be due to micro-layering caused by the packing procedure. We believe that the issue must be resolved. The large difference in residual saturations (17% to 27%) has enormous practical implications. We recommend a careful investigation of the role of clay minerals with an emphasis on possible packing induced heterogeneities.

- **Further investigate capillary trapping and mobilization at high capillary numbers.** We expect that the correlation between residual saturation and capillary number depends on the soil pore structure, and that it will vary from soil to soil. Our apparatus was not able to very fully explore this relationship for mobilization and did not attempt to do so for initial trapping. Micromodels should also be used to address these issues.

- **Investigate effects of dissolution on residual saturations.** The position of a capillary trapped blob within the pore space has a strong influence on mass transfer between phases. If a large portion of the blob surface is in contact with only a thin film of water, as certainly seen in our pore casts and micromodels, then the transfer rate may be limited by advection or diffusion in the film. Preliminary videotaped micromodel observations indicate that the flowing water moves around the blobs, through the unoccupied pores, with little water movement in the films to help advect organic components away (Mason *et al.*, 1988). We suggest additional micromodel experiments using a fluorescent dye as a soluble component, or fluorescent microspheres, with image enhancement to bring out the concentration distribution in the water phase. We could then observe the flow of water on a pore scale, especially through water films and wedges surrounding the blobs. Similar techniques could be use to examine flow in the films of the vadose zone experiments.

- **Investigate wetting phase relative permeability as a function of reduced residual saturation.** Compositional models are numerical codes which simulate multi-phase flows with interphase transfers such as solubilization. 'Black oil' models focus on more sophisticated representation of the multi-phase flow, but at the expense of neglecting compositional behavior. The two approaches are being integrated by various researchers, allowing better predictions of the migration of organic pollutants. These models need estimates of relative permeabilities to each of the fluids. In particular they need the wetting phase relative permeability at residual saturation. When residual non-wetting phase saturations are reduced by mobilization, volatilization, or solubilization the wetting phase relative permeability increases [$k_{rw}(S_{or})$ *at* $0 < S_{or} < S_{or}^*$; see Sections 3 & 9]. Increases in permeability result in either increased water flow under constant head boundary conditions, or increased residence time under constant flux conditions. In either case an accelerated rate of dissolution is the ultimate result. It is our expectation that the distribution of organic liquid, after having undergone significant dissolution, will be much different than the distribution of an organic phase subjected only to hydraulic forces. Hence, it is hypothesized that two systems, each having the same fluid saturations, will not have the same fluid permeabilities due to different distributions of the fluids — because in each case the saturations are achieved by a different process. Accurate measures of relative permeabilities at reduced residual saturations may be as important as good estimates of the mass transfer coefficients for predicting pollutant migration.

- **Continue experiments and theoretical modeling of residual saturations caused by heterogeneities.** The effects of heterogeneities on multi-phase flow were explored in Section 9. In effect, heterogeneities dramatically increase the residual saturation of organic liquids and the accessibility of that saturation to the passing groundwater. Further laboratory and theoretical research is needed on this issue. We suggest additional micromodel studies, with quantitative measurements of the effluents and the saturations (using image analysis), on a wide variety of heterogeneities. Sandbox experiments can then be conducted on those heterogeneities identified by the micromodel studies as most important. We also suggest that the simple mathematical model presented be extended. Other mathematical models should be developed using simulation (eg. like that in Ababou *et al.*, 1988) or spectral approaches (like that in Yeh *et al.*, 1985a,b,c; Mantoglou and Gelhar, 1987; or Welty and Gelhar, 1989). Finally, field experiments on organic liquid movement should pay special attention to this issue.

- **Investigate the influence of surface wetting on multi-phase flow behavior and the movement and capillary trapping of organic liquids.** We usually assume that soils are water wet or hydrophillic. However, wetting can be altered by physical, chemical or biological means (Anderson, 1986a; Wilson, 1988). It appears likely to us that some of the compounds present in organic waste solutions, or even in gasoline, can alter wettability. Schiegg (1980) observed such changes in his laboratory study, and we saw some in ours (although not under controlled conditions). The major chemical mechanism is adsorption, particularly of polar oxygen-, nitrogen-, or sulfur-containing compounds (Anderson, 1986a; Morrow et al, 1986). In the laboratory organochlorosilane compounds are typically adsorbed onto sandstone cores, glass beads, and etched-glass micromodels to alter wettability in fluid flow experiments (Anderson, 1986a, 1988). The organosilane reacts with the silica surface leaving its organic portion exposed, thus presenting a hydrophobic surface to the pore space. Chemical modification of clays and other soils has recently been investigated, with a focus on sorption behavior by hydrophobic surfaces in aqueous media (Boyd *et al.*, 1987; Bouchard *et al.*, 1987; Mortland *et al.*, 1986). Although these changes were made to alter sorption behavior it is reasonable to hypothesize that the altered wettability will effect the behavior of fluids. Surfactants can also change wettability. In addition to influencing the behavior of fluids, wetting disturbs chemical partitioning between phases, and the diffusion/dispersion of chemicals within each fluid phase. In short, the entire transport system is influenced by wettability. **We suggest the following research issues (Wilson, 1988):**

  - ○ Can soil wetting be altered in the natural environment and under antropogenic stress? If so, how? Does wetting alteration require aging?
  - ○ Is wetting actually altered to any significant extent in the environment, or is this simply an academic problem?
  - ○ Where is wetting altered? What is the spatial pattern and heterogeneity? What does heterogeneous wetting look like through an SEM?
  - ○ Does wetting recover? If so, how? How long does it take?
  - ○ What are the effects and consequences of a change in wetting? In particular how does it influence fluid flow and chemical transport including sorption? How does it affect colloid transport? How does it affect bacterial growth and migration? How does bacterial growth affect wetting?
  - ○ Can the consequences be mitigated? If so, how?

- **Study the effects of large Bond numbers on residual saturations in the saturated zone.** When dense organic liquids move downward through the saturated zone gravity forces may play a significant role in reducing the initial amount of capillary trapping, particularly in coarse grained soils. Experiments should be conducted to explore whether this issue is important and to determine the effect it has on residual saturations, and blob size and shape distributions.

- **Determine the conditions required for the onset of fingering as dense organics move downward through the saturated zone.** Many halogenated solvents are more dense and less viscous than water — attributes which promote flow instabilities (gravity fingering) as an organic phase percolates downward through an aquifer. Of special interest in this problem are the roles of capillarity and heterogeneity. In the case of a non-wetting phase displacing a wetting phase, capillary forces appear to promote fingering, while layering in the soil transverse to flow appears to promote stability. Further micromodel, sandbox, and mathematical models of these issues are needed.

- **Employ micromodels to observe colloid transport in a pore network.** In particular, observe attachment-detachment of colloid particles to pore walls as a function of pore size distribution, pore network pattern, wetting, colloid size and charge. Colloids could be made observable through optical microscopes by using fluorescent microspheres to represent them.

- **Employ micromodels to observe bacterial transport and colonization.** Micromodels with fluorescent bacteria could be used to study bacterial motility, attachment, detachment, and colonization (see, eg, Bitton and Marsell, 1979; Marsell, 1985; Pringle and Fletcher, 1983; Van Loosdrecht et al., 1987a,b).

Vadose Zone Research

- **Study the movement and ultimate distribution of non-spreading organic liquids; compare to spreading organic liquids.** In three-phase (air/organic/water) systems in which the organic liquid is of intermediate wettability, some organics spread between the water and air phases while others, such as halogenated solvents, do not. The propensity of a given organic liquid to spread can be predicted from the spreading coefficient, $\Sigma = \sigma_{aw} - (\sigma_{ow} + \sigma_{ao})$. In Section 10 we presented some photomicrographs from a micromodel study which indicate that the spreading coefficient can have a profound influence on how the organic phase moves and where (especially on a pore scale) it ends up. This can be particularly important to remediation via soil venting. We suggest additional quantitative and visualization experiments.

- **Investigate the behavior of organic liquids in the transition zone between the vadose and saturated zones. Determine the equilibrium saturation.** Particularly for organic liquids lighter than water, the low suction range in and just above the capillary fringe is where all the "action" occurs as light organics reach the water table and begin to migrate laterally to form a lens. Unfortunately, this is where the balance of forces governing movement for the three fluid phases becomes much more complicated (and perhaps the least understood). Later we suggest improvements in our apparatus to permit this experiment to be carried out. Another approach would be to measure saturations in a sandbox model constructed in a fashion that permits the lateral redistribution of the organic phase (eg, Schiegg, 1980). Such experiments are being conducted at a variety of laboratories around the country.

- **Explore the effect of heterogeneities on behavior in the vadose zone.** This is simply an extension of the work recommended above for two phase flow.

- **Determine the conditions required for the onset of gravity fingering as liquid organics move downward through the vadose zone.** All liquid organics are more dense and viscous than the gas phase in the vadose zone. The greater density promotes flow instabilities (gravity fingering) as an organic phase percolates downward toward the water table. Capillarity and heterogeneity play a significant role in this process. There is significant literature on the two phase flow instability issue. There is little on three phase flow instability. Further micromodel, sandbox, and mathematical models of these issues are needed.

- **Employ micromodels to study the movement and behavior of colloids and microorganisms, and the efficacy of soil venting.** The first two items are simply extensions of the work recommended above for two phase flow. The third item addresses the issue of water-gas mass transfer coefficients as a function of pore size, pore distribution, spreading coefficient, and fluid saturations.

General Recommendations for Research

- **Investigate mobilization via surfactant floods.** Surfactant floods can be used in an attempt to mobilize residual organic liquid saturations by reducing interfacial tensions and capillary numbers, or simply by emulsifying the organic liquid. Both of these mechanisms should be explored in micromodel and column experiments for typical combinations of organic liquids, surfactants, and soils.

- **Compare 2- and 3-phase flow in micromodels to results from cellular automata (CA).** Cellular automata has recently been used to mathematically model multiphase fluid flow on a pore scale (D. Rothman, personal communication, 1988; B. Travis and K. Eggert, personal communication, 1989). For example, two phase flow is represented by 'red' and 'blue' particles. The particles interact on a grid using rules that satisfy the conservation laws of mass and momentum. Rothman invented other rules to describe the relative affinity of a red particle for another red particle and similar rules for blue particles, allowing CA models to simulate interfacial tensions. Red or blue properties can also be assigned to the walls, in order to represent wetting and its alteration. We believe that CA can be extended to three fluid phases. By changing the interfacial tension rules it may be possible to accurately describe the movement of a spreading or non-spreading intermediate wetting phase (organic liquid) on a pore scale in the vadose zone.

- **Investigate 'irreducible' wetting phase saturation dependence on history, and non-wetting phase velocity, and determine its relevance to contamination problems.** At residual saturation the wetting phase is continuous and is composed of an interconnected network of films, rings and wedges. The wetting phase liquid can move through its interconnected network, draining the films and rings, and reducing the residual wetting phase saturation. Most models of pore pressure-saturation assume a fixed and known 'irreducible water saturation'. We recommend a study of the effect of the non-wetting phase flow rate on the amount and distribution of the wetting phase residual. We expect that the flow rate must vary over orders of magnitude before the change in residual is significant. Further research is needed to determine this relationship, its importance to fluid flow, and its relevance to conditions encountered in the field.

- **Conduct field experiments to confirm laboratory observations.** In particular, attempt to obtain undisturbed soil samples containing residual organic liquids under both saturated and vadose zone conditions. Using quick freezing techniques (see below), observe the distributions of fluids on a pore scale. Make quantitative measurements of fluid saturations using, for example, distillation. Compare results to laboratory observations.

RECOMMENDED IMPROVEMENTS IN EXPERIMENTAL EQUIPMENT & PROCEDURE

General Issues for Soil Column Experiments

- **Provide better control on soil sample variability.** Most of our experiments were conducted on the Sevilleta sand, which we selected as our standard soil for a variety of reasons (see Section 3). This is an aeolian soil, and we were not always able to re-sample it so as to obtain 'exactly' the same material. We believe that residual non-wetting phase saturations may be more sensitive to this variability than some other soil properties (eg. porosity, permeability). Consequently, great care should be taken in future work to insure that a sufficient stock of material is on hand to complete all experiments. Naturally this material should be properly handled and stored so as to minimize segregation and to avoid undesired clumps and aggregates.

- **Conduct mercury and nitrogen gas porosimetry on the soil samples,** in order to yield estimates of the actual pore size distributions for the soils tested in the various experiments

Residual Saturation Measurements – Short Column Experiments

- **Modify the experimental procedure in order to observe and record capillary numbers, so as to insure low capillary number conditions.** This modification would insure that there is no danger of comparing residual saturations taken under low capillary number conditions, to those taken under conditions that would result in a lower initial residual saturation.

- **Improve the apparatus, or develop a new apparatus, to handle low permeability soils like the Palouse loam.** We were not able to make significant measurements of residual saturation for the Palouse loam because it was difficult to supply sufficient presure to force organic liquid nito the soil. This problem can be circumvented with a high-pressure system, including a high-pressure fluid delivery pump, a column built to withstand high pressures, and a bottom membrane with a very high non-wetting phase entry pressure.

- **Consider the development of a new apparatus capable of controlling pressures in all fluid phases.** Such equipment has been developed by others (eg. Lenhard and Parker, 1987b; A. Demond, personal communication, 1988), but is expensive to construct and operate. To make a large number of measurements additional improvements to this type of experimental equipment is warranted, motivated by both economics and science.

- **Improve the apparatus and procedure to permit observation of conditions in the transition zone between the vadose and saturated zones.** Results from our transition zone experiments gave what we believe to be unreasonably high equilibrium organic liquid saturations, reported in Section 10. During organic liquid drainage, water was unable to re-imbibe into the soil. Under low applied suctions representing the capillary fringe and just above, re-imbibing water would have displaced organic liquid resulting in lower equilibrium organic saturations than the values we measured. The largest change in forces acting on the organic liquid occurs in the capillary fringe, and just above, where the transition from the vadose zone to saturated zone conditions is most pronounced. The apparatus mentioned immediately above would eliminate this problem.

- **Investigate the influence of different column packing procedures on residual saturations.** In particular, compare dry vs. wet packings on a variety of soils, with an emphasis on the nature of packing induced heterogeneities. This type of experiment would also be relevant to the many large scale sandbox experiments currently being planned or conducted. This investigation is different than the typical packing study which does not examine residual saturation.

Residual Organic Liquid Mobilization – Long Column Experiments

- **Develop a long column with a water wet wall for future mobilization experiments.** The organic liquid wet PVC walls of our long column may have influenced the distribution and amount of organic liquid in the column, prior to the water flood. The resulting residual organic liquid saturations may have been biased. We recommend that future mobilization experiments be conducted in a column with water wet walls. We initially designed a glass version of the long column, using a stretched version of the glass short column. Pressure taps in the column were designed so that they could be installed by a glassblower. Concerned that the column would be too fragile, and that we would accidentally break these glass taps off, we switched to the easier to work with PVC. As it turned out, we accidentally broke off some of the PVC taps.

- **Improve the apparatus and procedure so as to handle higher capillary numbers.** We found that the long column apparatus was unable to pump at a sufficient flow rate to achieve significant mobilization for the soil we tested. This problem can be overcome by improving the pump and plumbing to handle higher flow rates and pressures. However, for the soils we examined this would mean Reynolds numbers greater than ten, an unlikely condition in the field. Optionally, the wetting and non-wetting fluids could be selected so that their interfacial tension (IFT) is significantly lower that that of the water and Soltrol used in our experiments.

- **Develop an experimental procedure to examine the effect of organic liquid aqueous solubility on residual saturations, their mobility, and aqueous phase relative permeability.** Suppose a multi-component organic liquid is at residual non-wetting phase saturation. Let each of the components have a significantly different solubility in the aqueous phase. Then assume that the more soluble component completely partitions to the aqueous phase, before there is any significant partitioning of the remaining components. For example, consider a two component organic liquid composed of a mixture of isopropyl alcohol and Soltrol. Then the production of alcohol at the end of the column is a measure of the solubilization of the alcohol, and can be correlated to the reduction of residual saturation of the mixture. As the residual saturation is reduced, the isolated blobs of capillary trapped residual become smaller, and some of the residual is mobilized. Part of this mobilized volume may coalesce down the column, while some may make it to the end of the column where it is observed. The aqueous phase relative permeability is measured before and after the solubilization. A three component mixture would provide a third point of data, or perhaps the two component experiment can be rerun with different proportions of alcohol and Soltrol to provide a much wide range of data.

In situ Visualization of Residual Saturation – Pore and Blob Casts

- **Develop pore casts of the pore space.** This will allow us to see into the actual pore space in which the fluids move. Pore casts have been made for sandstones and carbonates by injecting Wood's metal, epoxy, or styrene. In these rocks the matrix is interconnected and can be removed with acid. The mineral grains of unconsolidated soils are not interconnected. Only the exposed grains can be removed. A three-dimensional serial reconstruction of the pore space can be made by sequentially sectioning the sample, using acid to remove new grains as they appear.

- **Develop a new short column with water wet walls for pore and blob casts.** As described in Section 7 we experienced some preferential flow of the styrene along the walls of the TFE column used in these experiments. It is not clear to what degree this influenced the visualization results. As the use of TFE for the column offered only minor advantages over other choices, we recommend that water wet materials be employed in the future, for those experiments using water as the wetting phase. TFE columns can still be employed when styrene is considered the wetting phase.

- **Investigate other monomers, initiators, and techniques for the saturated zone pore & blob casts.** We experienced several problems with styrene as the monomer for these experiments. Once the inhibitor was removed its viscosity began to increase. This lead to an acceleration of the experimental time table, with the result that the pore and blob casts may be biased. The styrene also shrank upon polymerization. We suggest that additional efforts be made to find fluids that can be hardened, but that have fewer problems than the styrene.

- **Reduce blob cast breakage.** We were unable to perform a size and shape analysis on the produced blob casts, partly because of breakage. We need to explore new materials and handling procedures that will reduce the incidence of breakage.

- **Investigate other monomers, initiators, epoxies, and techniques for the vadose zone pore casts.** We experienced several problems with fluids used in these experiments. Principally this involved the changing viscosities of the fluids, which did not appear to have always drained to equilibrium. This was especially a problem with the epoxy representing the intermediate wetting phase. We also had air bubbles entrained in the epoxy. These problems affected fluid distributions and interfaces in the pore casts. Additional efforts could be directed toward finding a better combination of porous media, fluids, and dyes to minimize these problems.

- **Investigate freezing fluids in place with liquid nitrogen.** Soils containing several fluid phases can be quick frozen with liquid nitrogen, and viewed under a scanning electron or optical microscope equipped with a cryogenic stage. An example of this approach is shown in Gvirtzman et al (1987), for the case of frozen water and air in a spoonful of soil. Jamine Wan of our group performed some preliminary experiments with a cryogenic on an optical microscope, using Traverse City soil, undyed Soltrol and water. She found that keeping the sample frozen is not very useful for samples containing two liquids. Instead, by slowly bringing up the temperature until the Soltrol begins to melt, the distribution of fluids is briefly visible and can be photographed. This technique holds promise for the visualization of fluid phase distributions in laboratory and field collected samples. In the lab it avoids the artificial nature of styrene and epoxy simulations of the various fluids, especially their increasing viscosity with time.

- **Improve thin sectioning of pore casts.** We found it difficult to make thin sections of the pore casts, whether done in local facilities or contracted out. The combination of an unconsolidated soil and an infill of various plastics made it difficult to cut and polish the sections without plucking or cracking the mineral grains. Improvements in this technology would certainly aid in the production of better photomicrographs.

Visualization of Multi-phase Flow in Micromodels

- **Improve the micromodel equipment and procedure to allow quantitative measurements.** Improved end reservoirs, incorporating oil- or water-wet etched channel porous membranes provide a mechanism for controlling capillary end effects. Pressures can be controlled and measured through these reservoirs. Etched pore cross-sections can be estimated using measurescopes, epoxy casts, and other techniques. Saturations can be estimated using a high resolution video camera, a frame grabber and image processing techniques. These quantitative techniques could be combined with mathematical models at the pore and network level (eg. Soll and Celia, 1988) in order to help explain the observations and to validate the models.

SECTION 4

CHARACTERIZING EXPERIMENTAL FLUIDS AND SOILS

In this section, characterization of the fluids and soils commonly used in several of the experiments is presented. Predictably, the section is divided into two main parts — fluids, and soils. Within each part, the methods used for characterization will be described, followed by the characterization results themselves.

FLUID CHARACTERIZATION

Measurements of fluid properties such as viscosity, specific gravity, surface tension, and interfacial tension were performed following procedures outlined by the American Society for Testing and Materials (ASTM, 1986). Viscosity was measured with Cannon-Fenske routine viscometers according to ASTM methods D445-83 and D446-85a. Specific gravity measurements were made as described by ASTM method D1429-76 (pycnometer procedure). An adaptation of ASTM procedures D 1590-60 and D 971-82 were used to determine surface tension and aqueous-organic interfacial tensions, respectively, with a Fisher Manual Model 20 tensiometer.

The surface tension procedure (D 1590-60) was slightly modified so that no centrifuging of the samples was done. In Section 7 of the ASTM procedures, the method of glassware cleaning was modified to follow the cleaning method of the interfacial tension procedure (D 971-82). The 100 ml beakers were first rinsed with petroleum ether, followed by two rinses of methyl ethyl ketone (2-butanone) and distilled water. A hot chromic acid solution was then used to remove any remaining contaminants. Five rinses of distilled water followed by three rinses of distilled-deionized water completed the procedure. The beakers were oven dried and allowed to cool to room temperature before use. In Section 9, the procedure for cleaning the platinum-iridium ring was also modified to follow the interfacial tension method. The ring was soaked in petroleum ether and methyl ethyl ketone after which it was flamed in a bunsen burner. The ring was allowed to cool 3 minutes between flaming and use.

Measured fluid properties

The measured properties of all fluids used in our laboratory experiments (except for styrene and the epoxies used in the blob and pore cast experiments) are shown in Table 4-1.

A 3000 ppm $CaCl_2$ solution was used as the aqueous phase in all column experiments. Distilled, de-ionized water was de-gassed by boiling. Enough calcium chloride dihydrate was added to the cooled water to bring the concentration to 3000 ppm. The solution was stored under a vacuum to keep it de-gassed. The properties of this aqueous phase are given in Table 4-1. The interfacial tensions of all the organic liquids were measured against this fluid.

liquid	specific gravity	density (g/cm^3)	kinematic viscosity (cst)	dynamic viscosity (cp)	interfacial tension with 0.3% $CaCl_2$ solution (dynes/cm)	surface tension (dynes/cm)
aqueous phase	1.003±0.002	1.000±0.002	0.98±0.01	0.98 ± 0.01	not applicable	72.0 ± 0.4
Soltrol-130	0.755 ± 0.002	0.753 ± 0.002	1.93 + 0.01	1.45 ± 0.01	47.8 ± 1.2	19.1 ± 0.3
kerosene	0.809 ± 0.002	0.807 ± 0.002	2.15 ± 0.01	1.73 ± 0.01	38.6 ± 1.2	26.8 ± 0.4
gasoline	0.733 ± 0.005	0.731 ± 0.005	0.66 ± 0.01	0.48 ± 0.01	22.9 ± 0.3	20.5 ± 0.3
n-decane	0.729 ± 0.002^{21}	0.727 ± 0.002^{21}	1.25±0.01	0.91 ± 0.01	44.5 ± 1.0	24.9 ± 0.3
benzene	0.877^{20}_{4} †	0.877^{20} †	0.745^{20} †	0.652^{20} †	not determined	28.9^{20} †
toluene	0.864±0.002	0.861±0.002	0.685^{20} †	0.590^{20} †	not determined	28.5 ± 0.5
p-xylene	0.858 ± 0.005	0.855 ± 0.005	0.70 ± 0.01	0.60 ± 0.01	35.8 ± 0.8	28.4^{20} †
PCE	1.609 ± 0.005	1.614 ± 0.005	0.54 ± 0.01	0.87 ± 0.01	41.8 ± 0.7	31.7^{20} †
carbon tetrachloride	1.602±0.002	1.599 ± 0.002	0.66 ± 0.01^{21}	1.05 ± 0.01^{21}	32.9 ± 0.8^{21}	28.2 ± 0.3^{21}

† Weast, 1986

TABLE 4-1. Measured properties of fluids used in experiments. All measurements were taken at temperatures between 22°C and 24°C except where noted by superscript, eg. ^{20} refers to 20° C. Values with the † symbol were taken from Weast, 1986.

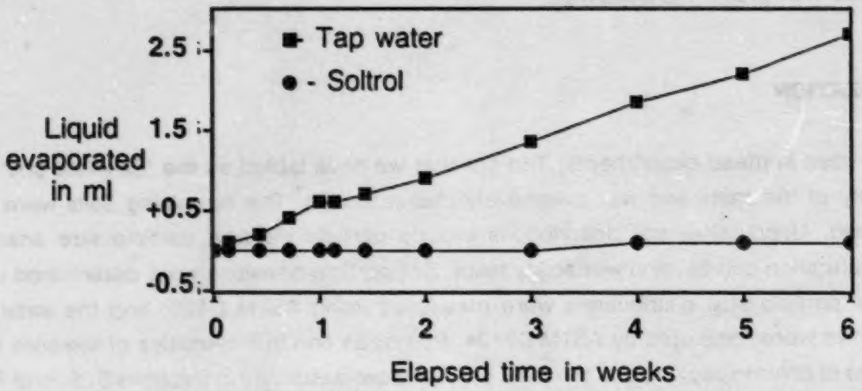

FIGURE 4-1. A simple experiment illustrating the relatively low volatility of Soltrol, compared to water.

Soltrol-130, a mixture of C_{10} to C_{13} isoparaffins produced by Phillips 66 Company, was the fluid most commonly used as the organic phase in our experiments. It is a colorless, combustible liquid having a mild odor, negligible solubility in water, and a relatively low volatility. For example, the simple experiment documented by Figure 4-1 illustrates the low relative volatility of Soltrol to water. Equal amounts of Soltrol and water were placed side by side in identical graduated cylinders and periodically checked visually for liquid loss caused by evaporation. Soltrol's low toxicity, solubility and volatility, coupled with its density contrast with water, made it an ideal organic liquid for our basic experiments. It was used in most short column saturated zone experiments and all micromodel, vadose zone short column, and saturated zone long column experiments. The properties of Soltrol as measured in the laboratory are given Table 4-1.

Residual saturations were measured in short columns for a variety of other organic liquids and compared to the Soltrol results (see Sections 9 & 10). Separate tests were conducted for n-decane, p-xylene, tetrachloroethylene (PCE), gasoline, and kerosene. These liquids were selected to be representative of several classes of organic liquids. Three are single-component liquids: n-decane was chosen to represent straight-chain aliphatics, p-xylene was chosen to represent aromatics, and PCE was chosen to represent halogenated hydrocarbons. Selection of a particular chemical to represent a given class of chemicals was based on the objectives of minimizing solubility and volatility, while maximizing the density contrast with water. Low volatility and solubility were desired to avoid competing physical processes. A large density difference between the organic liquid and water was desired because the soil columns were weighed, exploiting the density difference between the fluids, to measure the fluid saturations. Larger density differences between the fluids led to more accurate measurement of the saturations. Multi-component mixtures were represented by gasoline and kerosene, as well as Soltrol-130. Gasoline was also represented by xylene for the lighter aromatic fraction and decane for the less volatile fraction. The composition of gasoline and kerosene vary with the supplier and the season. One batch of each was purchased locally for the tests. Care should be applied when generalizing our results to other gasoline or kerosene mixtures.

Gasoline components benzene and toluene, and the solvent carbon tetrachloride were characterized, but not tested for residual saturation. The volatility or solubility was too high to permit accurate experiments with present procedures.

SOIL CHARACTERIZATION

Four soils were used in these experiments. The soil that we have labled as the 'Sevilleta soil' was used for the majority of the tests and was extensively characterized. The remaining soils were only partially characterized. Quantitative soil descriptions include particle density, particle size analysis, capillary pressure-saturation curves, and wettability tests. Soil particle densities were determined using ASTM D584-83. Soil particle size distributions were measured using ASTM D422, and the saturated hydraulic conductivities were measured by ASTM D2434. Porosities and bulk densities of the soils were measured at the time of column packing and the methods used are described in Sections 5, 6, and 7, for each experiment. Soil capillary pressure-saturation relationships were determined using equilibrium methods (Vomocil, 1965). Wettabilities of the soils to water and the organic liquid were by the Amott method (Amott, 1959) and the USBM method (Donaldson, 1969). Saturated hydraulic conductivity and intrinsic permeability were determined using the steady flow method. Relative permeability was determined for two of the soils using the unsteady state method of Jones and Roszelle (1978).

Capillary Pressure-Saturation Test

Soil capillary pressure-saturation relationships were determined using equilibrium methods (Vomocil, 1965). Hanging column type equilibrium stepwise water-air, water-organic, and air-organic displacement experiments were performed under both drainage and imbibition conditions to determine the capillary pressure functions. The experiments were performed using prepared soil columns. The effective column length was kept short (5 cm) in order to keep fluid saturations relatively constant along the length of the column, and to optimize column weight for gravitimetric measurements. A longer column would have necessitated the use of a balance with significantly lower accuracy. Standard equilibrium procedures were altered for the water-organic liquid displacement experiments to accommodate conditions involving two liquid phases. Figure 4-2 shows this modified set up. Tubing was used to connect the tops of the burets to seal the system and reduce volatilization. The soil column was prepared as described later in Section 5 for a water saturated column. The soil column was attached to burets containing organic liquid (buret A) and water (buret B). The capillary pressure was increased stepwise. At each step the system was allowed to equilibrate (about 24 hours were required). The capillary pressure head was measured in terms of the wetting fluid, water, as;

$$H_c = \frac{\varrho_o\, h_1 + \varrho_w\, h_2}{\varrho_w} \qquad (4\text{-}1)$$

where: $H_c = -\varrho_w\, g\, P_c$ = capillary pressure head, often called the *suction head*, expressed in cm of wetting phase, in this case H_2O

P_c = capillary pressure = $P_{non\text{-}wet} - P_{wet} = P_o - P_w$ (pascals)

h_1 = height of the organic liquid level in buret A above the center of the column (cm)

h_2 = height of the water level in buret B below the center of the column (cm)

ϱ_o = organic liquid density (g/cm^3)

ϱ_w = aqueous fluid density (g/cm^3)

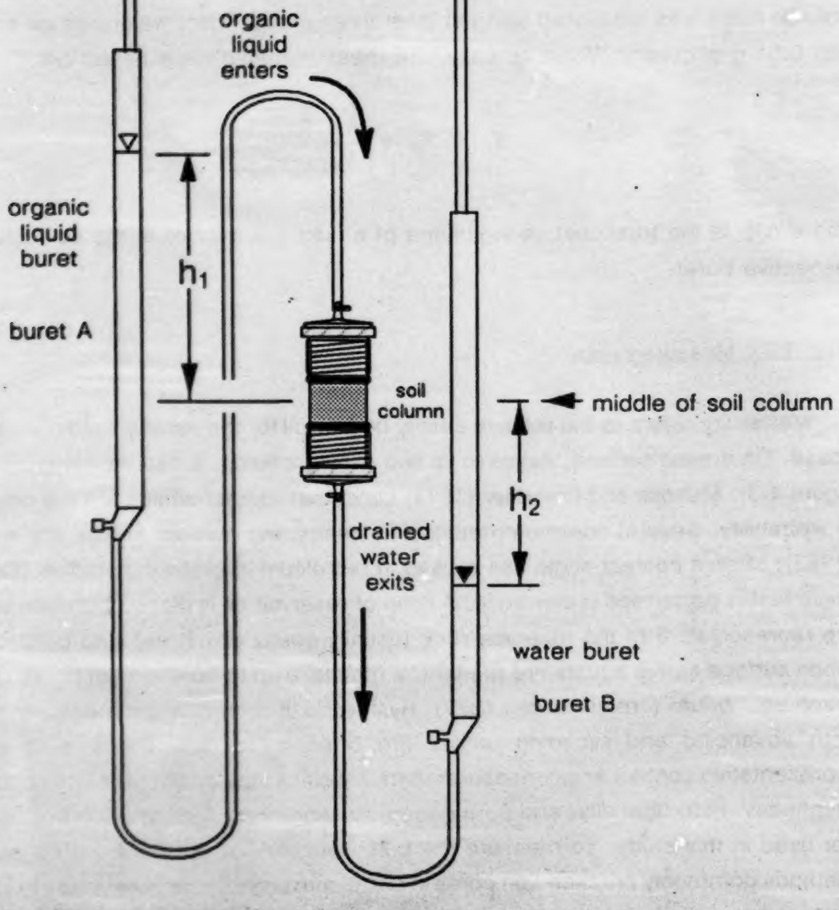
organic liquid enters
organic liquid buret
buret A
h_1
soil column
middle of soil column
h_2
drained water exits
water buret
buret B

FIGURE 4-2. Setup for the organic liquid and water capillary pressure – saturation relationship.

Fluid saturations were measured both gravimetrically (by weighing the column after equilibration had been achieved in each step) and volumetrically (by measuring the volume change of the fluids in each buret). Gravimetrically, saturations were measured as :

$$S_w = S_{wp} + \frac{\Delta M}{\Delta \varrho \ V_p} \tag{4-2}$$

$$S_o = 1 - S_w \tag{4-3}$$

where: S_w = water saturation (–)

S_{wp} = water saturation at previous step (–)

ΔM = change in column mass from the previous step (g)

$\Delta \varrho$ = density difference between the fluids, $\varrho_w - \varrho_o$ (g/cm^3)

V_p = pore volume of the column (cm^3) (Section 5 describes how V_p was measured)

Column mass was measured using at least three independent weighings on a Mettler PE 1600 balance with 0.01 g accuracy. Volumetrically, the measurements were based on:

$$S_i = S_{ip} + \frac{\Delta V_i}{V_p} \tag{4-4}$$

where ΔV_i is the total change in volume of a fluid (i = w or o) in the soil column as measured in the respective buret.

Wettability Measurements

Wettability refers to the relative affinity of the soil for the various fluids — water, air, and the organic phase. On a solid surface, exposed to two different fluids, it can be measured by contact angle (see Figure 4-3). Melrose and Brandner (1974) claim that contact angles are the only unambiguous measure of wettability. Several common methods for measuring contact angles are summarized by Adamson (1982); often a contact angle cell is used in petroleum engineering studies (Craig, 1971). The contact angle test is performed under brine. A drop of reservoir oil is placed between two polished crystals that are representative of the reservoir rock (usually quartz or calcite) and contact angles are measured. When surface active agents are present, it may take up to hundreds of hours of interface aging time to reach equilibrium (Treiber et al., 1972). Hysteresis in contact angle measurements is common, so that both advancing and receding angles are often measured. There is some question as to how representative contact angle measurements are since they do not take into account the effect of surface roughness, heterogeneity, and pore geometry (Anderson, 1986b). Contact angle measurements were not used in this study. To measure the bulk wettability of our soils, we employed adaptations of two methods commonly practiced on cores in petroleum engineering: the Amott test and the USBM method. Both methods rely upon characteristics of organic/water capillary pressure-saturation curves to determine the wettability of the porous media.

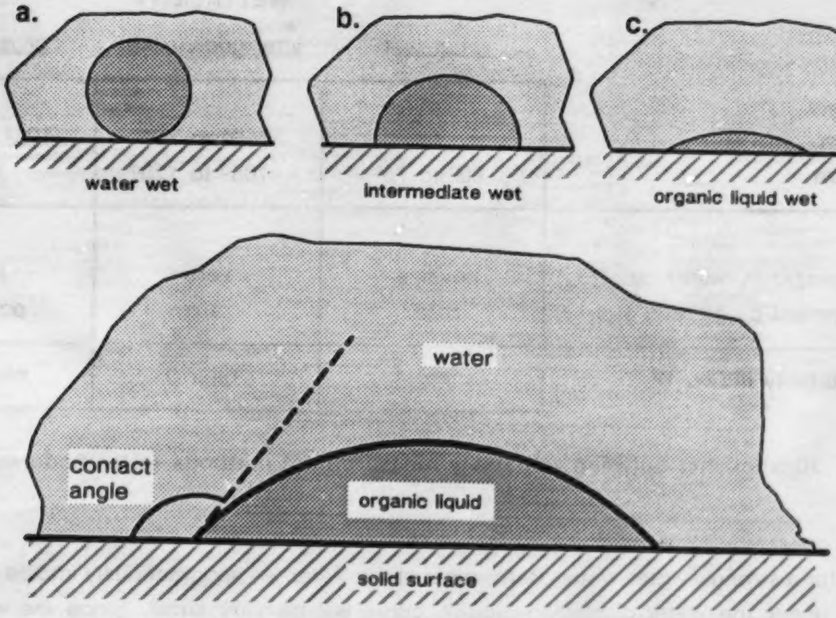

FIGURE 4-3. Contact angle measurement on a clean, smooth solid surface.

The Amott (1959) test measures the wettability of soil as a function of the displacement properties of the soil-water-oil system. Four displacement operations are performed on the soil, and the ratio of spontaneous imbibition to forced displacement is determined for both the water and organic phases. The technique is similar to that required to determine capillary pressure-saturation relationships for two fluid phases. The four displacements are :

1) spontaneous displacement of organic liquid saturated core or column by water.

2) forced displacement of organic liquid saturated core or column by water.

3) spontaneous displacement of water saturated core or column by organic liquid.

4) forced displacement of water saturated core or column by organic liquid.

This test is based on the fact that the wetting fluid will spontaneously imbibe into the core, displacing the non-wetting phase. When the displacement-by-water ratio (δ_w) approaches one and the displacement-by-oil ratio (δ_o) is zero, the core is water-wet. If the opposite is true, the core would be oil-wet. The main problem with the Amott test is its insensitivity at near neutral wettability (Anderson, 1986b).

The USBM test compares the areas under two fluid phase capillary pressure-saturation curves as a measure of average wettability (Donaldson et al., 1969). When a soil is water-wet, the area under the organic-displacing-water capillary pressure curve (A_1) is larger than the water-displacing-organic curve

	WETTABILITY		
	water-wet	intermediate-wet	organic-wet
contact angle			
minimum	0°	60° to 75°	105° to 120°
maximum	60° to 75°	105° to 120°	180°
Amott test			
displacement-by-water ratio (δ_w)	positive	zero	zero
displacement-by-oil ratio (δ_o)	zero	zero	positive
USBM wettability index, *W*	near 1	near 0	near -1

TABLE 4-2. Relationship between wettability measurement methods (after Anderson, 1986b).

(A_2). In fact, for a strongly water-wet system, most of the water will spontaneously imbibe into the soil, and the area under the water-displacing-organic curve will be very small. Since the work of fluid displacement is proportional to the areas under the capillary pressure curve (Morrow, 1970), the USBM wettability index in essence measures the ratio of work needed for organic phase to displace water, to the work needed for the opposite displacement. The USBM wettability index, *W*, is given as:

$$W = \log \frac{A_1}{A_2} \tag{4-5}$$

Table 4-2 shows the wettability criteria for each of the three quantitative methods.

Relative Permeability

Relative permeabilities were measured in long columns (see Section 6). The columns were initially water saturated. Organic liquid was drained into the column, reducing water to its wetting phase residual saturation, S_{wr} . This was followed by a water flood, or imbibition of water, to reduce the organic liquid to its non–wetting phase residual saturation, S_{or} . Fluid outflows and pressure drops across the column were monitored during these two displacement steps. A graphical version of the 'unsteady state method', which is based on the Buckley-Leverett model of immiscible fluid displacement, was used to calculate relative permeability-saturation curves for each fluid (Jones and Roszelle,1978). In the drainage step the water saturation and the relative permeability to water, k_{rw} , began at unity and were reduced as organic liquid displaced water from the column. The solid lines in Figure 4–4 illustrate typical results expected from this first displacement step. As the displacement continued, the water approached residual saturation — at which time the relative permeability of the water approached zero. In the imbibition step, as the water saturation increased, the relative permeability of the water also increased. The saturation and permeability of the organic phase became reduced until the organic phase was discontinuous and immobile within the pore space — i.e. this second displacement step caused the organic phase to be reduced to its residual saturation. The water relative permeability did not fully recover to unity, because of the presence of residual organic liquid. The dashed lines in Figure 4-4 indicate typical results obtained from this displacement step.

Sevilleta Soil

The 'Sevilleta sand' is a well sorted, medium grained, aeolian sand, taken from a sand dune in the Sevilleta Wildlife Refuge, located 15 miles north of Socorro, New Mexico. This sand was chosen for three reasons. First, it is a uniform, homogeneous soil with a fairly high hydraulic conductivity, a very low percentage of fine particles, and a very low organic content. These properties made the Sevilleta sand easy to use during the development of the short and long column experimental techniques. Second, the sand is easy to obtain. The Hydrology program maintains a field site at the location from which the soil is taken. Third, the Sevilleta dune sand has been previously in several hydrologic studies here at Tech (eg., McCord et al. 1988a,b). This permitted a comparison of soil characterization results with those of previous studies.

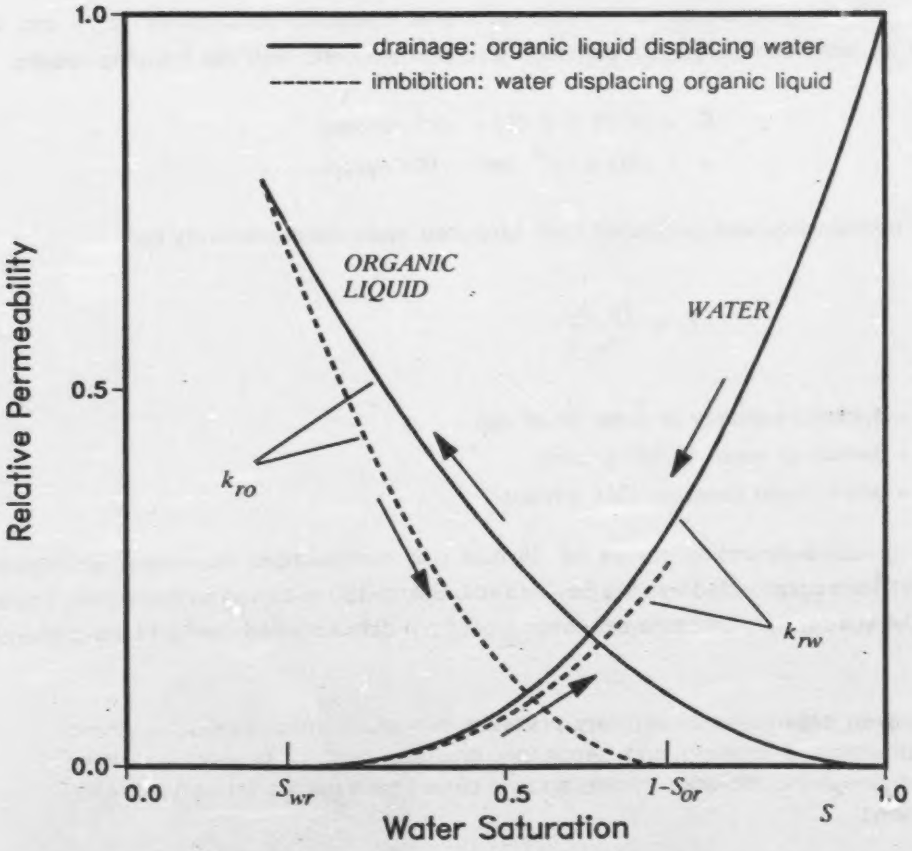

FIGURE 4-4. **Generic representation of relative permeabilities versus saturation for the displacements performed in steps 1 and 2 of the long column experiments.**

The particle density of this sand was determined to be 2.65 ± 0.02 g/cm from five replicate measurements. Six sieve tests were conducted to measure the particle size distribution of the Sevilleta soil. There was excellent agreement between tests with all curves falling essentially on top of one another. The results of one test are presented in Figure 4-5, along with the results for two other tested soils. The particle size distribution classifies the Sevilleta soil as a uniform medium grained sand, with a median particle diameter of about 0.3 mm (300 microns) and a uniformity coefficient (d_{60}/d_{10}) of less than 2.

An SEM photomicrograph of a sample of the sand is shown in Figure 4-6. The grains are sub-angular to sub-rounded. The SEM picture shows a particularly angular grain. (Also note the web of graphite paint that the grains are sitting on; this is an artifact of the SEM procedure.) A mineral characterization of the sand indicates that it is composed mostly of quartz grains (72 ± 5% by number), with lesser amounts of feldspar(11 ± 2%) and lithic fragments (16 ± 3%). The lithics were generally much smaller in size than the other mineral grains; they compose about 5% of the sand by volume. An organic carbon analysis was conducted at North Carolina State University (courtesy of Dr. Cass Miller) and yielded an organic carbon content of 0.02%, an almost negligible amount.

Eleven replicate measurements of water-saturated hydraulic conductivity (K_w) and intrinsic permeability (k) were conducted in a constant head permeameter with the following results:

$$K_w = (1.03 \pm 0.20) \times 10^{-2} \text{ cm/sec}$$
$$k = 1.03 \times 10^{-7} \text{ cm}^2 = 104 \text{ darcys}$$

The intrinsic permeability was calculated from saturated hydraulic conductivity by:

$$k = \frac{K_w \ \mu_w}{\varrho_w \ g} \tag{4-6}$$

where: μ_w = dynamic viscosity of water (0.98 cp)
ϱ_w = density of water (0.997 g/cm^2)
g = gravitational constant (981 cm/sec^2)

Capillary pressure-saturation curves for all fluid pair combinations (air-water, air-organic, and organic-water) were constructed with the Sevilleta soil. Soltrol-130 was used as the organic liquid phase in all trials. The soil capillary pressure-saturation plots from data acquired during 12 experimental trials include:

- **seven organic-water capillary pressure curves**, of which two curves have drainage, imbibition, and secondary drainage cycles, three curves have drainage and imbibition cycles, and two curves have the main drainage branch only;
- **two air-organic capillary pressure curves**, one curve with drainage, imbibition, and secondary drainage cycles, and one curve of the main drainage branch only; and,

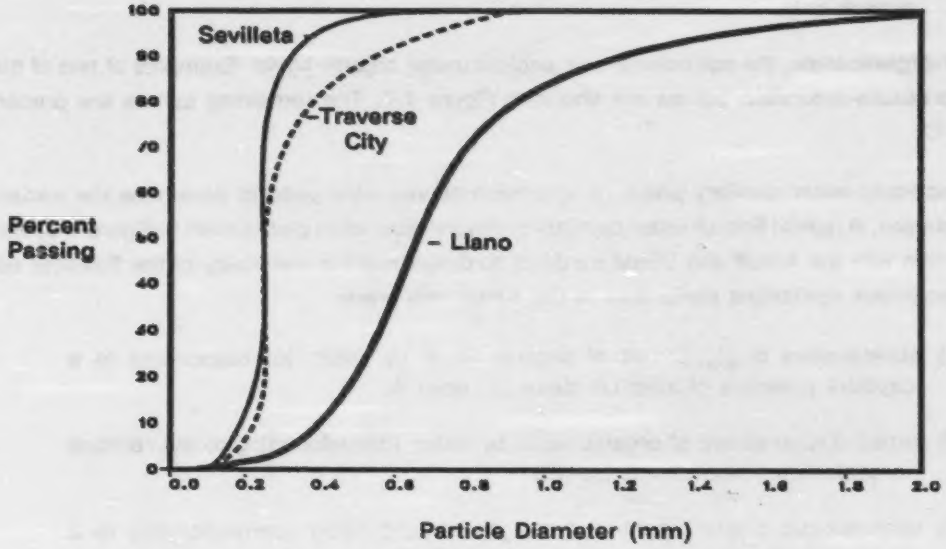

FIGURE 4-5. Particle size analysis for three of the soils used in this study.

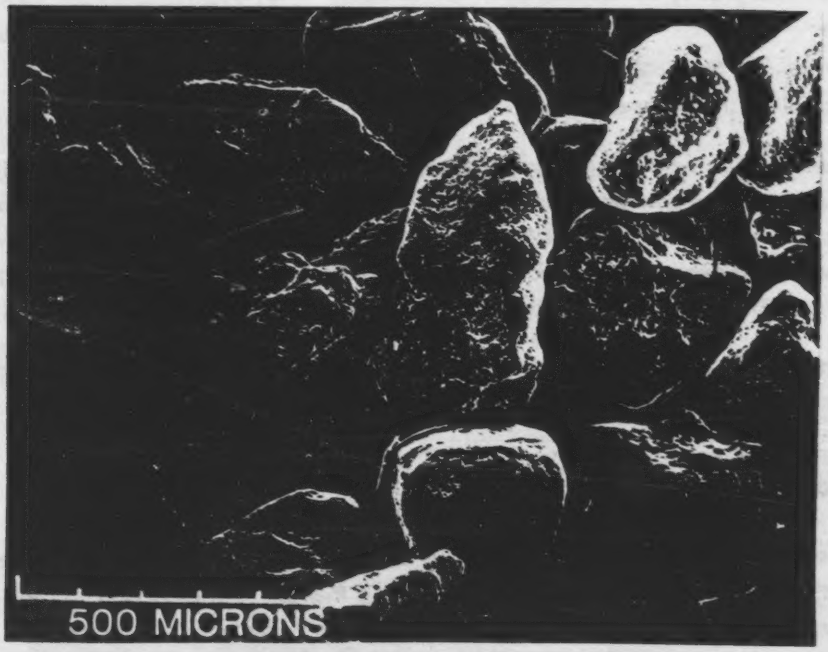

FIGURE 4-6. SEM photomicrographs of Sevilleta sand.

- **three air-water capillary pressure curves,** of which two curves have the main drainage and imbibition cycles, and the third curve has the main drainage branch only.

For the air-organic trials, the soil column was packed under organic liquid. Examples of two of these 12 capillary pressure-saturation curves are shown in Figure 4-7. The remaining curves are presented in Appendix C.

Organic liquid-water capillary pressure-saturation curves were used to determine the wettability of the Sevilleta soil. A typical Soltrol-water capillary pressure-saturation plot (shown in Figure 4-8) was used in conjunction with the Amott and USBM methods to determine the wettability of the Sevilleta soil. The four displacement operations performed in the Amott test were:

1) spontaneous displacement of organic liquid by water (corresponding to a capillary pressure of zero on curve 2); point **A**;

2) forced displacement of organic liquid by water (corresponding to the residual organic liquid saturation); point **B**;

3) spontaneous displacement of water by organic liquid (corresponding to a capillary pressure of zero on curve 3); point **C**; and,

4) forced displacement of water by organic liquid (corresponding to irreducible water saturation or residual wetting phase saturation); point **D**.

Preferentially water-wet soils have displacement ratios, $\delta_w = (S_{wA} - S_{wD})/(S_{wB} - S_{wD})$, approaching 1.0 and displacement-by-organic ratios, $\delta_o = (S_{wB} - S_{wC})/(S_{wB} - S_{wD})$, of zero. Organic liquid-wet soils give reverse results. The Sevilleta soil is strongly water-wet, not only to Soltrol, for which $\delta_w = 0.98$ and $\delta_o = 0.0$, but for all of the other organic liquids utilized as well.

The USBM test compares the areas under capillary pressure curves as a measure of wettability. When a soil is water-wet, the area under the organic-displacing-water capillary pressure curve (shaded) is larger than the area under the water-displacing-organic curve (black). In a strongly water-wet system, most of the water spontaneously imbibes into the soil, and the area under the water-displacing-organic curve is very small. This is the case for Soltrol in the Sevilleta soil, as shown in Figure 4-8.

Sevilleta sand relative permeability under drainage was measured during the long column test. The results, shown in Figure 4-9, are not considered reliable.

Traverse City Soil

The Traverse City soil sample was supplied to us by EPA's Kerr lab from their biodegradation field demonstration site in Traverse City, Michigan. The site is located at a U.S. Coast Guard Air Station Superfund fuel spill. The soil is a clean, beach sand, composed primarily of sub-rounded to rounded quartz grains, with some dolomite and igneous and metamorphic particles (Twenter, 1985). It has a particle density of 2.65 ± 0.01 g/cm^3 and a saturated hydraulic conductivity of 1.0×10^{-2} cm/s. An organic carbon analysis conducted on soil samples from a nearby well indicated the soil had an organic

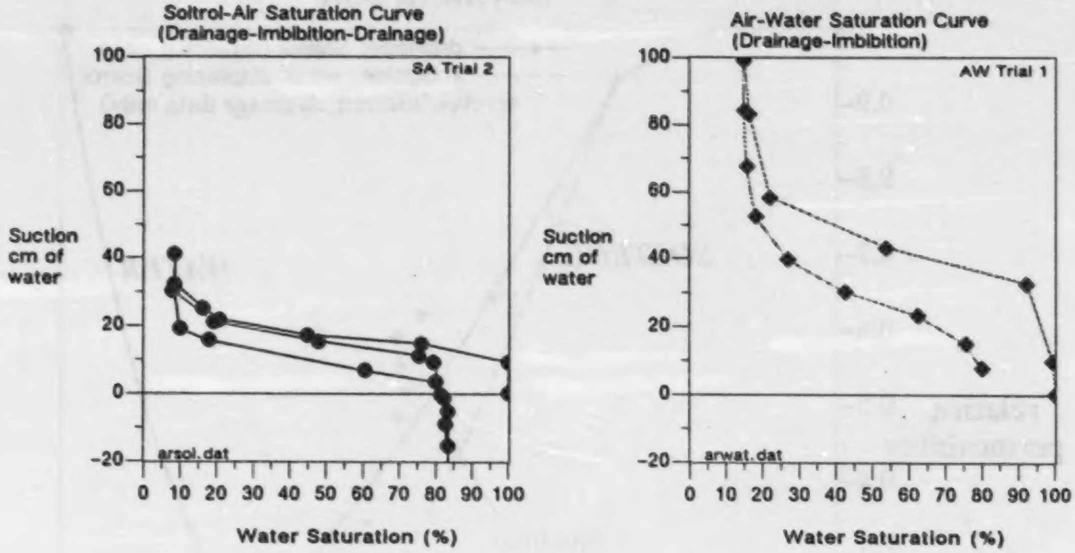

FIGURE 4-7. **Typical Sevilleta sand capillary pressure-saturation curves.**

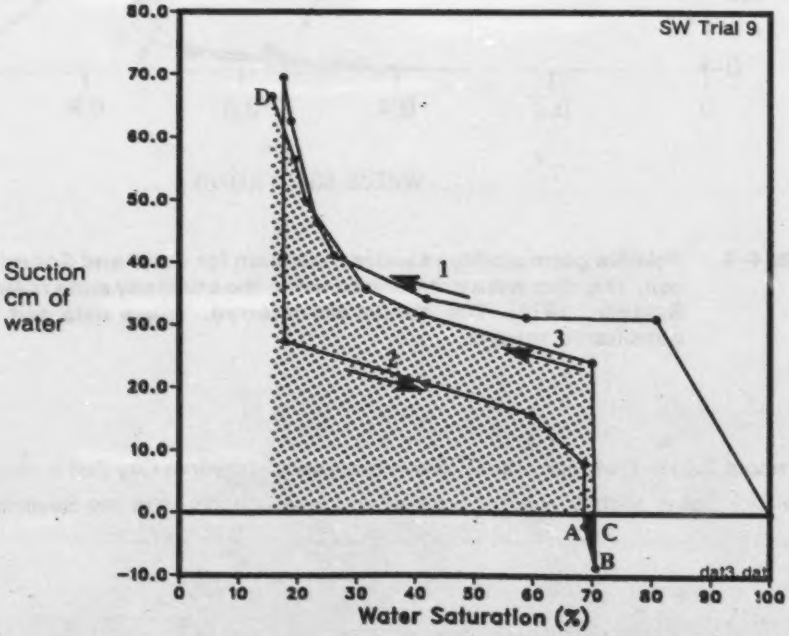

FIGURE 4-8. **A typical organic liquid-water capillary pressure-saturation curve used to determine wettability, in this case for Soltrol-130 in Sevilleta sand.**

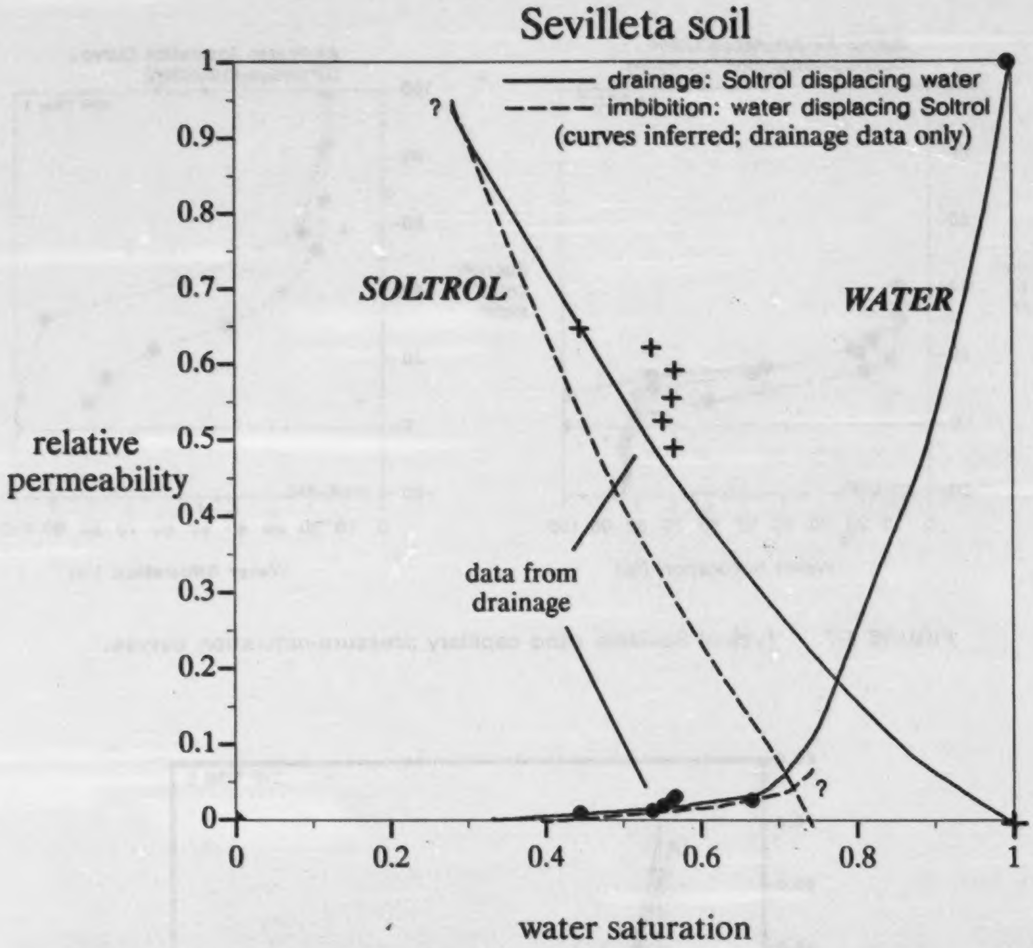

FIGURE 4-9. Relative permeability vs water saturation for water and Soltrol in the Sevill soil. The data were determined using the unsteady state method (Jones Roszelle, 1978). The curves are inferred. These data and curves are considered reliable.

carbon content of about 0.01% (Twenter, 1985). Sieve analysis of Traverse City Soil is plotted in Figure 4-5. The Traverse City Soil is slightly coarser grained and less uniform than the Sevilleta Sand.

Llano Soil

The Llano soil sample was obtained from the escarpment of the Llano de Albuquerque, remnants of a fluvial plain deposited and then eroded by the Rio Grande and the Rio Puerco, west of Belen, New Mexico. The soil sample is a clean, coarse, fluvial sand. It has a particle density of 2.66 ± 0.01 g/cm^3, and a saturated hydraulic conductivity of 1.6×10^{-1} cm/s. Sieve analysis of the Llano soil is plotted in

Figure 4-5. The sample is more coarse grained and much less uniform than either the Sevilleta or Traverse City soils. Relative permeability, as measured and inferred during our long column test (see Section 6) is shown in Figure 4-10.

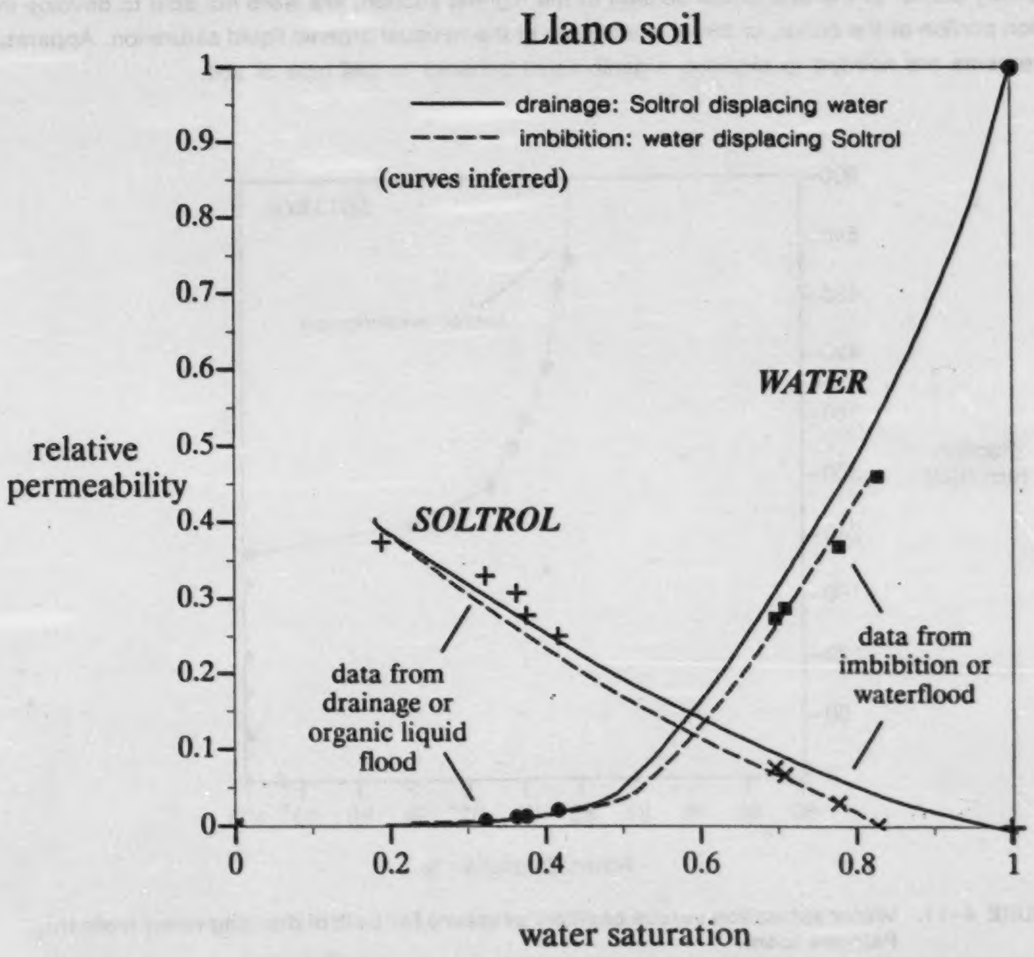

FIGURE 4-10. Relative permeability vs water saturation for water and Soltrol in the Llano soil. The data were determined using the unsteady state method (Jones and Roszelle, 1978). The curves are inferred.

Palouse Loam

The Palouse loam soil is an agricultural soil from eastern Washington. It provides a good contrast to the Sevilleta, Traverse City and Llano soils because of its much finer texture (15% sand, 80% silt, 5% clay) and its higher organic carbon content, 1.5% (R. Bowman, personal communication). The water-saturated hydraulic conductivity of the soil was measured to be 5×10^{-6} cm/s using a falling head test, and the particle density was measured to be 2.67 ± 0.02 g/cm^3.

Figure 4-11 is a capillary pressure-saturation curve for the Palouse loam, constructed for a water saturated being drained by Soltrol. The Soltrol did not readily drain the loam over the range of suctions available in our laboratory using the short glass columns and applied vacuums. The maximum Soltrol saturation reached was 11.7%, with an corresponding water saturation of 88.3%. Soltrol broke through the capillary barrier at the end of the column at the highest suction. We were not able to develop the imbibition portion of the curve, or the final estimate of the residual organic liquid saturation. Apparatus improvements are needed to examine organic liquid behavior in this type of soil.

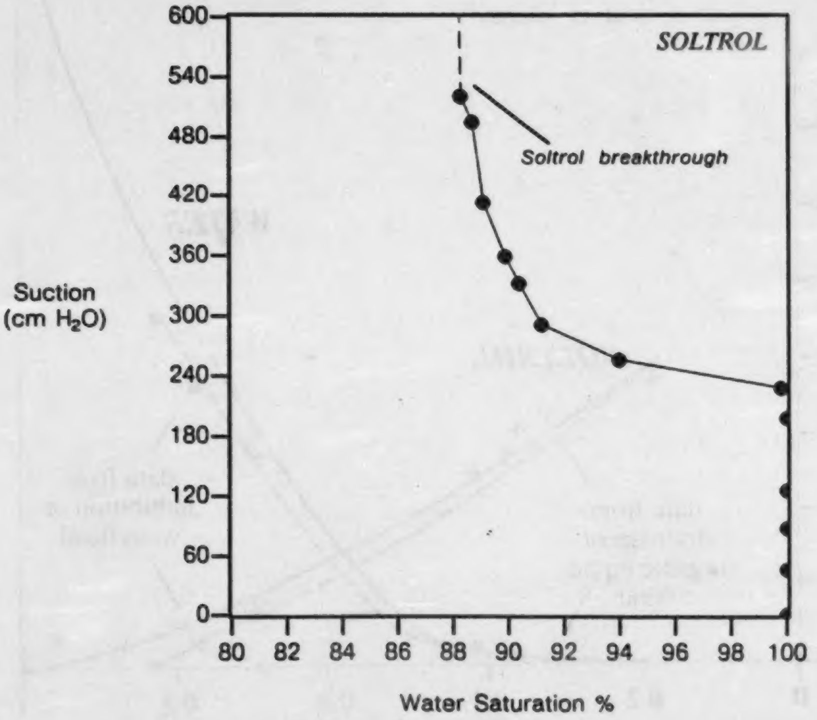

FIGURE 4-11. Water saturation versus capillary pressure for Soltrol draining water from the Palouse loam.

SECTION 5

SHORT COLUMN EXPERIMENTAL METHODS

Bench top short column experiments were performed to measure the residual organic liquid saturations of soils under either vadose zone or saturated zone conditions, providing a direct means to compare the amount of organic liquid trapped in the vadose zone to the amount trapped in the saturated zone. The Sevilleta soil was used in most of these experiments. It is a uniform, medium-sized, quartz sand. Soltrol-130, a mixture of C_{10} to C_{13} isoparaffins with negligible solubility in water, served as the organic phase. The aqueous fluid used in the experiments was water with 3000 ppm calcium chloride added to prevent dispersion of clays.

In other saturated-zone experiments kerosene, regular leaded gasoline, n-decane, p-xylene, and tetrachloroethylene were used to directly compare the differences in residual saturations to different classes of organic pollutants. Residual saturations were also measured for several soils under saturated-zone conditions and these results were compared to the Sevilleta results and the published results of petroleum reservoir engineers.

A short glass chromatographic column with threaded Teflon™ tetrafluoroethylene (TFE) endcaps was used to contain the soil sample. The glass column had an inside diameter of 5 cm and an effective internal length of about 5 cm. The column was kept short so that — especially in the vadose zone case — saturations remained fairly constant over the length of the column. The short column also maximized the accuracy of the gravitimetric measurements of saturation, since the greater weight of a longer column would have required the use of a greater capacity but less accurate balance. Finally, the short column allowed for easy packing with soil, and minimized deairing times. Water or oil wet membranes were used on the lower endcap to minimize capillary end effects. A paper filter placed on the upper endcap prevented clay-sized particles from leaving the column. Over the course of an experiment, the change in column mass was used, in conjunction with the known density difference between the fluids, to measure saturations. Soils and liquids were exposed only to glass, Teflon, and chemically resistant tubing during the experiments.

In the saturated zone experiments, organic liquid was introduced into an initially water-saturated soil sample until the so-called irreducible water saturation was reached. Water was then re-introduced into the soil displacing most of the organic liquid, but leaving behind some discontinuous blobs of organic liquid trapped by capillary forces. The fraction of the pore space occupied by these trapped blobs is the residual saturation. The experiment represents a scenario in which organic liquid percolates into the saturated zone and is, in turn, displaced by ambient groundwater flow, leaving behind a residual organic liquid saturation.

In the vadose zone experiments, an initially water-saturated soil sample was drained with air under an applied suction until an equilibrium was reached. The drained soil represented vadose zone conditions in which the pore space is occupied by both air and water. As organic liquid was introduced (simulating a spill or leak), it displaced air and water as it percolated through the soil. Organic liquid was then drained from the soil under an applied suction, simulating the downward movement of organic liquid as it passes through the vadose zone toward the water table. Again, capillarity caused some organic liquid to become trapped in the pore space.

In this section, we begin by describing the fluids and soils used in these experiments and the rationale for our choices. (A detailed characterization of the fluids and soils used in the experiments is presented in Section 4.) We then describe the short column apparatus, followed by detailed procedures of how the apparatus was used to measure fluid saturations under two-phase (saturated zone) and three-phase (vadose zone) conditions. We conclude the section by discussing the limitations of the apparatus and possible errors that may occur when running these experiments.

FLUIDS AND SOILS (see Section 4)

The aqueous fluid used in all experiments was distilled, de-ionized, de-aired water with 3000 ppm $CaCl_2$ added to prevent dispersion of clays. Saturated zone residual organic liquid saturations were determined for six organic liquids; three of the liquids were mixtures (regular leaded gasoline, kerosene, and Soltrol-130), and three were single-component liquids (n-decane, p-xylene, and tetrachloroethylene). Soltrol-130 was also used to develop the experimental procedure and to perform the vadose zone short column experiments. The other organic liquids selected for use in the experiments were chosen to be representative of several classes of organic liquid pollutants often present at landfills, hazardous waste sites, and accidental spills.

Sevilleta sand was used to refine the test apparatus and procedure. To hold all variables but the independent variable of interest constant, this soil was also used in all experiments comparing residual saturations in the saturated zone to those in the vadose zone, and for all comparisons of residual saturations between organic liquids. The Traverse City soil and Palouse loam were used in several trials of the short column saturated zone experiment. The Llano soil was used in the long column (see Section 6).

EXPERIMENTAL APPARATUS

Each apparatus used in the short column experiments consisted of a short glass chromatographic column with tetrafluoroethylene (TFE) endcaps (Figure 5-1), and associated plumbing. The glass column and TFE endcaps were manufactured by Ace Glass, Inc. The glass column was specially fabricated to our specifications: 5 cm inside diameter and 5 cm effective internal length between TFE endcaps. The effective column length was kept short in order to keep fluid saturations relatively constant along the length of the column. The endcaps were screwed into threaded ends on the glass column and sealed against the column with o-rings.

A 5 mm thick fritted-glass disk with a 20 micron average pore diameter was placed into the taper of the bottom endcap as a filter support. A water-wet Magna 66 nylon filter with a 0.22 micron pore diameter, designed to allow water, but prevent organic liquid from leaving the column, was glued along

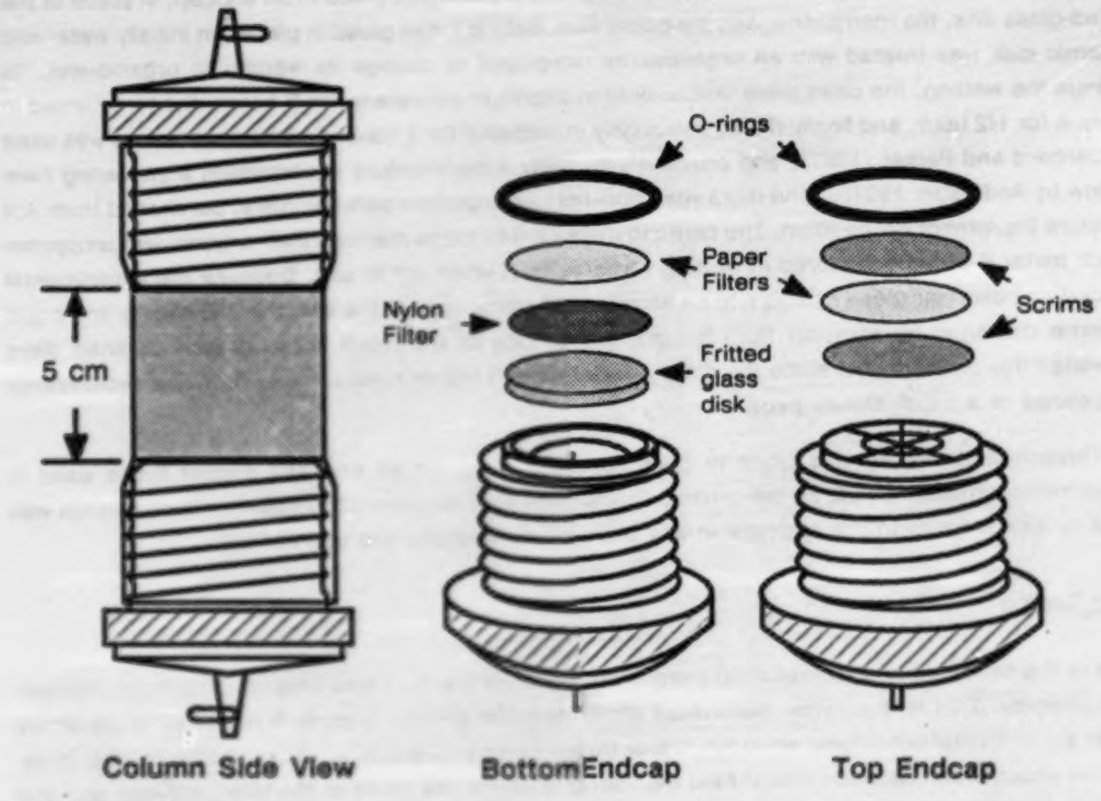

FIGURE 5-1. The short column apparatus, vith blow-up views of the endcaps and filters.

the edges to the fritted-glass disk. A paper filter waslaced over the nylon filter to protect the nylon from abrasion by the soil.

A network of small channels, approximately 1 mm deep and 1.5 mm wide, were machined into the surface of the top endcap, in a pattern similar to tht shown in Figure 5-1. The grooves allowed for a more uniform flow of fluids between the endcap andhe soil. A paper filter was sandwiched in between two polypropylene scrims and glued to the endcap. he paper filter kept fine soil particles from leaving the column. The outer scrim kept the paper filter fom tearing when the endcap was screwed down against the soil. The inner scrim decreased cloggingby preventing the paper filter from sagging back into the grooves.

In vadose zone experiments, endcaps with organi-wet filters were used as part of the experimental procedure (as described later in this section unor '*vadose zone experiments*'). Endcaps with organic-wet membranes, which allow organic liqui to pass through but not water or air, were constructed in one of two ways. By the first methd, the endcaps were constructed identically to water-wet endcaps, but an organic-wet TFE filter waslued in place instead of a water-wet nylon filter. The TFE filters, purchased from Gelman Sciences, hadn average pore diameter of 0.5 microns. By the second method, an organic-wet ceramic disk was simply glued into place in an endcap, in place of the fritted-glass disk, the membrane, and the paper filter. Before it was glued in place, an initially water-wet ceramic disk was treated with an organosilane compound to change its wetting to organic-wet. To change the wetting, the disks were first soaked in chlorotrimethylsilane for 2 hours, then immersed in toluene for 1/2 hour, and finally rinsed thoroughly in methanol for 1 hour. A similar procedure was used by Lenhard and Parker (1987), and previously by many experimenters in petroleum engineering (see review by Anderson, 1987a). The disks were one-half bar, high-flow ceramic disks, purchased from Soil Moisture Equipment Corporation. The ceramic disks were found to maintain their organic-wet properties much better if they were stored in wetting (organic) fluid when not in use. Because the experimental procedure called for these endcaps to be screwed into place against the soil, the TFE membrane could become damaged by abrasion from the soil grains. Use of the much more rugged ceramic disks alleviated this problem, but since the disks offered a much higher resistance to flow, the experiments proceeded at a much slower pace.

Devcon 2-ton epoxy was used to glue filters and disks on all endcaps except those used in experiments employing PCE as the organic liquid. Since PCE dissolved the epoxy, silicon sealant was used to attach filters to the endcaps in any experiments involving the use of PCE.

Filter Testing

For the saturated and vadose zone experiments to run properly, it was essential that filters maintain their integrity. That is, the nylon filters must allow only water and not organic liquid or air to penetrate under experimental conditions; while the TFE or treated ceramic filters must allow organic liquid to pass, but not water or air. Capillary forces held the wetting phase in the pores of the filter, allowing only that wetting phase to pass through. Non-wetting fluids could not pass through the filter, as long as the non-wetting phase entry pressure of the filter was not exceeded.

An air-entry test was used as a simple means to test the integrity of a filter and its glued seal to the endcap. The wetting fluid (water or organic liquid) was pulled through the filter and endcap under suction using a vacuum pump (see step 1 in Figure 5-2), until the filter and any void space in the end reservoir behind the filter was completely saturated. The suction on the vacuum pump was set to a performance standard and run for a couple of minutes at that level. The endcap was removed from the wetting fluid with the vacuum suction continuing (see step 2 in Figure 5-2). If air breached the filter (seen as air bubbles in the tubing leading out of the endcap within 1 to 2 minutes), then the filter failed the air-entry test and was not used. Filters which allowed no air to penetrate them passed the air-entry test and were used in experiments.

The performance standards were set with a margin of safety so that filters could be assured of maintaining integrity under experimental conditions for any combination of wetting and non-wetting fluids (water-air, organic liquid-air, water-organic liquid). For example, about 60 cm of water suction was needed to bring the Sevilleta sand close to irreducible water saturation. This suction was doubled to 120 cm (9 mm Hg) to ensure a margin of safety. To account for the fact that air was not always the non-wetting phase, the integrity test standard was corrected by the ratio of interfacial tensions. For Soltrol this correction was:

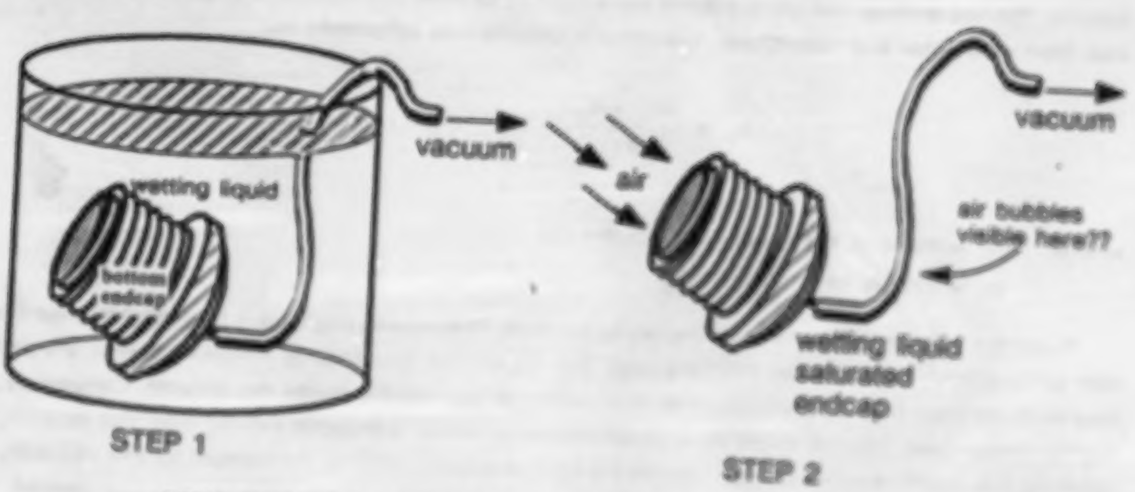

FIGURE 5-2. Air entry test for bottom end cap filter and seal.

$$120\ cm\ H_2O\ (water/soltrol) \times \frac{\sigma_{wa}}{\sigma_{ws}} = 185\ cm\ H_2O\ (water/air) = 14\ cm\ Hg \qquad (5\text{-}1)$$

where: σ_{wa} = 73.6 dyne/cm = water/air interfacial tension = water surface tension
σ_{ws} = 47.8 dyne/cm = water/Soltrol interfacial tension

The performance standard for this particular air-entry test was set at 14 cm Hg.

Column Volume Measurement

Accurate measurement of the column volume was important because it was used in subsequent calculations of bulk density, porosity, pore volume, and fluid saturations. To measure the column volume, the column was weighed empty, filled with water, and weighed again. The difference between the two weights divided by the density of water yielded the column volume, V_c. Allowances were made for volume inside the column occupied by filters, the grooves in the top endcap, and how tightly the column was screwed together to give what we call the 'effective column volume' (V_{ce}), the volume occupied by soil and the fluids of interest. What follows is a detailed description of the procedures used to accurately measure the effective column volume.

The mass of the empty column (M_c) was determined by weighing the core body, endcaps with valves, and o-rings using a Mettler PE 1600 balance with 0.01 g accuracy. The bottom endcap was weighed while still full of water from the filter test, and the top endcap was weighed before the filters were glued into place. The column was then assembled. The bottom endcap was screwed into the glass column and tightened in place using a bench vise. The top endcap was only hand tightened into the glass column. The top endcap and glass column were marked to show this reference alignment. The column was filled with water and reweighed. The column volume was calculated as:

$$V_c = \frac{M_{w_1} - M_e}{\rho_w} \qquad (5\text{-}2)$$

where: M_{w_1} = mass of the water-filled column (g)

ρ_w = density of water (g/cm³)

Packing a column with soil was an imprecise science. The column might have been slightly over-filled with soil one time, slightly under-filled the next. The top endcap could not be screwed down to the same degree in an over-filled column resulting in a slightly larger volume inside the column. Conversely, a slightly under-filled column might have been tightened down somewhat further than the reference, resulting in a slightly smaller column volume than the reference volume. To account for this variability in column volume from one packing to the next, a correction factor for endcap tightening was desired. To accomplish this, the valve on the top endcap was opened and the previously hand tightened endcap was tightened in a bench vise. As the column volume was made smaller by the tightening, water squirted out through the opened valve. A new mark, aligned with the glass column mark, was made on the top endcap. The offset length between marks (L_o) was recorded, the column was reweighed, and the new mass (M_{w_2}) was recorded. The column tightening correction factor (C_t) was calculated as:

$$C_t = \frac{M_{w_1} - M_{w_2}}{L_o \, \rho_w} \qquad (5\text{-}3)$$

The volume of the top endcap (including the volume of the grooves, the connecting hole in the endcap, and the valve) was measured in a manner similar to the method used to measure the gross column volume. The endcap was weighed empty, the endcap was filled with a liquid of known density, and the column was reweighed. Similar to before, the mass of the full endcap minus the mass of the empty endcap divided by the liquid density provided a measure of volume which could be occupied by fluid in the endcap. Because the endcap was made of Teflon, which is oil wet, an organic liquid did a much better job than water of wetting the surface and filling the grooves.

The volume of the filter, scrims, and glue on the top endcap reduced the volume of the column available to sand and fluids and also needed to be accounted for. The volume of the paper filter and the polypropylene scrims was calculated by simply multiplying the cross-sectional area by the measured thickness. The endcap, filter, and scrims were weighed prior to gluing the filter and scrims onto the endcap. After the glue had hardened, the endcap was reweighed. The difference between the two weights was the weight of the glue, and when divided by the glue density yielded the glue volume. The density of hardened glue was determined using the ASTM [illegible].

The effective column volume was determined by accounting for the volume in the top endcap behind the filters (including grooves, connecting hole, and valve), the volume of the paper filter and scrims on the top endcap, the volume of glue on the top endcap, and the correction for how tightly the top endcap was screwed in place. So we calculated the effective column volume as:

$$V_{ce} = V_c - V_{groove} - V_{filter} - V_{glue} - C_t \ L_c \qquad (5\text{-}4)$$

where: V_{ce} = effective column volume (cm^3)

V_c = original column volume (cm^3)

V_{groove} = volume of the top endcap grooves (cm^3)

V_{filter} = volume of the paper filter and polypropylene scrims (cm^3)

V_{glue} = volume of the glue (cm^3)

C_t = column tightening correction factor (cm^2)

L_c = length shy of mark (cm)

This procedure may seem to be somewhat elaborate, but was easy for an experienced technician to master. By measuring all of the volumes suggested by equation 5–4 we reduced experimental error and provided repeatable results. Some of the corrections in this equation would have proven less significant in a longer column, but that would have required the use of a larger capacity balance to handle the greater weight of the column. The available larger balances were much less accurate than the Mettler PE 1600 balance.

SOIL PACKING

The glass column was packed by hand in small increments under about 1 cm of water. A previously determined mass of soil was gently poured into a vertically oriented column. The water was controlled by a buret connected to the column through the bottom endcap. The soil was tamped into place using a modified metal spatula (bent flat and turned 90 degrees at one end). The column was packed to a depth of about 5 cm, reaching the top end, just at the base of the upper column threads. The soil was carefully leveled and the top endcap was screwed into place. If the top endcap alignment mark was offset from the mark on the glass column, the distance was measured as the length shy of mark (L_c). The effective column volume was calculated according to equation 5-4.

Occasionally, several attempts at sealing the top endcap needed to be made before the top endcap was successfully screwed into the column and the o-ring was seated properly. After the initial attempt, soil often had to be added or removed from the column before a tight o-ring seal was obtained and the endcap could be tightened in a vise. Any soil removed from the column was oven dried overnight and combined with the leftover soil. The mass of soil in the column, M_s, was simply the original mass of soil minus any leftover soil.

The mass of soil packed into the column was used in determining the bulk density, ϱ_b, the pore volume, V_p, and porosity, n, of the soil pack:

$$\varrho_b = \frac{M_s}{V_{ce}} \tag{5-5}$$

$$V_p = V_{ce} - \frac{M_s}{\varrho_s} \tag{5-6}$$

$$n = 1 - \frac{M_s}{\varrho_s \; V_{ce}} \tag{5-7}$$

where: M_s = mass of soil in the column (g)
ϱ_s = particle density of the soil (g/cm^3)

Upon completion of packing, the column was reconnected to the buret tubing to test the top endcap's o-ring seal for water leakage. O-ring leakage was tested by closing the top endcap valve, opening the lower endcap valve and buret valve, and raising the input buret height, thus increasing the pressure on the o-ring seal. It was usually immediately apparent if the seal leaked, requiring the endcap to be refitted. A good o-ring seal was obvious, with the black o-ring appearing flat against the glass column wall. Only rarely did the seal leak when the top endcap was tightened down using a bench vise. On the other hand, when the top endcap was hand tightened, o-ring seal leakage was more common.

After the column had been tested for leakage, silicon sealant was placed between the outside of the glass column and the top endcap. This prevented any change in column mass due to evaporation of any water accidentally trapped in the threads between the glass column and top endcap.

In two of the experimental trials, the column was packed with coarse lenses within a finer matrix. Sevilleta soil was split into two fractions for these trials, which were packed dry. The dry packing procedures used were identical to those used to to achieve heterogeneous packings in the pore cast experiments. A description of the procedures can be found in Section 7.

Some of the Palouse loam short columns were also packed under dry conditions. Wet packing was difficult in this material. This problem is discussed at the end of this section under the topics '*possible sources of error*' and '*limitations*'.

DEAIRING

The column was flooded with 20 to 30 pore volumes of deaired water in order to remove any gas bubbles trapped in the porous matrix or plumbing. Entrapped gas dissolved into the deaired water and was carried out of the column. After every 100 ml of water added, the column was disassembled from its plumbing and weighed. The column gained mass as entrapped air was removed from the column and replaced by water. The column mass eventually stabilized as all entrapped air was removed. Operationally, we used three consecutive unchanging measurements of column mass to indicate the complete removal of entrapped air. The deairing of the soil column took anywhere from 5 to 10 days for a sandy soil (eg. Sevilleta, Llano, Traverse City), and up to 3 weeks for an initially dry silty-clay soil (Palouse loam). The mass of the column at this point was called the initial column mass (M_1). The water-saturated column could now be used for capillary pressure-saturation tests (see Section 4), the saturated zone experiment (see below and Section 9), or the vadose zone experiment (see below and Section 10).

SATURATED ZONE EXPERIMENTS

Saturated zone residual organic liquid saturation was determined by introducing organic liquid into a water saturated packed soil column (organic liquid flood), then displacing the organic liquid by water (water flooding). These experiments simulated conditions beneath the water table.

Step 1: Organic Liquid Flooding

Once the column had been packed with soil and any entrapped air removed, organic liquid was flooded into the column simulating the movement of organic liquid into the saturated zone. To maintain a stable displacement front, the column was flooded from top to bottom for the case of an organic liquid lighter than water (Figure 5-3), or flooded from below when an organic heavier than water was used. The organic liquid was injected under sufficient head so that the water saturation was reduced to the so-called irreducible water saturation, but the head was kept low enough to prevent organic liquid from breaking through the nylon filter on the bottom endcap.

All organic and aqueous liquids were loaded into the burets by a siphoning procedure to reduce aeration of the fluids. To avoid contact with hazardous vapors, p-xylene, tetrachloroethylene, and gasoline were loaded into burets with a vacuum suction under a fume hood. The openings at the top of the burets were sealed to each other by a stopper and tubing arrangement (not shown in Figure 5-3) to close the system and limit emission of fumes.

The organic liquid flooding was continued for at least 24 hours or until the column weight stabilized, indicating that the fluid saturations had reached equilibrium. A stabilization of fluid levels in both the inflow and outflow burets also indicated that the system had reached equilibrium and fluid saturations had stabilized. Fluid production at the bottom endcap was observed to ensure that only water was produced (verifying that the nylon filter had maintained its integrity and no organic liquid had breached the filter). After stabilization, the column was detached from the burets and the column mass, M_2, was measured (using at least three independent weighings on a Mettler PE 1600 balance with 0.01 g accuracy). The fluid saturations were determined employing the density difference between the organic liquid and water:

$$S_o = \frac{M_1 - M_2}{\Delta\varrho \; V_p} \tag{5-8}$$

$$S_{wr} = 1 - S_o \tag{5-9}$$

where: S_o = Organic liquid saturation (-)

$\Delta\rho$ = Density difference between water, ρ_w, and the organic liquid, ρ_o, (g/cm^3)

S_{wr} = Residual water saturation (same as irreducible water saturation, S_{wi}) (-)

Modifications to the procedure were made in an attempt to introduce organic liquid (Soltrol) into the Palouse loam soil. Because the soil was fine-grained and water wet, the Soltrol did not readily enter the column. Compressed air was used to increase the pressure behind the Soltrol and force it into the water-saturated soil column. One tubing line was connected to an air compressor and split with a tee. One split line went to a mercury manometer board to record the pressure and the other line was connected to the buret containing Soltrol, through a stopper inserted on top of the buret. In this manner, a capillary pressure of about 500 cm of water was induced on the Palouse loam. Still, we had great difficulty pushing Soltrol into the soil.

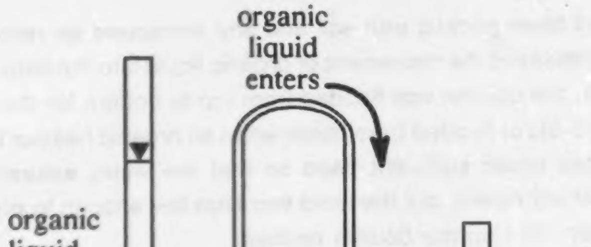

FIGURE 5-3. **Saturated Zone Test Step 1: Organic liquid flood into a water saturated column.**

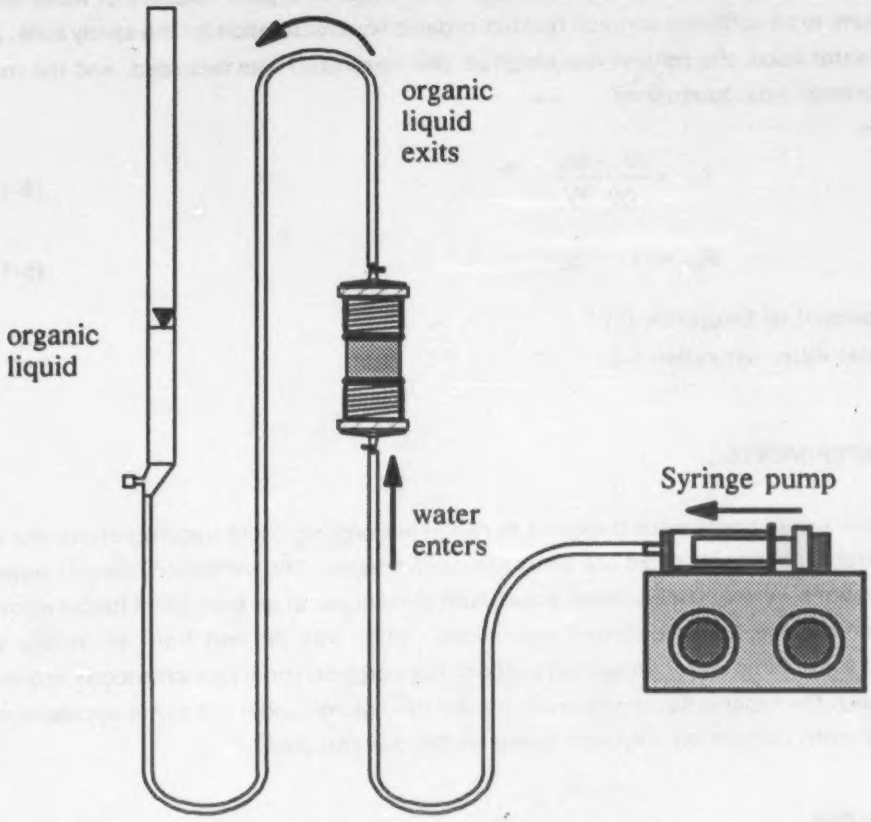

FIGURE 5-4. Saturated Zone Test Step 2: Waterflooding at low velocity to reduce the organic liquid to its residual saturation.

Step 2: Water Flooding

Following the organic liquid flood, the column was slowly flooded with water in order to displace the organic liquid. The sandy soils (eg, Sevilleta, Llano, Traverse City) were flooded at a rate of about 0.3 ml/min. The Palouse loam was flooded at a much slower rate.The water flood was intended to simulate the action of ambient groundwater displacing the organic liquid and leaving behind trapped organic liquid at residual saturation. As shown in Figure 5-4, the column was flooded from bottom to top to promote a stable displacement of the less dense organic liquid. When an organic liquid denser than water was used, the column was flooded from above, displacing the denser fluid out the bottom. A syringe pump, or a carefully controlled and monitored buret flow was used to push the water through the column at a low velocity to make sure the displacement proceeded under low Bond number and low capillary number conditions (see Section 9 for definitions of Bond and capillary numbers). The waterflood continued until no additional organic liquid was produced (as indicated visually through the transparent tubing and by an unchanging column mass). Introduction of about nine pore volumes of water through the column was found to be sufficient to reach residual organic liquid saturation for the sandy soils. At the conclusion of the water flood, the column was weighed, the mass (M_3) was recorded, and the residual organic liquid saturation was determined:

$$S_{or} = \frac{M_1 - M_3}{\Delta\rho \ V_p} \qquad (5\text{-}10)$$

$$S_w = 1 - S_{or} \qquad (5\text{-}11)$$

where: S_{or} = Residual oil saturation (–)
S_w = Final water saturation (–)

VADOSE ZONE EXPERIMENTS

The vadose zone experiments were designed to represent organic liquid trapping above the water table where air, water, and organic liquid are simultaneously present. The simulated residual water and organic liquid saturations were obtained under equilibrium conditions, at an equivalent height above the water table. To achieve the aforementioned saturations, water was drained from an initially water saturated, de-aired soil column under an applied suction. Then organic liquid was introduced into the top of the column. Finally, the organic liquid was drained from the column under the same applied suction. These experiments were performed only with Soltrol in the Sevilleta sand.

Step 1: Water Drainage

Beginning with a de-aired, entirely water saturated column of known mass (M_1), a suction was placed on the column, draining water through the nylon filter and out the bottom endcap (see Figure 5-5). Air entered through the top endcap, replacing the drained water in the soil's pore space. The water-wet nylon filter allowed water, but not air to pass through the bottom of the column. The suction was applied by lowering the water level in the buret beneath the column in the same fashion as when determining water/air capillary pressure-saturation functions. Figure 5-5 shows the configuration used for applying a suction Δh to the column. The elevation difference Δh was measured from the middle of the soil column to the water level in the buret in centimeters of water. Equilibrium was reached when the water level in the buret stabilized and the column weight no longer changed.

Upon reaching equilibrium, the column was weighed and the mass (M_4) was recorded. Air saturation was a function of the suction applied and was measured at a particular equilibrium suction as :

$$S_{a,initial} = \frac{M_1 - M_4}{\rho_w \ V_p} \qquad (5\text{-}12)$$

$$S_{w,initial} = 1 - S_{a,initial} \qquad (5\text{-}13)$$

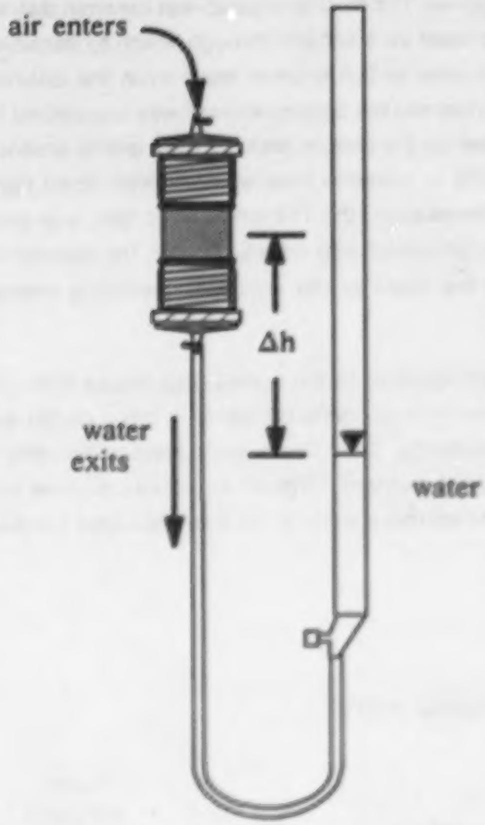

FIGURE 5-5. **Vadose Zone Test Step 1: Water being drained with air under an applied suction.**

where: $S_{a,initial}$ = air saturation following water drainage (-)
$S_{w,initial}$ = water saturation following water drainage (-)

The density of water, ρ_w, was used in the denominator of equation (5-12), instead of the density difference between fluids as in previous equations. The density of the air is negligible, and in any case the measurements were made on a balance exposed to air at room temperature and pressure.

The saturations found by this method were the fluid saturations for the soil under equilibrium conditions Δh centimeters above the water table. One reason the effective column length was kept short (5 cm) was to ensure reasonably constant fluid saturations along the length of the column.

Step 2: Organic Liquid Flooding

Once the water had been drained from the column, organic liquid was introduced to simulate the effect of organic liquid percolating through the vadose zone. Before proceeding with the organic liquid flood, the bottom endcap with the water-wet filter was removed from the column and replaced with an identical endcap with an organic-wet TFE filter or organic-wet ceramic disk in place of the nylon filter. The TFE filter or ceramic disk was used as a vehicle through which to introduce the organic liquid into the column. In a later step it was used to pull organic liquid from the column under suction. To change endcaps, the column was inverted and the bottom endcap was unscrewed from the soil column. Any soil grains clinging to the paper filter on the bottom endcap were gently brushed back into the column. The replacement endcap with a TFE or ceramic filter was screwed down tightly in place to ensure good contact with the soil. Prior to installation, the TFE or ceramic filter was tested for integrity and the end reservoir behind the filter was saturated with organic liquid. The column was then reweighed (M_3) to account for any difference in the mass of the endcaps. Switching endcaps appeared to cause little disruption of the soil packing.

The column was once again attached to the burets (see Figure 5-6). Organic liquid was introduced through the organic-wet bottom endcap. Because water is more dense and air is less dense than the organic liquid used in the experiments, the column was turned horizontally to inhibit density instabilities that might occur in a vertical displacement. Organic liquid was pushed through the column under low capillary number conditions until no more water or air was produced (verified by a stable column mass,

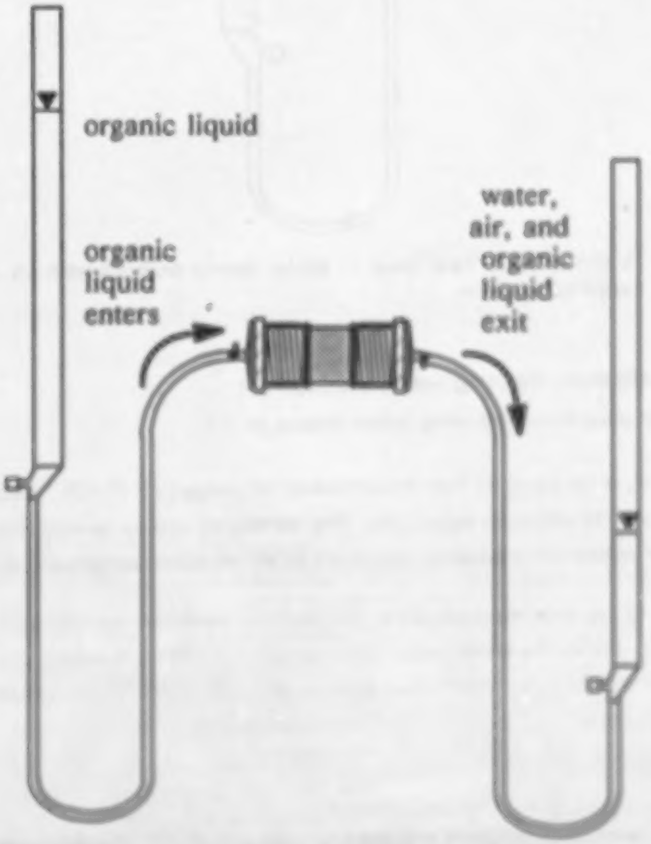

FIGURE 5-6. Vadose Zone Test Step 2: Organic liquid flood in a column already drained by air.

M_6). This step usually required about 300 ml of organic liquid to be pushed through the soil column before the mass stabilized, and took 2 to 3 days to complete.

Once the fluid saturations had equilibrated, the volume of water produced from the soil pack was measured. The volume of water produced was measured by collecting the outflow (water and organic liquid) in a TFE flask and withdrawing the water from the bottom of the flask with a syringe. The water, as well as a small amount of organic liquid pulled into the syringe, was then injected into a graduated cylinder to determine the volume of the water produced (V_{wp}). The new water saturation was then calculated as:

$$S_w = S_{w,initial} - \frac{V_{wp}}{V_p} \tag{5-14}$$

With the water saturation known, the organic liquid saturation (S_o) and the air saturation (S_a) could be found using mass measurements of the column before (M_5) and after (M_6) the organic liquid flood:

$$S_o = \frac{M_6 - M_5 - \rho_w V_{wp}}{\rho_o V_p} \tag{5-15}$$

$$S_a = 1 - S_w - S_o \tag{5-16}$$

Step 3: Organic Liquid Drainage

In the final step of this process, organic liquid was drained from the column under an applied suction. The organic liquid saturation was reduced to an equilibrium saturation for a given height above the water table. For sufficiently large suctions, this represents the residual organic liquid saturation in the vadose zone. This residual remains interconnected, unlike the saturated zone's disconnected blobs. Figure 5-7 shows the set-up for organic liquid drainage. It was very similar to the set-up used earlier in step 1, for draining water from the soil column (Figure 5-5). The drainage was a stable displacement, in which air entered from the top displacing organic liquid downward through the lower organic-wet filter. The elevation difference, Δh, for this step was equal to the Δh used in the previous water drainage step. For instance, if the suction used in the water drainage step was 70 cm of water, in the organic liquid drainage step the applied suction was 70 cm of organic liquid. Although in each case the fluid column in the buret was dropped the same distance beneath the soil column to induce suction, the capillary pressures induced in each of these steps was not the same. The difference in capillary pressures was scaled by the relative densities of the water and organic liquid phases.

The displacement proceeded until the organic liquid and air saturations equilibrated (the water saturation remained unchanged during this step). The equilibrated column was weighed (M_7) and the final organic liquid, water and air saturations were determined:

$$S_o = \frac{M_7 - M_1 - \rho_w V_{w}}{\rho_o V_p} \qquad (5\text{-}17)$$

$$S_a = 1 - S_w - S_o \qquad (5\text{-}18)$$

POSSIBLE SOURCES OF ERROR

Several sources of experimental error were associated with performing multi-phase flow experiments to determine residual organic liquid saturations. Possible sources of error included:

- incomplete removal of entrapped gas.

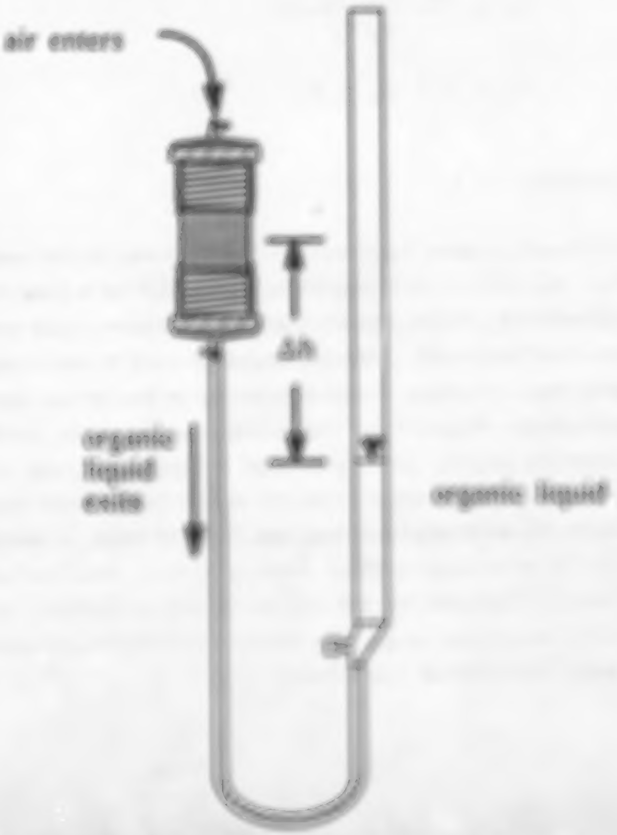

FIGURE 5.7. Vadose Zone Test Step 3: Organic liquid drained by air.

- changes in fluid densities due to changes in laboratory temperature,
- capillary end effects,
- lack or loss of filter integrity,
- faulty seals in the system leading to leakage or evaporative losses,
- trapping of fluids in the outflow and reservoir,
- packing variability (from one soil packing to the next),
- dry packing,
- soil sample variability,
- limited column length, and
- error associated with the precision limits of the measuring devices.

What follows is a brief discussion of each of these sources of error.

Entrapped Gas

As soil was packed into a soil column, some gas was trapped in the pore space. For a water-wet system, trapped gas tends to reside in pores which would probably otherwise trap organic liquid (see for instance, Kyte et al., 1956, and our photographs in Section 10). Residual saturations measured in the presence of trapped gas would be expected to be lower than residuals measured under strictly two-phase conditions.

Entrapped gas presents other problems because its saturation may not remain constant over the duration of the experiment; some of it may dissolve into the liquid phases. When gravimetric measurements are used to determine fluid saturations, the loss of entrapped gas over the course of the experiment would indicate a lower residual saturation than is actually present (for an organic liquid less dense than water).

Entrapped gas was eliminated by flushing the column with several pore volumes of degassed water. As degassed water moved through the column, trapped gas dissolved into the water phase and was carried from the column prior to beginning the experiment. The column gained weight as the pore space previously occupied by gas was then occupied by water. All entrapped gas was assumed to be removed once the column weight stabilized.

Variable Laboratory Temperature

The worst and most persistent problem encountered during this project was our inability to control temperature variations in our laboratory. As the temperature in the laboratory fluctuated, so too did the densities of the fluids used in experiments, introducing error into gravimetric determinations of fluid saturations. In addition, we had observed fluctuations in column weight that were larger than could be accounted for by density effects alone. It is believed that as the temperature rose, dissolved gasses came out of solution and were trapped in the soil — this gas may have subsequently re-dissolved as the temperature fell. This problem was especially acute when liquids containing volatile components, such as gasoline, were used.

Large temperature fluctuations in the laboratory over the course of an experiment led to poor reliability of the results. Measured residual saturations of Soltrol in Sevilleta sand are plotted against laboratory temperature variation in Figure 5.6. The temperature range in this figure represents the difference between maximum and minimum observed room temperatures recorded during an experiment. Measurements were made periodically in the early experiments, while the others were recorded on a strip chart. This figure illustrates the large variation of residual saturations that were measured when temperatures were not held constant over the course of an experiment. The experiments conducted with small temperature variations (< 2°C) show much less scatter than experiments conducted under less controlled temperature conditions.

To remedy the problem of fluctuating temperatures during the experiments, a constant temperature cabinet was constructed. Experiments performed within the constant temperature box displayed a noticeably smaller variation of residual saturations than experiments performed prior to completion of the box.

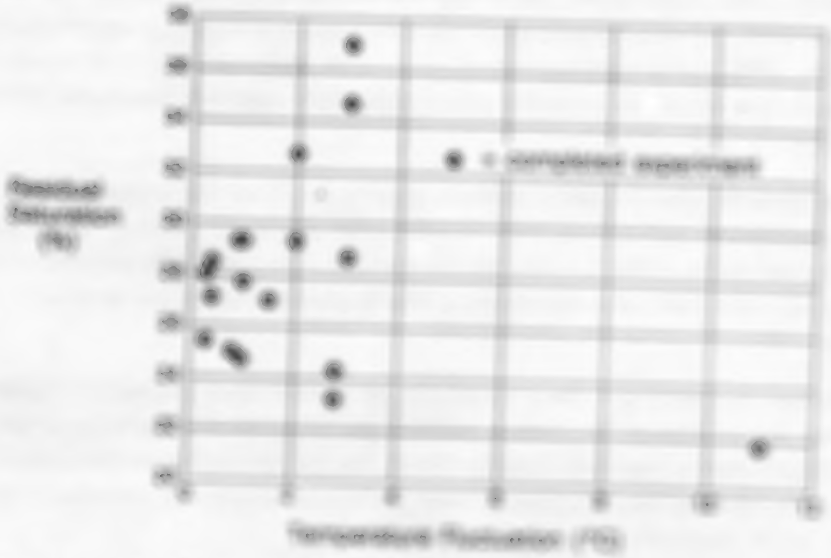

FIGURE 5.6 Temperature range and its effect on the accuracy of results.

Capillary End Effects

Capillary end effects can become important sources of experimental error in multiphase fluid experiments. An example of capillary end effect, for [illegible] displacing water in a micromodel, is shown and discussed in Section 8. Filters that allow only a single phase to pass through reduce these effects. For example, a water wet filter at the discharge end of the short column prevents the non-wetting phase, the organic liquid, from breaking through. A similar filter, for oil advancing into a water filled micromodel, is demonstrated in Section 10. The water and oil wet filters used in the short column appear to have performed at least as well. Inspection of saturated [illegible] pore casts constructed with the [illegible] column (Section 7) and water wet filters revealed a minimal capillary end effect, extending less than [illegible] into the soil. A longer column would have minimized this effect even more. However, there are other problems with long columns, including packing, cleaning, and accurate recording of column mass, as discussed earlier.

Filter Integrity

If filter integrity was not maintained, end effects were not eliminated and the non-wetting fluid could have become trapped in the reservoir behind the filter. In soil column flooding experiments, each filter was tested for integrity prior to use, and [illegible] filters were [illegible] the soil which could have caused leakage. For experiments [illegible] screens were used instead of filters because of their greater durability.

Leaking Seals

The endcaps were sealed to the column using O-rings. Each apparatus was pressure tested for leakage prior to use.

Outlet End Reservoir

[illegible]

Packing Variability

[illegible]

[illegible]

[illegible]

[illegible]

[illegible]

[illegible]

[illegible]

[illegible]

[illegible]

[illegible]

[illegible]

saturations were dependent upon measures of fluid densities, soil particle density, total soil weight, total column volume, and measures of the column mass at several points in the progress of an experiment. All these measures have some error (or uncertainty) associated with them and these errors are routinely propagated through the calculations used to determine fluid saturations. We used a worst case error approach in which we assumed all errors were additive. Since some measurement errors would be expected to cancel each other out, this worst case approach was a conservative estimate of the total measurement error.

LIMITATIONS OF THE APPARATUS AND TECHNIQUE

The experiments with Palouse loam pointed out some of the limitations of our apparatus. Because of the fine-grained nature of the soil, it was difficult to supply sufficient pressure to force organic liquid into the soil. We used pressure equivalent to more than seven meters of Soltrol to overcome the entry pressure for a non-wetting phase. Even if we had been able to inject the organic liquid with sufficient pressure, we might well have also exceeded the entry pressure of the nylon filter on the bottom endcap, resulting in failure of the filter. In order to accommodate fine-grained soils, the apparatus would have to be re-designed as a high-pressure system, including a high-pressure fluid delivery pump, a column built to withstand high pressures, and a bottom membrane with a very high non-wetting phase entry pressure.

Our inability to inject an organic phase into the Palouse loam is not a total loss. It indicates that fine-grained, water-wet soils (which do not shrink and crack in the presence of organics) can serve as an effective barrier to organic liquid movement in the subsurface.

Another limitation of the experimental technique occurred in the vadose zone experiments. Several trials of the vadose zone experiment were run using high applied suctions to measure the saturation of organics left behind a front of organics percolating through the vadose zone high above the water table. Additional vadose zone experiments were performed over a range of applied suctions. These experiments were run to give an idea of the saturation distributions that can be expected in the transition zone between the saturated zone and the vadose zone. Results from these transition zone experiments gave what we believe to be unreasonably high equilibrium organic liquid saturations, reported in Section 10. The limitation of our experimental procedure was that, during the organic liquid drainage step, water was unable to re-imbibe into the soil. Under low applied suctions representing the capillary fringe and just above, re-imbibing water would have displaced organic liquid resulting in lower equilibrium organic saturations than the values we have measured. The largest change in forces acting on the organic liquid occurs in the capillary fringe and just above where the transition from the vadose zone to saturated zone conditions is most pronounced. Unfortunately, the experimental procedure used to measure three-phase saturations over this range was found to be inappropriate. This low suction range is important particularly for organic liquids lighter than water because it is the zone in which gravimetrically light organic liquids spread, forming a lens on the water table.

SECTION 6

LONG COLUMN EXPERIMENTAL METHODS

Organic liquid residual saturation in the saturated zone can be reduced by mobilizing some of the blobs through an increase in hydraulic gradients and water flow rate (Wilson and Conrad, 1984). This concept has long been known in petroleum reservoir engineering and involves increasing the viscous forces of the groundwater flow above a threshold value needed to overcome the capillary forces trapping the larger blobs (see, eg., Anderson, 1987b; Chatzis and Morrow, 1981; Chatzis et al., 1984,1988; Morrow, 1979; Morrow et al., 1988; Taber, 1969). Alternatively, the interfacial tension between the water and the organic liquid can be decreased below an equivalent threshold (see e.g., Tuck et al., 1988). This is the principle behind surfactant floods in enhanced oil recovery (eg., Taber, 1981). Reduction of residual saturation by mobilization is also of interest in aquifer remediation studies.

The saturated zone hydraulic mobilization of the residual saturation of Soltrol-130 was correlated to capillary number for the Sevilleta and Llano soils, both unconsolidated aquifer materials. Experiments of this kind had previously been conducted in consolidated petroleum reservoir cores (eg., Chatzis and Morrow, 1981; Chatzis et al., 1984,1988) and in glass beads (eg., Morrow et al., 1988), but not for unconsolidated materials typical of shallow aquifers that are particularly susceptible to organic pollution. The capillary number represents a ratio of viscous (flowing) forces to capillary forces.

Each experiment began with a long water-saturated column, into which organic liquid was injected, followed by the injection of water under low capillary number conditions to reduce the organic liquid to its residual saturation. Absolute and relative permeabilities were measured during these floods. After the water flood the organic liquid was reduced to residual saturation under low capillary number conditions. In the last step the water flow rate through the column was increased incrementally. Above a critical flow rate (i.e., a critical capillary number), the residual organic liquid saturation in the column became reduced as the force of water flow began to overcome the capillary forces holding the organic liquid in place. By measuring the reduction of residual saturation versus flow rate and pressure drop, a correlation was constructed relating the mobilization of trapped organic liquids to capillary number. At each residual organic liquid saturation, the relative permeability to water was measured under steady-state conditions.

A long column was used in these experiments in an attempt to maximize the accuracy of pressure gradient measurements. The long column also minimized end effects, but at the cost of increased difficulty in packing, longer degassing times, and lower accuracy gravimetric saturation measurements. The long column also allowed us to make measurements of relative permeability during the flooding stages using the unsteady state method (Jones and Roszelle, 1978).

LONG COLUMN APPARATUS

The set-up for the long column experiment is shown in Figure 6-1. The column itself was constructed from a 105 centimeter long, 2.5 inch I.D., schedule 80 PVC pipe, and could accommodate soil packed to

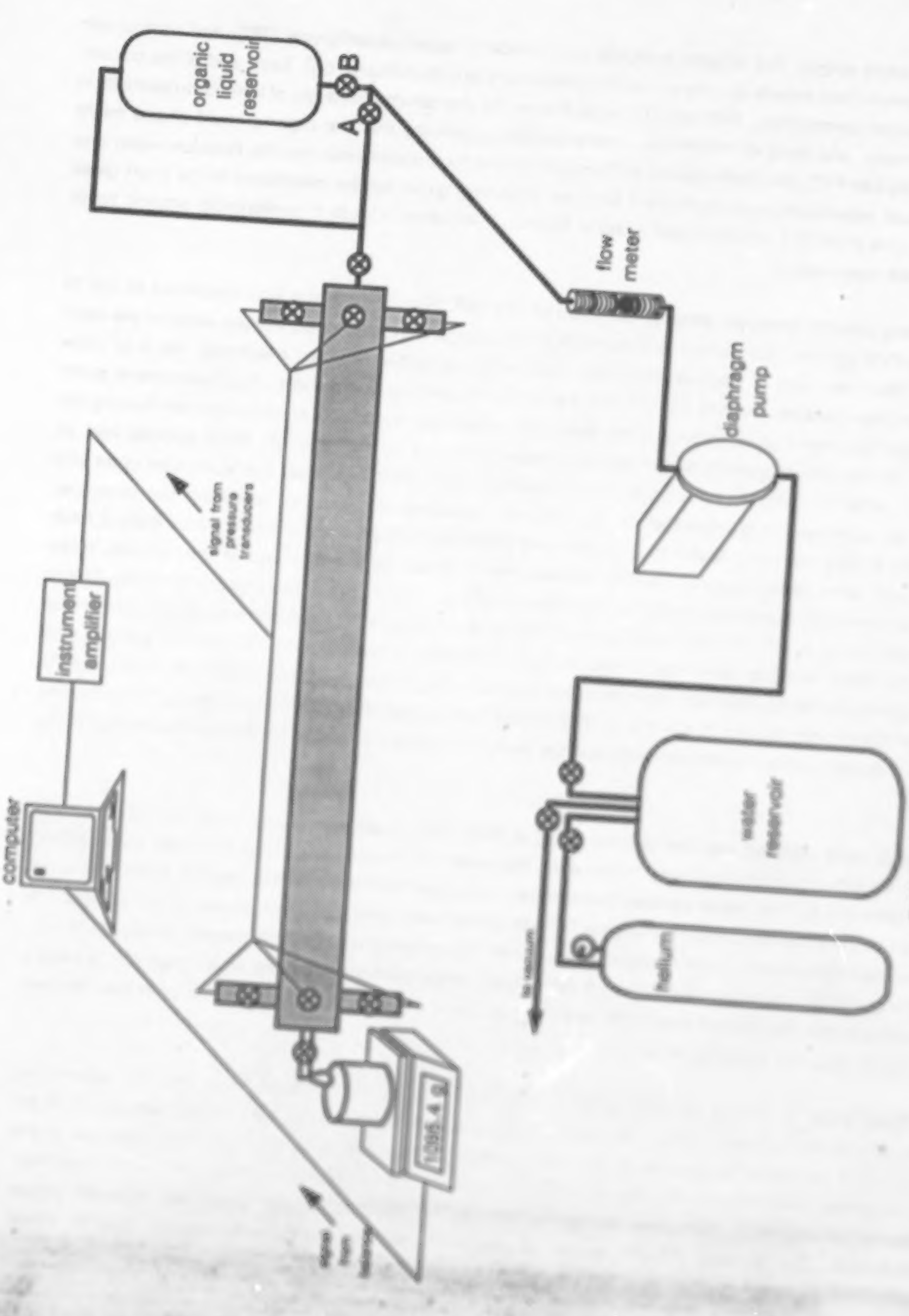
organic
liquid
reservoir
A
B
flow
meter
diaphragm
pump
water
reservoir
helium
to vacuum
instrument
amplifier
computer
signal from
pressure
transducers
1095.4 g
signal
from
balance

FIGURE 5-1. Long column experimental setup

about 100 cm in length. The column endcaps were made of tetrafluoroethylene (TFE) and sealed with o-rings. Construction details for one end of the column are shown in Figure 6-2. Each end of the column was of identical construction. PVC and TFE were chosen for the column because of their non-reactivity in this experiment, and ease of machining. There is some possibility that the organic liquid phase might preferentially wet PVC, but there was no evidence for this in the experimental results. Residual water and organic liquid saturations were equivalent to those observed under similar conditions in the short glass columns. (The short TFE columns described in Section 7 did show effects of preferential organic liquid wetting; see Appendix A.)

The long column endcaps were constructed of TFE rod. Part of each rod was machined to just fit inside the PVC cylinder. Grooves to accommodate two o-ings were machined into the sides of the each endcap. The inner face of each endcap had radial and concentric grooves machined into it to allow better fluid flow between the soil sample and the 1/16 inch endcap center hole. A polypropylene scrim and a paper filter were glued to each inner face. The paper filter kept fine soil particles from leaving the column and the polypropylene scrim kept the paper filter out of the grooves. Each endcap had an aluminum plate screwed into the back. Four threaded rods passed through the aluminum plate and through an aluminum ring mounted on the column, providing a means of attaching the endcaps, essentially bolting them on. Nupro plug valves were threaded through the aluminum plates behind each endcap and were sealed against the TFE endcap with o-ings. Near either end of the column, three pressure transducers were mounted into the sidewall of the column. Each transducer was screwed into the female end of a 1/4 inch NPT male-female PVC valve. A porous ceramic disk was glued to the male end of the valve, and the valve was threaded into the sidewall of the column. The column sidewall was thickened where the transducers were mounted by machining a short length of 3 inch PVC pipe to just fit over the column and by gluing it in place. The thicker column wall allowed enough threads to be tapped into the sidewall to hold the transducers, and the thicker wall provided a stop for the aluminum ring on the column.

Fluids were injected into the column using a Pulsa 680 diaphragm pump, and the flow rate was monitored with a Gilmont float-type (rotameter) flowmeter. The water phase was prepared as described in Sections 4 & 5. Only water passed through the pump and flowmeter. When organic liquid was to be injected into the column, valve A in Figure 6-2 was closed and valve B opened, so that water entered the organic liquid reservoir displacing organic liquid from the reservoir and into the column. While not in use, water was stored under vacuum to keep it de-gassed. When pumping from the water reservoir, a helium atmosphere was maintained above the water to help keep the water as de-gassed as possible. (Helium gas has a very low solubility in water.)

Three pairs of Omega PX-800 series pressure transducers were tapped into the PVC sidewall at either end of the column to measure pressure drops across the length of the column. One set of 20 psi transducers measured pressures in the water phase; another 20 psi set measured pressures in the organic phase; and the third set, having a 200 psi capacity, measured water phase pressures under high pressure conditions — pressures exceeding the 20 psi capacity of the other set of water phase transducers. The Omega PX-800 series pressure transducers were selected for use in these experiments because of their high accuracy and low weight.

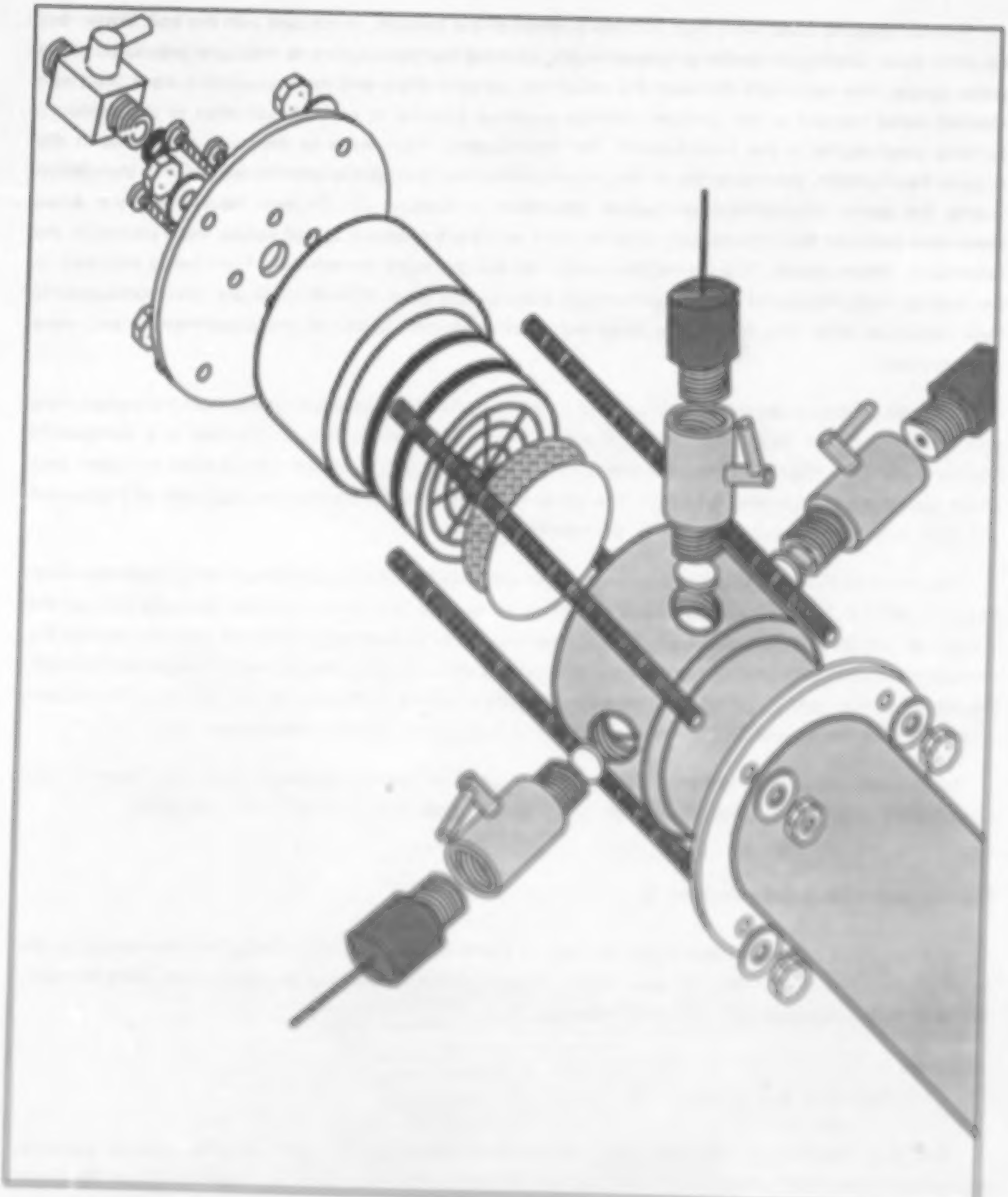

FIGURE 6.2. Long column construction details.

Porous ceramic disks were built into the sidewall of the column, in contact with the soil. Water-wet ceramic disks functioned similar to tensiometers, allowing the transducers to measure pressures in the water phase. The reservoirs between the water-wet ceramic disks and the transducers were filled with distilled water instead of the calcium chloride aqueous solution to reduce corrosion of the pressure sensing diaphragms in the transducers[1]. For transducers which were to measure pressures in the organic liquid phase, the wettability of the ceramic disks was changed to organic-wet prior to installation (using the same organosilane procedure described in Section 5). Organic liquid filled the small reservoirs between the organic-wet ceramic disks and the transducers. Ball valves were placed in the reservoirs. When closed, the valves prevented the low-pressure transducers from being exposed to damagingly high pressures. The organic liquid transducers were difficult to degas, and consequently their response time was excessive. They were not essential to any of the experiments, and were disconnected.

A 10 volt DC power supply served as input to the transducers. Full-scale output from the transducers was 100 millivolts. A Metrabyte DASH-16 analog-to-digital interface board, installed in a CompuAdd Standard PC-AT personal computer, transformed analog signals from the transducers to digital data which could be stored in the computer. The signal from the transducers was boosted with an instrument amplifier to meet the requirements of the interface board.

The mass of fluids produced from the column was measured using a Mettler PM 11 balance which has a 11,000 ± 0.1 gram capacity. Since the densities of each fluid phase and the flow rate through the column at any given time were known constants, the mass of fluid produced was used to monitor the production of both fluid phases from the column as a function of time. Also, by employing mass balance, the displacement data could be used as an independent means of measuring saturations in the column — a check on the standard gravimetric method of measuring column saturations.

The Lotus 'Measure' software package was used to record readings from the balance and transducers at specified intervals and to download the data into a Lotus 1-2-3 worksheet.

FLUIDS AND SOILS (see Section 4)

The column was packed with either Sevilleta or Llano soil. A 3000 ppm $CaCl_2$ solution served as the water phase, and Soltrol 130 was used as the organic phase because of its very low solubility in water. Soil and fluid properties are reported in Section 4.

COLUMN PACKING and SATURATION

The long column was packed under procedures similar to the short column packing methods described in Section 5. The column was aligned vertically with the bottom endcap in place at the lower end. The bottom endcap was connected to a buret which supplied $CaCl_2$ solution to the column. During packing, the head in the buret was maintained so that the soil was packed into the column under approximately 2 cm of water to reduce the amount of entrapped air in the column. Oven-dried soil was poured through a funnel into the column and was tamped into place. Once the column was full, the top endcap was bolted down tightly against the soil. The effective length of the soil in the column varied slightly from one experiment to the next depending on just how much soil was packed into the column. The mass of the soil packed into the column was recorded.

---

[1] Any osmotic pressure generated by using distilled water in these small reservoirs and the $CaCl_2$ solution in the column was negligible compared to the water pressures existing in the column.

The procedures for removing entrapped air from the long column were similar to those described in Section 5. At the conclusion of the packing procedure, entrapped air typically occupied from 5 to 7 percent of the pore space. To remove the entrapped air, the column was flushed with de-gassed $CaCl_2$ solution at a slow rate. The column gained weight as the entrapped gas solubilized into the water phase and was removed from the column. The column was weighed periodically, and once the weight had stabilized the column was assumed to be de-gassed.

At the conclusion of the de-gassing procedure several useful quantities were calculated. The pore volume of the column, V_p (in cm^3), the volume occupied by soil in the column, V_s (in cm^3), and the total column volume, V_T (in cm^3), were determined by:

$$V_p = \frac{M_T - M_s - M_c}{\rho_w} \qquad \text{(6-1)}$$

$$V_s = \frac{M_s}{\rho_s} \qquad \text{(6-2)}$$

$$V_T = V_p + V_s \qquad \text{(6-3)}$$

where: M_T = total column mass at the conclusion of de-gassing (g)
M_s = mass of soil (g)
M_c = apparent weight of the empty column (g)
ρ_w = density of the water phase (g/cm^3)
ρ_s = particle density of the soil (g/cm^3)

The bulk density of the soil, ρ_b (in g/cm^3), the porosity, n, and the effective length of the soil in the column, L (in cm), were determined from:

$$\rho_b = \frac{M_s}{V_T} \qquad \text{(6-4)}$$

---

6. Apparent column weight is the weight of the column [illegible]

$$n = \frac{V_v}{V_t} \qquad (3\text{-}5)$$

$$L_e = \frac{V_t}{A} \qquad (3\text{-}6)$$

where: A = internal cross-sectional area of the column ([illegible] cm²). Finally, since the effective length of the column was a little longer than the distance between the pressure transducers, a pressure correction coefficient, C, was calculated.

$$C = \frac{L_e}{L} \qquad (3\text{-}7)$$

where: L = distance between pressure transducers ([illegible] cm).

This correction factor was used to provide a linear estimate of the pressure drop across the entire length of the soil pack in the column. The effective pressure drop across the column, ΔP_e, was calculated from the measured pressure drop, ΔP, as follows:

$$\Delta P_e = C\,\Delta P \qquad (3\text{-}8)$$

MEASURING ABSOLUTE PERMEABILITY, RELATIVE PERMEABILITY, AND SATURATION

In these experiments, the absolute permeability, k, was defined as the intrinsic permeability measured under fully water-saturated conditions. Following column de-gassing, the absolute permeability was determined by injecting water into the horizontal column at a constant rate and measuring the pressure drop across the column as well as the outflow of water. Darcy's law was used to solve for the permeability, k. Rearranging Darcy's law gives:

$$k = \frac{Q\,\mu_w\,\Delta L}{A\,\Delta P} \qquad (3\text{-}9)$$

where: Q = flow rate (in cm³/sec)

ΔP = pressure drop

ΔL = L = length between pressure taps

A = gross cross sectional area of the column.

For the horizontal column, where the dynamic viscosity of water, μ_w, was [illegible], the length, ΔL, was [illegible] cm, the area, A, was [illegible] cm², the pressure drop, ΔP, was measured in [illegible] and permeability, k, was in cm², this becomes:

$$k\ (\text{in cm}^2) = [illegible]\ \frac{Q}{\Delta P} \qquad (3\text{-}10)$$

Because the data collection system was automated, the pressure drop, the flow rate, and hence the permeability were measured every 10 seconds. The absolute permeability and error reported for each experimental trial was the mean and standard deviation of these measurements.

Step 1: Organic Liquid Displacing Water

In this first displacement step, organic liquid displaced water from the soil column reducing the water saturation to its irreducible value. During this process the relative permeability of both water and organic liquid were measured as a function of fluid saturations using the unsteady state method.

Referring again to Figure 6.1 on page 66, water was initially injected into the column (valve A open, valve B closed) until the desired flow rate had been established (as determined from the flow meter). Once the flow rate had stabilized, valve A was closed and valve B opened to allow organic liquid to enter the column. During organic liquid injection, pressure data and the mass of fluid outflow from the column were continuously recorded. The pressures of each fluid phase were measured at both ends of the column. A pressure drop in the organic phase significantly different from the pressure drop in the water indicated the presence of capillary pressure gradients across the length of the column, violating an important assumption of the unsteady state method. The experiments were run at sufficiently high flow velocities that capillary pressure gradients were negligible. The cumulative mass of the produced fluids were also continuously measured. Cumulative mass of the outflow, taken together with the flow rate and the fluid densities, was used to determine the cumulative production of each fluid. Cumulative mass measurements taken at early time (when only water was being produced) were used to more accurately quantify the flow rate. The entire contents of the organic liquid reservoir (a total of about 2-3 pore volumes) were injected into the column. Relative permeabilities, k_{rw} and k_{ro}, were calculated using the unsteady state method graphical procedure of Jones and Roszelle (1978).

At the conclusion of the initial organic liquid injection, the column was weighed to determine the average organic liquid saturation, $\bar{S}_o$, in the column:

$$\bar{S}_o = \frac{M_i - M_f}{V_p \, \Delta\rho} \qquad (6.1)$$

where M_f was the final column mass following organic liquid injection, and $\Delta\rho$ ($\rho_w - \rho_o$) was the density difference between fluids. The gravimetrically determined organic liquid saturation was compared with the average organic liquid saturation calculated from the material balance:

$$\bar{S}_o = \frac{V_{oI} - V_{oE}}{V_p} \qquad (6.2)$$

where V_{oI} = the volume of organic liquid injected into the column (cm³)
V_{oE} = the volume of organic liquid produced from the column (cm³)

It then was $\bar{S}_w = 1 - \bar{S}_o$.

[illegible]

$$[illegible]$$

[illegible]

[illegible]

[illegible]

$$[illegible]$$

[illegible]

$$[illegible]$$

[illegible]

[illegible]

[illegible]

[illegible]

[illegible]

[illegible]

- ○ [illegible]
- ○ [illegible]
- ○ [illegible]
- ○ [illegible]
- ○ [illegible]
- ○ [illegible]
- ○ [illegible]
- ○ [illegible]
- ○ [illegible]
- ○ [illegible]
- ○ [illegible]
- ○ [illegible]
- ○ [illegible]

[illegible]

[illegible]

[illegible]

[illegible]

[illegible]

[illegible]

[illegible]

[illegible]

[illegible]

[illegible]

[illegible]

[illegible]

[illegible]

[illegible]

[illegible]

[illegible]

[illegible]

[illegible]

[illegible]

[illegible]

[illegible]

[illegible]

[illegible]

[illegible]

[illegible]

[illegible]

plate screwed to the backs. An external groove was cut in the cylinder into which fit a 10 cm diameter aluminum split ring. Four threaded rods passed through the aluminum plates and split ring and provided a means of attaching the endcaps, essentially bolting them on. Four o-rings, one on each end of the cylinder and one on each of the endcaps, securely sealed the column and created a purely mechanical method of holding filters in place.

The inner face of the endcaps had radial and concentric grooves machined into them to allow better fluid flow between the soil sample and the 1/16 inch endcap center hole. In addition, a round fritted glass disc (50 mm diameter, 5 mm thick) was fitted on top of the groove pattern of the lower endcap as a support for filters. Nupro® plug valves were threaded through the aluminum plates and sealed against the TFE rod with Viton® o-rings.

A Magna 66 nylon filter with pore diameters of 0.22 μm, held in place by an o-ring, was used on the bottom endcap. It acted as a semi-permeable membrane; when water-wet the filter would allow water to pass but not a non-wetting phase, such as styrene. The nylon filter was covered with a paper filter to prevent abrasion against the sand. A paper filter alone was used on the upper endcap to prevent fine soil particles from leaving the column. In experiments which required epoxy drainage, Millipore's 0.2 μm Durapore® (polyvinylidene difluoride) filters were used in place of the water-wet nylon filters.

FLUID AND SOIL CHARACTERIZATION

Although styrene's immiscible behavior with water, its low viscosity, and its ability to harden while in contact with water, make it useful for simulating non-aqueous phase liquid movement through soils, it does have several drawbacks. For example, it initially has a low viscosity, but once initiated the viscosity increases over time. This indicates that polymerization begins as soon as initiator is added, albeit slowly(see Figure 7-2). Styrene's volume also shrinks by about 17% as it hardens (Boyer, 1970). This must be noted when making optical measurements. However, the interfacial tension of the styrene with $CaCl_2$ solution was found to remain constant over time (35.3 dynes/cm) even when initiator was added.

Dyes were added to the styrene in order to improve its visibility, but they changed fluid properties. For example, 9,10-diphenylanthracene (maximum adsorption 260 ηm) was added to styrene (0.6% by weight as recommended by McKeller and Wardlaw, 1988) causing the styrene to fluoresce blue under ultraviolet light. Addition of the dye caused the interfacial tension (IFT) with $CaCl_2$ solution to decrease from $\sigma_{ow} = 35.3 \pm 0.3$ to 30.9 ± 3.0 dynes/cm, and also caused viscosity changes, as shown by Figure 7-2. Other dyes tried, such as oil blue N (IFT σ_{ow} of styrene + dye = 20.2 ± 0.5 ; surface tension σ_{oa} of styrene + dye = 31.8 ± 0.3 dynes/cm) and phthalocyanine blue did not work well enough to justify further characterization.

Tracon's Tra-Bond® 2114 epoxy was used in several experiments, in addition to styrene, to represent the wetting or non-wetting phase. Rhodamine B (maximum adsorption 543 ηm), a red-orange fluorescent dye, was dissolved in benzyl alcohol and added to the Tra-Bond® 2114 epoxy, but no characterization was done beyond that stated in Table 7-1. The benzyl alcohol caused a dramatic decrease in the resin's viscosity but only a slight decrease in its surface tension. In the three-phase

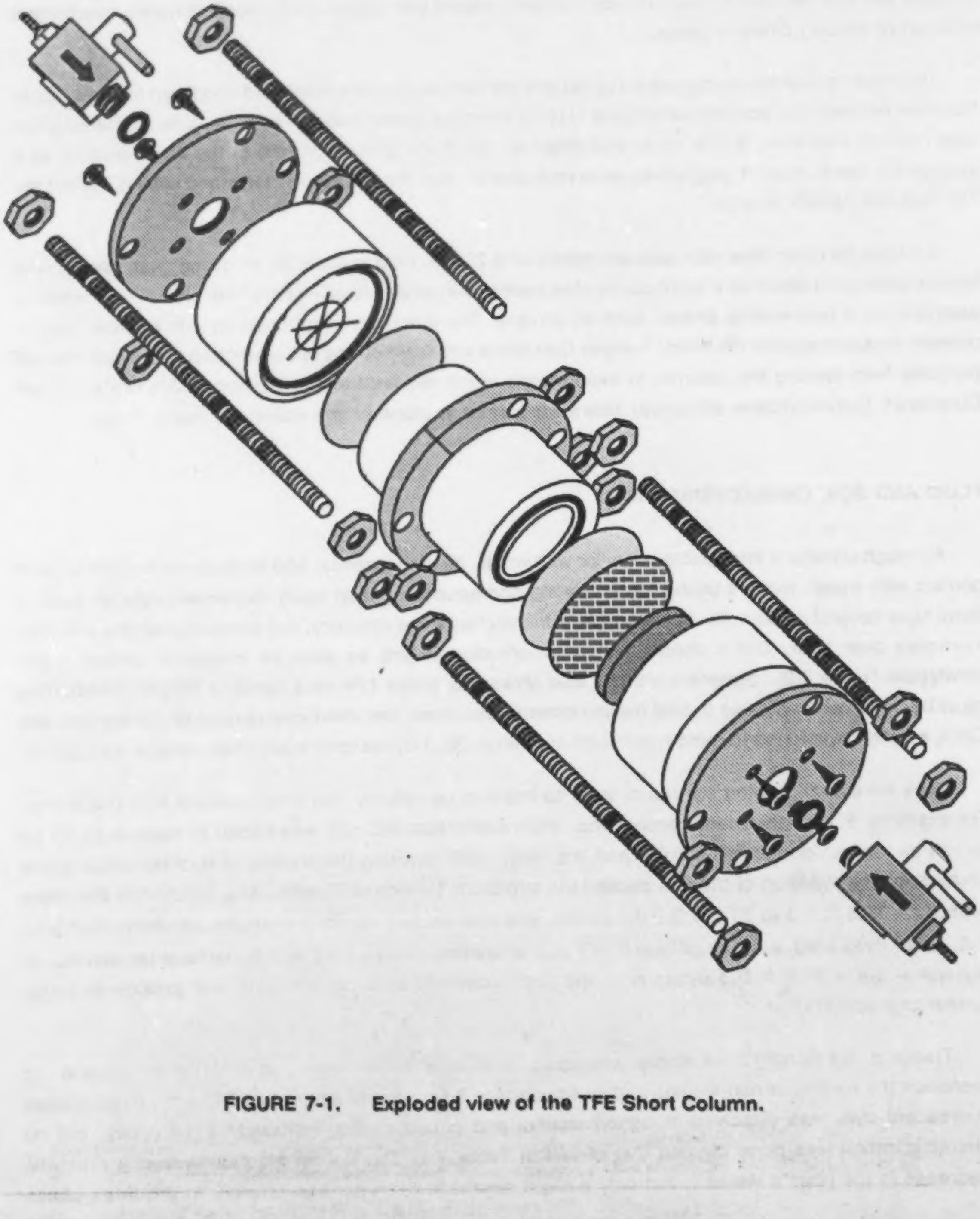

FIGURE 7-1. Exploded view of the TFE Short Column.

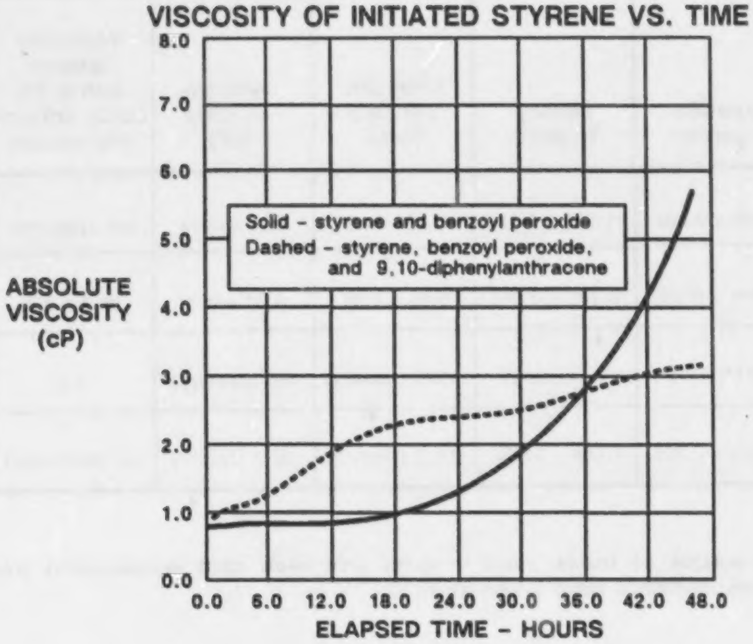

FIGURE 7-2. Viscosity of initiated styrene vs. time.

experiments benzyl alcohol (40% by weight) was added to the Tra-Bond ® 2114. This reduced the viscosity to about 50 cP and decreased the surface tension to 38 ± 1 dyne/cm.

Several other epoxy resins were considered but none performed well enough in preliminary tests, to be used in actual experiments. Shell Chemical's Epon® 8132 epoxy, Dow Chemical's D.E.R ® 324, and Polysciences' Ultralow® epoxy underwent tests for viscosity, the ability to harden in the presence of water, compatibility of the liquid epoxy with other hardened epoxies, and dye solubility. All the liquid resins were soluble with styrene.

Shell's Epon 8132, when mixed with a hardening agent (DETA or diethylenetriamene) in a ratio of 100:13 had a viscosity of approximately 600 centipoises. The viscosity can be decreased with the addition of benzyl alcohol. To test the resin's resistance to moisture during the curing process, several drops of the Epon 8132 mixture were covered with water and left to harden. Several of the resin's components separated, when the drops came into contact with the water, and the resin failed to harden. Liquid Epon 8132 did not react with any of the other hardened epoxies. Addition of benzyl alcohol to the resin, as a thinner, however, did result in some surficial tackiness of the other hardened epoxies. Observations of hardened samples showed that the Epon resin would dissociate over time. Small pock marks on the surface, filled with an amber fluid, were observed to form over a period of months. This phenomenon may have been due to water vapor, or other chemical vapors, in the atmosphere reacting with the epoxy. For this reason no tests of dye solubility were performed.

liquid	specific gravity	density (g/cm³)	kinematic viscosity (cst)	dynamic viscosity (cP)	interfacial tension with 0.3% $CaCl_2$ solution (dynes/cm)	surface tension (dynes/cm)
aqueous-phase	1.003 ± 0.002	1.000 ± 0.002	0.98 ± 0.01	0.98 ± 0.01	not applicable	72.0 ± 0.4
styrene	0.906 ± 0.002	0.903 ± 0.002	0.89 ± 0.01	0.81 ± 0.01	35.3 ± 0.3	31.9 ± 0.3
Tra-Bond® 2114	1.204 (factory)	1.2 (factory)	545 (factory)	597 (factory)	< 2	40.9 ± 0.5
Ultra-low resin	1.072 ± 0.002	1.069 ± 0.002	18.7 (factory)	20.0 (factory)	not determined	36.6 ± 0.6

TABLE 7-1. Properties of fluids used in pore and blob cast visualization experiments. All measurements were taken at 23°C.

Dow Chemical's D.E.R. 324, when mixed with Henkel's Versamid® 150, had a viscosity comparable to Shell's Epon 8132, approximately 600 centipoises. Again the viscosity could be decreased using benzyl alcohol as a solvent. The D.E.R. 324 performed better than the Epon 8132 when tested for hardening in the presence of water. A thin film of epoxy, in contact with the plastic container, hardened, but the majority of each drop remained a white viscous gel. Liquid D.E.R. 324 did not react with any of the other hardened epoxies. The solubility of fluorescent dyes in D.E.R. 324 was low; neither 9,10-diphenylanthracene, rhodamine B, nor coumarin 6 would dissolve to any great extent in the resin. The resin did take on the dye's color faintly, but large clumps of dye would remain isolated in the liquid. Interestingly, the undyed D.E.R. 324 resin fluoresced a light blue under ultraviolet light.

Polysciences' Ultralow® is a multi-component resin with a viscosity of 20 centipoises. It does not harden in the presence of moisture. Due to its low viscosity Ultralow was a prime candidate for use in the three phase simulation, but it was found that Ultralow reacted with, and softened, hardened styrene. All three dyes were readily soluble in the resin. During the resin's curing process, however, Ultralow darkens to a dense amber color. The coloring tended to dominate any dyes dissolved in the resin.

A 3000 ppm $CaCl_2$ solution was used as the aqueous phase in all the saturated zone experiments. Distilled, de-ionized water was de-gassed by boiling. Enough calcium chloride dihydrate was added to the cooled water to bring the concentration to 3000 ppm. The solution was stored under a vacuum to keep it de-gassed.

Measurements of fluid properties such as viscosity, density, surface tension, and interfacial tension were performed following procedures outlined in Section 4. The Sevilleta sand was used in all of the successful experiments described in this report. Its properties are also reported in Section 4.

SATURATED ZONE EXPERIMENTAL PROCEDURE

Packing and Degassing

Both homogeneous and heterogeneous sand-pack experiments were performed in the TFE columns. The packing and degassing procedures for the homogeneous case are reviewed first, followed by the heterogeneous case. Equations are then presented for calculating pore volume, bulk density, and bulk porosity, after packing.

Before packing a column with soil to be used in a homogeneous saturated zone experiment, the lower endcap with filters was tightly bolted to the TFE cylinder, and the cylinder and endcap were attached to an 18 cm Hg vacuum. Then the column was inverted and placed in a large beaker of $CaCl_2$ solution. Liquid was drawn through the filters, fritted glass disc, and associated plumbing to saturate them with water (see, eg., Figure 5-2). When air bubbles were no longer observed, the column was removed from the vacuum and the filters checked visually for integrity. The water-wet filters should have prevented the flow of the non-wetting air phase. If the filters did not allow air flow the whole column was dried and weighed. This was called the empty column weight, M_c. Mettler PE1600 and PM11 scales, with 1600 ± 0.01 gram and 11000 ± 0.1 gram capacities respectively, were used for the gravimetric measurements in these experiments.

Next, a buret filled with $CaCl_2$ solution was attached to the bottom endcap and the solution was allowed to fill the column to a depth of 2 cm. Oven dried Sevilleta sand, which had been weighed previously, was then poured and packed into the column, taking care to keep the packing surface below the solution surface. Lab spatulas, bent to a 90 degree angle, were used to pack the soil down. The process of filling the column with $CaCl_2$ solution and then packing soil was repeated until the solution level was approximately 2 cm from the top of the cylinder. At that point capillary rise of the solution was used to saturate the soil/sand as much as possible, since there was nothing to prevent overflow of liquid from the column. Sand packed above the end of the cylinder was carefully scraped off with a lab spatula and collected together with spilled sand. After drying, it was combined with unused sand. The mass of soil in the column, M_s, was simply the difference between the initial soil mass minus any leftover. O-rings and a paper filter were placed on the cylinder to seal and prevent the escape of clays and other fines, respectively, and the upper endcap was lowered onto the column and bolted on.

Some trapped air remained on or between soil particles, especially near the top of the column, and had to be removed. The column was slowly flooded with degassed $CaCl_2$ solution to solubilize and remove the trapped air. The solution was introduced through the bottom endcap and out the top endcap. Periodic gravimetric measurement of the column was used to determine whether or not an equilibrium had been established. When the column reached equilibrium all the entrapped air had been removed from the column and the plumbing (see similar procedure for the short column, Section 5). Twenty five pore volumes (~800 ml) of degassed $CaCl_2$ solution usually solubilized the trapped air and removed it from the column.

The heterogeneous sand pack column experiments were performed using the Sevilleta sand, split with a size 50 sieve (≈ 296 microns) into coarse and fine portions, approximately 45% and 55% by mass, respectively. The finer fraction was used as a matrix to surround 3 stringers or lenses, composed of the coarser fraction. The stringers were roughly circular in cross-section. The major difference in packing technique between the homogeneous and the heterogeneous cases was that the heterogeneous columns were packed dry. The TFE cylinder and water saturated bottom endcap were assembled as described earlier, in the homogeneous packing procedures, but no $CaCl_2$ solution was allowed to flow into the column while it was being packed. This was to preserve the paper forms which were used to separate the coarse stringers from the fine sand.

The three paper cylinders were constructed with diameters calculated so that the sum of their cross-sectional areas would equal approximately 45% of the cross-sectional area of the column. This was done so that any given cross-section would roughly have the same percentage of grain sizes as a cross-section through a homogeneous column.

A 6 to 7 mm thick layer of the fine sand was placed on the bottom of the column assembly and the paper cylinders were pushed down into it. This held the forms upright. Then the fine sand was carefully poured and packed around the forms, so as not to collapse them, until the level of the sand was three-fourths of the way to the top of the column. At that point the coarse sand was packed, using a lab spatula, into the paper cylinders. They were filled to approximately 6 to 7mm from the top of the column. The rest of the matrix was then filled with the fine sand. The three paper forms were slowly pulled out of the column and any remaining volume was filled with the fine sand.

$CaCl_2$ solution was then pushed upwards, through the bottom endcap, wetting the sand. Settling of the sand was observed, and more fine sand as added to the top of the column. When the sand-pack was totally wetted, excess sand was removed from the top of the column and the upper endcap was attached, as described earlier. Degassed $CaCl_2$ solution was flooded through the column until a gravimetric equilibrium was attained. These same methods were used for heterogeneous packings in the quantitative short glass column experiments (see Section 5).

The mass of water in both homogeneous and heterogeneous packed columns was determined from:

$$M_w = M_1 - M_e - M_s \qquad (7\text{-}2)$$

where: M_w = mass of water in the column (g)

M_1 = de-gassed, water saturated, sand packed column mass (g)

M_e = mass of the empty column (g)

M_s = mass of soil in the column (g)

Estimates for pore volume, soil volume and total effective column volume were also calculated from these gravimetric measurements:

$$V_p = \frac{M_w}{\varrho_w} \qquad (7\text{-}3)$$

$$V_s = \frac{M_s}{\varrho_s} \tag{7-4}$$

$$V_T = V_p + V_s \tag{7-5}$$

where: V_p = pore volume of the column (cm^3)
V_s = volume of soil sample in the column (cm^3)
V_T = total volume of the column (cm^3)
ϱ_w = density of water (g/cm^3)
ϱ_s = particle density (g/cm^3)

Finally, the bulk density, ϱ_b , and bulk porosity, n , of the soil pack were determined:

$$\varrho_b = \frac{M_s}{V_T} \tag{7-6}$$

$$n = 1 - \frac{M_s}{\varrho_s \ V_{ce}} \tag{5-7}$$

where: M_s = mass of soil in the column (g)
ϱ_s = particle density of the soil (g/cm^3)

The bulk density and porosity formulae represent a bulk or mass average value for the heterogeneous columns. The actual volumes, densities, and porosities of the fine matrix and coarse stringers were not individually measured.

Styrene Preprocessing

Styrene monomer is commonly sold containing an inhibitor to prevent polymerization during transport and storage. Distillation of styrene has been the preferred method to remove the inhibitor, but the distillation process is quite involved due to styrene's volatility. In order to simplify the laboratory procedure, inhibitor removal columns developed by Aldrich Chemical Company (cat.# 30,632-0) were used to remove the 4-tert-butylcatechol inhibitor from the styrene.

Inhibited styrene, held in a separatory funnel, was slowly dripped into the column and then collected in a beaker or flask at the bottom of the column. Each inhibitor removal column has the capacity to remove inhibitor, at 15 ppm, from up to 4 liters of styrene. The uninhibited styrene was weighed and benzoyl peroxide, 1% by weight, was added as an initiator. Benzoyl peroxide was chosen as an initiator because it was found to preserve the water wetness of the soil sample (Chatzis and Morrow, 1984). Dyes were then added to the styrene.

Styrene Flooding

The initiated, dyed styrene was transferred from the flask to a 100 ml buret which was attached to the upper endcap of the de-gassed column. To eliminate the possibility of air entering the column, the

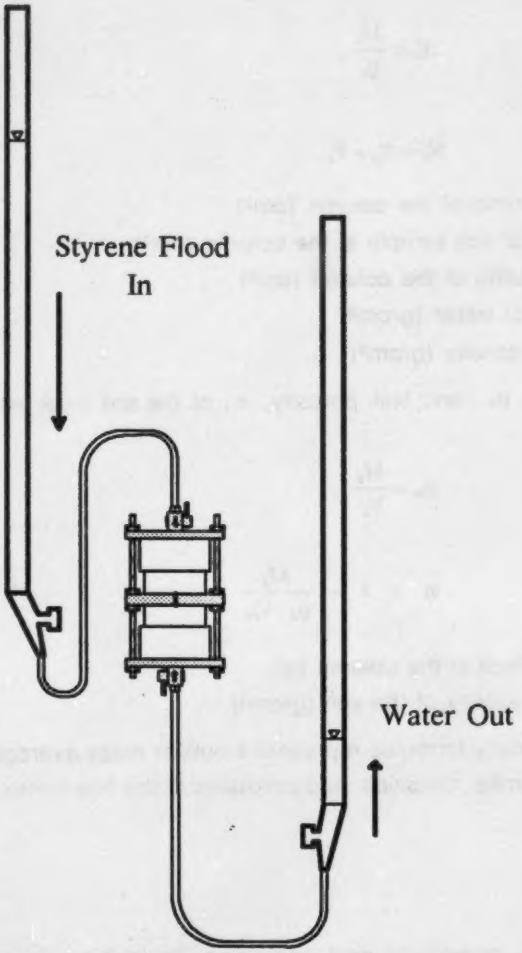

FIGURE 7-3. **Experimental setup of a styrene flood.**

column was first inverted and the tubing attached while a slow stream of styrene flowed from the buret. The column was righted and the styrene elevated to a head of approximately 1 meter above the column. Valves on the water and styrene burets, and those on the column, were opened and styrene flowed into the column, as illustrated in Figure 7-3. During the flooding, the head on the column decreased as styrene left the buret. Head drops of 30 to 40 cm, depending on the column, were common. Water, displaced by the styrene, passed through the nylon filter and left the column via the lower endcap. The displaced water was collected in a flask and later discarded.

Experiments with Soltrol-130 have shown that the column-buret system actually required close to 48 hours before residual or irreducible water saturation (S_{wr} or S_{wi}) was reached. The time dependent nature of styrene's viscosity, however, required the experiment to be completed within 24 hours of initiation. Experiments running longer would be of questionable value since the viscosity would be increasing. Besides, many organic liquids of interest generally have viscosities close to that of water (see Table 7-2). Attempting to displace a more viscous fluid with a less viscous fluid (i.e., displacing viscous styrene with less viscous water) can lead to results different from those obtained from a displacement experiment where the ratio of viscosities is near one. The ratio of the non-wetting fluid viscosity to the wetting fluid viscosity is often referred to as the 'mobility ratio' in petroleum reservoir engineering. High, or adverse, mobility ratios can lead to increased trapping of the non-wetting phase in saturated zone experiments caused by viscous instabilities.

After 18 hours the valves on the burets and column were closed. The outflow tubing and buret were checked to see that no styrene was produced. Styrene in the outflow line indicated a leak in the filter which would invalidate the experiment. The upper (styrene) tubing was carefully removed, noting any spills and cleaning them off the column; the column was inverted and the lower ($CaCl_2$ solution) tubing was removed. The TFE column was weighed and the mass recorded as M_2. The fluid saturations were calculated as:

$$S_o = \frac{M_1 - M_2}{\Delta\varrho \; V_p} \tag{7-8}$$

$$S_w = 1 - S_o \tag{7-9}$$

where: S_o = oil saturation (%)
S_w = water saturation (%)
V_p = pore volume (g/cm^3)
$\Delta\varrho$ = density difference between fluids (g/cm^3)

The results of these calculations are given in Appendix A.

Water Flooding

Styrene was drained from its buret and the other buret was filled with de-gassed $CaCl_2$ solution. The column, at initial organic saturation, was re-attached to the two burets, the water buret to the lower

benzene	0.65
toluene	0.59
m-xylene	0.62
gasoline	0.48
soltrol-130	1.45
kerosene	1.73

TABLE 7-2. Absolute viscosities of selected organic liquids at 20° C in Centipoise. Data from laboratory measurements (section 4) and Weast, 1986.

endcap and the styrene buret to the upper endcap. The $CaCl_2$ solution buret was raised to a head of approximately 1 meter and all the valves in the system were opened.

$CaCl_2$ solution entered the lower endcap and flowed upward, displacing the less dense styrene. Connected, or continuous styrene, left the column and no water was produced until approximately 60-70% of a pore volume had passed. For a relatively short period of time after water breakthrough occurred, both styrene and water were produced from the column. A total of 6-7 pore volumes of $CaCl_2$ solution were flushed through the column in order to ensure equilibrium between the aqueous phase and the organic residual.

The burets were disconnected from the column, as described above, and the column was weighed again. This mass was recorded as M_3. The residual organic saturation was then calculated as

$$S_{or} = \frac{M_1 - M_3}{\Delta\varrho V_v} \tag{7-10}$$

Calculated residual styrene saturations for the Sevilleta sand are reported in Appendix A.

Styrene Polymerization

The styrene residuals were hardened by placing the column in a pressure vessel, pressurizing it to 80 psig and then heating the vessel at 85 degrees centigrade for 40 hours.

The pressure vessel was a 40 cm tall aluminum cylinder (I.D. 10 cm) with 1.3 cm thick walls. The bottom was sealed with a flanged aluminum plate welded to the outer wall. The top was sealed with an o-ring held between the top cap and the face by 10 threaded studs set into the cylinder face. A Nupro® plug valve, with associated fittings, was threaded into the top cap.

Eight hundred ml of degassed $CaCl_2$ solution were poured into the vessel. The column was placed into the pressure vessel with the valves on both ends open and enough $CaCl_2$ solution was added to cover the column with liquid. The liquid acted to prevent nitrogen from entering the sand pack and also as a diffusion barrier for any oxygen that may be present in the vessel atmosphere.

After the column was sealed into the pressure vessel, a 60 cm Hg vacuum was applied to the head space to evacuate as much atmosphere as possible, then a dry nitrogen source was connected to the plug valve and the vessel was pressurized to 80 psig. Checking for leaks in the seal was done by submerging the vessel under water. If no leaks were detected, the vessel was placed in a laboratory oven and heated.

Observation of Styrene Residuals

To complete the saturated zone simulation, either the styrene blobs were removed from the sand matrix or the water/wetting phase was replaced by an epoxy. The first method produced individual styrene residual 'blob casts', whose shapes and sizes were viewed optically or with a scanning electron microscope. The second method yielded polished epoxy slabs, the 'pore casts', in which the relationships between soil grains, the wetting phase, and the non-wetting phase were studied.

The styrene blob casts were removed from the matrix by dissolving the sand grains with acids. A small portion of the styrene-sand pack was carefully removed from the column with a spatula, placed in a TFE beaker, and dried. The dry sample was covered with one of several concentrated acids and allowed to dissolve for several days after which the sample was filtered through a TFE filter, washed with water, and covered with another acid. This process was repeated with concentrated hydrofluoric acid, sulfuric acid, nitric acid, hydrochloric acid, phosphoric acid, and chromic acid. This combination of acids dissolved essentially all of the matrix and left the resistant styrene blob casts, as well as some insoluble inorganic residue. Several styrene blob casts, as photographed with a scanning electron microscope, are shown in Section 9 (Figures 9-20 and 9-22).

To construct the pore casts, the column was taken out of the pressure vessel, and the top endcap was removed. The column and endcap were placed back in the oven at 75-80 degrees centigrade and allowed to dry for 48 hours. The dried column was reassembled and attached to a pressure vessel filled with 0.5% by weight rhodamine B dyed Tra-Bond® 2114 epoxy resin. Resin was forced through the soil sample from the bottom of the column with air pressure. Four or five pore volumes of resin were forced through the column in order to remove as much air as possible. Time was of the essence, since the Tra-Bond epoxy would generally harden within 1 hour, depending on the mix of resin to hardener. Twenty-four hours were allowed for the Tra-Bond epoxy to properly set. The consolidated core was then removed from the column by cutting longitudinally through the teflon sleeve in two spots, and peeling the teflon away.

Rock saws owned by the New Mexico Bureau of Mines and Mineral Resources were used to section the core into 6 or 7 approximately seven mm thick discs. One face on each disc was covered with a thin layer of undyed Tra-Bond® 2114 epoxy to fill in holes left by plucked grains, and create a solid surface for polishing. To remove air bubbles trapped under the epoxy, each disc was placed in a vacuum dessicator for 5 minutes under a 60 cm Hg vacuum. When the epoxy layer dried, the disc was cut on a Bureau of Mines trim saw into 9 pieces: 8 edge pieces and one rectangular middle piece. The smaller pieces were easier to polish and hence provided better optical surfaces. Lap (grinding) wheels were used to grind the epoxy layer down to a flat surface.Two-hundred-twenty and 400 grit powders were used to remove the majority of the epoxy coating, and 10 minutes of polishing with 14.5 μm and 9.5 μm grit provided the final surface. Some of these pieces were sent to a commercial firm to be processed into thin sections.

Photomicrography was done using one of the two in-lab Zeiss SR stereoscopes, or New Mexico Tech's Petroleum Recovery Research Center's Nikon Opti-Phot epifluorescent microscope system. Examples of these photomicrographs are shown in Figures 9-18, 9-19, and 9-21 of this report.

VADOSE ZONE EXPERIMENTAL PROCEDURES

Attempting to simulate organic liquid transport in the vadose zone using styrene and epoxies presented several difficulties. In the vadose zone, there are three fluid phases: water, air, and the organic liquid. In these visualization experiments, all three phases obviously could not be fluid simultaneously since most epoxies and styrene monomer are miscible. It was decided to simulate the three fluid phases by a sequence of two phase experiments in which the wetting phase of each experiment would be hardened. Styrene was used as the first wetting phase, and nitrogen was used to drain the styrene to a wetting phase residual saturation. Assuming this saturation would not change with the presence of an intermediate wetting phase, the styrene was hardened. Epoxy was then flooded into the column and drained with gas to simulate the intermediate wetting phase. The remaining void space was filled with a second epoxy to simulate the gas phase.

This approach raised a question about surface energies. Would differences between solid-liquid wetting relationships and the liquid-liquid interfacial tension cause serious differences between the simulation and reality? The styrene, acting as a wetting phase, was drained to some residual saturation and hardened. The next intermediate-wetting phase, epoxy, interacted with the immobile 'wetting phase' as it was flooded through the column and subsequently drained. In order to decrease the surface energy of the system, the second phase should have spread out in a thin film over the wetting phase whether the 'wetting phase' is solid or liquid. A liquid at residual wetting saturation would be relatively immobile as it is trapped by an interaction of capillary, viscous, and buoyancy forces. It may not be as immobile as a solid, yet simple wetting experiments have shown that a non-wetting liquid will not displace a wetting liquid from a surface; rather, a thin film of the wetting phase will exist between the solid surface and the intermediate or non-wetting phase (Morrow, 1974). So in this sense, a solidified wetting phase may be a reasonable approximation of a fluid wetting phase, as long as flow in the wetting phase is not significant (Amaufule and Handy, 1982). Granted, there are differences between a liquid propagating over a solid surface versus a liquid surface, but the final results will be similar: a minimization of surface energy.

Wetting Phase

Initially, due to its excellent wetting characteristics, styrene was chosen to represent the wetting/aqueous phase. A column was packed with Sevilleta sand, under dyed initiated styrene, following procedures described previously in the saturated zone methods. Then it was drained with air. Polymerization of the styrene failed, however, because of the air in the sand pack. Oxygen in the air attached to the free radical chain of the styrene, effectively stopping the polymerization process. The sand pack was left as a gooey, viscous mess.

Polysciences' Ultralow® epoxy, dyed with coumarin 6 (maximum absorption 458 ηm), was tried in an attempt to bypass the styrene problem. Packed as the wetting phase, it hardened sufficiently to hold the sand together, but the dye, in the thin layers and pendular rings of the epoxy, did not fluoresce sufficiently for easy viewing. We decided to try styrene again, in the absence of oxygen.

An I^2R (Instruments for Research and Industry) glove bag was purchased, inside of which a column could be packed in a nitrogen atmosphere. The inert nitrogen atmosphere made it possible for the styrene chains to polymerize unhindered by oxygen molecules. The glove bag was connected to a tank of dry nitrogen, inflated, and purged to remove any air. Sand, dyed initiated styrene, packing materials, the pressure vessel, and the column with a nylon filter were put into the bag and the bag was purged two more times. A vacuum line with a reservoir outside the bag to collect styrene and tubing attached to a buret were punched through the side of the bag. With these lines, styrene could be removed from, or introduced into, the bag.

Using the vacuum line, styrene was pulled through the bottom endcap of the column to remove atmosphere from behind the nylon filter. Styrene, which had passed from the column to the vacuum reservoir, was transferred to the buret, which in turn was attached to the lower endcap of the column. This source of styrene was used to pack the column in a method similar to that described earlier, for the saturated zone TFE column.

After the packing of the column was completed, a paper filter was placed over the sand and the upper endcap was bolted on. Approximately five pore volumes of styrene were pushed from the buret upward through the column and out to the vacuum reservoir. Nitrogen trapped in the sand pack was removed in this manner. The hydraulic gradient between the buret and the reservoir provided the impetus for styrene flow, so the vacuum was not used. After the styrene flooding, the column was considered saturated. The term 'considered saturated' is used because no gravimetric measurements were made to determine if an equilibrium was attained. Nitrogen may still have been present within the the sand pack or in the lower endcap, but costs of styrene and dye prevented a more thorough de-gassing procedure.

Draining the column to a residual wetting phase saturation was done by applying tension to the sand pack by lowering the styrene buret below the column. Still within the glove bag, the vacuum line was removed from the upper endcap. Styrene drained through the nylon filter to the buret while nitrogen entered the column through the upper endcap. Initially, the styrene-air interface was lowered to 50 cm below the column, and the column allowed to equilibrate. After 1 hour, the buret was lowered another 25 cm and allowed to equilibrate for 2 hours.

The residual styrene was polymerized following the method described in the saturated zone experiment. A difference in procedure to note is that the column was placed into the pressure vessel while still within the glovebag, so that the nitrogen atmosphere was maintained. Also, no water was present within the pressure vessel in which to submerge the column, only nitrogen gas.

Intermediate Wetting Phase

In most experiments, after the styrene had been polymerized, the TFE column was disassembled and cleaned. Hardened styrene clogged the fritted glass disc, froze the plug valves, and filled the grooves in the endcaps. Soaking the valves and endcaps in toluene dissolved the styrene. The fritted glass disc was discarded.

A new fritted glass disc and new filters were used to reassemble the column. In the first experiment, a nylon filter was used at the lower end of the column, as in the two phase simulation. It was found that Tra-Bond® 2114 and Polysciences' Ultralow® epoxy did not wet the nylon sufficiently to prevent air breakthrough during drainage, so the nylon filter was eliminated from further consideration. Further experiments and a search through the literature led to the purchase of Millipore's 0.2 µm Durapore (polyvinylidene difluoride) filter. With a water-wet air entry value of 50 psig, Durapore filters provided better, although not perfect, epoxy drainage.

Ultralow epoxy dyed with coumarin 6 was used in a first attempt to simulate an intermediate-wetting phase. The time required to flood and drain a column, 1 to 1.5 hours, seemed to make the choice obvious. Ultralow had no time constraints and it required heating to cure, while the Tra-Bond hardened after approximately 1 hour at room temperature. Unfortunately, the Ultralow proved to be incompatible with the dyed styrene. In preliminary tests, the Ultralow softened the hardened styrene but not to the point of destruction. While flooding the Ultralow through the sand-styrene pack, however, the epoxy leached the 9,10-diphenylanthracene dye from the styrene, leading to a homogenization of dyes and an overall decrease in intensity of both of the dyes. This failure led to an increase of interest in the Tra-Bond resin.

Tra-Bond® 2114 resin with rhodamine B dye, 0.5% by weight, and benzyl alcohol, 40% by weight, were pulled under a vacuum into a small stainless steel pressure cylinder. The upper end of the cylinder was removed from the vacuum and reattached to a source of dry air with a pressure of 40 psig. The lower end of the pressure cylinder was connected with tubing to the bottom end of the reassembled column, as shown in Figure 7-4. A short length of tubing led from the upper endcap of the column to a drainage beaker. The applied air pressure forced resin upwards through the lower endcap displacing air. Approximately one pore volume of the moderately viscous resin was forced through the column in a 45 minute period.

Draining the column was accomplished by turning off the air source, removing the upper drain tubing, and attaching a vacuum line to to pressure cylinder. Thirty cm Hg of tension were applied to the

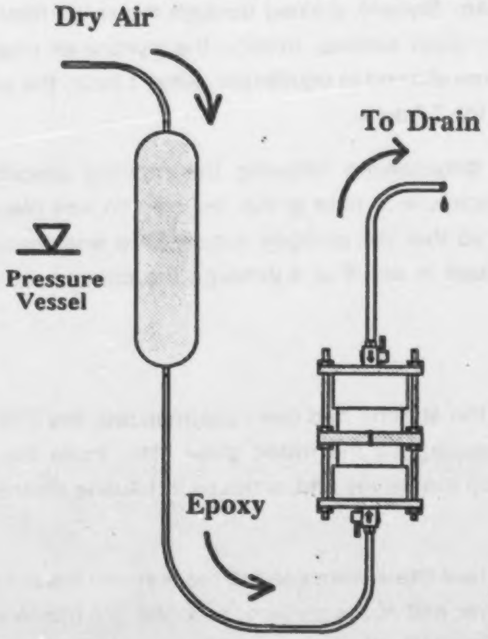

FIGURE 7-4. Intermediate-wetting phase flood.

column and this drained approximately 50% of the intermediate-wetting phase volume. The column was allowed to drain until the excess resin in the drainage beaker showed signs of hardening. This was about 1 hour after the hardener was added to the resin. At that time, the valves on the column were closed, and the pressure cylinder was disconnected from the system. As the hardening time of an epoxy is dependent on the volume of the epoxy, the fluid within the column was still semi-liquid when the tension was removed.

It took 24 hours for the epoxy to cure after which the column was disassembled and cleaned. Benzyl alcohol was used to flush epoxy from the pressure bottle and to dissolve epoxy from within the endcaps.

Non-Wetting Phase

The third fluid phase to be added to the column represented the non-wetting air phase. Again Tra-Bond epoxy was used, but this time it was dyed with coumarin 6. Preliminary experiments indicated that the epoxy resin's liquid phase would not react with its solid phase, so no problems of dye leaching were anticipated, and none were encountered.

As no drainage of the third phase was required, this step was the easiest of all. The dyed epoxy was pulled into the stainless steel pressure cylinder, as described earlier, and flooded into the column through the bottom endcap. After breakthrough occurred, the excess resin was collected in a beaker and discarded. Forty-eight hours were required for the epoxy to cure.

When the core had cured sufficiently, the teflon cylinder was cut away and the core was prepared for observation as 'pore casts', as described previously for the saturated zone experiments.

POSSIBLE SOURCES OF ERROR

Several sources of experimental error were associated with the pore and blob cast experiments. All of those errors listed and discussed in Section 5 apply here. However, recall that with pore and blob casts we mainly seek qualitative visual pictures of the residual saturation, rather than quantitative measurements. Possible sources of additional error are:

- TFE Column Weight,
- high styrene density,
- error propagation,
- styrene viscosity changes,
- effects of time constraints on saturated zone experiments,
- TFE column wettability
- styrene shrinkage,
- movement of styrene blobs after hardening,

- breakage of styrene blob casts,
- heterogeneous sand packing,
- fluid properties as a function of the presence of dyes,
- time constraints on wetting phase saturation in the vadose zone experiment,
- incomplete drainage of the intermediate wetting phase saturation in the vadose zone experiment, and
- finite thickness of pore cast sections.

What follows is a brief review of these issues.

TFE Column Weight

The pore and blob cast experiments produced quantitative results as well as results pertaining to flow visualization. Unfortunately, the experimental methods made these quantitative results too inaccurate to be included with the main body of saturated zone residual saturation data presented in Section 9. Perhaps the largest source of error in the styrene experiments was the mass of the TFE column itself. The column weighed much more than the glass short-columns used in the quantitative experiments. It had to be weighed, during the gravimetric determinations of saturation, on the high capacity Mettler PM 11 balance, which has an accuracy of 0.1 grams. The glass short-columns, in contrast, were weighed on a Mettler PE 1600 balance, with an accuracy of 0.01 grams. The difference in accuracy of the scales propagated through the error calculations and led to much larger error bars on the data obtained during the styrene experiments.

Styrene Density

Another factor contributing to the lower quantitative accuracy in these results was the density of the styrene. In comparison to Soltrol-130, styrene is the denser — 0.90 versus 0.75 g/cm^3. The larger density of styrene led to a smaller value of $\Delta\varrho$, the difference between the density of water and the organic phase, which was plugged into the equations for organic saturation, S_o, and residual saturation, S_{or}. The smaller value of $\Delta\varrho$ led to greater uncertainty in the saturation measurements.

Error Propagation of the Residual Saturation Measurements

The glass short column experiments residual saturations commonly had errors of ±2-3%, while the styrene experiments had errors of ±6-8%. When we considered that 6-8% was sometimes up to 50% of the residual saturation measurement, it seemed prudent to consider these less accurate results separately. The TFE column residuals are presented in Appendix A.

Styrene Viscosity

Styrene's low viscosity increases over time, once it is initiated (see Figure 7-2). This led us to run the experiments more quickly than we desired, in order to avoid the adverse effects of a high viscosity organic liquid.

Effects of Time Constraint

In the saturated zone experiments styrene saturations, S_o , commonly reached values of 70 ± 6%. In experiments with Soltrol-130 in the short glass columns S_o values were commonly around 85% (see Section 9). Clearly the water saturation at this point was greater than its residual wetting value (S_{wr} , = irreducible water saturation, S_{wi}). Observed residual styrene saturations for the Sevilleta sand were generally 15 ± 7%. These values are significantly lower than those observed with Soltrol-130 in Sevilleta sand filled short glass columns(about 27%; see Section 9).

We hypothesized that the time constraint put on the experiment by styrene's ever increasing viscosity did not allow enough time for the column to come to an equilibrium condition during the styrene flood. Therefore, the maximum organic saturations were consistently lower than those obtained with the glass short-columns. This led to consistently lower organic residual saturations after the water flood. Several experiments were performed to investigate this phenomenon and are also reported in Appendix A (see Table A-1). In one experiment, trial 0-6, Soltrol-130 was flooded into and drained out of a TFE column following procedures dictated by the viscosity time constraints of the styrene procedure. The residual saturation obtained matched those commonly found when performing experiments with styrene in the TFE column (19%). Another experiment, trial 0-5, was also performed using Soltrol-130 in the TFE column, but followed procedures described in Section 5 of this report. Since sufficient time for the system to come to equilibrium was allowed, a value of residual saturation was obtained (27%) which closely matched those found when using Soltrol-130 in a glass column. These results, which are presented in detail later, suggest that the differences in residual saturation values were related not to differences in fluid characteristics, but to the amount of time the liquid/soil system had in which to equilibrate.

TFE Column Wettability

The wettability of the column walls was also found to affect the amount of time required to reach an equilibrium during the organic liquid flood. That is, how well an organic liquid wetted the column side wall affected how the liquid travelled through the column. TFE, which formed the walls of the column in these styrene experiments, was preferentially wet by the organic phase, whereas the glass-walled columns used in the short column experiments were preferentially wet by water.

In an attempt to study a non-wetting phase front advance in the TFE columns, an experiment was conducted in which only one-third of a pore volume of styrene was introduced into a water-saturated TFE column. The experiment was halted at that point and the column was heated to polymerize the styrene. When the column was dissected, all the styrene was found around the edges of the sand-pack in contact with the column walls or endcaps (see Figure 7-5b). The central core of the sand-pack had not yet been contacted by styrene. This result indicated that because styrene wet TFE, but not the sand, the advancing styrene followed the walls preferentially (see Figure 7-5a). Subsequent drainage of water from the center of the column was slowed because the styrene had already achieved a high saturation at the bottom of the column, interfering with water drainage. Due to the time constraints imposed on the styrene experiments, the slower drainage of water resulted in lower maximum organic saturations which contributed to lower residual saturations.

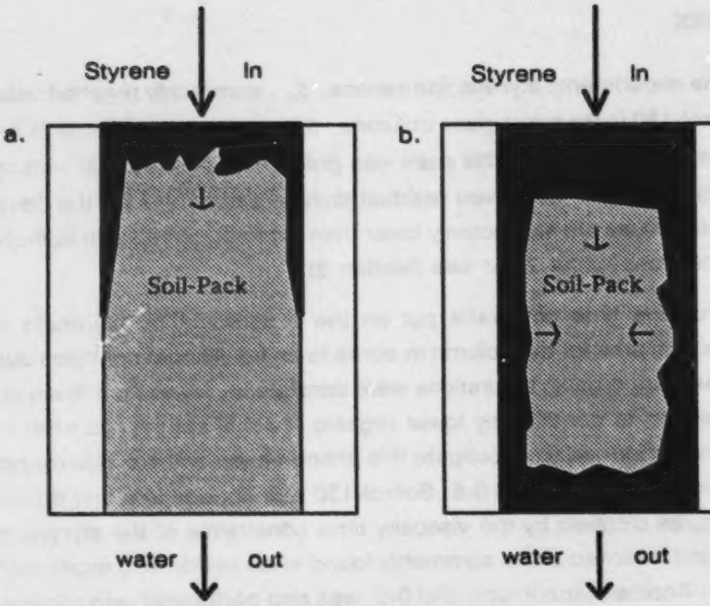

FIGURE 7-5. Cross-section of styrene flooding into a water-saturated column with organic wet walls: a) early time; b) late time.

If this non-uniform displacement was typical for styrene, it is probable that the resulting spatial distribution of polymerized sytrene blobs may not faithfully simulate the residual organic distributions in the glass columns and perhaps in the field. This problem is one reason why statistical analyses of blob size and shape using blob and pore casts may be premature for unconsolidated soils. We suggest the development of a water-wet column in future blob and pore cast experiments.

Shrinkage of Styrene Volume after Polymerization

Styrene's volume also shrinks by about 17% as it hardens (Boyer, 1970). This must be noted when making optical measurements of the hardened styrene blobs in the blob or pore casts.

Movement of Styrene During the Construction of Saturated Zone Pore Casts

In the saturated zone pore cast experiments, the water phase was replaced by an epoxy. It is likely that each hardened styrene blob moved somewhat within the pore space surrounding it. Movement was restricted by the proximity of the pore walls and, for complex, branching blobs, by their interweaving within the pore network. There is a very minimal possibility that small hardened blob singlets may have migrated to an adjacent pore during the epoxy flood. This possibility is inhibited by the large size of the singlet blobs compared to the available pore throats.

Blob Cast Breakage

Although the styrene blob casts were chemically resistant, they were quite brittle and fragile. The transfer of a blob from filter paper to a microscope slide for observation often resulted in the breakage of the blob. It was not clear that the blob casts recovered from the acid bath were wholly unbroken. Some photomicrographs of broken blobs are presented in Section 9.

Heterogeneous Sand Packs

The heterogeneous sand pack column experiments were performed using the Sevilleta sand split into two fractions. The geometry of the packing was not well controlled. The properties of the two fractions was not measured. Future experiments should approach this issue more quantitatively.

Dyes and Fluid Properties

Dyes were added to the styrene in order to improve its visibility, but they changed fluid properties, Addition of 9,10-diphenylanthracene dye caused styrene's interfacial tension (IFT) with $CaCl_2$ solution to decrease from $\sigma_{ow} = 35.3 \pm 0.3$ to 30.9 ± 3.0 dynes/cm and also caused viscosity changes, as shown by Figure 7-2.

Time Constraints in the Wetting Phase Saturation of the Three Phase Experiments

Styrene was used to represent the wetting phase saturation in the vadose zone experiments. Because, once initiated, styrene's viscosity changes with time only about five pore volumes of styrene were pushed through the column. The column was then considered saturated. The term 'considered saturated' is used because no gravimetric measurements were made to determine if an equilibrium was attained. Nitrogen may still have been present within the the sand pack or in the lower endcap, but costs of styrene and dye prevented a more thorough de-gassing procedure.

Incomplete Drainage of Intermediate Wetting Phase in the Three Phase Experiments

The high viscosity of the epoxy prevented complete drainage of the resin in the three phase experiments.

Finite Thickness of the Pore Cast Sections

Some of the pore casts were thin sectioned. These sections were not two dimensional sections through the porous media. The styrene, epoxy, and quartz are all translucent to transparent. Fluorescing materials (eg, styrene blobs) below the surface were visible at the surface. Consequently, blobs seen in the pore casts are somewhat three-dimensional. Surface staining is a technique used in biology and geology to insure that only the surface materials are being view. However, both styrene and epoxy take up the surface dyes, so that it was not possible to use this approach to distinguish the different simulated fluid phases. We suggest that future work further explore surface staining techniques to overcome this problem.

LIMITATIONS OF THE TECHNIQUE

We had hoped to conduct statistical analysis of size and shape blob casts. However, two of the problems that we encountered led us to reconsider. First, the preferential wetting of the TFE column walls may have led to a final non-uniform distribution of residual saturation over the column cross-section. Blob populations taken from this sample might not be representative. Second, the samples of blob casts we examined showed many broken casts (see photomicrographs in Section 9). These two problems led us to conclude that the experimental procedure was not yet mature enough to conduct the statistical study as part of this research project. We recommend future efforts in this direction.

We represented the three phase saturations by a sequential application of fluids. These experiments assumed that a liquid at residual wetting saturation would be relatively immobile as it is trapped by an interaction of capillary, viscous, and buoyancy forces. It may not be as immobile as a solid, but a thin film of the wetting phase should exist between the solid surface and the intermediate or non-wetting phase (Morrow, 1974). A solidified wetting phase may be a reasonable approximation of a fluid wetting phase, as long as flow in the wetting phase is not significant (Amaufule and Handy, 1982). Although we feel that there is a similarity between a liquid propagating over a solid surface and a liquid propagating over a similar immiscible liquid surface, this experimental approach is unproven. Other experimental techniques should be developed to study pore scale fluid distributions in the vadose zone. Quick freezing of very low temperatures is one such technique (see, eg., Gvirtzman *et al.*, 1987).

SECTION 8

MICROMODEL EXPERIMENTAL METHODS

Micromodels are physical models of a pore space network, created by etching a pattern onto two glass plates which are then fused together. The pores have complex three dimensional structure, although the network is only two dimensional. The advantage of performing multiphase flow experiments using micromodels is that they give us the ability to actually see fluids displace one another both in a bulk sense and in individual pores. Displacement photographs of the entire model allow examination of the bulk displacement processes, while photomicrographs taken through an optical microscope permit observation of details on a pore level. Etched glass micromodels provide an excellent method with which to study the mechanisms controlling the transport and capillary trapping of organic liquids because the structure of the pore network and the wettability of the system can be closely controlled.

Mattax and Kyte introduced the 'capillary micromodel' in 1961 as a method to make detailed observations of fluid interface movements. Their technique allowed them to precisely control the pore geometry and its variability; factors difficult to control in bead-pack models. They created their models by first mechanically scribing pore-network patterns on a wax-coated plate, and then by contacting the exposed glass surface with hydrofluoric acid. Unfortunately, this method relied on the patience and manual dexterity of the model maker. Davis and Jones (1968), Chatzis (1982), and McKellar and Wardlaw (1982) improved the manufacturing process by adapting a common photo-etching procedure to glass. By generating a pore-network pattern by photo-reproduction instead of by mechanical means, they were able to manufacture large, complex models with pore sizes that approximated those found in oil reservoir rocks. Their technique, similar to one used for making printed circuits in the electronics industry, involved 'photographing' the desired patterns on glass plates coated with an ultraviolet-sensitive resin and etching the plates with hydrofluoric acid. The micromodel construction procedures described below were modifications of Chatzis's methods as well as those developed by Eastman Kodak (1975, 1979).

Etched glass micromodels have been used to study a variety of petroleum and chemical engineering problems. For example, Chatzis and Dullien (1983) used micromodels to investigate capillary trapping during two phase flow in a pore doublet. Wardlaw (1982), Chatzis *et al.* (1983,1988), and many others have examined displacement in complex two dimensional pore networks, using water flooding and various enhanced recovery techniques.

This section first addresses the fabrication of glass micromodels used in these experiments. The experimental procedures for saturated zone conditions are then explained, including comments on fluid preparation. This is followed by a description of the experimental procedures used in the three-phase experiments.

MICROMODEL CONSTRUCTION

The manufacture of micromodels was a difficult process, requiring an enormous investment of time and effort to learn. However, once the technique was perfected, the whole construction process lasted only three or four days. A glass mirror, stripped of its protective enamel backing to reveal a copper layer, was coated with a photosensitive resin. A transparency of a desired pore-network pattern was placed on the coated mirror surface and was exposed with ultraviolet light. The unexposed resin beneath the opaque portions of the pattern was removed with xylene. The copper beneath the pattern was removed with nitric acid, and the glass beneath the copper was etched with hydrofluoric acid (HF). A mirror-image pattern was etched on another piece of mirror, and the two etched halves were fused together in a muffle furnace to form the completed micromodel.

Pattern Preparation

Pore-network patterns were created by modifying commercially available drafting pattern films with drafting pens. A local photographer reduced each pattern to a standard size and transferred it and a mirror image to plastic transparencies. The emulsion side of each transparency contacted the coated glass plates; transparencies laid emulsion-side up on a plate allowed too much light to leak under the pattern during exposure to UV light. The patterns included 'reservoirs' at each end of the network through which fluids were added and removed in the completed micromodel. An example of a pore-network pattern is shown in Figure 8-1.

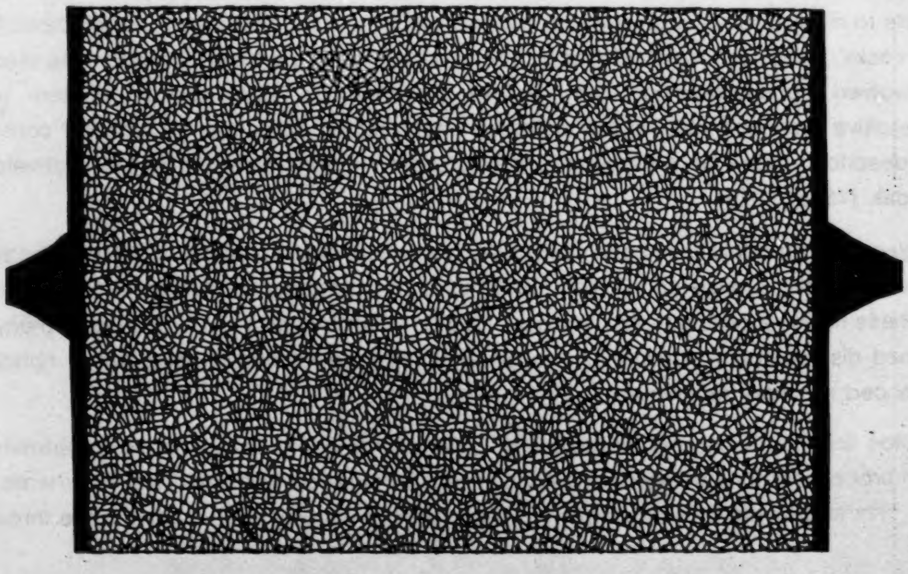

FIGURE 8-1. Pore-network pattern for the homogeneous model.

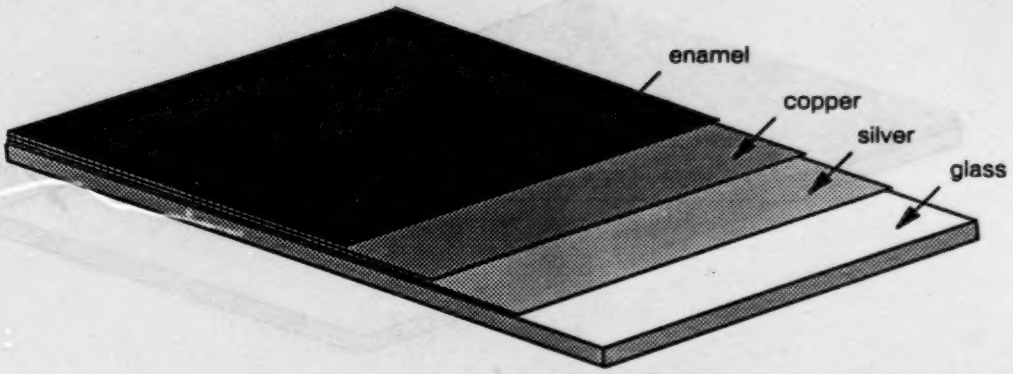

FIGURE 8-2. **Mirror construction.**

Mirror Preparation

Ordinary mirrors are manufactured by coating a piece of glass first with a silver layer, then a copper layer, and finally a protective enamel backing (see Figure 8-2). Mirrors were used in micromodel construction as a matter of convenience: the copper layer provided a binding surface for the photosensitive resin described in the next portion of this section, and the enamel backing served to protect the copper during transport and storage. A less convenient alternative to mirror glass would have been to coat plain glass with copper in a high-vacuum chamber by evaporation.

A 5 X 8 inch (12.7 X 20.3 cm) piece of mirror glass was prepared for coating with resin by first placing it, enamel side up, in a hot 50% by weight solution of NaOH to remove the protective backing. The solution was kept as hot as possible without actually boiling (approximately 90° C). During the next 5-10 minutes, the integrity of the enamel was tested by gentle scraping with teflon tongs. When the backing scratched easily, the mirror was taken from solution and the enamel was removed from the plate by gentle rubbing with a Viton-gloved hand under a stream of hot tap water. If the plate was left for greater times in solution, the backing slid off easily with no rubbing necessary; however, for these longer soaking times, the NaOH slightly corroded the copper beneath the enamel layer. If any enamel was left on the plate after the rinse, the affected portion was reinserted into the solution for a short time and then re-rinsed. Some experimentation was necessary to find a brand of mirror with enamel (Willard mirror glass, for instance) that could be removed completely and easily. After the backing was removed, the plate was rinsed with distilled water and dried in an 80° C oven (Figure 8-3).

Pattern Exposure and Development

Kodak Thin Film Resist (KTFR), an ultraviolet-sensitive resin, was used to transfer the pore-network pattern to the mirror surface. In a darkened room, 1 part KTFR by volume to 2 parts xylenes were mixed. A mirror plate stripped of its protective backing was held horizontally, copper side up, and coated with

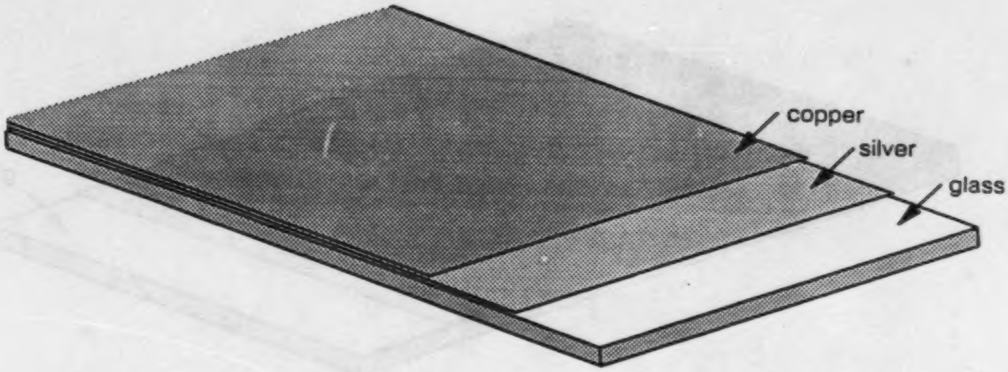

FIGURE 8-3. **Mirror with enamel removed to reveal copper surface.**

approximately 10 ml of resist mixture. The plate was tipped in various directions to evenly distribute the resin over the copper surface in a layer of uniform thickness (see Figure 8-4). The plate was tilted vertically and allowed to air dry until the coating was no longer sticky to the touch (generally 20-30 minutes). If long HF etching times were expected, the plate was baked in an 80° C oven for 10 minutes to help the resin adhere to the copper surface. The disadvantage of baking was that the resin was difficult to remove in later steps. Unused coated plates were stored in a dark place.

After the coating was dry, the patterned transparency was placed emulsion-side down on the coated mirror surface, covered with a clear piece of glass to ensure good contact between the pattern and the surface, and placed under a 1600 microwatt per centimeter long-wave ultraviolet light source at a distance of 24.5 cm. The assembly was exposed to the UV source for approximately 12 minutes as illustrated in Figure 8-5.

Exposure times were found to be a function of the thickness of the resin coating, the intensity of the light source, and the distance of the light source from the plate. A thick coating (an undiluted KTFR

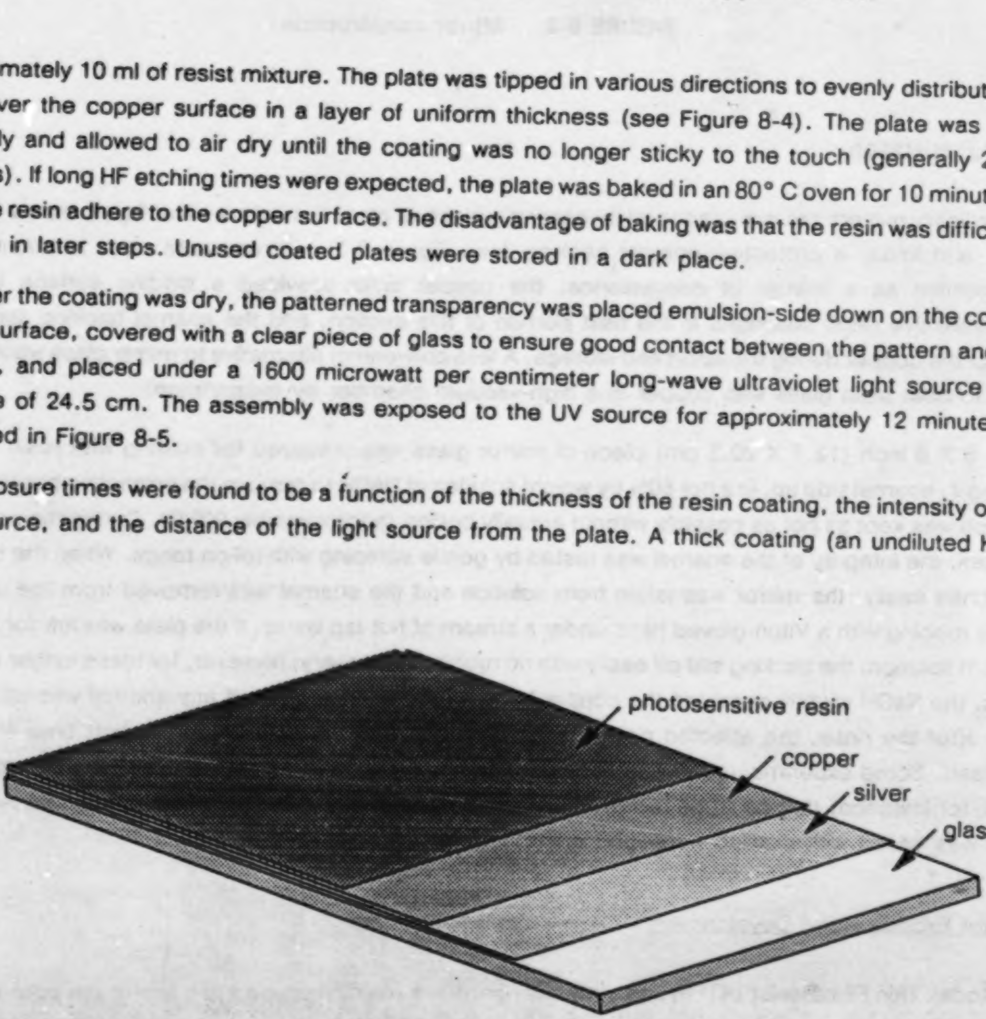

FIGURE 8-4. **Copper surface coated with Kodak Thin Film Resist (KTFR).**

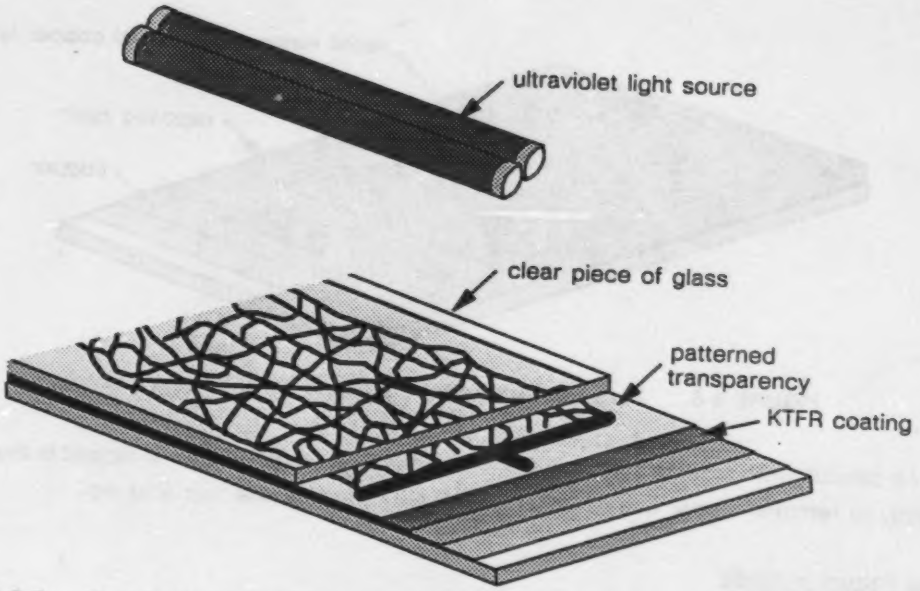

FIGURE 8-5. **Pore-network pattern exposed with UV light onto coated copper surface.**

mixture) better protected the non-pore areas from HF during the etching step but required greater exposure times than for a thin coating. However, thin coatings made by diluting KTFR with xylene reproduced fine details more faithfully and required smaller exposure times than for thick resist layers. It was also found that exposure time decreased with a shortened distance between the light source and the model, and with increased intensity of the light source. Exposure times were also affected by the age of the resin: the older the bottle of KTFR, the longer the exposure times needed (it requires months of aging on shelf to increase exposure times).

When the exposure was complete and while the room lights were still dim, the plate was removed from under the UV light and the surface was sprayed with xylene. The plate was tipped back and forth for about 1 minute to wash away the undeveloped resist representing the pore-network pattern (see Figure 8-6). The plate was rinsed with warm tap water, then distilled water, after which the normal room lighting was restored. If the pattern was not visible, more xylene was applied, and the plate was rinsed again. The plate was shaken to remove excess water droplets and was placed in an 80° C oven for 10 minutes. The plate was removed and cooled before the next step.

Etching Copper

The cooled model was placed in a 50% by weight solution of HNO_3 for approximately 10 seconds, or until the copper and silver layers unprotected by resist (the pore-network pattern) had dissolved to reveal the underlying glass surface, as illustrated in Figure 8-7. The plate was rinsed quickly with cold tap water and then with distilled water. After the plate had been dried in an 80° C oven, the pattern was examined under a microscope for imperfections. Small undissolved portions of the network were

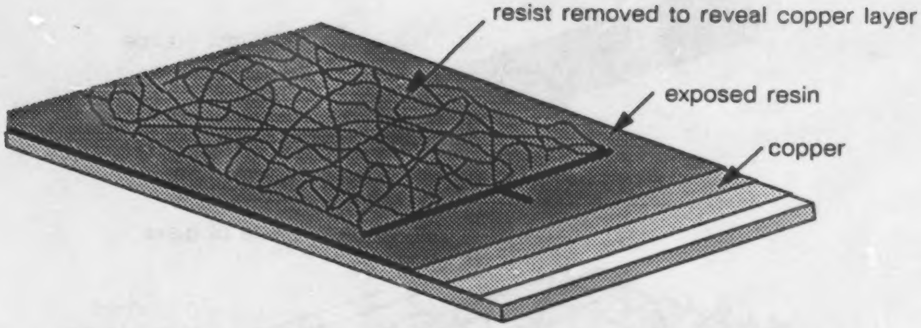
resist removed to reveal copper layer
exposed resin
copper

FIGURE 8-6. **Pore-network pattern exposed on the resin coating.**

removed carefully with a dental tool or scriber. If necessary, the plate was re-dipped in the HNO_3, then re-rinsed, to remove copper and silver left in the network after the first acid dip.

Etching Pattern in Glass

All areas of glass that were to remain unetched, such as the model edges and back, were coated with excess resist mixture and allowed to dry. The model was placed pattern-side up in a tray of concentrated HF for about 15 minutes. Longer etching times were used for models requiring deeper pores. When the model was removed from solution, it was promptly rinsed in cold water, and the network was scrubbed with a wire brush to remove siliceous deposits formed during etching. The resist was removed with a razor blade, the copper and silver with HNO_3, and the model was washed with detergent, rinsed with distilled water, and allowed to dry.

Model Assembly

A mirror-image micromodel half was produced by the above methods using a mirror-image transparency. Inlet and outlet ports were drilled with a diamond drill bit in the reservoir areas of one of the

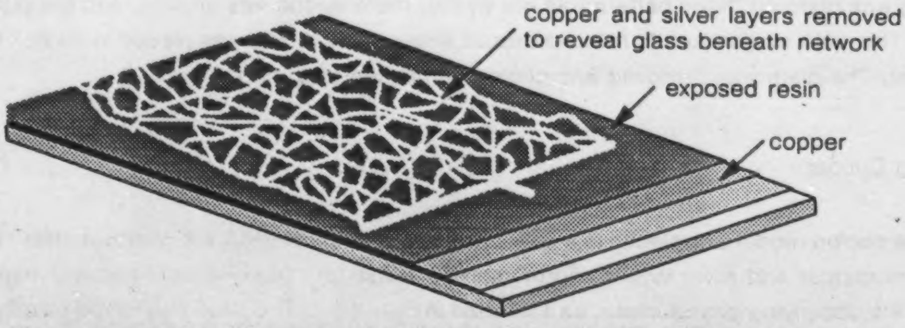
copper and silver layers removed
to reveal glass beneath network
exposed resin
copper

FIGURE 8-7. **Copper and silvers layers under the pore network pattern removed to reveal the underlying glass plate.**

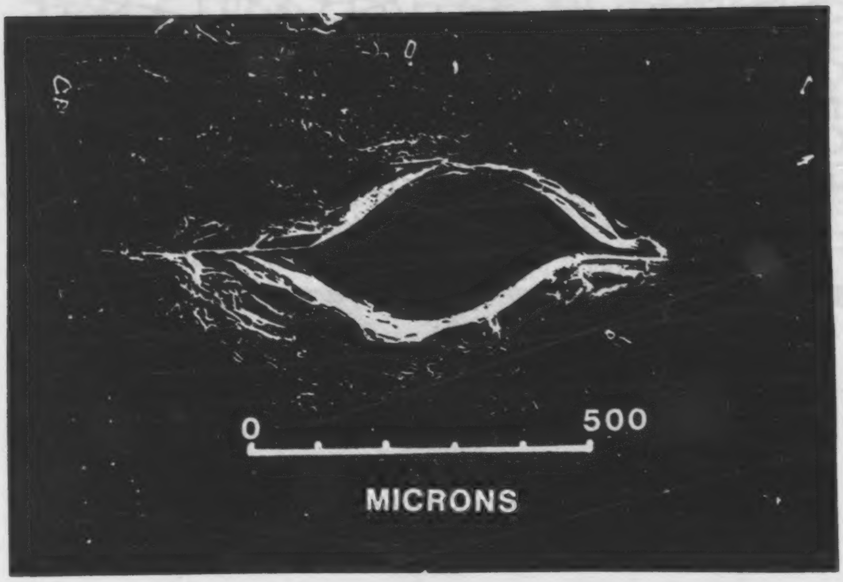

FIGURE 8-8. **SEM photomicrograph of the cross-section through a typical pore within a micromodel.**

plates. The two halves were aligned under a microscope, and cyanoacrylate glue was wicked in between the plates from the edges to temporarily hold them together. The model was placed in a muffle furnace and fused at 720° C for 15 minutes. Longer fusing times resulted in smoother, smaller pores; however, if a model was left too long in the furnace, some of the pores closed and the network became disconnected.

A completed micromodel has pores that are eye-shaped (see Figure 8-8). During multi-phase displacements, the most wetting phase tends to preferentially fill the wedges on either side of the pore. We believe that this mimics behavior in natural soils, in which the wetting phase tends to remain as pendular rings at grain-to-grain contacts.

MICROMODEL EXPERIMENTAL PROCEDURE

In the two-phase micromodel experiments, as in the two-phase short column experiments, an initially water-saturated and degassed micromodel was flooded with Soltrol at a prescribed rate to simulate the movement of an organic liquid into the saturated zone. After the fluid saturations stabilized, the model was flooded with water at low velocity. The organic liquid still in the model after water injection remained as residual saturation 'blobs': immobile and disconnected pockets of organic liquid which have been trapped by capillary forces. The two-phase experiments represented a scenario in which an organic liquid percolated into the saturated zone, then was displaced by ambient groundwater flow, and finally was left behind as residual organic liquid saturation.

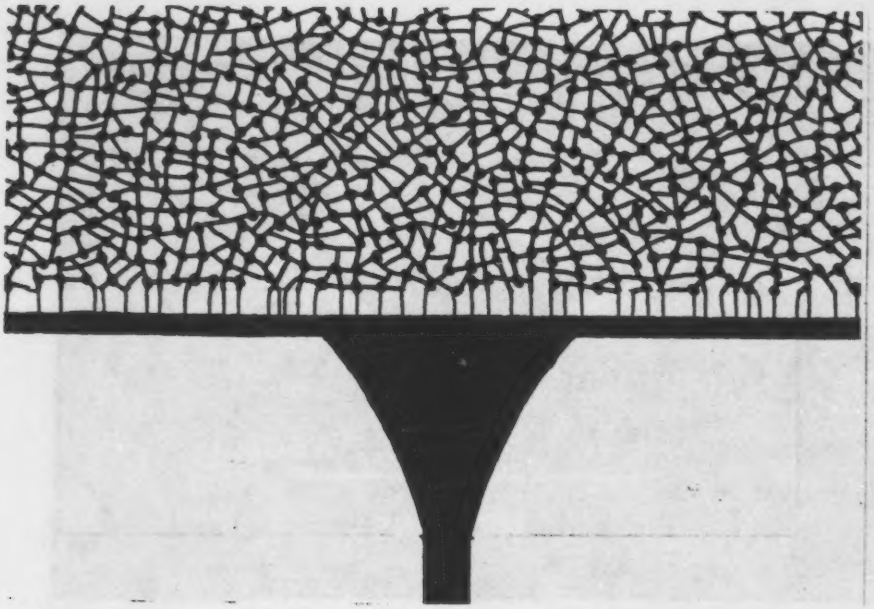

FIGURE 8-9. **Photograph of network pattern showing the capillary barrier built into one end of a micromodel.**

In the three-phase experiments, an initially water-saturated micromodel was drained with air under an applied suction. The magnitude of the applied suction determined the water saturation remaining in the model. Organic liquid was then injected into the column under low-flow conditions, simulating the infiltration of organic pollutants into the vadose zone. After equilibrium conditions were reached, the organic liquid was again drained with air. The three-phase experiments represented a scenario where an organic liquid percolated through the vadose zone to the water table, leaving behind trapped organic liquid.

During flooding or drainage, a capillary end effect was sometimes observed at the bottom of the model (see Figure 9-2a, for example). A cure to this problem was developed rather late in this study. The pore-network pattern was altered so that it included a series of small pores in one of the end reservoirs, as illustrated in Figure 8-9. These small pores served as a capillary barrier, a function equivalent to that of the nylon filters described in Sections 5 and 7. Only some of the three-phase experiments were run with these capillary barriers in place.

Fluid Preparation

The fluids used in the micromodel experiments were air, water, and Soltrol-130. The aqueous phase was prepared by combining 10 milliliters of blue food color with one liter of distilled water. The water was degassed. The organic phase was prepared by combining 0.90 grams Oil Red O with one liter of Soltrol-130, and then by straining the mixture through a coarse paper filter. The micromodels were cleaned with chromic acid, thoroughly rinsed with distilled water, and were saturated with the aqueous phase prior to the experiments.

Two-Phase Experimental Procedure

The micromodels were initially saturated with water by connecting each one to a circulating pump and a reservoir of the aqueous phase as shown in Figure 8-10a. Water was then flushed through the model until all entrapped air was removed. Then, Soltrol was injected at a prescribed rate into each model with a Sage Instruments model 351 syringe pump. After the fluid saturations stabilized, the syringe pump flow direction was reversed and the model was flooded with water. Capillary forces trapped the remaining organic liquid as immobile, disconnected blobs.

Micromodels were oriented either vertically or horizontally during the two-phase experiments. For vertically-positioned micromodel experiments, the syringe pump was connected to the top fitting of the model and was flooded with Soltrol from the top to the bottom (Figure 8-10b). In the horizontally-oriented experiments, the syringe pump was arbitrarily connected to the left fitting, and Soltrol was flooded into the model from left to right (Figure 8-10c). The pore networks shown in Figure 8-1 and in Figures 8-12 and 8-13 were run vertically. The network in Figure 8-13 was run in both the horizontal and vertical positions. Micromodels based on other patterns were prepared, but results from those experiments are not presented in this report (see, eg, Conrad *et al.*, 1989).

Three-Phase Experimental Procedure

As in the two-phase experiments, the micromodels in the three-phase experiments were de-aired with a circulating pump. With the model positioned vertically, the micromodel was drained with air under a suction applied by the syringe pump, which had been connected to the bottom fitting (Figure 8-11a). After the syringe pump had been removed and re-attached to the model's top fitting, organic liquid was

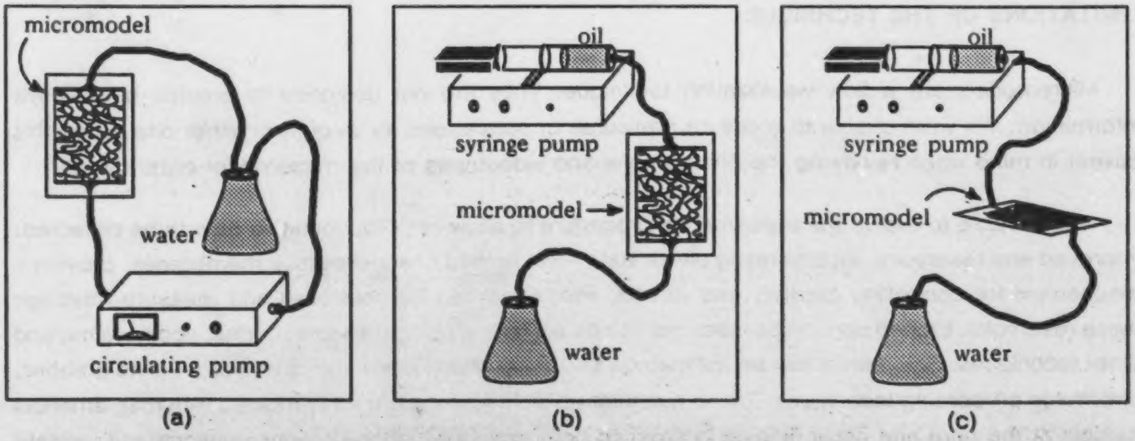

FIGURE 8-10. Two-phase micromodel experimental set-up.

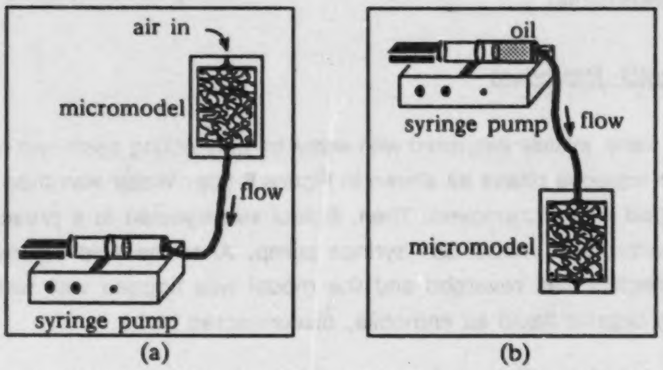

FIGURE 8-11. Three-phase micromodel experimental set-up.

introduced into the top of the model to simulate the infiltration of an organic liquid into the unsaturated zone (Figure 8-11b). After equilibrium conditions were reached, that is, after the fluid saturations stabilized, the syringe pump was re-attached to the bottom fitting and the micromodel was once again drained with air.

Although we had a desire to control fluid pressures in each of the phases during this experiment, we were not able to develop a cost effective apparatus to do so. We attempted to place various wetted porous membranes in the model to control the pressures and eventually perfected this technique using narrowly etched channels. This improvement came late in the project and we will exploit it in future work. Glass bead pack micromodels, glued together with epoxy, would present no such problem, but it is more difficult to make visual observations in them than in the etched glass micromodels. There is also the issue of the competing wetting properties of the glass and the epoxy that holds the beads together.

LIMITATIONS OF THE TECHNIQUE

Micromodels are a flow visualization technique. They are not designed to provide quantitative information. We were unable to measure pressures or saturations, or to control either one. Keep this caveat in mind when reviewing the photographs and videotapes of the micromodel experiments.

It is possible to evolve the experimental procedure to allow semi-quantitative data to be collected. Improved end reservoirs, incorporating oil- or water-wet etched channel porous membranes, provide a mechanism for controlling capillary end effects. Pressures can be controlled and measured through these reservoirs. Etched pore cross-sections can be estimated using measurescopes, epoxy casts, and other techniques. Saturations can be estimated using a high resolution video camera, a frame grabber, and image processing techniques. These quantitative techniques could be combined with mathematical models at the pore and network level in order to help explain experimental observations and validate theoretical models.

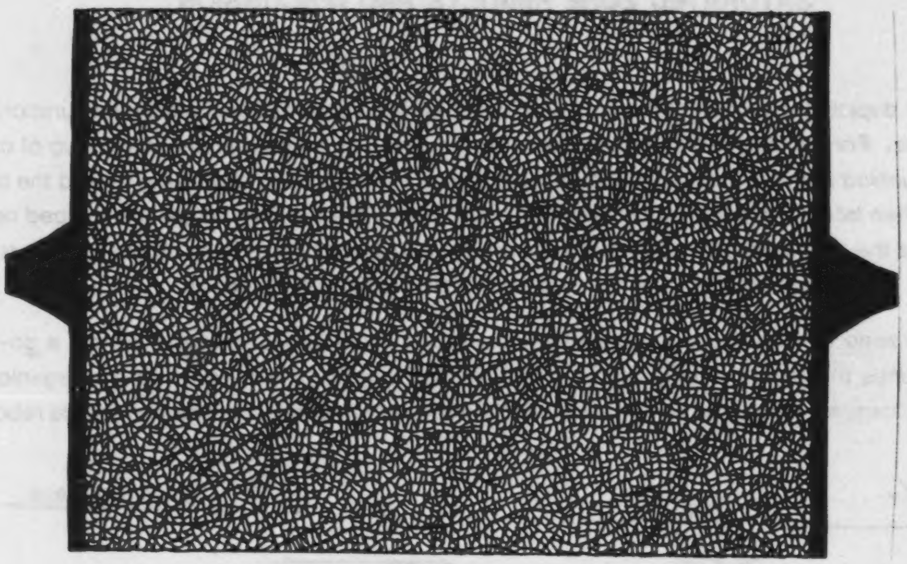

FIGURE 8-12. Pore-network pattern for the 'aggregated' model.

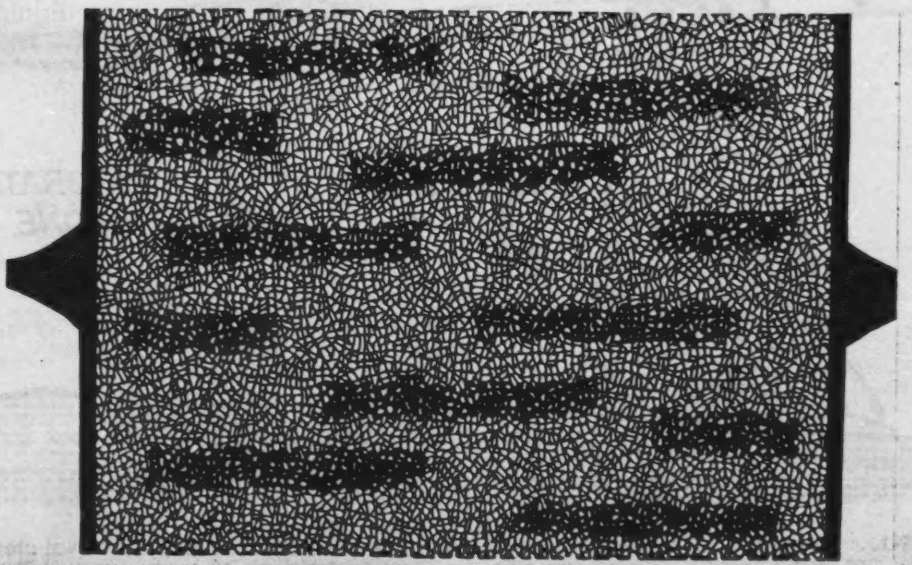

FIGURE 8-13. Pore-network pattern for the heterogeneous 'coarse lens' model.

SECTION 9

SATURATED ZONE RESULTS AND DISCUSSION

Figure 9-1 depicts the portion of the aquifer that includes the organic liquid residual saturation in the saturated zone. For an organic liquid more dense than water (left below), an incoming slug of organic liquid leaves behind a trail of capillary trapped residual as it makes its way downward toward the bottom barrier, and then laterally along that barrier. Within and below the capillary fringe the trapped residual organic shares the pore space only with water. In the saturated zone there is no air phase. The residual organic liquid in the saturated zone is the subject of this section of the report.

Saturated zone residual is also found when an organic liquid less dense than water, a so-called 'floater', reaches the capillary fringe and water table (right below). The weight of the organic liquid depresses the capillary fringe and water table, and then redistributes laterally. The water table rebounds,

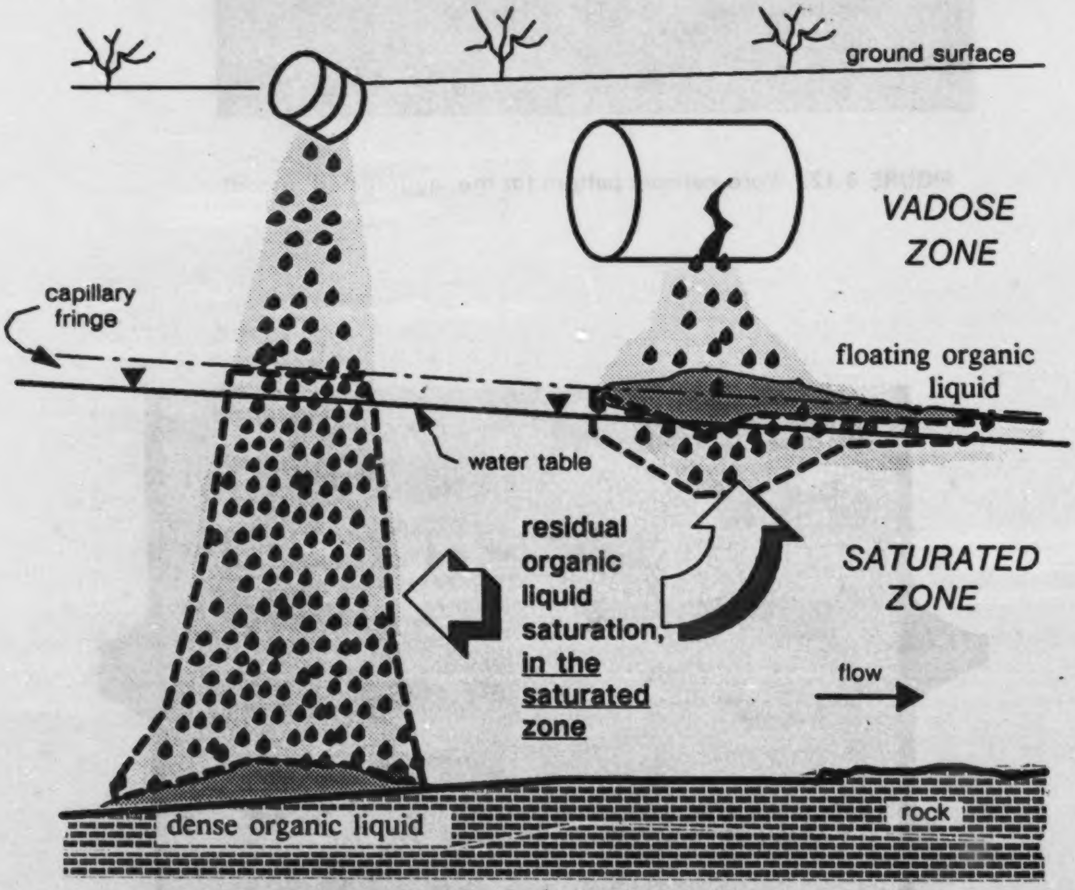
ground surface
VADOSE ZONE
capillary fringe
floating organic liquid
water table
residual organic liquid saturation, in the saturated zone
SATURATED ZONE
flow
dense organic liquid
rock

FIGURE 9-1. **Schematic of residual organic liquid trapped in the saturated zone. Not clearly shown is the residual organic liquid trapped in the capillary fringe portion of the saturated zone.**

and some organic liquids are left behind, within the saturated zone that is defined by the capillary fringe and below. A third possibility for the capillary trapping of residual organic liquids in the saturated zone is also associated with a 'floater'. As the water table rises in response to recharge or other hydrologic controls, some of the 'floater' is trapped and remains behind.

This section on organic liquid movement and capillary trapping in the saturated zone contains eight main parts:

- $\bullet_1$ review of basic concepts, capillary trapping mechanisms, petroleum experience, and mobilization issues,
- $\bullet_2$ flow visualization of displacement and capillary trapping in a micromodel,
- $\bullet_3$ capillary trapping and residual saturation in an unconsolidated soil: the Sevilleta sand,
- $\bullet_4$ residual saturations for various organic liquids,
- $\bullet_5$ residual saturations for various soils,
- $\bullet_6$ influence of the rate of initial organic liquid invasion on irreducible water saturation and organic residual saturation,
- $\bullet_7$ influence of the rate water flow rate on residual organic liquid mobilization, and
- $\bullet_8$ residual saturations in heterogeneous soils.

The first part is a brief review of background information, including a brief discussion of published experiments on sandstones and glass beads. Next, is the description of displacement and capillary trapping in a homogeneous micromodel. It visually illustrates many of the issues that are raised in the review. Third, we present the results of our study of the Sevilleta sand, including quantitative measurements of Soltrol residual, and photomicrographs of blob and pore casts. We examine the hypothesis that the Sevilleta sand should exhibit a behavior more like that of glass beads, than that of sandstone. In the fourth part we test the hypothesis that residual saturation is largely independent of organic liquid composition, by making measurements for a variety of single and multi-component organic liquids. Next, we examine residual saturations in a variety of soils, and test the hypothesis that residual saturations should be similar in soils that have a similar grain size distribution. Sixth, we investigate how the rate of initial invasion of a non-wetting organic liquid may influence irreducible water saturations and, later, organic residual saturations. Seventh, we study the possible hydraulic mobilization of residual organic liquid, by increasing groundwater velocities. We validate Wilson and Conrad's (1984) conclusion that this is largely an unrealistic aquifer remediation alternative, unless interfacial tensions are reduced significantly. Eighth and last, we investigate the hypothesis that porous media heterogeneity can dominate displacement and trapping mechanisms. We present flow visualization results from micromodels representing 1) an aggregated soil (strings of interconnected macropores separating clumps of micropores), and 2) a soil with discontinuous stringers (lenses of coarse pores within an otherwise homogeneous model). The character of these displacements are contrasted with homogeneous displacements. The discontinuous stringers experiments were duplicated in short column studies, yielding both pore casts of the trapping in a heterogeneously packed sand column, and quantitative measurements of increased trapping. The micromodel and column results are supported by a new theoretical model. Based on the interplay between viscous and capillary forces, this model explains why the trapping is strongly dependent on fluid flow rate when there are discontinuous stringers or related heterogeneities.

The discussion of our results includes special paragraphs that address implications for various aspects of groundwater contamination characterization and remediation. Not surprisingly, these paragraphs are labeled *'Implications for ...–'*.

REVIEW OF CAPILLARY TRAPPING PHENOMENA IN POROUS MEDIA

Capillary trapping of oil during displacement by water has been studied for years in the context of petroleum recovery from oil reservoirs. A very few examples of this large literature are: Anderson, 1988; Chatzis *et al.*, 1984, 1988; Craig, 1971; Hornof and Morrow, 1988; Melrose and Brandner, 1974; Mohanty *et al.*, 1980; Moore and Slobod, 1956; Morrow, 1979;, 1894; Morrow and Songkran, 1981; Morrow and Chatzis, 1982; Ng *et al.*, 1978; Pathak *et al.*, 1982; Salathiel, 1973; Taber, 1969,1981; and Yadav *et al.*, 1987. These authors are primarily concerned with the mechanisms of oil trapping during a waterflood. Capillary trapping of residual oil leads to a reduction of economic oil recovery. Some enhanced oil recovery techniques are largely aimed at reducing the amount of capillary trapped residual, by changing miscibility (eg, a CO_2 flood) or interfacial tensions (eg, a surfactant flood). In groundwater hydrology we too are concerned with the capillary trapping of residual saturation, and with its removal. The review given below focuses on these two issues. However, unlike petroleum engineers, we are also concerned with the mechanisms that initially brought the 'oil' into the aquifer in the first place. In the 'oil patch' that is the province of petroleum geologists, and it involves issues that are quite different than ours. Consequently, we can expect little help from the oil patch on these mechanisms.

There were three major forces acting in both oil recovery, and in organic liquid behavior in groundwaters: **capillary forces, viscous forces,** and **gravity or buoyancy forces.** Capillarity is the result of the interplay of cohesive forces within each fluid phase, and the adhesive forces between the solid phase and each of the fluids. The capillary force is proportional to the interfacial tension at the fluid-fluid interface and the strength of fluid wetting to the solid surface, and inversely proportional to the pore size. Viscous or dynamic forces are proportional to the permeability and to the pressure gradient, while buoyancy is a gravitational force proportional to the density difference between the fluids. For multiple fluid phases in an aquifer at typical aquifer flow rates, capillary forces often dominate over viscous and buoyancy forces. As we shall see, the dominance of capillarity explains the trapping of residual organic liquid.

The review starts by assuming that there is an oil or organic liquid saturated porous medium (with some residual water saturation), with the organic liquid being displaced by water. As the water flood progresses through the medium some of the organic liquid is trapped by capillary forces and remains behind as residual. We first review the fundamental concepts of interfacial tension, wettability, and capillarity. Then we examine the two major mechanisms for capillary trapping when two fluid phases are present: snap-off and by-passing (Mohanty *et al.*, 1980; Chatzis *et al.*, 1983; Wilson and Conrad, 1984).

We then review some of the published experimental measurements for residual oil saturations, as measured for sandstones and glass beads by petroleum researchers. Finally, we review the relative role of viscous, gravity and capillary forces in the mobilization of residual.

Fundamentals

Interfacial Tension (after Adamson, 1982) —

In the interior of a homogeneous fluid, a molecule is surrounded on all sides by other like molecules exerting cohesive forces between one another. At the interface between two immiscible fluids however, there are few if any like molecules across the interface. A molecule at the interface is attracted to molecules of its own phase by a force greater than the force attracting it to molecules of the 'immiscible' phase across the interface. The cohesive forces acting on a molecule inside a fluid phase, and on a molecule at the interface (liquid-gas or liquid-liquid) between fluid phases are illustrated in Figure 9-2a. This unbalanced force draws molecules along the interface inward and results in the tendency for the fluid-fluid interface to contract. If the interface is stretched, it acts like an elastic membrane. The restoring force seeking to minimize the interfacial area between the two immiscible fluids, is called the interfacial tension, σ . When encountered between a liquid and a gaseous phase, this same force is called the surface tension, γ .

Wettability —

Figure 9-2b illustrates a possible configuration of two immiscible fluid phases in contact with the solid phase (walls) of a cylindrical tube. At the line of contact where the two fluid phases meet the solid phase, both the cohesive forces within the fluids and the adhesive forces between the solid and each of the fluids are at work. Suppose that one of these fluid phases is water (fluid 1), and the other is an organic liquid (fluid 2). If the adhesive forces between the solid and the water phase are greater than the cohesive forces inside the water itself, and greater than the forces of attraction between the organic phase and the solid, then the solid-water contact angle, θ , will be acute and the water will 'wet' the solid (Hillel, 1980, p.44). The contact angle provides the only direct measurement of wettability. As an example of a contact angle, on clean glass liquid water forms an acute contact angle θ of about 25.5° in the presence of air. Water is a strong wetting fluid relative to air for this surface, but not necessarily for other surfaces, such as TFE (tetrafluoroethylene). Further discussion of wettability can be found in Section 4 of this report.

Capillarity —

As a result of the contact angle, a meniscus is formed between the fluid phases (Figure 9-2b). The narrower the tube, the smaller the radius of curvature. Similar to the curvature produced by a pressure difference across a membrane, the presence of curvature implies a pressure difference across the fluid-fluid interface, called the capillary pressure:

$$P_c = P_{nw} - P_w = \sigma C = \frac{2\sigma}{r_c} = \frac{2\sigma \cos\theta}{r_t} \qquad (9\text{-}1)$$

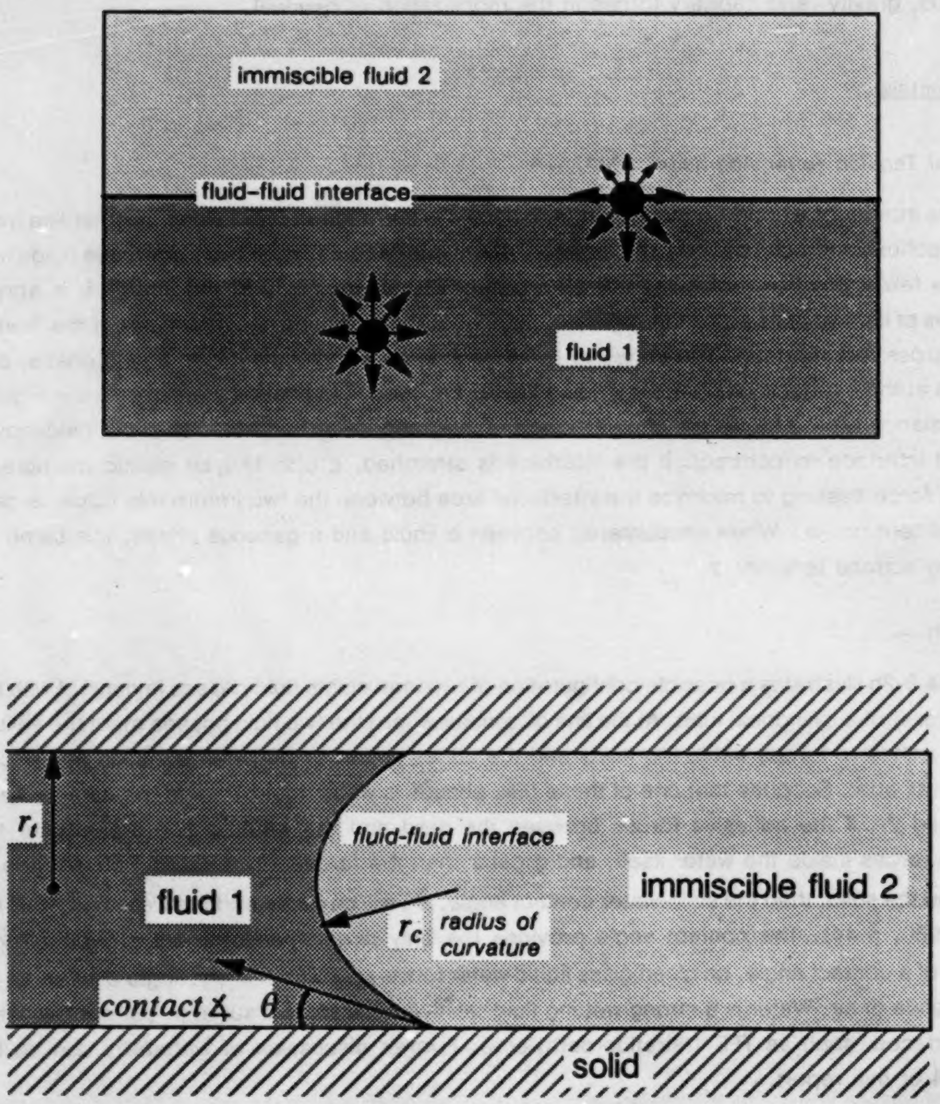
immiscible fluid 2
fluid-fluid interface
fluid 1
r_t
fluid-fluid interface
fluid 1
immiscible fluid 2
r_c radius of curvature
contact ∡ θ
solid

FIGURE 9-2. **Two sketches illustrating fundamentals: a) cohesive forces acting on a molecule inside a fluid and at its interface with another, immiscible fluid (after Hillel, 1980); and b) hydrostatic equilibrium of two fluid phases in contact with a solid phase (after Melrose and Brandner, 1974).**

where: P_c = capillary pressure

P_w = pressure in the wetting phase (fluid 1 in the figure)

P_{nw} = pressure in the non-wetting phase (fluid 2 in the figure)

σ = fluid-fluid interfacial tension

C = curvature of the fluid-fluid interface

r_c = radius of curvature

θ = contact angle, measured through the wetting fluid

r_t = radius of capillary tube

The most common example given to illustrate capillarity is that of the capillary rise of water in a straight thin tube, or straw (see Figure 9-3). The pressure difference between the wetting and non-wetting fluid, at the interface inside the tube, causes the water to rise into the tube, above the level of the free surface.

These same forces operate on the pore scale in saturated, and unsaturated, porous media. The capillary fringe is a notable example. Also, the interplay of the various wettabilities and interfacial tensions of different fluids, and the capillary forces they give rise to, leads to trapping of fluids within pores, as the fluids migrate through, or drain out of, a system. These capillarity induced trapping mechanisms are discussed below.

Capillary Trapping Mechanisms

When two fluid phases are present, and the non-wetting fluid is being displaced by the wetting fluid, there are two major mechanisms for capillary trapping: snap-off and by-passing.

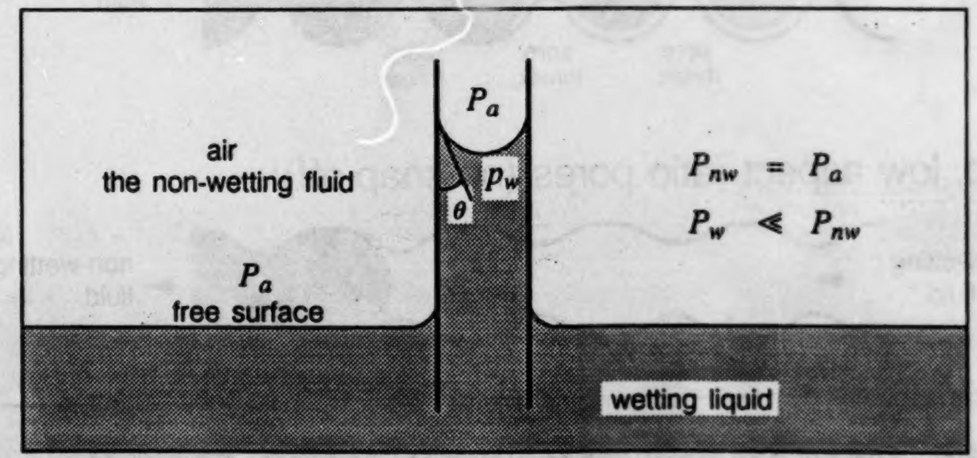

FIGURE 9-3. Capillary rise in a slim tube.

Snap-off —

Snap-off occurs as non-wetting fluid in a pore is displaced from a pore body into a pore throat. The mechanism strongly depends on wettability and the aspect ratio — the ratio of pore-body diameter to pore-throat diameter (Wardlaw, 1982).

Consider the case of water displacing an organic liquid from a tube with a non-uniform pore diameter, as shown in Figures 9-4 and 9-5. The walls of the tube are smooth and strongly water wet. The water contact angle is acute, the water-organic liquid interface is curved, and the water phase 'wicks' along the pore wall. In high aspect ratio pores, the pore throats are much smaller than the pore bodies (Figure 9-4a and Figure 9-5). When the thin layer of water phase reaches the exit pore throat, a large blob of organic liquid still remains in the pore (Figure 9-5). Snap-off occurs as the water continues through the exit throat leaving behind the now disconnected singlet blob. In a sequence of high aspect ratio pores, a singlet blob is trapped by snap-off in each pore (Figure 9-4a). Pores in a pack of uniform sized glass beads have a high aspect ratio, explaining the prevalence for singlet blobs observed by Morrow and Chatzis (1982) and Chatzis et al. (1988). For low aspect ratio pores, in which the pore throats are almost as large as the pore bodies, the organic fluid can be completely displaced, as shown in Figure 9-4b.

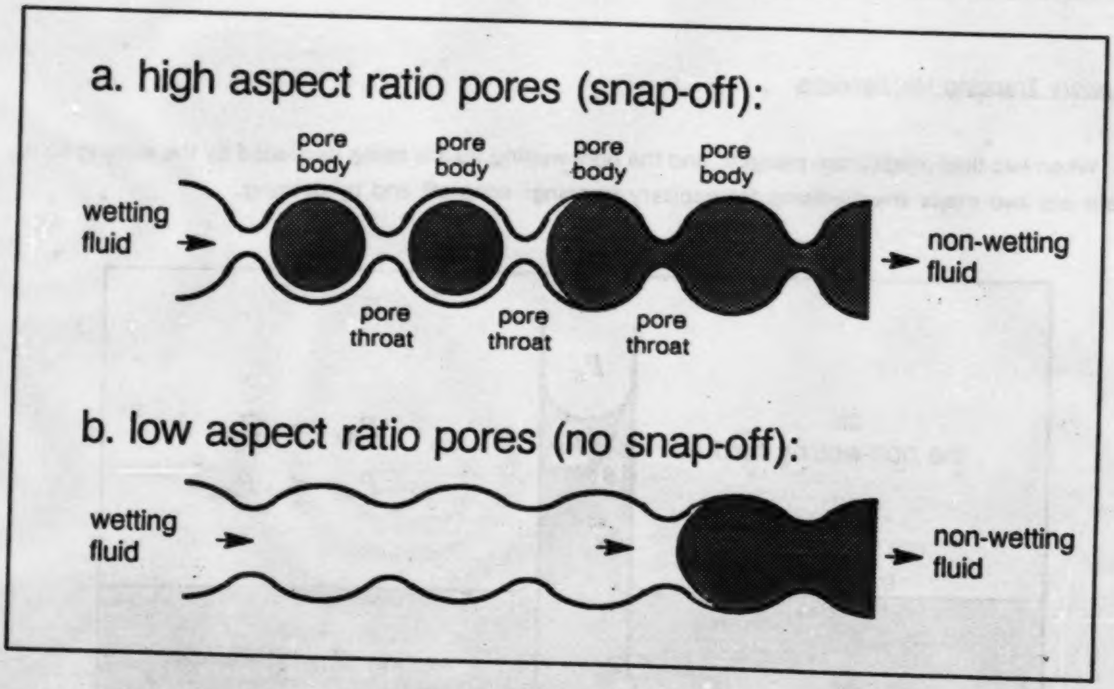
a. high aspect ratio pores (snap-off):
pore body
pore body
pore body
pore body
wetting fluid
non-wetting fluid
pore throat
pore throat
pore throat
b. low aspect ratio pores (no snap-off):
wetting fluid
non-wetting fluid

FIGURE 9-4. **Effect of pore aspect ratio on organic liquid trapping in a tube of non-uniform diameter (after Chatzis et al., 1983).**

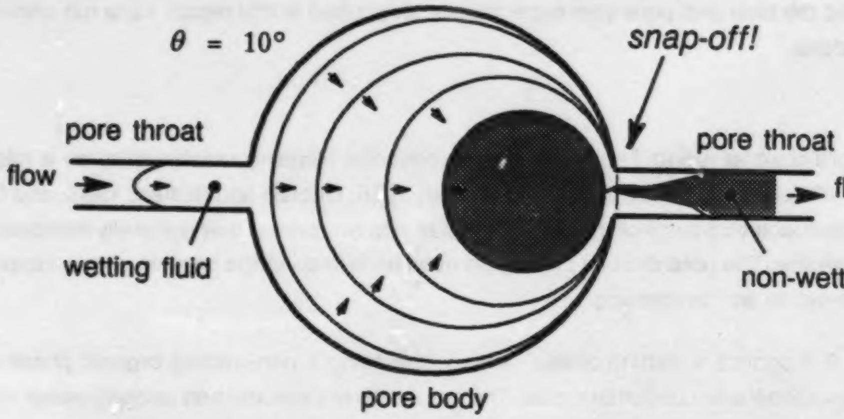
θ = 10°
snap-off!
pore throat
flow
wetting fluid
pore throat
flow
non-wetting fluid
pore body

FIGURE 9-5. **Wetting fluid displacing a non-wetting fluid from a circular, high aspect ratio pc under strongly wet conditions (after Wardlaw, 1982).**

Trapping is a function of wetting and contact angle as well as pore geometry. The combined effect of contact angle and pore geometry control the curvature of a fluid-fluid interface and determine the potential for snap-off (Wardlaw, 1982). Figure 9-6 depicts an interface with a 90 degree contact angle passing from a pore throat through a high aspect ratio pore body with smooth walls. The intermediate contact angle of 90° causes the curvature of the interface to remain relatively small. As the interface reaches the exit throat, little organic phase remains in the pore and no trapping occurs (Wardlaw, 1982). In rough walled pores, there is probably some trapping of the retreating phase in the

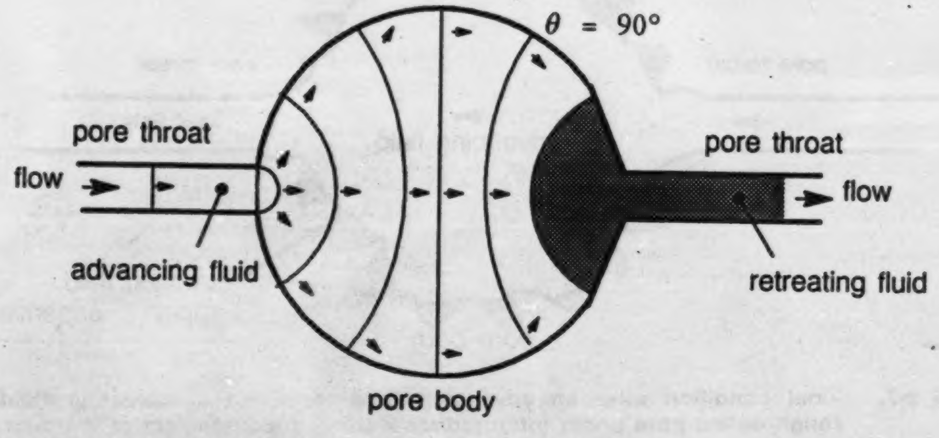
θ = 90°
pore throat
flow
advancing fluid
pore throat
flow
retreating fluid
pore body

FIGURE 9-6. **One fluid displacing another from a circular, high aspect ratio pore, under intermediate wetting conditions (after Wardlaw, 1982).**

asperities along the wall (see Figure 9-7). Photomicrographs of the Sevilleta sand (Figure 4-6) and its pore casts (shown later in this section) indicate that this material had smooth walls. In any event all of the micromodels, and the blob and pore cast experiments, described in this report were run under strongly water wet conditions.

By-passing —

The pore doublet model has been used to describe trapping mechanisms on a microscopic scale (Rose and Witherspoon, 1956; Moore and Slobod, 1956; Chatzis and Dullien, 1983; and Chatzis et al., 1983). A pore doublet consists of a tube which splits into two pores, one generally narrower than the other, and then rejoins. The pore doublet concept is used here to describe organic phase trapping by the mechanism referred to as 'by-passing'.

Figure 9-8 depicts a wetting phase (water) displacing a non-wetting organic phase in a pore doublet under several different circumstances. The pore walls are smooth and strongly water wet. Figure 9-8a demonstrates circumstances under which no trapping occurs. The advancing water phase enters the narrower pore opening first (stage 1). In each pore, the total pressure drop driving flow is the sum of the capillary pressure and the dynamic pressure drop caused by flow (Moore and Slobod, 1956). For the pore doublet to have any physical meaning, the flow rates (and dynamic pressure drop) should be low enough to approximate aquifer conditions. On a pore scale, under such conditions, capillary forces are much larger than the dynamic viscous forces. Capillarity then controls advance of the wetting front causing water to fill the narrower pore (Chatzis and Dullien, 1983). The water-organic interface remains stable at the entrance to the wider pore (stage 2). When the water reaches the downstream node (where the pores rejoin), it forms a stable meniscus with the organic liquid because the cross-section at the downstream node is greater than at the entrance to the wider pore. In instances where a stable meniscus can be maintained at the downstream node, water can then push organic out of the wider pore (stage 3).

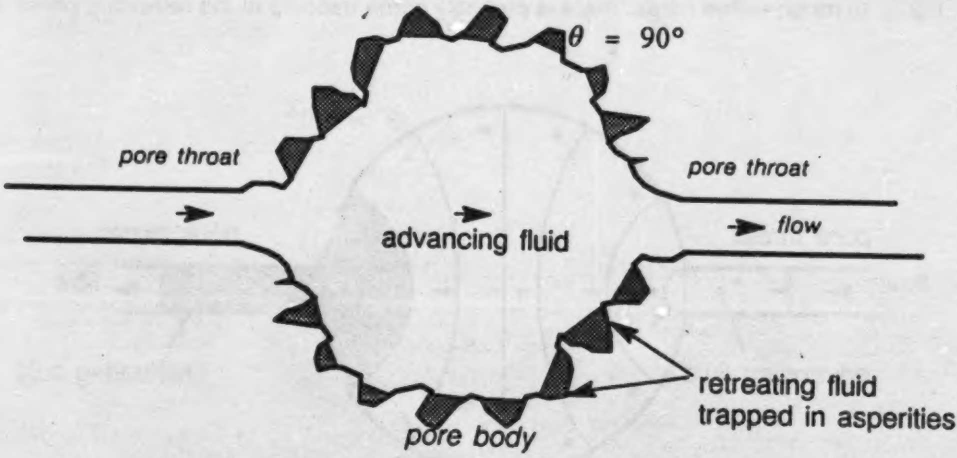

FIGURE 9-7. **Final condition after an advancing fluid displaced a retreating fluid from a rough-walled pore under intermediate wetting conditions (after Wardlaw, 1982).**

The menisci rejoin at the downstream node (stage 4). In this case, the water has displaced the organic liquid completely from the pore doublet and no trapping has occurred.

The displacement sequence for the pore doublet shown in Figure 9-8b illustrates the by-passing mechanism of trapping. As before, the water enters the narrower pore first. However, as water reaches the downstream node, it does not stop because no stable interface is formed (Figure 9-8b, stage 2). The organic liquid in the wider pore has become disconnected from the main body of organic liquid and is now unable to drain from the pore. This liquid has become 'by-passed' by the advancing water (stage 3).

Figure 9-8c uses a pore doublet model to demonstrate both snap-off and by-passing trapping mechanisms. Once again, water enters the narrower pore first (stage 1). Due to the high aspect ratio in the narrower pore, snap-off occurs (stage 2). Water continues to move through the narrower pore and through the downstream node. No stable meniscus is formed and organic liquid in the wider pore is by-passed (stages 3 and 4).

While the pore doublet model allows the organic liquid to be by-passed in at most one pore, in a porous medium the organic phase in several pores may be collectively by-passed leaving an organic blob which extends over the several pores. In contrast, blobs trapped by snap-off extend over one pore

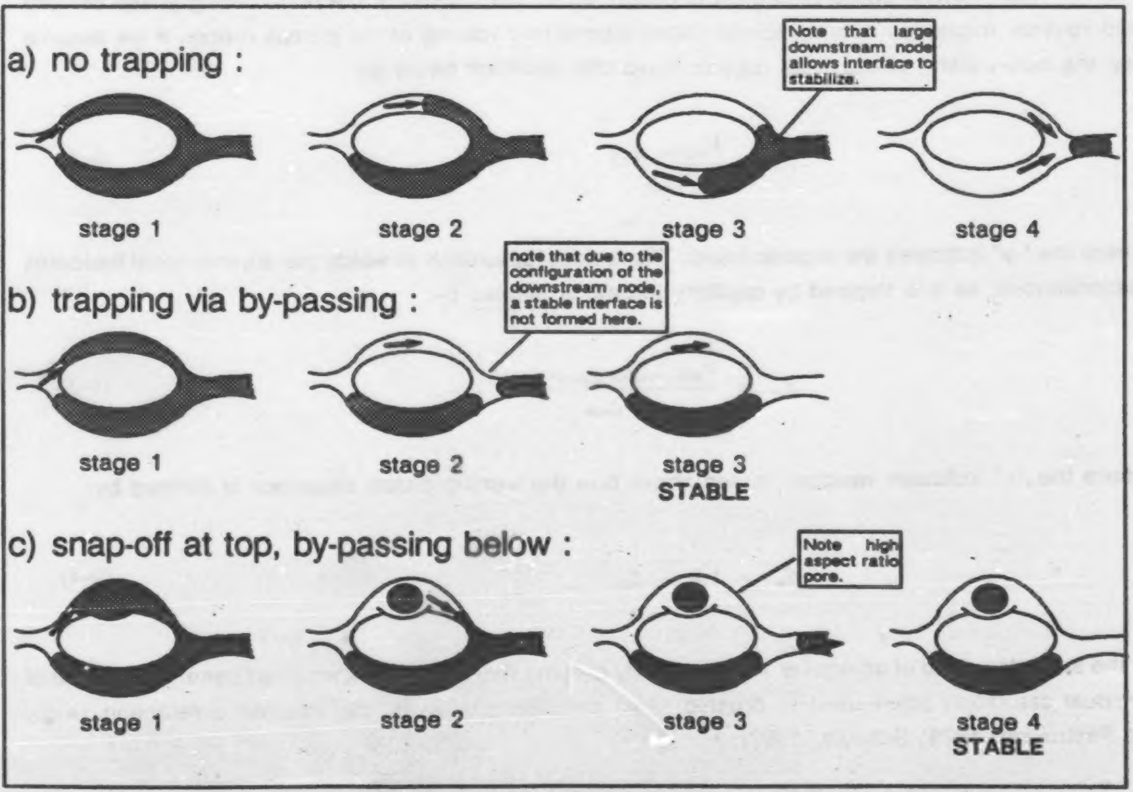
a) no trapping :
Note that large downstream node allows interface to stabilize.
stage 1
stage 2
stage 3
stage 4
b) trapping via by-passing :
note that due to the configuration of the downstream node, a stable interface is not formed here.
stage 1
stage 2
stage 3
STABLE
c) snap-off at top, by-passing below :
Note high aspect ratio pore.
stage 1
stage 2
stage 3
stage 4
STABLE

FIGURE 9-8. Sketches illustrating trapping mechanisms using the pore doublet model (after Chatzis et al., 1983)

only. As pore aspect ratio decreases, the proportion of organic liquid trapped by by-passing, relative to snap-off, increases, and blobs become larger and more complex. Soil or rock heterogeneity also encourages trapping through by-passing, as will be shown later in this section (see also Chatzis et al., 1983). Wettability, pore aspect ratio, and soil (or rock) heterogeneity are important factors influencing trapping.

Quantitative Measurements of Residual Saturation

Quantitative measurements of residual non-wetting phase saturation have been made in many petroleum reservoir cores and in glass bead packs (see, eg.: Anderson, 1988; Chatzis *et al.*, 1983, 1984, 1988; Hornof and Morrow, 1988;; Mohanty *et al.*, 1980; Moore and Slobod, 1956; Morrow, 1979;, 1894; Morrow and Songkran, 1981; Morrow and Chatzis, 1982; Morrow *et al.*,1988). In one type of experiment a core or pack is saturated with a wetting phase. Then the wetting phase is displaced by a non-wetting phase, reducing the wetting phase to its so-called irreducible saturation. Finally the non-wetting phase is displaced by wetting phase at a low flow rate (low capillary number) to yield a residual non-wetting phase saturation. Typically, water is the wetting phase and a hydrocarbon is the non-wetting phase. (Our experiments are essentially the same; see Sections 5,6,7 & 8.)

Non-wetting phase saturation is measured as the volume of the non-wetting phase per unit void volume, measured over a representative elementary volume of the porous media. If we assume that the non-wetting phase is an organic liquid this definition becomes:

$$S_o = \frac{V_{organic\ liquid}}{V_{voids}} \tag{9-2}$$

where the "o" indicates the organic liquid. The residual saturation at which the organic liquid becomes discontinuous, as it is trapped by capillary forces, is defined by:

$$S_{or} = \frac{V_{discontinuous\ organic\ liquid}}{V_{voids}} \tag{9-3}$$

where the "r" indicates residual. In two phase flow the wetting phase saturation is defined by:

$$S_w = 1.0 - S_o \tag{9-4}$$

In the saturated zone of an aquifer we can usually assume that water is the wetting phase. A measure of residual saturation often used in organic liquid pollution studies is the volumetric retention (e.g., de Pastrovich, 1979; Schwille, 1967):

$$R = \frac{liters\ of\ residual\ organic\ liquid}{cubic\ meters\ of\ soil} = S_{or} \times n \times 10^3 \tag{9-5}$$

where n is the soil porosity.

In strongly water-wet Berea sandstones, Chatzis and Morrow (1981) found residual organic liquid saturations, S_{or} , between 27% and 43%. Chatzis et al. (1988) found that the majority of the blobs in Berea sandstones were 'singlets', or 'doublet' occupying two pore bodies and the pore throat in between. The largest complex blobs, which were often branched, tended to be no larger than 10 pore bodies in size. Fifty percent of their blobs had an 'equivalent diameter' in the range of 30 to 130 microns, consistent with measured pore sizes in Berea sandstone (Wardlaw and Taylor, 1976).

In water-wet, uniformly-sized glass beads, Morrow and Chatzis (1982), Chatzis et al. (1983), and Morrow et al. (1988) found residual organic liquid saturations, S_{or} , between 14 and 16%. Bead size did not seem to make any difference, as long as the wetting phase velocity was low (low capillary number). Most of the blobs were trapped as singlets (58%), much more so than in sandstone. Once again the largest blobs measured on the order of 10 pore bodies long. Although by number there were more singlets than any other blob size, they held less than 15% of the volume of the residual saturation (see also Figure 6 in Wilson and Conrad, 1984). Blobs spanning five or more pore bodies held at least 50% of the residual, even though they constituted less than 24% of the blob numerical population.

When they sintered the glass beads (consolidated the beads by fusing them together in a furnace), Morrow *et al.* (1988) found residual organic liquid saturations, S_{or} , between 20% and 30%, although they did not feel that these numbers are reliable. The sintered beads should have better simulated the sandstone cores. The reported saturations are consistent with this hypothesis.

Residual Organic Mobilization

Consider the residual saturation of organic liquid shown in the stable pore doublets, to the right of Figure 9-8b and 9-8c. If the pressure gradient and Darcy velocity of the wetting phase are increased sufficiently, some of the trapped blobs begin to move because of an increase in the viscous force (Hornof and Morrow, 1988). This process is called mobilization. The pressure gradient must be sufficiently high to squeeze the blobs through pore throats. At the leading edge of the blob, organic liquid is displacing water (drainage), while at the trailing edge water is displacing organic liquid (imbibition). The dynamic pressure difference required to support mobilization is proportional to the difference in these drainage and imbibition capillary pressures (Melrose and Brandner, 1974).

A critical element in mobilization is the length of the blob in the direction of flow. For a fixed dynamic pressure gradient the longer blobs are easier to mobilize, because a greater pressure difference can be established across them. The amount of residual saturation reduction by hydraulic mobilization can strongly depend on how the trapped organics are distributed on a pore scale. If, for instance, many of the trapped blobs are relatively long and complex ganglia formed by by-passing, they can be more easily mobilized than if the majority of blobs are singlets resulting from snap-off. Once mobilized, blobs do not always maintain their size. The larger mobilized blobs can break up into smaller blobs, with a significant fraction being only temporarily mobilized (Chatzis *et al.*, 1984). Also, as moving blobs collide with other blobs, the blobs may coalesce (Ng *et al.*, 1978). If substantial coalescence occurs, a bank of mobilized organic liquid may form. The factors controlling blob break-up and coalescence are not, as yet, well understood.

Mobilization can be aided by a difference in density between the water and the organic liquid. If the organic liquid is lighter than water, the blob will be buoyant and tend to rise vertically. If the blob is heavier than water it will tend to sink. The vertical migration of the blob due to the density difference is resisted by the capillary forces which trapped the blob in the first place. If the hydraulic gradient can be aligned so that viscous and buoyant forces reinforce each other, their combined force may be sufficient to induce mobilization.

There are many factors that influence initial trapping and subsequent mobilization: the geometry of the pore network; fluid-fluid properties such as interfacial tension, and density ratio; fluid-soil interfacial properties which determine wetting behavior; the applied water phase pressure gradient and its alignment with gravity (Morrow and Songkran, 1981). When only two fluid phases are present these factors can be incorporated into two dimensionless numbers. The ratio of viscous forces to capillary forces is known as the capillary number, N_c , while the ratio of gravity forces to capillary forces is the Bond number, N_B :

$$N_c^1 = \frac{k \, \nabla P_w}{\sigma} \tag{9-6}$$

$$N_B^1 = \frac{\Delta\varrho \, g \, R^2}{\sigma} \tag{9-7}$$

where: k = intrinsic (absolute) permeability of soil
∇P_w = water phase pressure gradient
σ = interfacial tension between the fluids
$\Delta\varrho$ = density difference between fluids
g = acceleration of gravity
R = representative grain radius

The superscript 1 in N_c^1 refers to the version of the dimensionless number. This model of the capillary number assumes that the hydrostatic forces are negligible. The ratio of forces represented by the capillary number can also be given in terms of the Darcy velocity in the water phase (see, e.g., Taber, 1981):

$$N_c^2 = \frac{q_w \, \mu_w}{\sigma} \tag{9-8}$$

where: q_w = specific discharge (darcy velocity) of the water phase
μ_w = viscosity of water

This version of the capillary number inherently accounts for relative permeability and the gravitational (hydrostatic) portion of the driving force — the $\nabla(\varrho_w \, g \, z)$ term in the expansion of q_w :

$$q_w = \frac{k_w \, k}{\mu_w} \nabla(P_w + \varrho_w \, g \, z) \tag{9-9}$$

where: k_{rw} = relative permeability for the water phase

z = elevation of the point of interest above the datum

N_c^2 can be obtained from N_c^1 by adding in the gravity term and multiplying by the relative permeability of water. Wilson and Conrad (1984) defined a related capillary number for groundwater situations:

$$N_c^3 = \frac{k\, \varrho_w\, g\, J_w}{\sigma} = \frac{K_w\, J_w\, \mu_w}{\sigma} \tag{9-10}$$

where: J_w = hydraulic gradient in the water phase, $\nabla\left(\frac{P_w}{\varrho_w\, g} + z\right)$

K_w = water-saturated hydraulic conductivity of the soil, $\frac{k\, \varrho_w\, g}{\mu_w}$

This definition of the capillary number does not contain the relative permeability built into (9-8), but does contain the gravity term neglected in (9-6). When hydrostatics are negligible, (9-10) reduces to (9-6).

The Bond number also has at least one other version. It can be given in terms of intrinsic permeability instead of a characteristic grain size:

$$N_B^2 = \frac{k\, \Delta\varrho\, g}{\sigma} \tag{9-11}$$

Morrow and Songkran (1981) used the Kozeny-Carmen equation (Carmen, 1937) to determine an approximate relation between the two forms of the Bond number for unconsolidated media of relatively uniform grain size. This second version of the Bond number may be more convenient to use for soils having a fairly wide grain size distribution — which makes selection of a representative grain size for use in N_B^1 rather arbitrary. Although buoyancy forces can aid mobilization, the following discussion will focus on viscous forces and the capillary number, referring the reader to work by Morrow[1] and to discussions later in this section and in the next section concerning the effects of significant gravity forces.

There is a minimum viscous force needed to mobilized trapped residual. Once the viscous force exceeded this critical value the residual saturation decreases. This process can be plotted in terms of capillary number, as shown in Figure 9–9. In the figure, the residual saturation is normalized by its initial value, S_{or}^*. This is, for example, the residual saturation measured in cores, packs, or columns, under low capillary number conditions (for example, 27 to 43% in sandstones, and 14 to16% in uniform size glass beads). Above the critical capillary number, N_c^*, viscous forces begin to overcome the capillary forces resulting in a reduction of the residual saturation. Equations (9–6) and (9–10) reveal that for a prescibed gradient the critical capillary number is much easier to exceed in a large grained soil where the intrinsic permeability, k, is high ;

---

[1] Morrow, 1979; Morrow and Songkran, 1981; Morrow et al., 1985; and Hornof and Morrow, 1987.

Chatzis and Morrow (1981,1984) performed a large number of experiments using sandstone cores to explore this correlation between capillary number, N_c^1 , and organic liquid saturation, S_{or} . First a residual organic liquid saturation, S_{or}^* , was established in the cores under low Bond and capillary number conditions. Then the gradient across the core was increased in a stepwise manner, and at each step residual organic liquid production was observed. A typical S_{or}/S_{or}^* vs. N_c^1 correlation curve for the sandstone is shown as the left-hand curve in Figure 9-9. The critical capillary number at which motion was initiated was typically $N_c^{*1} \approx 2 \times 10^{-5}$ for sandstones. N_c^{**} denotes the capillary number necessary to displace all of the blobs; $N_c^{**1} \approx 1.3 \times 10^{-3}$ for sandstones. Fifty percent of the residual organic liquid is removed when $N_c^1 \approx 3 \times 10^{-4}$. The left hand correlation in Figure 9-9 holds for a wide variety of sandstones and organic fluids, provided that the organic liquid is the non-wetting fluid.

Similar experiments were performed for glass beads by Morrow and Chatzis (1982), and Morrow *et al.* (1988). Using a variety of sizes of uniform beads, and various organic liquids they obtained another correlation, in terms of S_{or}/S_{or}^* vs. N_c^2 , which is shown as the solid line in Figure 9–10. It has been translated to N_c^1 so that it can be shown as the right-hand curve in Figure 9-9. It looks nothing like the sandstone curve. A significantly larger capillary number (i.e. more gradient) is required to mobilize the blobs in uniform glass beads. This is explained by the very large aspect ratio of the bead pack pores relative to sandstones, and the dominance of capillary trapping by snap-off. Sintering the beads (melting them together slightly) reduces the aspect ratio and produces a curve much closer to the sandstone curve , as shown by the x's in Figure 9–10 (Morrow and Chatzis,1982; Morrow *et al.*, 1988). In a similar

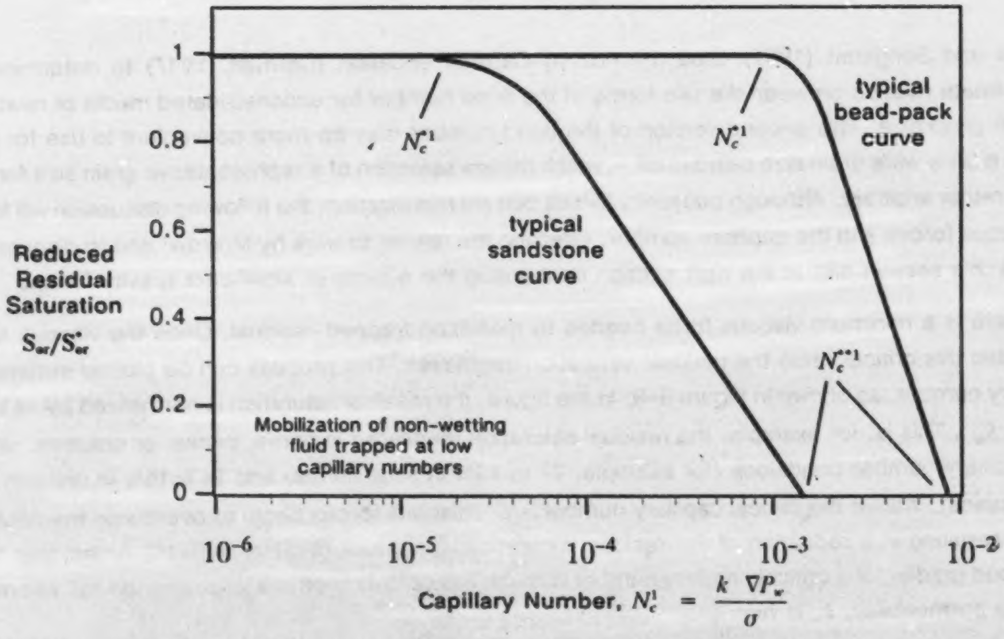

FIGURE 9-9. **Relationship between residual saturation and capillary number for sandstones and glass beads. The sandstone curve is from Chatzis and Morrow (1981,1984); the bead-pack curve is based on work reported in Morrow and Chatzis (1982), and Morrow et al. (1988).**

study using air, Morrow and Songkran (1981) found a that critical Bond number ($N_B{}^1$) of about 0.005 was needed to reduce trapping in glass beads.

Gravity and viscous forces also play a strong role in the initial capillary trapping of the organic liquid. If the wetting phase velocity is high enough, or if the density difference between fluids is large enough, the trapping mechanism is not as efficient (see, eg., Mohanty *et al.*, 1980), and less residual is trapped in the first place (Chatzis and Morrow, 1981,1984; Morrow and Songran, 1981; Morrow *et al.*, 1988). The results depicted in Figure 9-9 were developed for very low capillary and Bond number original displacements. The capillary number was then increased to mobilize the residual. Contrast this to the dashed curve Figure 9-10, which depicts glass bead experiments in which the original rate of displacement was varied over a much wider range. In this graph the reference residual saturation, S^*_{nr}, is that measured for a low capillary number original displacement. Initially displacing the continuous non-wetting fluid at a high rate, with the wetting fluid, significantly reduces the residual. Put another way, it is easier to avoid trapping residual non-wetting phase, than it is to mobilize it afterward (Morrow *et al.*, 1988). In sandstones the difference is not nearly so dramatic (see, eg., Chatzis and Morrow, 1981,1984).

In groundwater situations we may see a similar behavior with dense organic liquids as they move downward through the saturated zone, particularly in coarse grained soils (where k is high). The Bond number may be high enough to reduce the amount of initial entrapment.

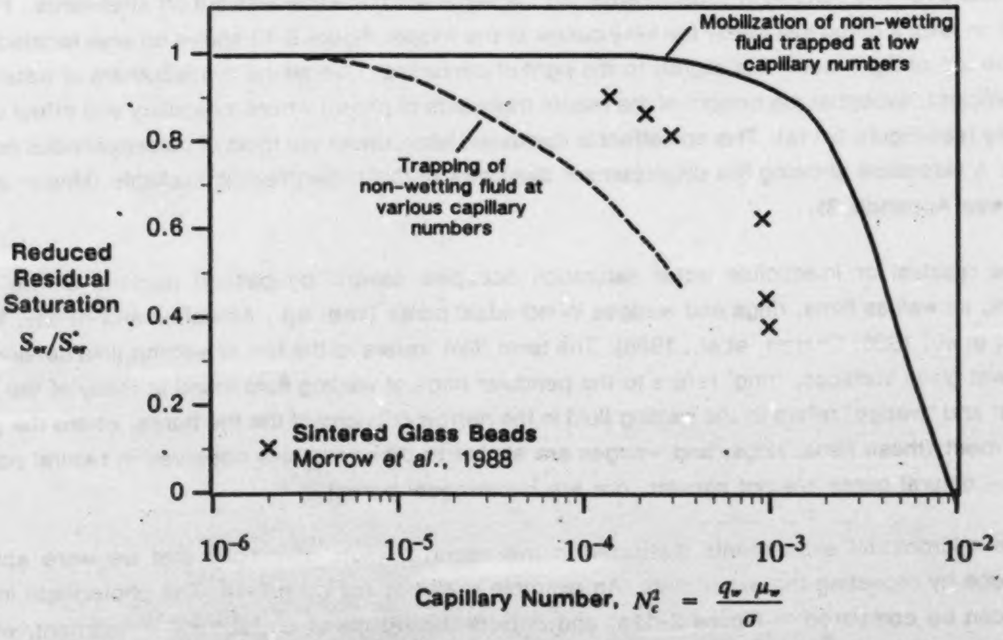

FIGURE 9-10. Residual saturation in uniform glass beads due to variable capillary number entrapment of the continuous non-wetting phase (dashed line), and due to mobilization of non-wetting phase originally trapped at a low capillary capillary number (solid line). After Morrow and Chatzis (1982) and Morrow et al. (1988).

MICROMODEL FLOW VISUALIZATION OF TWO PHASE DISPLACEMENT AND CAPILLARY TRAPPING

Flow visualization techniques in a homogeneous micromodel illustrate the process of organic liquid invasion of the saturated zone and subsequent displacement by flowing groundwater — resulting in trapped organic phase being left behind. It visually illustrates many of the issues that were raised in the review. Later, these micromodel results are compared to micromodel results for higher flow rates, heterogeneous media, and the vadose zone (in Section 10).

Organic Liquid Invasion into a Water Saturated Homogeneous Micromodel (Wilson et al. 1988)

A water-wet etched glass micromodel experiment (Figures 8-1 & 9-11) serves as good example of the displacement process of organic liquid movement into a water-saturated homogeneous soil. The water-saturated micromodel was oriented vertically, and flooded from the top with an organic liquid, red dyed Soltrol, at a relatively slow rate of 0.096 ml/min using the techniques described in Section 8. The steady state condition, at the end of the organic liquid invasion, is shown in the upper photographs of Figures 9-11 through 9-13. Figure 9-11a depicts the entire model at equilibrium, while Figures 9-12a & 9-13a depict close-ups. In these photos the red dyed Soltrol appears dark gray; the water was not dyed. The Soltrol continues to flow the model at the rate of 0.096 ml/min, but the Soltrol and water saturations have stabilized. The saturation pattern remained the same when the flow was cut off afterwards. Figure 9-12 is an area located just below the very center of the model. Figure 9-13 shows an area located very near the top of the model, and slightly to the right of centerline. Overall the displacement of water was fairly efficient, except at the bottom of the model (right side of photo) where a capillary end effect came into play (see Figure 9-11a). This end effect is discussed later, under the topic of heterogeneous porous media. A videotape showing the displacement dynamics of this experiment is available (Mason et al., 1988; see Appendix B).

The residual or irreducible water saturation occupies several by-passed pockets of the pore network, as well as films, rings and wedges in individual pores (see, eg., Amaefule and Handy, 1982; Dullien, et al., 1986; Chatzis, et al., 1988). The term 'film' refers to the film of wetting fluid covering all water wet glass surfaces; 'ring' refers to the pendular rings of wetting fluid found in many of the pore throats; and 'wedge' refers to the wetting fluid in the narrow crevices of the the pores, where the glass plates meet (these films, rings, and wedges are similar to those that are observed in natural porous media - natural pores are not circular, nor are micromodel pores).

The micromodel experiments illustrated in this report depicts conditions that we were able to reproduce by repeating the experiment. An example is shown in Figure 9-14. The photograph in this figure can be compared to Figure 9-11a, and depicts the results of an identical experiment, where Soltrol has advanced into the micromodel, displacing water. The character of the saturation pattern is similar for both experiments, only the details vary. The two-phase flow field appears to be a stochastic process, with the same mean behavior, but a different detailed realization for each experimental replication.

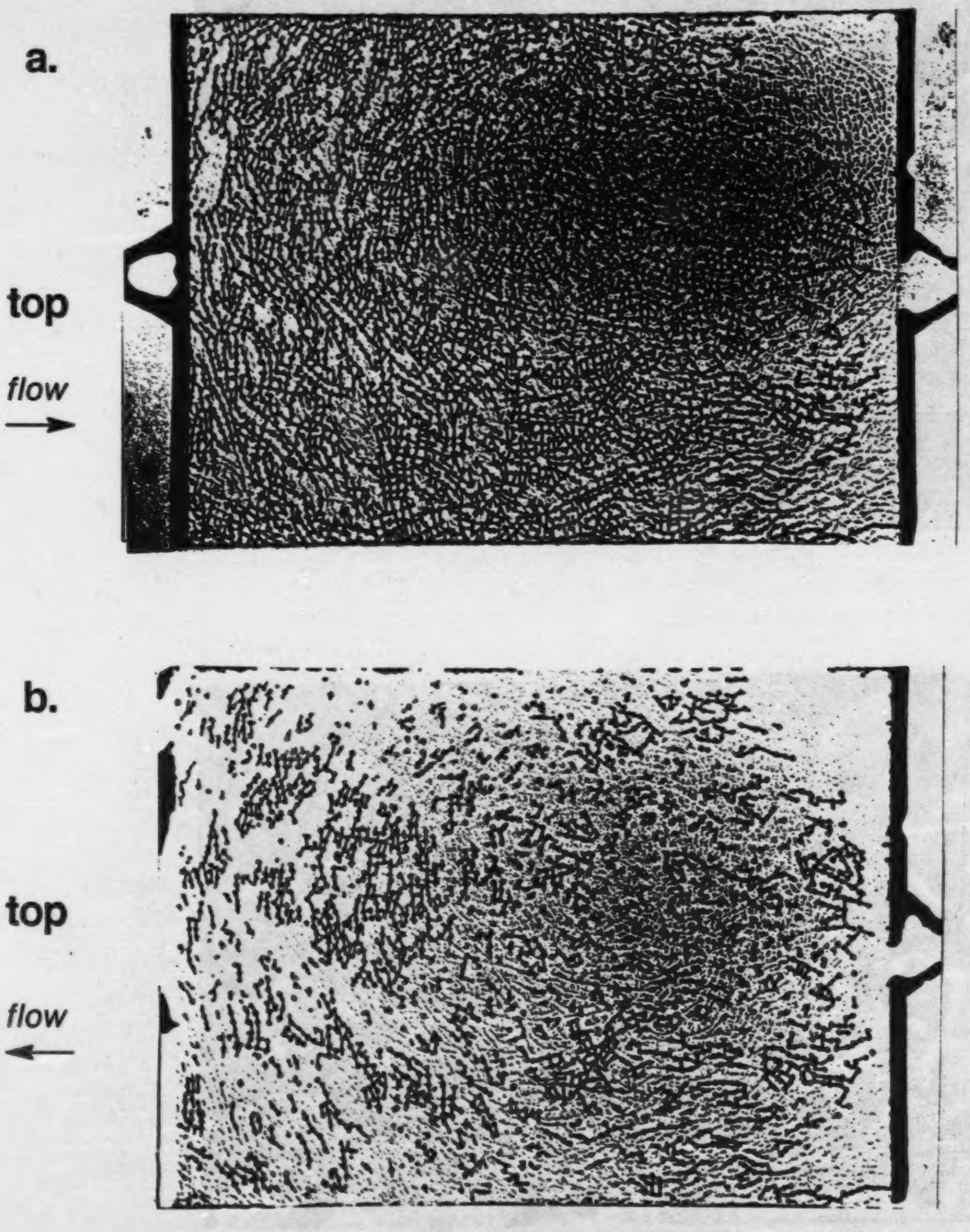

FIGURE 9-11. In the upper photo (a) Soltrol displaced water from the left (the top of the model) to the right (the bottom of the model), yielding a residual (irreducible) wetting phase saturation. In the lower photo (b) Soltrol was displaced by water from the right (the bottom of the model) to the left (the top) yielding a residual non–wetting residual saturation. Soltrol was dyed red and appears dark grey; the water was not dyed. The photos record steady state flow conditions at the end of the displacements.

Reproduced from
best available copy.

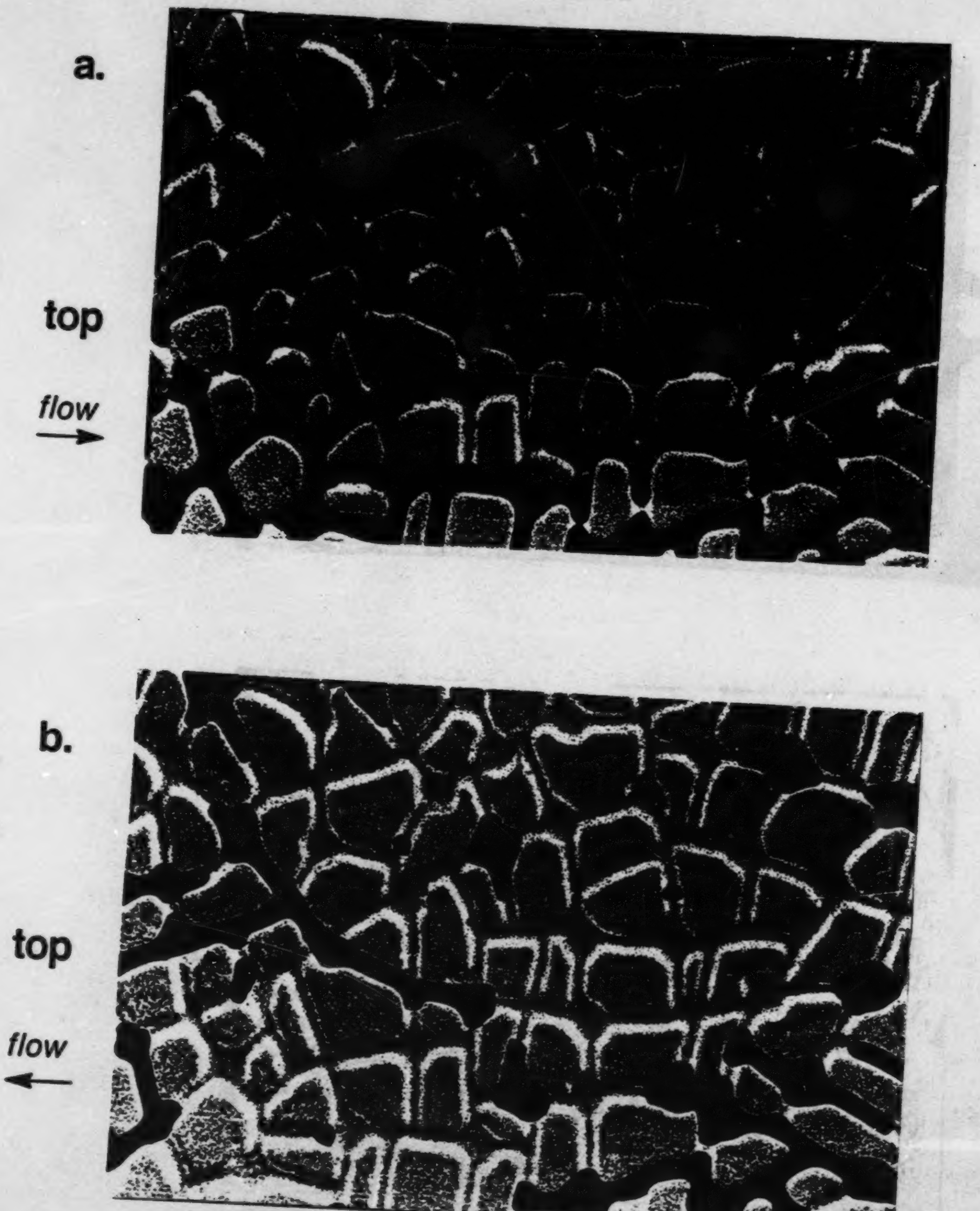

FIGURE 9-12. Detail from Figure 9–11 showing conditions following the displacement of the water by Soltrol (a. upper photo), and at residual non–wetting phase saturation (b. lower photo). The area is located just below the very center of the model.

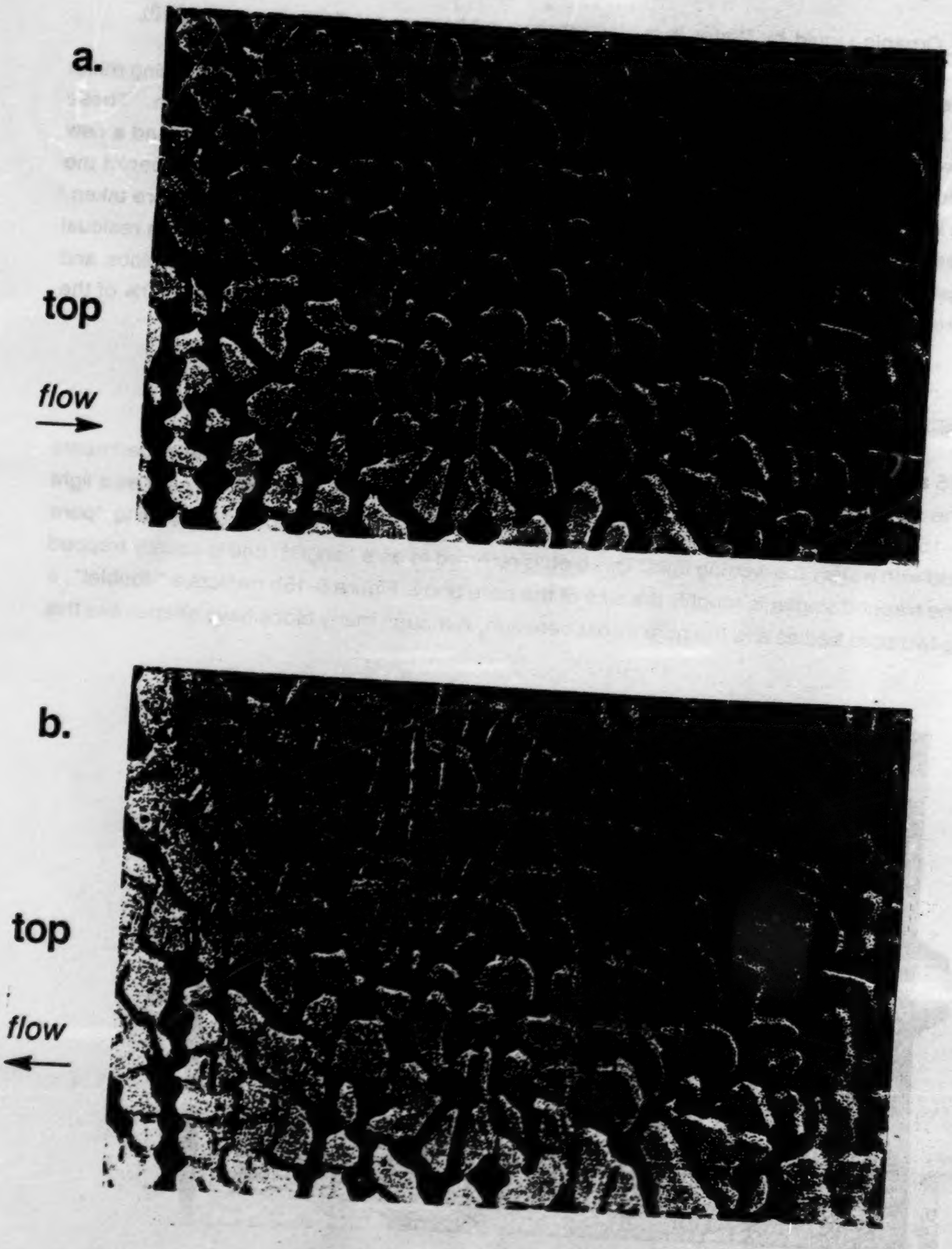

FIGURE 9-13. Detail from Figure 9–11 showing conditions following the displacement of the water by Soltrol (a. upper photo), and at residual non-wetting phase saturation (b. lower photo). The area is located near the top of the model, just to the right of the centerline.

Displacement of Organic Liquid by Water in a Homogeneous Micromodel (Wilson et al. 1988)

In the next step water was displaced upward through the micromodel at the same rate, pushing much of the Soltrol out, but leaving behind a capillary-trapped, residual Soltrol saturation. These displacements were also captured on videotape (Mason et al., 1988). When the model reached a new steady state, additional photos were taken. The lower photos of Figures 9-11b through 9-13b depict the residual organic liquid left behind. Water continued to flow through the model as the photos were taken. The saturation pattern did not change when the flow was cut off. As seen in these photos, the residual organic liquid saturation in these strongly water-wet models is composed of disconnected blobs and ganglia which are fairly evenly distributed throughout the model and appear to occupy up to 30% of the pore space.

Microscopic Inspection of Blob Size and Shape in Micromodels

Figures 9-15 and 9-16 present 'pore scale' close-ups of typical blobs taken from similar experiments conducted in the same micromodel.The water was dyed blue in Figure 9–15, and may appear as a light grey. Figure 9-15a is a photomicrograph of a blob trapped in a 'pore body'. The surrounding 'pore throats' are filled with water, the wetting fluid. This blob is referred to as a 'singlet' and is usually trapped by snap–off. The trapped singlet is roughly the size of the pore body. Figure 9-15b depicts a 'doublet', a blob occupying two pore bodies and the pore throat between. Although many blobs have shapes like this

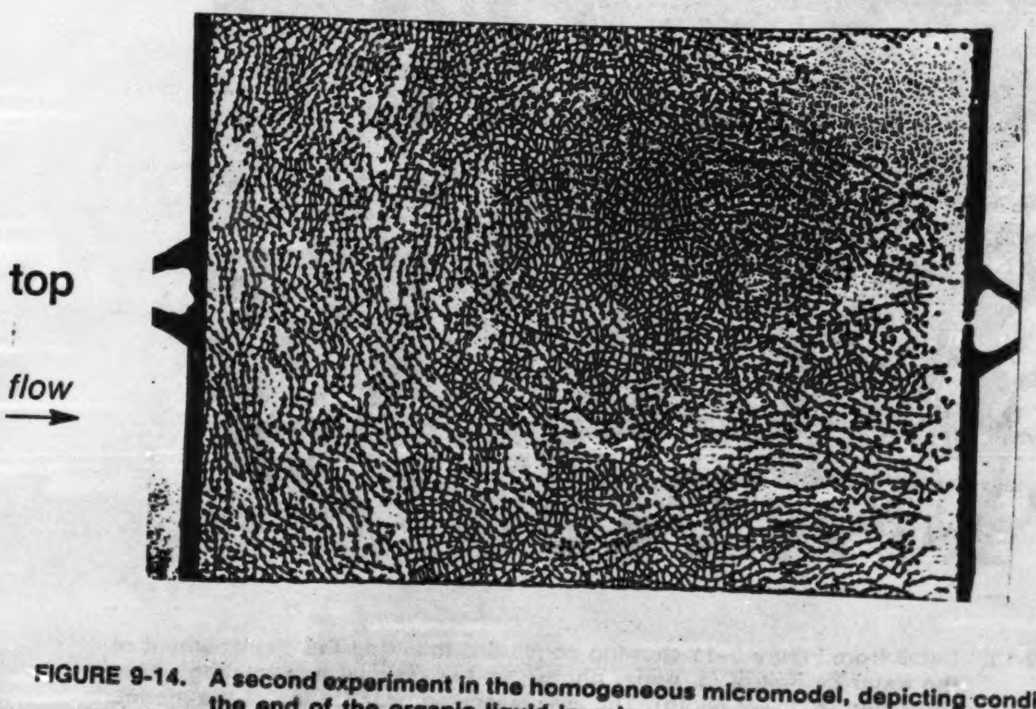

FIGURE 9-14. A second experiment in the homogeneous micromodel, depicting conditions at the end of the organic liquid invasion–compare to Figure 9-11a .

Reproduced from
best available copy.

a.

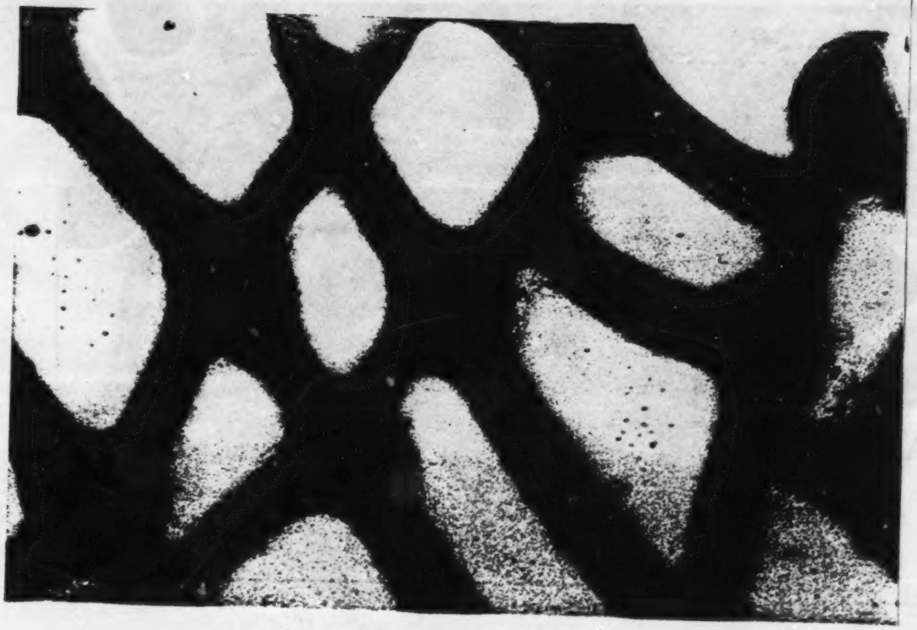

b.

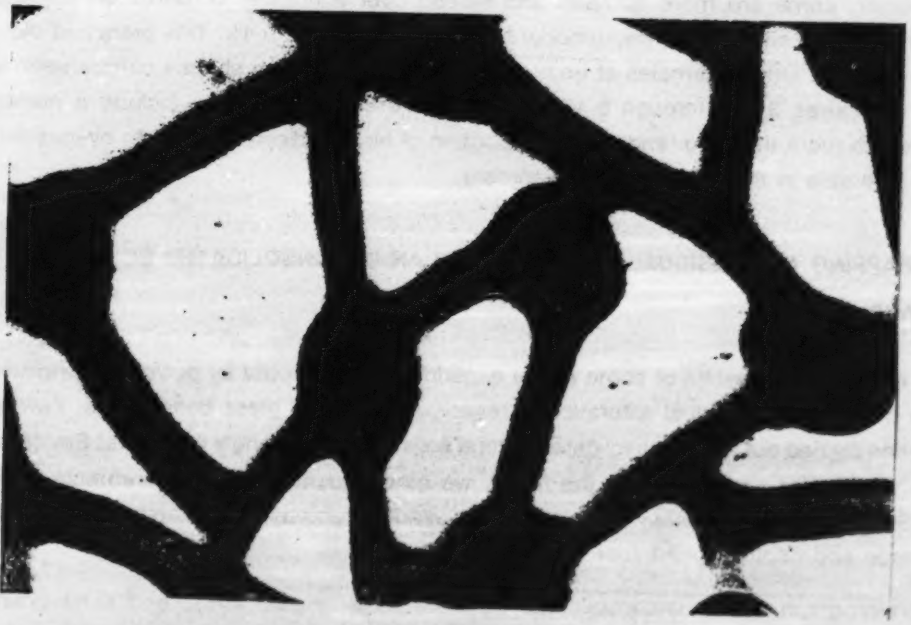

FIGURE 9-15. Photomicrographs of (a) a singlet blob occupying one pore body in the upper photo, and (b)a doublet blob occupying two pore bodies and a pore throat in the lower photo. The water is dyed blue (light grey); the Soltrol is dyed red (dark gray).

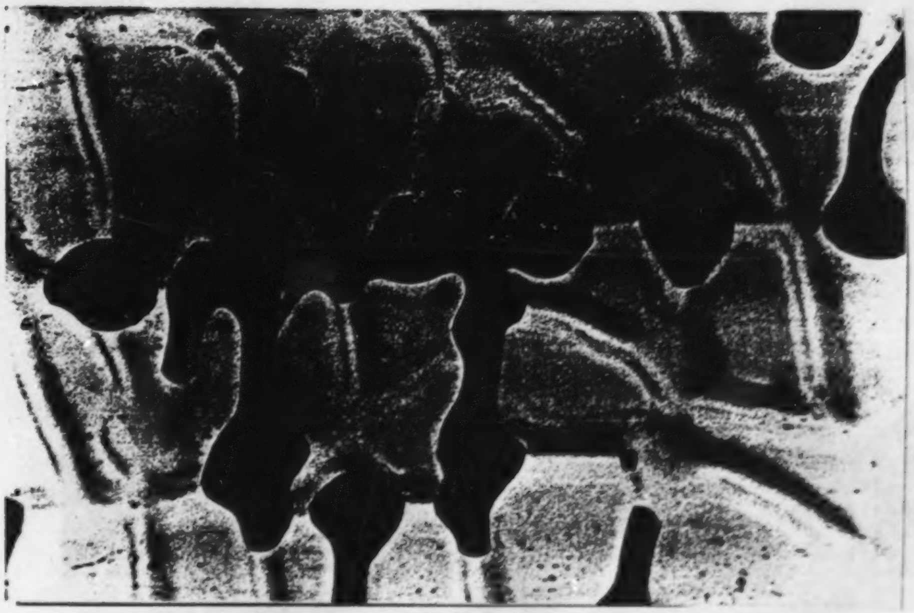

FIGURE 9-16. Photomicrograph of a complex blob as observed in the micromodel.

singlet and doublet, some are more complex and extend over a number of pores bodies and the connecting pore throats, such as the micromodel blob shown in Figure 9-16. This branched blob was presumably by-passed. Other examples of both simple and complex blob shapes can be seen in the upper photos of Figures 9-11b through 9-13b. These more complex shapes include a number of branched blobs with more than two 'ends'. The population of blobs indicates that both by-passing and snap-off were operable in the micromodel experiment.

CAPILLARY TRAPPING AND RESIDUAL SATURATION IN AN UNCONSOLIDATED SOIL: the SEVILLETA SAND

Earlier we reviewed the results of some of the experiments conducted by petroleum engineers to study capillary trapping and residual saturation in reservoir cores and glass bead packs. Few similar studies have been carried out for unconsolidated natural soils. Using a strongly water-wet Sevilleta sand for the media, and water and Soltrol for the fluids, we made quantitative measurements of Soltrol residual (see Sections 4 & 5). In other experiments we used styrene as the organic phase, which we hardened in place and photographed (see Section 7).

The photomicrograph of the unconsolidated Sevilleta sand (Figure 4-6), and sand grain size distribution curve (Figure 4-5), appear to resemble those of (unconsolidated) uniform glass beads, more than of (consolidated) sandstone. Thus we hypothesize that sand should exhibit a behavior more like that of glass beads, than that of sandstone. That is, the snap-off mechanism of trapping should be more common in the uniform Sevilleta sand, than it is in a sandstone,and the residual saturation should be dominated by singlet and doublet blobs.There should be relatively few large and complex blobs.

	porosity (%)	bulk density (g/cm³)	maximum organic liquid saturation (%)	residual organic liquid saturation (%)
all 22 experiments	34.3 ± 1.2	1.741 ± 0.033	84.7 ± 3.4	28.0 ± 3.8
good temp. control 13 experiments	33.9 ± 0.6	1.752 ± 0.016	85.1 ± 2.8	27.1 ± 1.7
poor temp. control 9 experiments	34.9 ± 1.7	1.724 ± 0.044	84.0 ± 4.1	29.3 ± 5.4

TABLE 9-1. **Soltrol residual saturation and other measurements in Sevilleta sand, for three temperature dependent categories (sample mean ± sample standard deviation).**

Correlation with porosity–

The earlier discussion on mechanisms focused on capillary trapping as a function of pore structure, among other factors. Each experiment recorded in Table 9-2 included measurements of porosity and bulk density. Presumably, these measurements give a measure of pore structure as controlled by the density of soil packing. A tendency for increased trapping with decreased porosity has been reported in the petroleum literature (Morrow et al., 1988). This is believed to be related to the fact that for more heavily cemented petroleum reservoir rocks, the pore throats (from which organic liquid is easily displaced by water) make up a smaller percentage of the total pore volume (Chatzis et al., 1983). Lower pore connectivity, another attribute of low porosity (heavily cemented) media, is also suspected of contributing to increased trapping (Pathak et al., 1982). Although the Sevilleta is an unconsolidated soil, we were concerned that we too might see some systematic change in residual saturations with change in porosity from one packing to the next. Figure 9-17 presents a plot of maximum organic liquid saturation and residual saturations for the 13 best samples in Table 9-2. In these results, there appears to be no discernible correlation between porosity and either the residual or maximum organic liquid saturations. Although the porosities varied somewhat, this variation did not seem to affect the measurements of saturation in any systematic way. The lack of correlation between S_{or} and n is probably due to the small range over which the porosities varied, and the unconsolidated nature of the soil.

Photomicrographs of Blob Casts and Pore Casts

Photomicrographs of polymerized styrene blobs embedded in epoxied Sevilleta soil pore casts, are shown in Figures 9-18 and 9-19. These pore casts were constructed in short TFE columns of Sevilleta soil using the techniques described in Section 7. Compare the singlet and doublets shown in Figure 9-18, from the soil column, to those in Figure 9-15, from the micromodel. The similarity between blob shapes in the two different media gives confidence that micromodels can reasonably be used to simulate the

trial	in box ?	porosity (%)	est. error (%)	bulk density (g/cm³)	est. error (g/cm³)	organic liquid saturation (%)				temp. range (°C)
						maximum	est. error	residual	est. error	
1	no	33.8	0.6	1.754	0.008	84.6	3.5	29.3	1.7	1.0
2	no	36.5	0.5	1.683	0.007	82.2	3.0	32.5	1.5	5.0
3	no	34.0	0.5	1.750	0.007	77.5	3.1	24.6	1.4	1.0
4	no	34.1	0.5	1.747	0.008	85.7	3.5	29.3	1.7	1.0
5	no	33.2	0.6	1.769	0.008	92.7	3.9	34.7	2.0	3.0
6	no	34.8	0.5	1.729	0.007	84.1	3.2	32.7	1.6	2.0
7	no	38.6	0.9	1.626	0.017	78.6	3.7	21.6	1.5	11.0
8	no	34.6	0.5	1.732	0.007	80.2	3.0	37.0	1.7	3.0
9	no	34.6	0.5	1.733	0.008	84.7	3.5	29.3	1.7	2.0
10	no	34.3	0.5	1.741	0.008	87.5	3.6	28.6	1.8	3.0
11	no	34.1	0.6	1.747	0.009	87.0	3.9	26.9	1.8	1.5
12	no	34.1	0.6	1.746	0.009	82.6	3.6	24.3	1.6	2.8
13	no	33.7	0.5	1.756	0.008	83.5	3.3	23.1	1.4	2.8
14	yes	34.9	0.5	1.726	0.007	87.0	3.4	27.9	1.6	0.3
15	yes	34.2	0.6	1.745	0.010	85.8	3.9	25.0	1.7	0.8
16	yes	34.7	0.6	1.730	0.010	88.2	3.9	28.5	1.8	0.4
17	yes	33.7	0.5	1.758	0.006	83.8	3.2	25.4	1.4	0.3
18	yes	34.1	0.6	1.747	0.009	85.6	3.7	27.1	1.7	0.4
19	yes	34.1	0.6	1.746	0.011	86.0	4.0	29.2	1.9	0.9
20	yes	32.8	0.6	1.781	0.010	88.3	4.1	27.6	1.9	1.0
21	yes	33.1	0.6	1.774	0.009	83.0	3.7	24.6	1.7	1.0
22	yes	33.2	0.5	1.771	0.007	84.1	3.4	26.6	1.7	1.1

TABLE 9-2. **Summary of Soltrol / Sevilleta sand saturated zone results.**

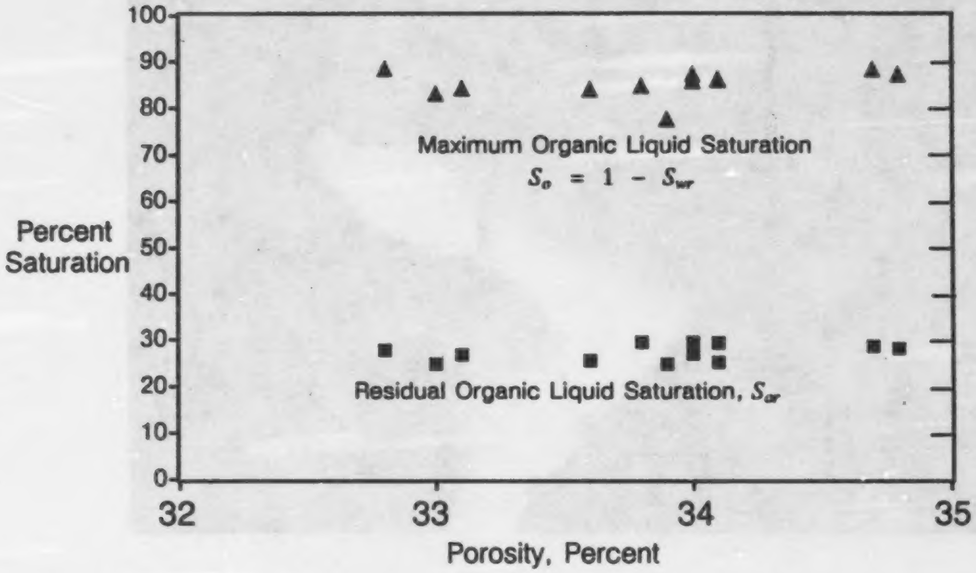

FIGURE 9-17. **Correlation of maximum Soltrol saturation (triangles), and residual Soltrol saturation (squares), to porosity in the Sevilleta sand.**

immiscible displacements taking place in the subsurface (Conrad et al., 1989). Figure 9-19 shows a variety of blobs in a similar pore cast. Some of these are singlets, while others are much more complex and have branches. The pore casts also reveal the position of the blobs within the pore space, and their position relative to the sand grains. In the pore throats, there appears to be only a thin film of water between the blob and the sand grain 'pore wall'. The micromodel mimics this behavior (Figure 9-15 and 9-16). For pore bodies occupied by organic liquid, sometimes there is a difference in the observed behavior found in the micromodels and the pore casts. Blobs in the micromodel appear to occupy most of each pore body they are found in, again leaving only a film of water between the blob and the 'pore wall'. Blobs in the Sevilleta pore casts sometimes share the pore bodies with significant amounts of water (see Figure 9–18b), perhaps due to greater surface roughness and irregularities in the pore walls of the Sevilleta sand. This is certainly not always the case (see Figure 9–19). Note that no attempt had been made to achieve similitude between the micromodel network and Sevilleta sand. One other factor to keep in mind: the styrene shrinks slightly as it polymerizes.

SEM photomicrographs provide a three-dimensional view. Views of polymerized styrene 'blob casts' from another Sevilleta soil column are shown in Figure 9-20a. The rough spots on the surface of these blobs is probably due to the SEM coating process. Once again there is a typical singlet (upper left), and a doublet (lower left). The singlet is almost spheroidal, with a length of 200 microns and a diameter of 100 or more microns. The doublet includes one pore body of roughly 100 microns in diameter, and another that appears to be almost 200 microns in diameter. At the pore throat, the doublet is only 20 microns in diameter. The two more complex shapes involve four (upper right) and six (lower right) pore bodies. The pore bodies of these more complex blob shapes appear to have a diameter of roughly 100 microns,

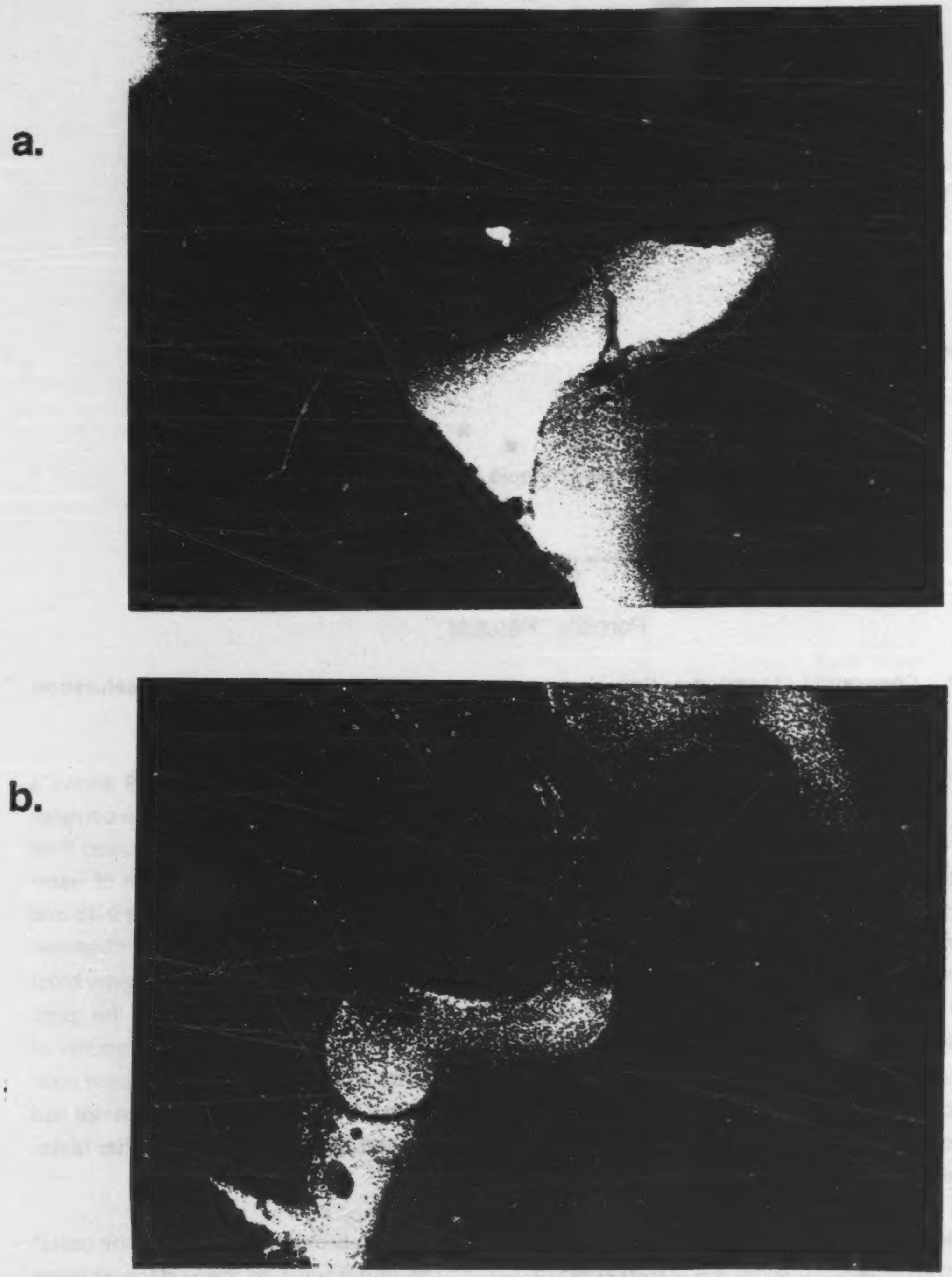

FIGURE 9-18. Sevilleta sand pore cast photomicrographs of (a) a singlet blob occupying one pore body, in the upper photo, and (b)a doublet blob occupying two pore bodies and a pore throat, in the lower photo. The styrene non-wetting phase is dyed blue (lightest grey); the epoxy wetting phase is dyed green (light gray). The solid grains show as dark colors, or in the case of translucent minerals, as a different shade of green (medium grey).

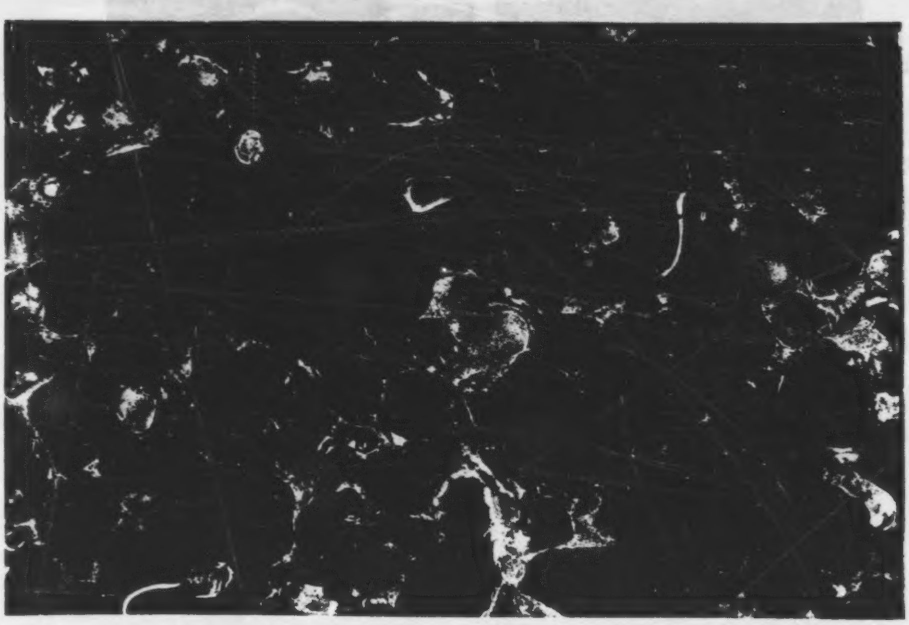

FIGURE 9-19. Sevilleta sand pore cast photomicrograph of a variety of blobs including some that are complex and branching. The styrene non-wetting phase is dyed blue (lightest grey); the epoxy wetting phase is dyed greenish yellow (light gray). The solid grains show as dark colors, or in the case of translucent minerals, as a different shade of green (medium grey).

while the typical throat diameter is less than 50 microns. Contrast these diameters with the grain size distribution of the very uniform Sevilleta soil, as given in Figure 4-5. The mean grain diameter is 300 microns. Few grains are larger than 500 microns, or smaller than 100 microns. The typical pore body blob diameter of 100 microns is smaller than the mean grain size. The blob lengths depend on the number of pore bodies involved. The singlet in Figure 9-20a is 200 microns long, the doublet bends through a length of 400 microns, the quadruplet is 800 micros long, and the contorted sextuplet is at least 800 microns long (part of the sextuplet is sticking up into the photo, and thus its entire length is not readily apparent). Several more complex, branching blob casts, taken from the same column, are shown in Figure 9-20b. These branched blobs often have holes in them, and 10 or more pore bodies. Presumably, the larger holes were partially filled with a sand grain when in the column. Perhaps the smaller holes contained only the 'pointed edge' of a grain.

At the beginning of this project, we anticipated taking pore casts and performing a statistical size and shape analysis. We referred earlier to similar analyses which have been conducted on blob casts taken from oil reservoir sandstone cores and glass bead packs (Morrow and Chatzis, 1982, Chatzis et al., 1983, and Chatzis et al., 1988). As discussed in Section 7, the pore casts taken from the Sevilleta

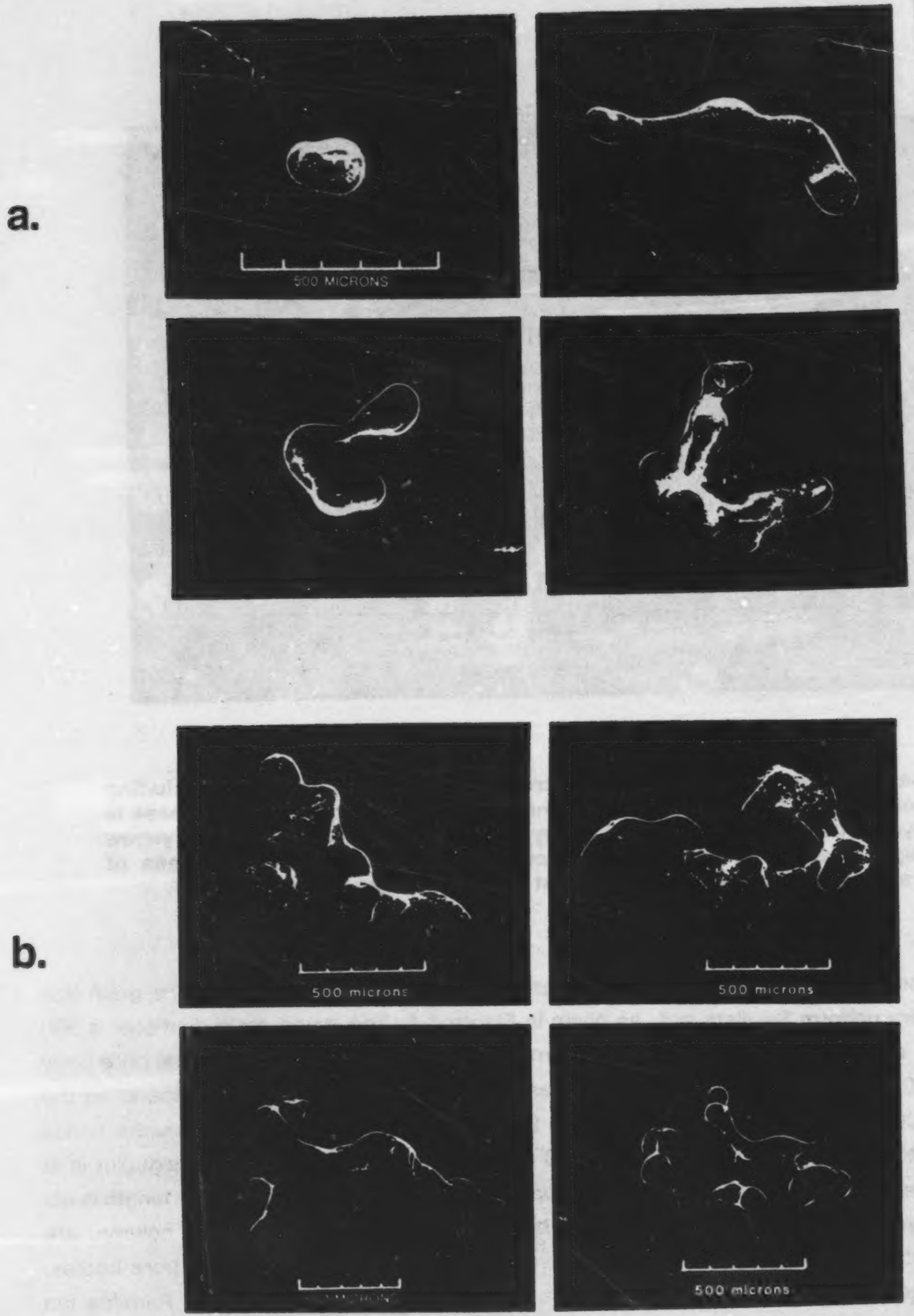
a.
500 MICRONS
b.
500 microns
500 microns
500 microns

FIGURE 9-20. Sevilleta sand blob cast photomicrographs of (a) non-branching blobs, and (b)branching blobs.

soil columns appeared to be too fragile for quantitative analysis using a Coulter Counter or even an image analyzer. Many of the larger casts broke into several pieces when handled. The right end of the blob cast depicted in the lower right photo of Figure 9-20b is broken. This complex blob of roughly 15 pore bodies was even bigger before it broke. The branched blob in the lower left also appears to have broken ends. Breakage of this kind would have severely biased a size analysis. The petroleum research samples must have also suffered from the same problem, and their results may be biased. A second approach would be to use image analysis on the sectioned epoxied pore casts. This proved beyond the resources of this project, but is strongly recommended in future research efforts. Also recommended is mercury and nitrogen gas porosimetry of the soil samples, in order to yield estimates of the actual pore size distribution.

Our size and shape analysis has been limited to visual inspection of the blob population through the microscope. Figure 9-21 is a photomicrograph of a Sevilleta sand pore cast, showing many blobs. Figure 9-22 is an SEM photomicrograph of a random sample of Sevilleta blob casts. These photographs document what we saw through the microscope. Many, if not most of the Sevilleta blobs are larger than a singlet or doublet. A closer inspection of the pore cast, with a stereoscope, shows that most of the blobs, which appear on the surface to occupy only one or two pores, actually extend down into the sample. Blobs commonly wind down and around into the pore network forming ‘ghosts’ at depth when viewed through the relatively transparent quartz sand. Figure 9-22 may also be somewhat misleading in reference to the size of the blobs. It must be remembered that many of the blob casts in the photomicrograph are broken. Even if the complex blobs do not outnumber the singlets and doublets, they clearly contain almost all of the residual saturation volume. Overall, it appears that the more complex blobs dominate the Sevilleta sand.

Discussion of Sevilleta Sand Experiments

We hypothesized that Sevilleta sand would behave more like glass beads, than like sandstone. The evidence does not support this hypothesis. The observed residual Soltrol saturations of 25–29% were much higher than the range of 18–20% that we anticipated, and the residual blobs were more complex. The Sevilleta sand appears to behave more like sandstones than glass beads. The complexity of the blobs may even exceed that of sandstones. We won't proposed an explanation for this behavior, until later when we contrast the results from the Sevilleta sand and other soils.

The high residual saturation level found in Sevilleta sand has important implications on aquifer contamination characterization and remediation. However, caution should be exercised when generalizing the results of experiments on only one soil.

Implications for aquifer contamination –

Twenty-seven percent of the Sevilleta sand pore space is occupied by immobile, discontinuous, blobs of Soltrol. If this estimate is typical for most organic liquids and sandy soils there is a tremendous storage capacity of organic liquid pollutants in the saturated zone. Expressed in terms of volumetric retention (9-5), the Sevilleta sand has the capacity to store over 90 liters of Soltrol per cubic meter of soil. For example, a single 10,000 gallon spill of an organic liquid could be absorbed in about

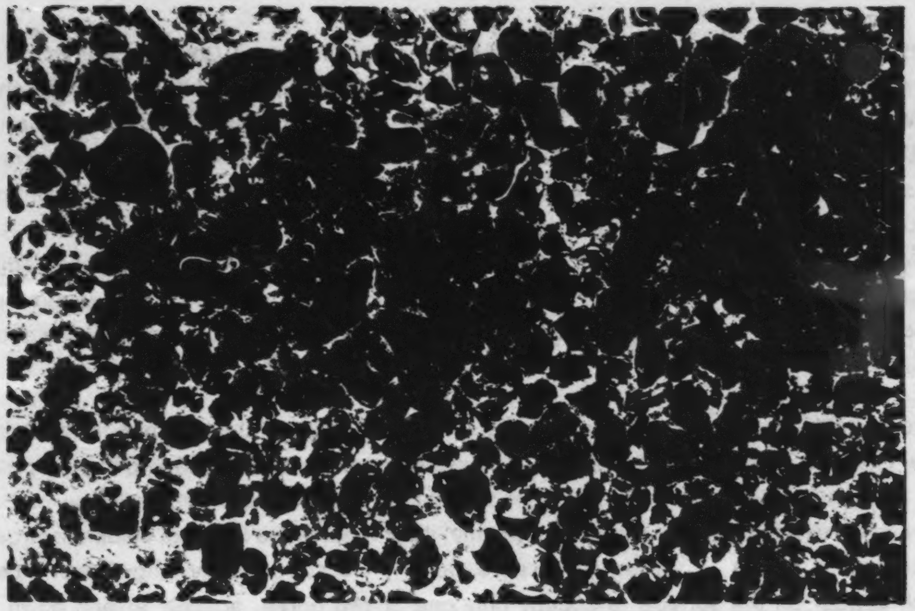

FIGURE 9-21. Photomicrograph of Sevilleta sand pore cast covering many pores.

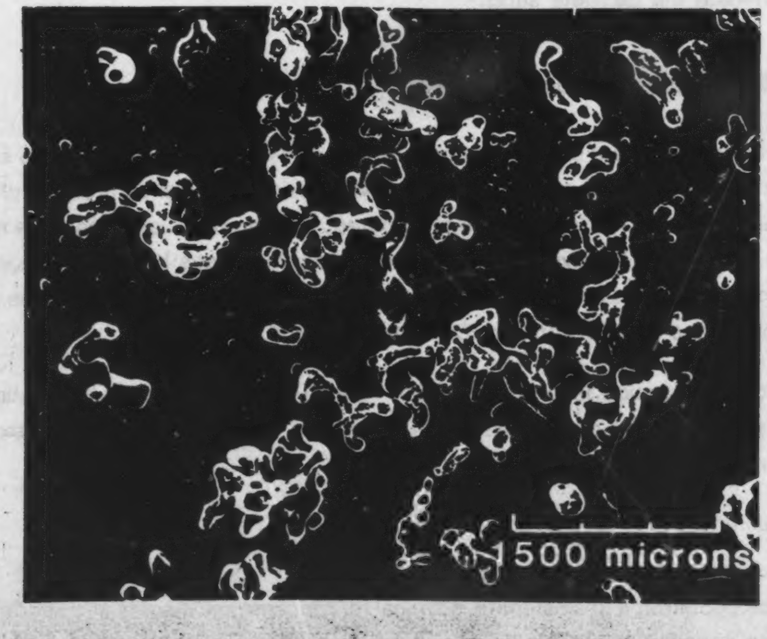

FIGURE 9-22. SEM photomicrograph of many blob casts from the Sevilleta sand.

420 m³ of saturated soil. This volume corresponds to a cube of soil with sides only 7.5 meters in length. Even if typical soil residual saturation is only half of this, and similar to that of glass beads, the capacity is still large.

Implications for biotransformation —

There are several implications of these observations on the study and practice of biotransformation of organic components. Microorganisms attached to the pore wall, at the water-solid interface, experience an environment that depends on their location. In blob-filled pore throats, the organisms have ready access to organic components that partition into the aqueous phase from the nearby blob surface. However, these organisms may not have a ready supply of other substrates, which can only diffuse (or flow) slowly through the thin water film that lines the pore throat (see Figures 9-18b, 9-19, 9-12b, 9-13b,9-15,and 9-16). In blob-filled pore bodies that have a surrounding water film, the same situation applies, as it does for microorganisms attached to the blob surface in these regions of thin aqueous films. In the other pores, occupied by flowing water, wall-attached microorganisms are readily exposed to available dissolved substrates, subject only to upstream substrate re-supply and biological consumption.

Migration of microorganisms is also probably influenced by the spatial distribution of blobs. It should be difficult for a seed population to find its way into regions with thin aqueous films because of their low flow rates and tortuous diffusion paths. In any event, most organisms would probably not thrive in these stagnant regions because of the substrate re-supply problem and the possibility of toxicity due to locally high concentrations of dissolved organics.

Implications for phase partitioning–

Blob size and shape influence the partitioning of organic liquid components to the aqueous phase. Mass transfer coefficients used in the mathematical models of this partitioning often employ the analogy of an equivalent spherical blob (e.g., Pfannkuch, 1984). Certainly singlets can be represented by a spherical model, but it is less clear that this model works for the multiple pore-body elongated blobs of Figure 9-20a , or branched blobs of Figure 9-20b . These large complex blobs may be fewer in number than the simple shapes, but they hold the majority of the liquid organic volume. Their surface area to volume ratio is also greater. For multi-component organic liquids it is easier for these more complex shapes to 'leach out' a lighter organic component than for a spherical blob of equal volume (this equivalent sphere may be much larger than a real pore). But break these complex shapes into many 'model' spherical singlets of realistic size, say 100 microns diameter for the Sevilleta sand, and the model leach rate increases dramatically. Coupled with this issue is the fact that there is a distribution of blob sizes and shapes in any sample (see Figures 9-21 and 9-22). An appropriate definition of equivalent sphere size has yet to be proposed, although work is progressing in that direction (eg, Powers *et al.*, 1988).

The position of a blob within the pore space also has a strong influence on mass transfer between phases. If a large portion of the blob surface is in contact with only a thin film of water, as certainly seen in our pore casts and micromodels, then the transfer rate may be limited by advection or diffusion in the film. Videotaped micromodel observations indicate that the flowing water moves around the blobs, through the unoccupied pores, with little water movement in the films to help advect organic components away (Mason *et al.*, 1988). This initial observation requires additional experimental confirmation.

As components of the organic phase partition from it, a blob gets smaller, and the residual organic saturation is reduced over time. Let's consider the solubilization of a one-component residual organic liquid. Simple compositional models of interphase mass transfer usually assume that a local equilibrium is reached between the phases. As groundwater passes through the zone of residual saturation, trapped organic liquid is dissolved by the water. In the case where a local equilibrium is in fact reached, only blobs at the extreme upstream end of the zone are dissolved. By the local equilibrium assumption, as soon as water comes into contact with organic liquid the solubility limit of the water with respect to the organic is reached. With time, blobs at the upstream become dissolved and completely disappear. Blobs not at the upstream end are not dissolved at all because passing water has already been completely saturated with organic liquid. If we look spatially at this equilibrium dissolution process as a function of time, we hypothesize that organic liquid saturation maintains a sharp front at the upstream end (Figure 9-23a), as does the dissolved concentration in the water phase (Figure 9-23b).

Often, when groundwater velocities are high enough or the dissolution kinetics are slow enough, the local equilibrium assumption no longer holds. In this case, the saturation distribution may look like that shown in Figure 9-24. A dispersed zone forms where traveling groundwater has not yet reached its solubility limit for the organic liquid. The dispersed zone is the region in which there is a reduced residual saturation ($0 < S_{or} < S_{or}^{*}$), and it looks like a backwards breakthrough curve. Downstream of the dispersed zone, the water has reached its solubility limit and can no longer dissolve organic liquid. The higher the velocity and the lower the interphase mass transfer rate, the larger the dispersed zone will be. It is in this sense that the rate of mass transfer between phases strongly depends upon the distribution of the residual saturation. For large, branched blobs, trapped by by-passing, mass transfer can be limited by a diffusional process. Substantial portions of large, branched blobs may be in contact with only thin water films along the walls of pores. Diffusion through these films to the main body of passing groundwater may sometimes be the rate-limiting step in solubilizing organic liquid into the water phase. If the dispersed zone is large enough, or the zone of trapped organics is relatively small, the solubility limit of the organic liquid in water may never be reached.

Dissolution from a multi-component organic phase is more complex. Many spilled organics — from gasoline and other fossil fuels to transformer oils containing PCBs to the mixed bag of organics that are sometimes found in industrial waste pits — are mixtures having many (sometimes hundreds of) organic components. The more soluble components of these mixtures can dissolve comparatively quickly, leaving behind less soluble components to leach out more slowly. There are also co-solvency effects to consider. Interaction between components can either enhance the solubility of a given component (co-solvency) or the interaction can reduce the solubility of that component (by a kind of salting-out process). And sometimes, for large branched blobs or by-passed regions of multi-component liquids, the mass transfer rate for a given component may become limited by rate of diffusion of that component within the organic phase to the organic/water interface. With all these complicating factors, the saturation distribution of the residual organic phase becomes much more complex than the simple curves shown for dissolution of a single-component liquid.

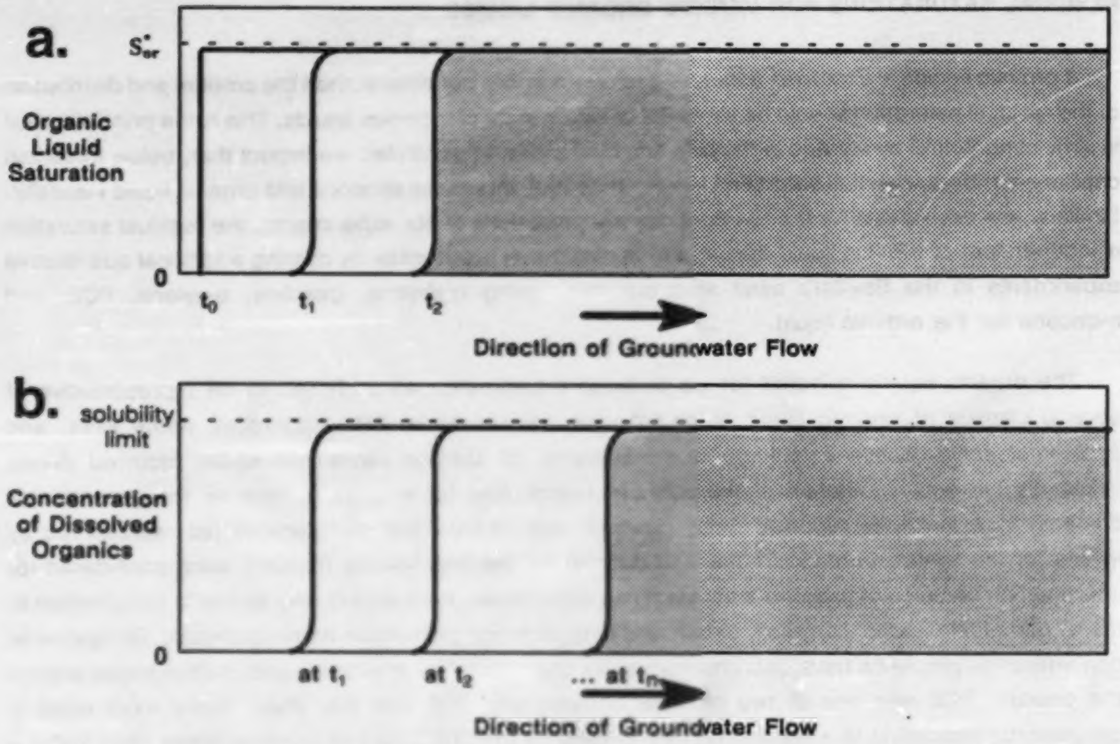
a.
S^*_{or}
Organic Liquid Saturation
0
t_0
t_1
t_2
Direction of Groundwater Flow
b.
solubility limit
Concentration of Dissolved Organics
0
at t_1
at t_2
... at t_n
Direction of Groundwater Flow

FIGURE 9-23. **The spatial distribution of a single-component residual organic liquid undergoing dissolution as a function of time when the local equilibrium assumption is invoked. Notice that a sharp front is maintained at the dissolution front for both the organic liquid saturation, (a), and for the concentration of the organic dissolved in the water, (b).**

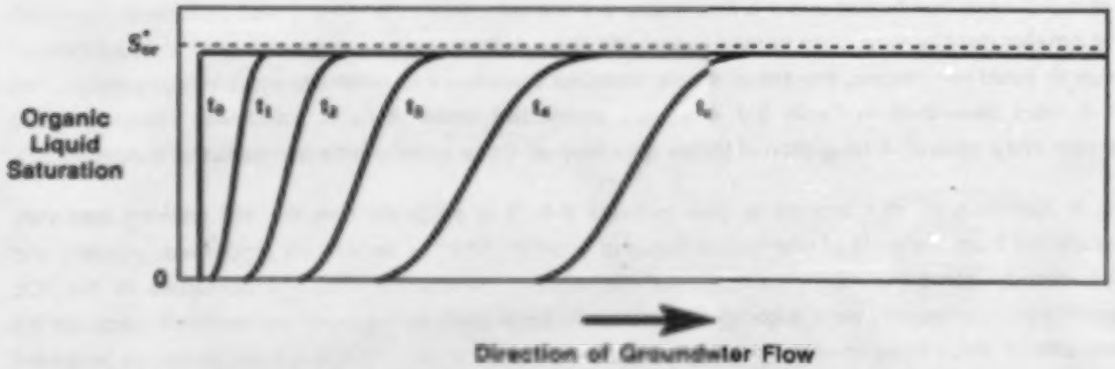
S^*_{or}
Organic Liquid Saturation
0
t_0
t_1
t_2
t_3
t_4
t_s
Direction of Groundwater Flow

FIGURE 9-24. **The spatial distribution of a single-component residual organic liquid undergoing dissolution as a function of time when a local equlibrium between the fluid phases is not reached. A dispersed zone forms and grow until a steady state is reached.**

RESIDUAL SATURATIONS FOR VARIOUS ORGANIC LIQUIDS

If organic liquids are trapped under low capillary number conditions, then the amount and distribution of the residual saturation should be similar for a wide variety of organics liquids. This is the principle used in simulating Soltrol by styrene in the pore and blob casts. In particular, we expect that, below threshold capillary numbers, residual saturation is independent of interfacial tensions and organic liquid viscosity. Similarly, we expect that for the low Bond number conditions of our experiments, the residual saturation is independent of organic liquid density. We tested these hypotheses by running additional quantitative experiments in the Sevilleta sand short columns, using kerosene, gasoline, p-xylene, PCE, and n-decane for the organic liquid.

The organic liquids selected for use in these experiments were chosen to be representative of several classes of organic liquid pollutants often present at landfills, hazardous waste sites, and accidental spills. Gasoline leakage from thousands of storage tanks and spills, incurred during transportation and distribution of the fuel, are responsible for a large number of the groundwater contamination incidents reported today. Gasoline and its individual components (as represented by xylene for the lighter aromatic fraction and decane for the less volatile fraction) were considered for investigation because of gasoline's abundant use and misuse. Kerosene is very similar in composition to the aviation fuel used in all military aircraft and long-distance passenger-carrying aircraft. Groundwater contamination problems have occurred from spills of aviation fuel at airfields and military bases around the country. PCE was one of two chemical carcinogens, TCE was the other, found most often in groundwater according to a report compiled in 1980 by the EPA Office of Drinking Water (Burmaster & Harris, 1982). PCE was also chosen because it represented the class of organic liquids that are denser than water.

The experimental results are presented in Tables 9-3 through 9-8. The eight kerosene experiments presented in Table 9-3 were run early in the project without the benefit of a constant temperature cabinet. The five gasoline experiments presented in Table 9-4 were conducted under good temperature control,as were the five n-decane experiment shown in Table 9-5. The six p-xylene tests summarized in Table 9-6 were conducted under a fume hood, but the temperature was fairly well controlled. Although the smaller density difference between water and the p-xylene resulted in greater error propagation for organic liquid saturations, the actual sample standard deviation was relatively small in comparison. The PCE tests described in Table 9-7 were also conducted under a fume hood with relatively good temperature control. A tabulation of the raw data from all these experiments can be found in Appendix D.

A summary of all the tests is given in Table 9-8. It is apparent that the soil packing was very consistent from the tests of one liquid to those of another. The soil dependent properties, porosity and bulk density, remained nearly constant over the most of the experiments. The porosities for the PCE experiments, however, were slightly but consistently lower than all the other experiments because the operator of these experiments tightened the top endcap on the column more than normal as an added precaution against leakage. This slightly lower soil porosity appeared to have no influence on the results.

We were concern about the variability of the maximum organic saturations shown in the tables, and whether this variability would substantially affect the residual saturation results. In running the

Trial	porosity (%)	error (%)	bulk density (g/cm³)	error (g/cm³)	Organic liquid saturation (%)				Temp. range (°C)
					maximum	error	residual	error	
1	33.1	0.4	1.765	0.002	73.3	2.0	28.1	0.9	5.0
2	33.0	0.4	1.769	0.003	52.8	1.6	28.3	0.9	4.0
3	33.7	0.4	1.751	0.003	78.9	1.6	27.3	0.9	3.0
4	33.2	0.5	1.765	0.003	70.1	2.0	25.3	0.8	3.0
5	33.8	0.5	1.747	0.003	73.8	2.1	23.8	0.8	3.0
6	33.7	0.4	1.750	0.002	73.1	2.0	23.3	3.2	5.0
7	33.3	0.3	1.760	0.001	80.1	2.1	25.4	0.8	2.0
8	35.0	0.5	1.721	0.008	80.9	2.8	29.0	1.5	7.0
Avg.*	33.6	0.6*	1.754	0.014*	72.9	9.0*	26.3	2.1*	——

* Average = sample mean ±standard deviation

TABLE 9-3. Summary of kerosene / Sevilleta sand saturated zone results.

Trial	porosity (%)	error (%)	bulk density (g/cm³)	error (g/cm³)	Organic liquid saturation (%)				Temp. range (°C)
					maximum	error	residual	error	
1	34.3	0.7	1.742	0.011	75.2	6.0	26.9	2.6	0.8
2	33.1	0.6	1.772	0.008	80.9	6.2	29.3	2.8	1.3
3	32.6	0.6	1.786	0.008	83.1	6.3	31.0	2.9	0.6
4	32.1	0.6	1.799	0.009	84.5	6.5	26.9	2.6	1.1
5	33.5	0.6	1.762	0.009	81.2	6.2	28.8	2.7	0.4
Avg.*	33.1	0.8*	1.772	0.022*	81.0	3.6*	28.5	1.7*	—

* Average = sample mean ±standard deviation

TABLE 9-4. Summary of gasoline / Sevilleta sand saturated zone results.

Trial	porosity (%)	error (%)	bulk density (g/cm³)	error (g/cm³)	Organic liquid saturation (%) maximum	error	residual	error	Temp. range (°C)
1	34.7	0.6	1.732	0.010	77.0	3.6	28.6	1.8	2.6
2	33.2	0.6	1.776	0.010	72.3	3.6	24.6	1.8	1.1
3	34.2	0.6	1.743	0.010	78.8	3.9	25.1	1.9	1.5
4	32.2	0.6	1.797	0.010	82.4	4.1	26.7	1.8	2.1
5	33.5	0.6	1.763	0.010	82.5	3.9	24.6	1.6	2.0
Avg.*	33.6	1.0*	1.762	0.026*	78.6	4.2*	25.9	1.7*	—

* Average = sample mean ±standard deviation

TABLE 9-5. Summary of n-decane / Sevilleta sand saturated cone results.

Trial	porosity (%)	error (%)	bulk density (g/cm³)	error (g/cm³)	Organic liquid saturation (%) maximum	error	residual	error	Temp. Range (°C)
1	34.1	0.6	1.747	0.009	62.0	8.1	24.3	4.0	2.6
2	33.0	0.6	1.753	0.011	79.6	11.1	23.7	5.3	1.1
3	32.8	0.6	1.781	0.009	72.4	9.8	21.3	3.9	1.5
4	32.6	0.6	1.786	0.009	78.2	10.0	20.1	3.6	2.1
5	34.0	0.5	1.748	0.008	78.2	8.7	26.2	4.3	1.3
6	33.0	0.5	1.754	0.008	78.6	8.7	21.8	3.7	0.6
Avg.*	33.3	0.6*	1.762	0.017*	75.3	9.4*	23.2	3.6*	—

* Average = sample mean ±standard deviation

TABLE 9-6. Summary of p-xylene / Sevilleta sand saturated cone results

Trial	porosity (%)	error (%)	bulk density (g/cm3)	error (g/cm3)	Organic liquid saturation (%)				Temperature range (°C)
					maximum	error	residual	error	
1	32.5	0.6	1.788	0.008	69.5	3.1	27.5	1.4	0.5
2	33.0	0.6	1.776	0.009	85.0	3.9	25.7	1.4	1.7
3	32.2	0.6	1.796	0.010	78.9	3.8	26.1	1.5	0.9
4	32.4	0.6	1.791	0.010	86.2	4.2	28.8	1.6	1.3
Avg.*	32.5	0.3*	1.788	0.009*	79.9	7.6*	27.0	1.4*	---

* Average = sample mean ±standard deviation

TABLE 9-7. Summary of PCE / Sevilleta sand saturated zone results.

Fluid	porosity (%)	bulk density (g/cm³)	maximum organic liquid saturation (%)	residual organic liquid saturation (%)
Soltrol (13 trials)	33.9 ± 0.6	1.752 ± 0.016	85.1 ± 2.8	27.1 ± 1.7
Kerosene (8 trials)	33.6 ± 0.6	1.754 ± 0.014	72.9 ± 9.0	26.3 ± 2.2
Gasoline (5 trials)	33.1 ± 0.8	1.772 ± 0.022	81.0 ± 3.6	28.5 ± 1.7
n-decane (5 trials)	33.6 ± 1.0	1.762 ± 0.026	78.6 ± 4.2	25.9 ± 1.7
p-xylene (6 trials)	33.5 ± 0.6	1.762 ± 0.017	75.5 ± 6.4	23.3 ± 2.6
PCE (4 trials)	32.5 ± 0.3	1.788 ± 0.009	79.9 ± 7.6	27.0 ± 1.4
all liquids	33.5 ± 0.8	1.761 ± 0.020	79.5 ± 7.1	26.4 ± 2.4

Average = sample mean ± standard deviation

TABLE 9-8. Average values for different organic liquids in the Sevilleta sand saturated zone experiments.

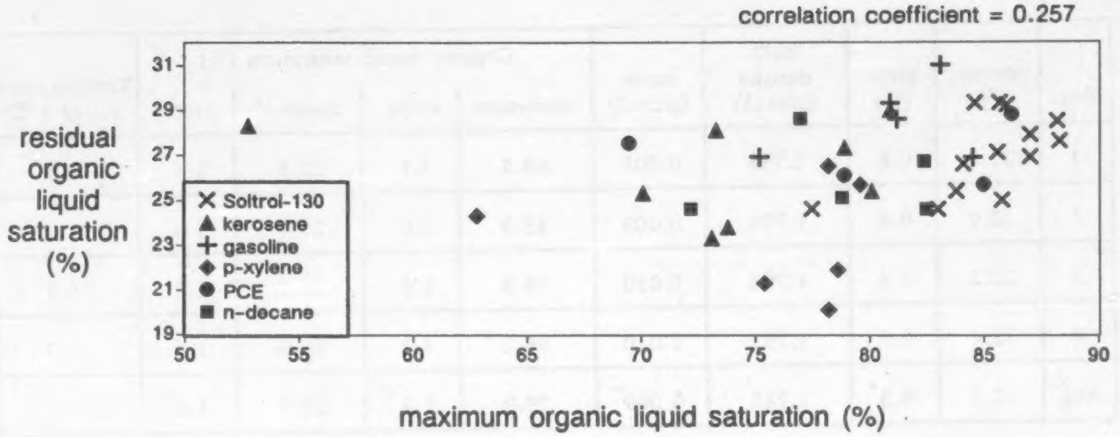

FIGURE 9-25. **Residual organic liquid saturation as a function of the maximum organic liquid saturation.**

experiments we avoided applying high suctions for fear of exceeding the breakthrough pressure of the bottom, semi-permeable membrane. As a consequence, we were not always certain that the water had been completely reduced to irreducible saturation and that the maximum organic saturation had been achieved. A plot of maximum organic liquid saturation versus residual saturation for all the experiments is shown in Figure 9-25. Visual inspection of the scatter plot does not reveal much correlation between maximum organic saturation and residual saturation, but least-squares regression analysis reveals a slight positive correlation.

Discussion of Experiments with Various Organic Liquids

The relationship between residual saturation and the type organic liquid is graphically displayed in Figure 9-26. The average residual organic liquid saturation, S_{or} , was relatively uniform, varying from a low value of 23.3% for p-xylene to a high value of 28.5% for gasoline, and similar to the value for Soltrol, 27.1%. The average residual saturation over all the fluids was 26.4%. All of the fluids were tested against one another for a statistically significant difference in the sample means using the student's t-test. Although the differences in residual saturations between the fluids appear to be small, the p-xylene results were found to be statistically different from each of the other fluids at the 97.5% confidence interval ($\alpha = 0.025$).

P-xylene was the most soluble of the organic liquids tested (~0.20 g/l). In each experiment, we flushed at least six pore volumes, or about 250 ml of water through the column to reach residual saturation. If we assume the water was flooded slowly enough so that the effluent water had reached equilibrium with the xylene, then as much as 0.05 g of xylene could have been removed from the column by dissolution, resulting in an underestimation of the residual saturation by as much as 1.0%. The reduction of xylene's residual saturation by dissolution may account for the significant difference in residual saturation between it and the other fluids tested. The residual saturations of kerosene and

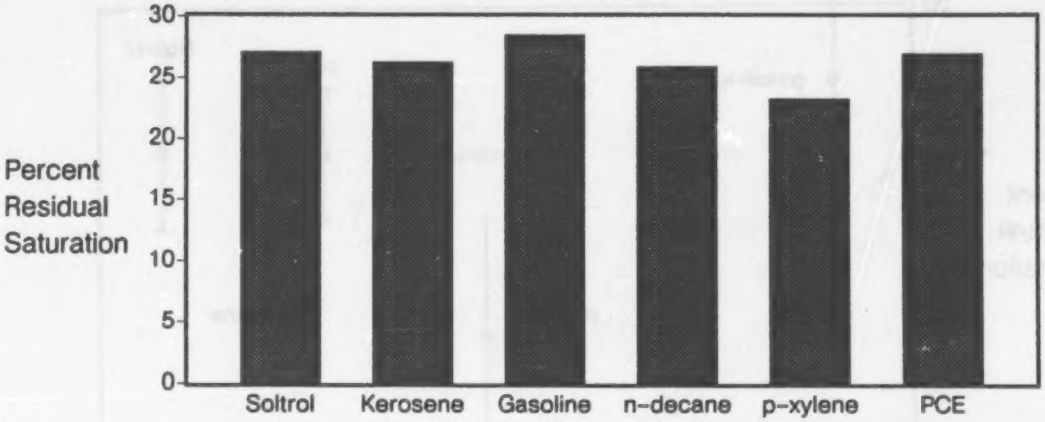

FIGURE 9-26. Residual organic saturation for tested organic liquids in the Sevilleta sand.

gasoline were also found to have statistically different sample means. At the 95% confidence interval ($\alpha = 0.05$), the difference was just barely significant (the calculated value of $t = 1.96$ was greater than the critical value of $t = 1.78$). This result may stem from some bias introduced by the poor temperature control for the kerosene experiments. None of the remaining combinations showed significant differences in residual saturations between fluids at the 97.5% confidence interval.

Influence of Interfacial Tension–

These same residual saturation results are again plotted in Figure 9-27, as a function of the interfacial tension (IFT) between water and the organic liquid (see Section 4 for IFT data). There appears to be no discernible correlation between IFT and S_{or} , just as we had hypothesized. The capillary forces (proportional to the IFT) so outweigh the other forces which may act to reduce trapping (buoyancy and viscous forces) that halving the interfacial tension — from an IFT of 47.8 for Soltrol to only 22.9 for gasoline — has no effect on the amount of organic liquid trapped. Indeed, at typical aquifer flow rates IFT's may have to be reduced by at least an order of magnitude or more before reaching the critical capillary number and any reduction in trapping occurs. This as can be illustrated in the following analysis.

Consider again the pore scale trapping mechanisms discussed earlier in this section. If we look at these mechanisms in a quantitative way, using — as an example — the flow rates of these experiments together with some observed characteristics of the Sevilleta sand, we can attempt some prediction of the reduction of interfacial tensions required to begin to lower residual organic saturations.

Let's consider the snap-off mechanism first. Wardlaw (1982) performed flow visualization experiments in glass micromodels using a single pore and pore throat to examine snap-off as a function of several properties including interfacial tension. An illustration of the pore and pore throat pair used in Wardlaw's experiments is given in Figure 9-5. For strongly water-wet systems, snap-off occurred for all fluid pairs studied even though the interfacial tensions ranged from 480 dyne/cm down to 0.1 dyne/cm. Trapping by snap-off was found to be insensitive to IFT down to 0.1 dyne/cm and it is expected that IFT's would have to be reduced still much further to avert the Haine's jump instability that leads to snap-off.

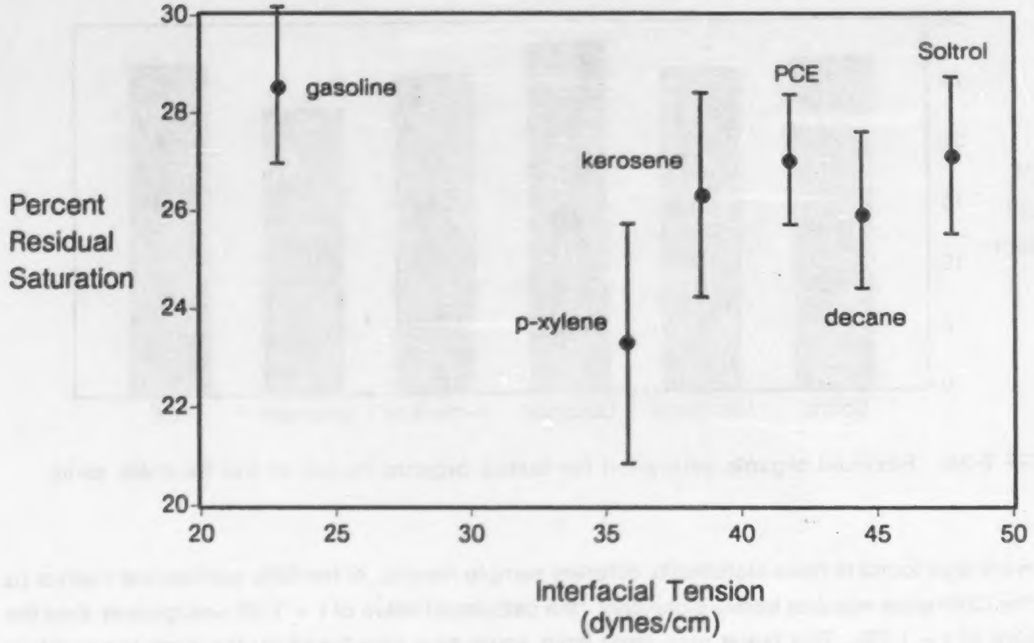

FIGURE 9-27. Residual organic saturation as a function of interfacial tension (IFT). The error bars represent the sample standard deviations taken from Table 9-8.

Although it appears that snap-off cannot be averted, perhaps for low enough IFT's the blob could become mobilized immediately after the Haine's jump caused its formation. Oh and Slattery (1979) in a theoretical study looked at the pressures required to mobilize blobs in a periodically constricting tube (similar to that shown in Figure 9-4). The critical dimensionless pressure needed for mobilization in a strongly water-wet pore with an aspect ratio of about four was:

$$\frac{\Delta P \ r_t}{2 \ \sigma} = 1.03 \qquad (9\text{-}12)$$

where: ΔP = Pressure drop across the blob
r_t = Radius of the pore throat
σ = Interfacial tension

As an example, we looked at the interfacial tension needed to mobilize the singlet blob pictured in Figure 9-18a. With a flux rate in our column experiments of about 2.5×10^{-4} cm/s, we estimated the pressure drop across the blob to have been about 3.7 dyne/cm². The pore throat radius was estimated to be about 50 microns and the aspect ratio to be 4. Using these estimates, the interfacial tension would need to be less that 0.01 dyne/cm to induce mobilization of the blob.

Now let's consider the by-passing mechanism. To prevent trapping in a pore doublet like the one shown in Figure 9-8, the velocities of the interfaces traveling through each pore would have to be about equal. That is, either the flow rate needs be increased, or the capillary forces reduced (by reducing the IFT) so that the water does not preferentially travel through the smaller pore of the doublet. To evaluate this, we used the equation presented by Moore and Slobod (1956) for computing competing velocities in a pore doublet:

$$\frac{v_1}{v_2} = \frac{\dfrac{4lQ\mu}{\pi r_2^2} + r_2^2\left(\frac{1}{r_1} - \frac{1}{r_2}\right)\sigma\cos\theta}{\dfrac{4lQ\mu}{\pi r_1^2} - r_1^2\left(\frac{1}{r_1} - \frac{1}{r_2}\right)\sigma\cos\theta} \qquad (9\text{-}13)$$

where: v_i = Velocity through pore i
l = Length of the pores
Q = Total flow rate through the doublet, $\frac{q\pi(r_1^2 + r_2^2)}{n}$,
q = Specific discharge
μ = Viscosity
r_i = Radius of pore i
σ = Interfacial tension
θ = Contact angle

We set the ratio of the velocities equal to one and solved for σ using reasonable values from our experiments in the Sevilleta sand. We let: $r_1 = 100\mu\text{m}$; $r_2 = 75\mu\text{m}$; $l = 400\mu\text{m}$; $\mu_o = \mu_w = 1\text{cP}$; the average flux rate, $q = 2.5 \times 10^{-4}$ cm/s; the porosity, $n = 0.33$, and the contact angle, $\theta = 0^0$. Under these circumstances, σ would have to be less than 2 dyne/cm to avert trapping by by-passing.

By looking at the pore scale mechanisms that cause trapping, and by relating these mechanisms to our particular experimental system, we have been able to show why S_{or} appears to be independent of IFT in these experiments — and why S_{or} would be expected to be independent of IFT for many commonly spilled organic pollutants in soils(shown in Table 9-8).

Influence of Viscosity and Density–

Figure 9-29 relates observed residual saturations to non-wetting phase viscosity. Residual saturations were hypothesized to be independent of viscosity and the results match expectations. Some variability in S_{or} might have been possible had fingering occurred, but since low flow rates were used the displacements were stable with respect to density, and the favorable viscosity ratio (μ_o / μ_w) prevented viscous instabilities.

A plot of observed residual saturation versus non-wetting phase density is shown in Figure 9-30. There appears to be no overall correlation between density and S_{or} and none was expected. However, fluids having a larger density difference with water tend to give more accurate results due to our gravimetric method of measuring saturations. For those organics lighter than water, there appears to be a decrease in S_{or} as the density of the fluids approach one (as the density difference between the

PRIORITY POLLUTANT	INTERFACIAL TENSION (dyne/cm)
carbon tetrachloride	45.0
PCE	47.5
benzene	35.0
chlorobenzene	37.4
ethylbenzene	38.4
toluene	36.1
phenol	39.3^{A} (40°C)
o-chlorophenol	42.25^{B}
naphthalene	28.8^{B}

A — Lyman et al., 1982
B — Weast, 1986

TABLE 9-9 **The interfacial tension of some priority pollutants with water at 20°C. The data were obtained from Girifalco and Good (1957) unless otherwise noted.**

organic and water approaches zero). This is the opposite effect one would expect had buoyancy played a role. This is probably a coincidental effect of the reduced measurement accuracy as ϱ_o approaches ϱ_w.

A larger density difference increases the buoyancy forces, but in this case we are well below the threshold for gravity induced reduction of trapping. However, had we been testing a very coarse soil — a gravely soil perhaps — we may not have been able to disregard buoyancy effects.PCE was the only organic liquid tested having a density greater than water. Even so, the residual saturation measurements do not appear to have been affected. THE PCE experiments were run with the column upside down from the other experiments to prevent any density induced instabilities. It is important to realize that on an aquifer scale, as a dense organic liquid percolates downward through the saturated zone, density induced fingering may well develop. This is most likely to occur in a layered soil, where a fine material overlies a coarse material. It may be possible to exceed critical Bond numbers in this situation.

Summary–

Residual saturation has been shown to be invariant with respect to fluid properties, at least over the range of fluid properties for common organic pollutants, and for the low capillary and Bond number conditions of these experiments.

Implications for measurements of residual saturation–

Although it seems reasonable to directly measure residual saturations of whatever organic liquid was spilled at a particular contamination site, it might be better to chose an ideal fluid with which to run residual saturation experiments. Unless some odd wetting behavior is anticipated, or unless some

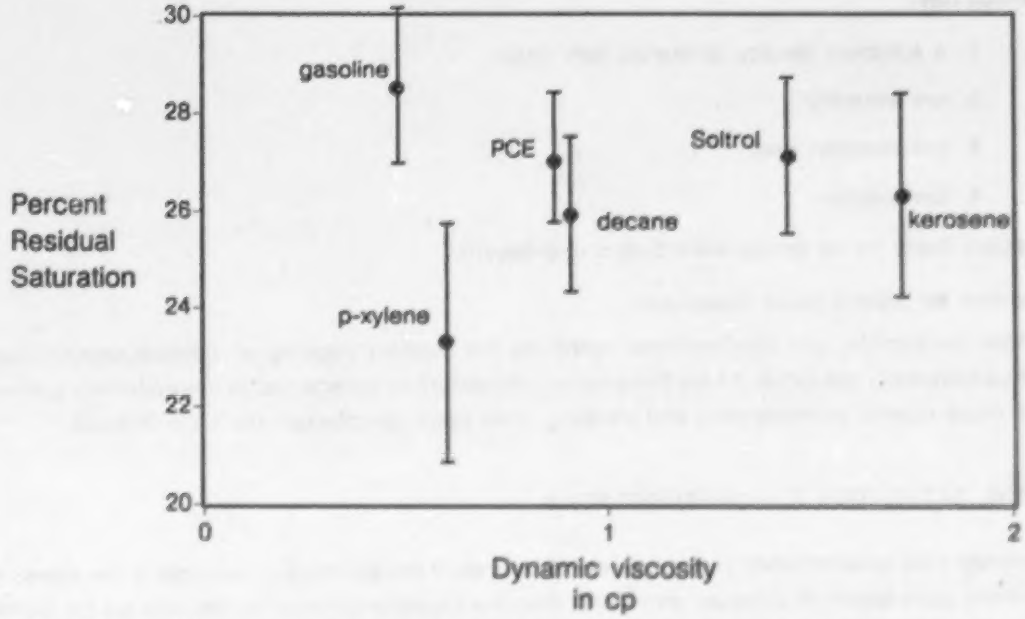

FIGURE 9-28. **Residual organic saturation as a function of non-wetting phase viscosity. The error bars represent the sample standard deviations taken from Table 9-8.**

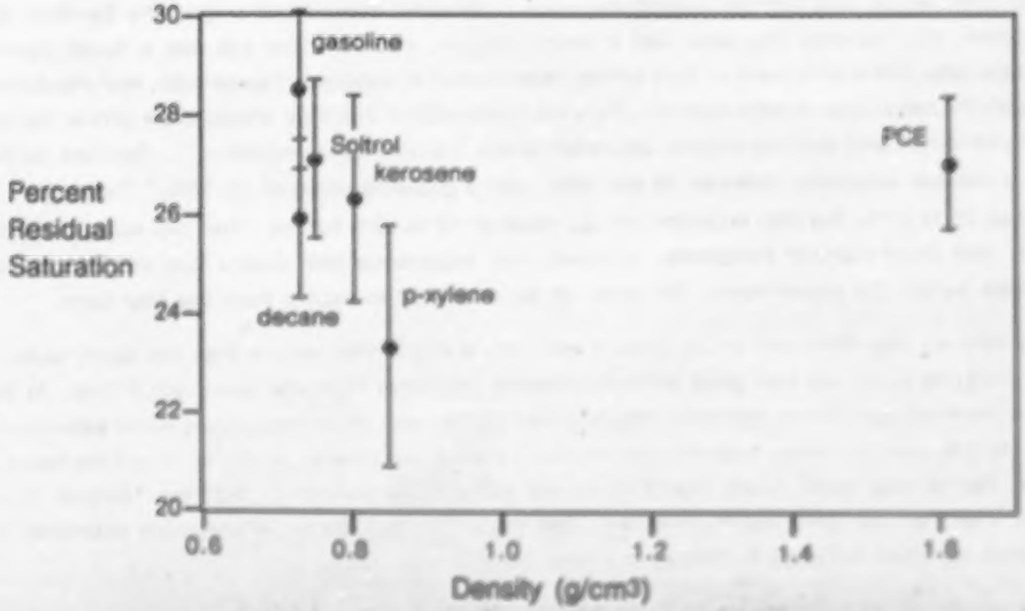

FIGURE 9-29. **Residual organic saturation as a function of non-wetting phase density. The error bars represent the sample standard deviations taken from Table 9-8.**

interaction between fluids or between fluids and the solid is expected, it is probably preferable to chose a fluid which has:

1. a sufficient density difference with water;
2. low solubility;
3. low volatility; and,
4. low toxicity.

The easiest fluids for us to use were Soltrol and decane.

Implications for organic liquid movement–

Under low capillary and Bond number conditions the capillary trapping of different organic liquids should be essentially the same. As we'll see below, the texture of the soil and its heterogeneity generally has far more control on movement and trapping, than does composition the organic liquid.

RESIDUAL SATURATION FOR DIFFERENT SOILS

Different soils have different pore sizes and structures. If the structure of two soils is the same, say two uniform glass beads of different diameters, then the capillary behavior of the soils will be identical when scaled by capillary and Bond numbers. If the structure is different, then the soils may not be scaled. For example, one soil structure may lead to capillary trapping of the non-wetting phase by snap-off, while another soil may be dominated by a by-passing mechanism. We examined capillary trapping in four soils: three sandy soils and a clay loam.

The three sandy soils that we investigated were of different depositional origin. The Sevilleta sand was aeolian, the Traverse City sand was a beach deposit, and the Llano soil was a fluvial deposit. Never-the-less, these soils were all fairly similar (see Section 4, especially Figure 4-5), and should have had much the same type of pore network. Thus we hypothesized that they should show similar capillary trapping behavior, and residual organic saturation levels. Recall that we expected "...Sevilleta sand to exhibit a residual saturation between 15 and 25%, with a probable value of 18-20%." The actual S_{or} value was 25 to 29%. We also expected an S_{or} value of 18 to 20% for the other two soils, under low capillary and Bond number conditions. However, our experience with Soltrol had us doubting this hypothesis before the experiments. We were not sure of what to expect from the clay loam.

The Palouse clay loam was an agricultural soil, with a much finer texture than the sandy soils. As shown in Figure 4-11, we had great difficulty draining the water from the loam with Soltrol. At high suctions the maximum Soltrol saturation reached was 11.7%, with an corresponding water saturation of 88.3%. At this point air broke into the column and we were not able to obtain an imbibition curve or residual Soltrol saturation. From Figure 4-11 we subjectively estimated that the residual Soltrol saturation for Palouse loam would have been less than 10%, but this is an unreliable estimate. The saturations reported in Figure 4-11 may not have been at equilibrium.

The results of our experiments on Traverse City and Llano soils using Soltrol are shown in Tables 9-10 and 9-11. All experiments were conducted under good temperature control conditions. The

Trial	porosity (%)	error (%)	bulk density (g/cm³)	error (g/cm³)	Organic liquid saturation (%) maximum	error	residual	error	Temp. range (°C)
1	34.4	0.6	1.738	0.009	85.1	7.3	17.0	2.4	0.7
2	35.7	0.6	1.705	0.010	84.6	6.8	15.8	1.9	1.9
3	36.0	0.6	1.696	0.009	86.6	6.9	19.3	2.2	1.7
4	33.9	0.6	1.753	0.010	88.0	7.2	18.4	2.1	1.1
Avg.*	35.0	1.0*	1.723	0.027*	86.1	1.5*	17.6	1.5*	----

*Average = sample mean ± standard deviation

Table 9-10 Summary of Soltrol / Traverse City soil saturated zone results.

Trial	porosity (%)	error (%)	bulk density (g/cm³)	error (g/cm³)	Organic liquid saturation (%) maximum	error	residual	error	Temp. range (°C)
1	37.2	0.6	1.665	0.009	90.2	3.7	18.5	1.4	1.6
2	37.5	0.6	1.656	0.009	91.9	3.8	15.8	1.3	1.3
3	37.5	0.5	1.656	0.008	92.2	3.6	14.4	1.2	1.8
4	38.1	0.5	1.640	0.008	88.0	3.4	13.9	1.1	1.4
5	37.2	0.6	1.664	0.009	90.2	3.7	16.5	1.3	1.7
Avg.*	37.5	0.4*	1.656	0.010*	90.5	1.5*	15.8	1.8*	----

*Average = sample mean ± standard deviation

Table 9-11. Summary of Soltrol / Llano soil saturated zone results.

average residual saturation of Soltrol in the Traverse City soil was 17.6%, while it was 15.8% in the Llano soil. These saturations were slightly lower than the range that we had initially hypothesized for this type of soil (18-20%), and almost 10% lower than the residual saturation found in the Sevilleta soil. As shown in Figure 9-30 and Table 9-12, this 10% difference is significant. In contrast, the minor S_{or} difference between the Traverse City and Llano soils is not significant.

Discussion of Experiments with Different Soils

We hypothesized that the three sandy soils would behave more like glass beads, than like sandstone. The evidence supports this hypothesis for the Traverse City and Llano soils. The observed residual Soltrol saturations of 14-19% were in the low end of the range of 18-20% that we had anticipated, and only slightly higher than the values observed for uniform glass beads.

A lower mean S_{or} value was observed for the Llano (15.8%), than for the Traverse City (17.6%). This difference is not statistically significant. We would expect the less uniform soil (Llano) to experience more trapping through by-passing, and thus to have a higher residual saturation. This was not the case in these experiments. The coarser material (Llano) would have had a higher capillary number during the imbibition (water flooding) phase of the experiment, because of its larger k value. Thus it is possible that the capillary number was too high during the water flood, and less Soltrol was originally trapped. The data qualitatively support this possibility, but not statistically. Our estimates for capillary numbers in these experiments are well below the threshold for this condition.

The grain size curves for the Sevilleta and Traverse City soils are almost identical, while the Llano curve indicates a coarser and less uniform material (see Figure 4-5). Why are residual saturations so different between two almost identical sands (Sevilleta and Traverse City), and so much alike in sands with much less similar grain sizes and distributions. Perhaps it is more appropriate to ask, *"Why are residuals in the Sevilleta sand so high?"*. After all, one would expect a uniform, unstructured sand like the Sevilleta to behave in a manner similar to glass beads -- as the Traverse City and Llano soils presumably did.

We hypothesize that while packing the columns with Sevilleta soil some small-scale layering developed. The Sevilleta sand contains a small but not negligible fine clay fraction not present in the Traverse City or Llano sands. This fine fraction is not readily observed in Figure 4-5, which reports the results of a dry sieve analysis. The clay content may have been as high as 1% by weight, and could have played an important role in the formation of fine layers in the column. We hypothesize that a fine layer settled at the top of each lift of the packed column. The thickness of the layers was presumably variable, depending on the time between lifts, and whether the packing process was interrupted. We did not actually observe layering, either in the sides of the short glass columns or in the pore casts (unfortunately, we did not cut the pore casts longitudinally, which might have shown the layers were they present). The layers would have caused the column to be heterogeneous. The effect of heterogeneities on multi-phase flow are explored in detail later in this chapter. In effect, heterogeneousness can dramatically increase residual saturation. Unfortunately, we developed this hypothesis too late in the project to be able to test it. None of the heterogeneities explored later correspond to this layering hypothesis. We recommend that future research efforts explore this issue further. Another hypothesis is

Fluid	porosity (%)	bulk density (g/cm³)	maximum organic liquid saturation (%)	residual organic liquid saturation (%)
Sevilleta (13 trials)	33.9 ± 0.6	1.752 ± 0.016	35.1 ± 2.8	27.1 ± 1.7
Llano (4 trials)	37.5 ± 0.4	1.656 ± 0.010	40.5 ± 1.6	15.8 ± 1.8
Traverse City (6 trials)	35.0 ± 1.0	1.723 ± 0.027	36.1 ± 1.5	17.6 ± 1.5
all sands	35.5 ± 1.8	1.71 ± 0.05	37.2 ± 2.9	20.2 ± 6.1

Average = sample mean ± standard deviation

TABLE 9-13. Average values of measured properties and saturations for different sandy soils, in the saturated zone experiments run with Soltrol.

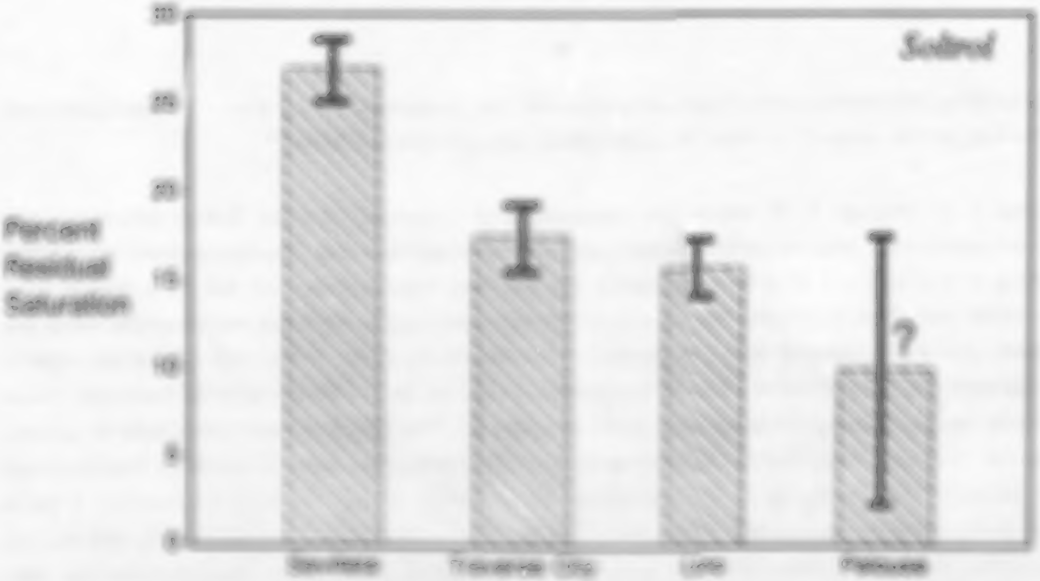

FIGURE 9-16. Residual organic saturation for Soltrol in sand soils. The error bars represent sample standard deviations, except for the [illegible] loam, where the error bar is a subjective indication of the poor quality of that experiment.

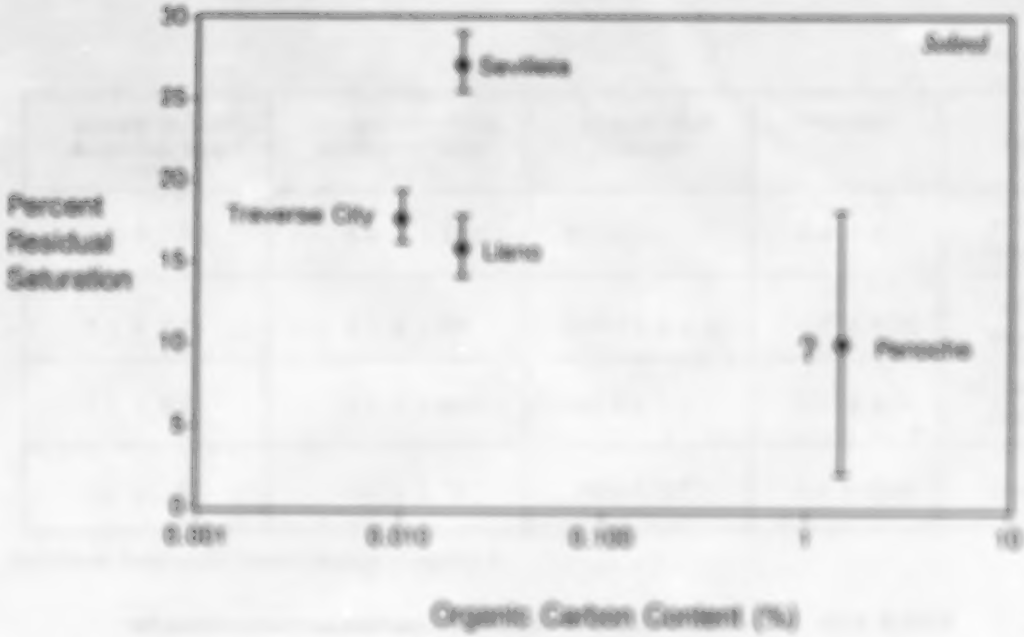

FIGURE 9-21. Residual organic saturation for Soltrol, as a function of organic carbon content in different soils. The error bars represent the sample standard deviations taken from Table 9-15. The organic carbon contents are of unknown uncertainty.

that clay swelling obstructed pore throats, and increased the propensity for by-passing. This hypothesis arose too late in the project to allow the appropriate clay mineralogy tests.

Figures 9-21 through 9-23 explore the relationship of observed residual Soltrol saturation and various soil properties: organic carbon content, porosity and permeability. Organic content may affect the wetting of the soil and thus would influence the trapping mechanisms. All the soils tested were strongly water wet. Thus we expect that the organic material was aggregated in a few locations within the pore space, rather than spread thinly over the mineral surfaces. As shown in Figure 9-21 the soil organic carbon content did not appear to have any systematic influence on capillary trapping. However, these experiments were not designed to elucidate such an influence. Porosity is a measure of pore structure, and thus may show a correlation to residual organic liquid saturation. Figure 9-22 indicates that the lower porosity material had the higher residual saturation. Presumably, the by-passing mechanism is more common in the lower porosity material (see, eg., Chatzis et al., 1983; Pathak et al., 1982). We are not convinced that the trend shown in the figure is reliable. For example, the Sevilleta may have been packed with layers, whereas we do not believe layering occurred for the other two soils. The Llano sand had the least uniform grain distribution, but the highest porosity. This is not what one would expect for consistent packings, from material to material. The correlation of porosity to residual saturation needs to be explored in future research. The influence of permeability on residual Soltrol saturation is shown in

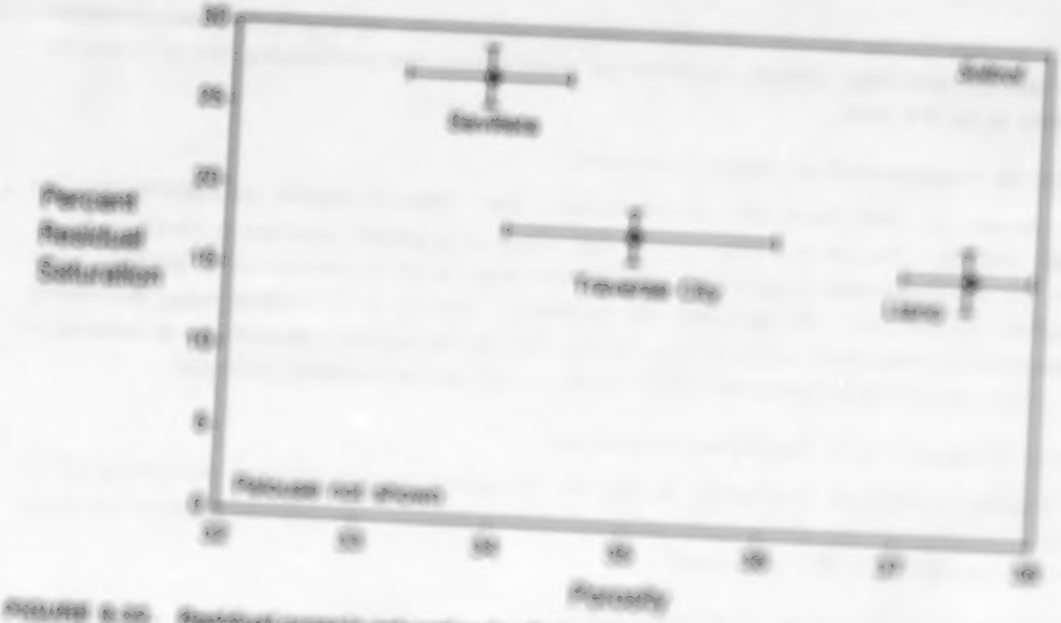

FIGURE [illegible]. Residual organic saturation for Soltrol, as a function of porosity in different soils. The error bars represent the sample standard deviations taken from Table [illegible].

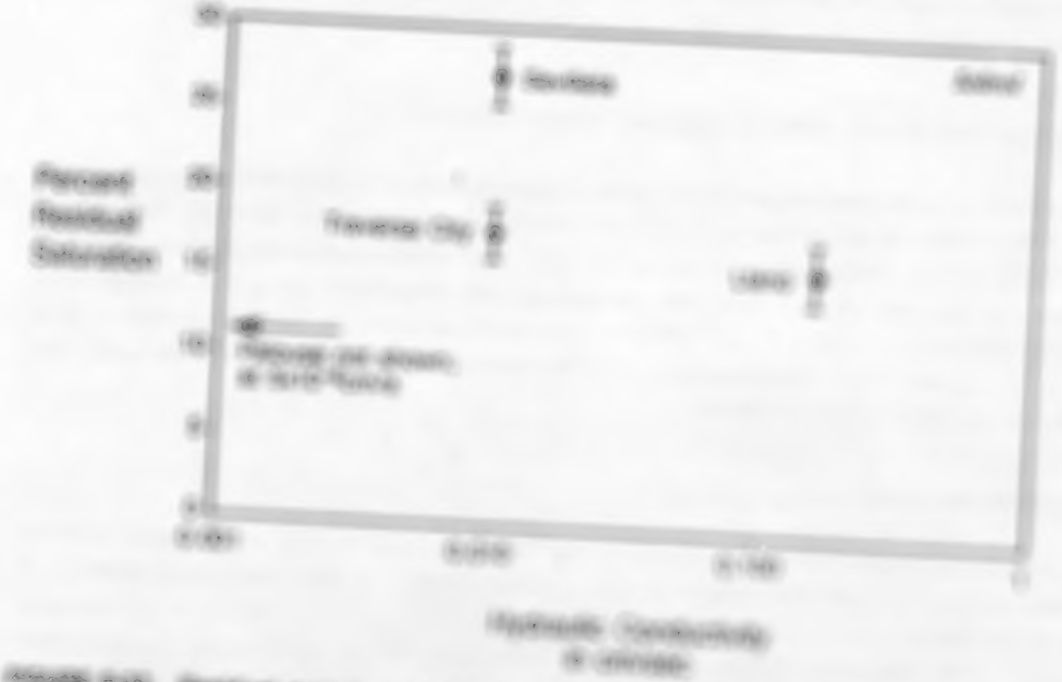

FIGURE [illegible]. Residual organic saturation for Soltrol, as a function of [illegible] hydraulic conductivity in different soils. The error bars represent the sample standard deviations taken from Table [illegible].

[illegible]

[illegible]

[illegible]

[illegible]

[illegible]

[illegible]

[illegible]

[illegible]

[illegible]

[illegible]

[illegible]

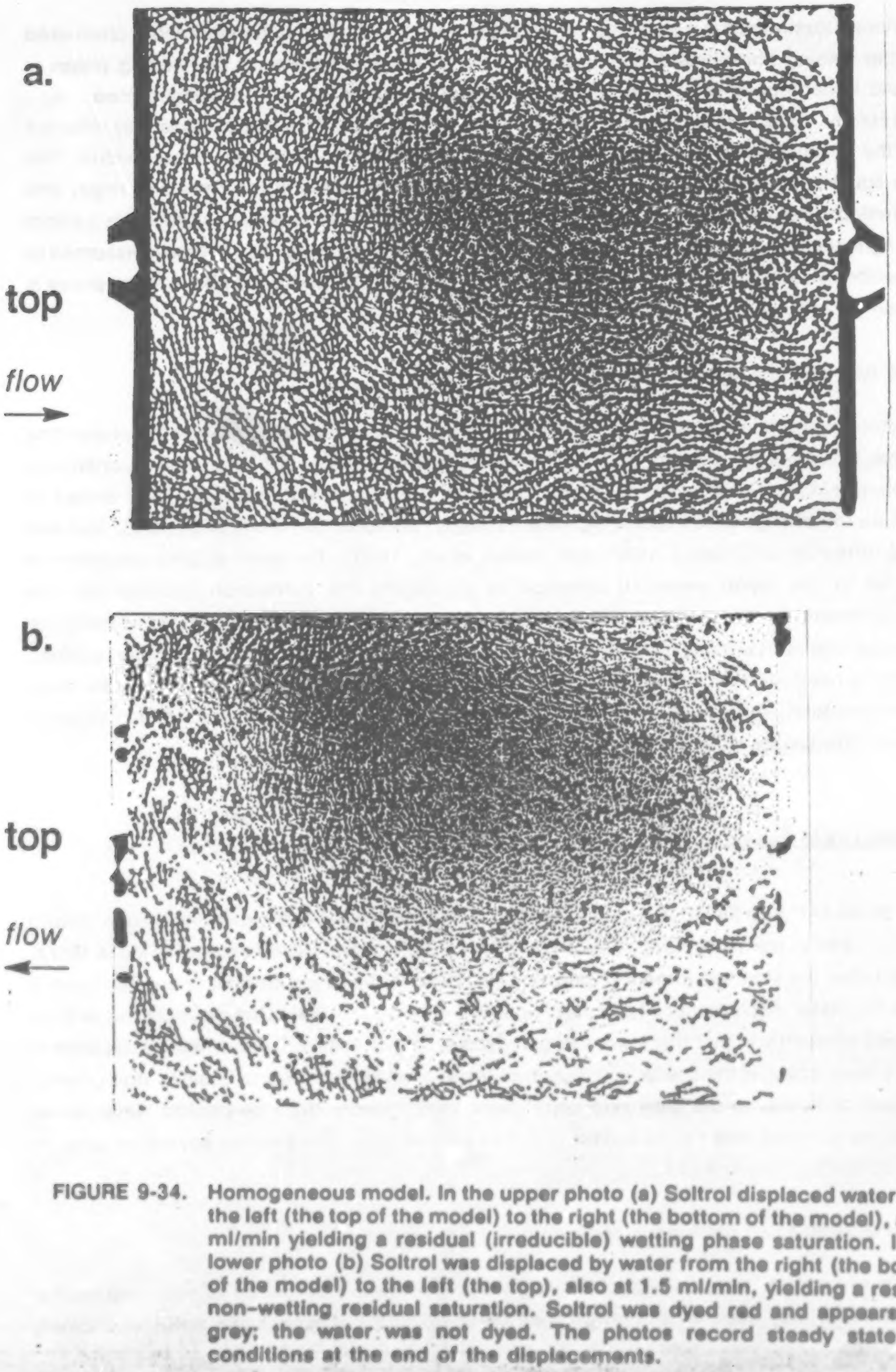

FIGURE 9-34. Homogeneous model. In the upper photo (a) Soltrol displaced water from the left (the top of the model) to the right (the bottom of the model), at 1.5 ml/min yielding a residual (irreducible) wetting phase saturation. In the lower photo (b) Soltrol was displaced by water from the right (the bottom of the model) to the left (the top), also at 1.5 ml/min, yielding a residual non-wetting residual saturation. Soltrol was dyed red and appears dark grey; the water was not dyed. The photos record steady state flow conditions at the end of the displacements.

This experiment illustrates the misleading nature of the term 'irreducible water saturation' often used to represent the wetting phase residual saturation. Even at residual saturation the wetting phase is continuous, and is composed of an interconnected network of films, rings and wedges (see, eg., Amaefule and Handy, 1982; Dullien, *et al.*, 1986; Chatzis, *et al.*, 1988) This is a considerably different situation than the discontinuous 'blobs' pictured in this report for the non-wetting phase residual. The wetting phase liquid can move through its interconnected network, draining the films and rings, and reducing the residual wetting phase saturation. Reducible wetting phase residual saturation is seldom considered in agriculturally oriented soil physics where the non-wetting phase, air, is usually assumed to be at static equilibrium. In petroleum geology and reservoir engineering, where the non-wetting phase is crude oil, it can be important although its usually ignored.

Implications to fluid flow modeling-

Several recent experiments provide some idea of the correlation between non-wetting phase flow and wetting phase residual for reservoir rocks. The wetting phase residual appears to be a continuous function of non-wetting phase flow rate, although the flow rate apparently must vary over orders of magnitude before the change in residual is significant (Handy, personal communication,1988; also see earlier work of Amaefule and Handy, 1982, and Dullien, *et al.*, 1986). The short column experiments described earlier in this report were not designed to investigate this correlation quantitatively.The micromodel experiments shown in this report and in Dullien *et al.* (1986), provide ample visual evidence that an increase of the non-wetting phase flow rate leads to a decrease of the wetting phase residual. Further research is needed to determine this relationship, its importance to fluid flow, and its relevance to conditions encountered in the field. In particular, most models of pore pressure-saturation assume a fixed and known 'irreducible water saturation'.

Residual Organic Liquid Saturation

The lower photo of Figure 9-34b depicts the residual Soltrol saturation at the completion of a upward displacement by water at the same 'fast' rate of 1.5 ml/min. The residual Soltrol saturation looks similar to that observed after the slow experiment (Figure 9-11b), despite the larger amount of organic liquid in storage before the water displacement (compare Figures 9-11a and 9-34a). One possible explanation for this increased efficiency is that there were larger viscous forces involved in the fast displacement. Perhaps a more likely cause is the spatial distribution of residual water and organic liquid in storage after the organic liquid advance. In the slow rate experiment the relatively large by-passed water zones remaining after the advance (see Figure 9-34a) provided pathways for the upwardly advancing water to by-pass large zones of organic liquid.

Implications for organic liquid movement, trapping and its modeling-

The amount of capillary trapped organic liquid, and therefore the efficiency of hydraulic aquifer remediation activities, may depend strongly on the rate at which the organic liquid pollutant originally invaded the aquifer.

INFLUENCE OF WATER FLOW RATE ON RESIDUAL ORGANIC MOBILIZATION

Earlier in this section we reviewed published evidence that sufficiently high rates of flow in the wetting phase can reduce the amount of capillary trapped non-wetting phase(eg., Melrose and Brandner, 1974; Ng *et al.*, 1978; Chatzis and Morrow,1981; Chatzis *et al.*, 1984; Hornof and Morrow, 1988; Morrow *et al.* 1988). This mobilization of the residual non-wetting phase can be correlated to capillary number (see, eg, Figures 9-9 and 9-10) and Bond number (Morrow and Songkran, 1981;Morrow *et al.* 1988). Aquifer remediation schemes may depend in whole, or in part, on the mobilization of the trapped organic liquid, by increasing the effective capillary number (Wilson and Conrad, 1984). Mobilization correlations exist for sandstones (Figure 9-9) and glass beads (Figure 9-10), but not for natural soils. We expect that the correlation depends on the soil pore structure, and that it will vary from soil to soil. Understanding this natural soil correlation would help define under what conditions it is possible to hydraulically mobilize trapped organic liquids — and when it is not possible. It would also help prevent inadvertent mobilization of organic liquids during laboratory experiments.

We investigated the mobilization of organic liquids in natural soils by mobilizing capillary trapped Soltrol in the Sevilleta and Llano soils. We hypothesized that, because soil texture considerations (see the grain size curves, Figure 4-5), the mobilization correlations for the Sevilleta and Llano soils should look more like that of glass beads, than like that of sandstones (see Figures 9-9 and 9-10). Given our experience with low capillary number residual saturations in these soils (see Table 9-12), we also expected that the Llano soil correlation would be the closest to the glass bead correlation.

The long column apparatus and procedure used in these experiments are described in Section 6. One experiment was performed on each soil. The soil packed columns were water saturated, drained with Soltrol, and then flooded with water under fairly low capillary number conditions. Once an initial residual Soltrol saturation was established the column flow rate was increased incrementally, and the residual saturation was re-measured at each step. Mobilization was indicated by a lower residual saturation. Table 9-13 and Figure 9-35 summarize the initial conditions for the mobilization portion of the experiments. The initial residual Soltrol saturations were within the range measured in the short column experiments.The mobilization results are given in Figure 9-36. We were not able to effectively mobilize a significant portion of the residual Soltrol saturation in either column, due to limited pump capacity (see Section 6).

Figure 9-36 contrasts our mobilization results with the published correlations for sandstones and uniform glass beads. The Llano data follows the glass bead correlation, up to the capillary number tested. The Sevilleta soil data deviates from the uniform glass bead curve, at a critical capillary number, $N_c^{1} = q_w \mu_w / \sigma$, of 8×10^{-5}. This critical capillary number is about 40 times higher than the value observed for sandstone (see the figure), but perhaps about one fourth of the value for glass beads. In fact, the Sevilleta data appears to follow the pattern observed by Morrow *et al.* (1988) for sintered glass beads (beads fused partially together in a furnace).

The observed data is consistent with our hypothesis. Both soils behaved much like glass beads, with the Llano soil being the closest. The hypothesis is not confirmed, however, because of a lack of data at higher capillary numbers

Soil	porosity (%)	bulk density (g/cm³)	water satuated hydraulic conductivity (cm/s)	maximum organic liquid saturation (%)	residual organic liquid saturation (%)
Sevilleta (1 trial)	37.2 (33.9)	1.66 (1.752)	1.9 (1.0) $\times 10^{-2}$	72.8 (85.1)	26.0 (27.1)
Llano (1 trial)	37.3 (37.5)	1.67 (1.656)	17 (16) $\times 10^{-1}$	81.1 (90.5)	17.2 (15.8)
Notes:	Apparently, the Sevilleta column was not packed at maximum density.			Drainage with Soltrol was halted before the maximum Soltrol saturation had fully stabilized.	

TABLE 9-13. Long column data for two different sandy soils run with Soltrol. The numbers in parentheses refer to the average values for the short colum experiments (taken from Table 9-12).

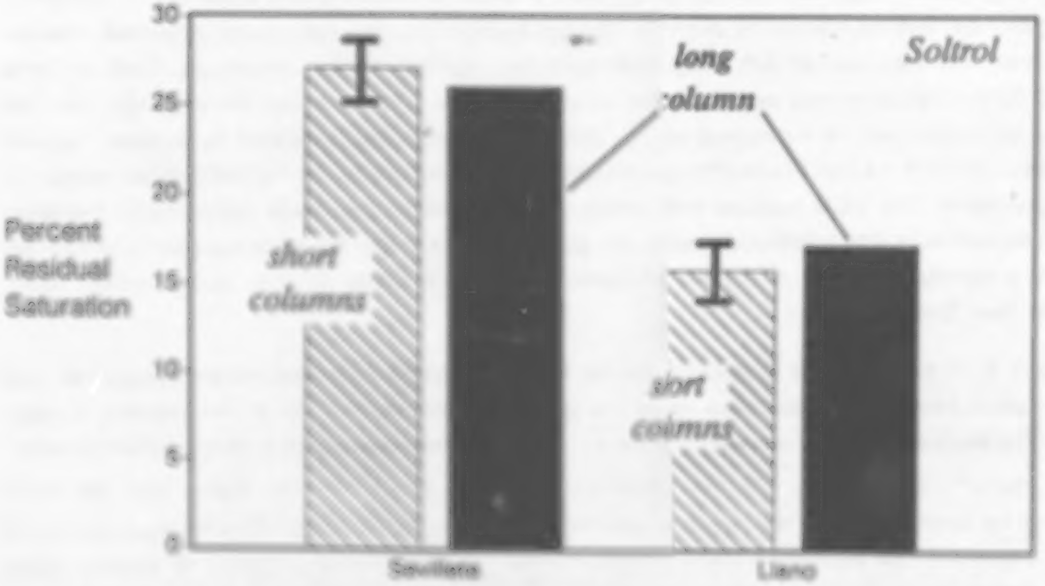

FIGURE 9-35. Residual organic saturation, in short an long columns, for Soltrol in the tested soils. The error bars represent sample standard deviations for the short column experiments.

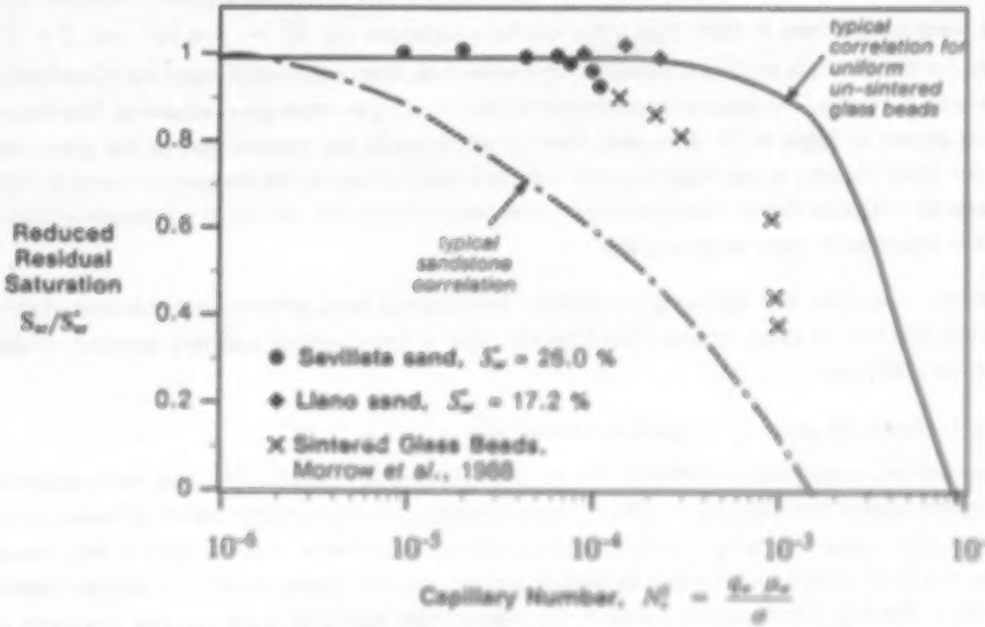

FIGURE 9-36 Relationship between Soltrol residual saturation and capillary number, N_c^{ℓ}, for Sevilleta sand and Llano sand. Its compared to sandstone data from Chatzis and Morrow (1981,1984) and bead-pack data from Morrow and Chatzis (1982), and Morrow et al. (1988).

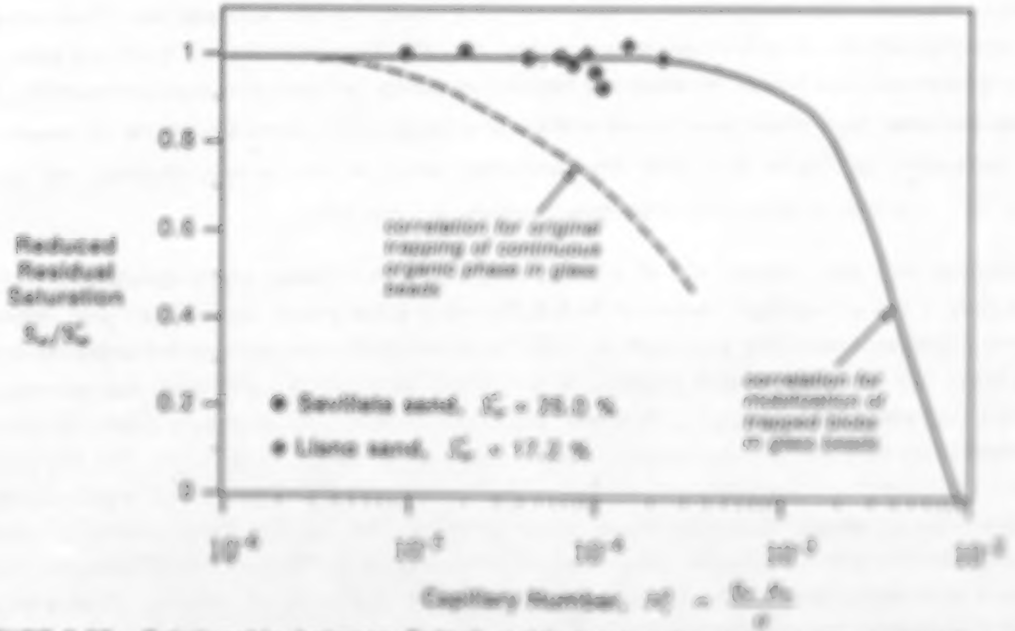

FIGURE 9-37. Relationship between Soltrol residual saturation and capillary number, N_c^{ℓ}, for Sevilleta sand and Llano sand. Its compared to correlations for un-sintered, uniform glass beads developed by Morrow and Chatzis (1982), and Morrow et al. (1988).

We also hypothesized that the initial residual saturations might be artificially low, because these saturations were established at fairly high initial capillary numbers (@ N_c^I = 9 × 10^{-6} and 9 × 10^{-5}, respectively, for the Sevilleta and Llano sands). If this were true, then we would expect the initial residual saturations to be lower than the values observed for the low capillary number short columns. This was not the case, as shown in Table 9–13. A weaker form of evidence is the comparison to the glass bead correlation for initial trapping at elevated capillary numbers, which is shown as the dashed curve in Figure 9–37. We see no evidence in this comparison for lower initial saturations. We have no reason to believe that the initial saturations were artificially low.

In summary, it appears that hydraulic mobilization in these two fairly uniform, unconsolidated sands may be much like that of glass beads. Glass beads have a large critical capillary number, making mobilization very difficult.

Implications for hydraulic removal of residual saturation —

Several schemes have been published in the literature and implemented in the field for hydraulically sweeping organic liquids from polluted aquifers. These schemes are presumably meant to sweep out the continuous organic liquid, knowingly leaving behind the residual. More often it seems that naivete prevails, and many designers assume that as long as ground water is flowing toward a collection system, eventually all of the organic liquid will make it. No matter how long one waits, unless gradients are increased above the critical level, none of the residual will be hydraulically removed (Wilson and Conrad, 1984).

Remediation schemes attempting to hydraulically remove capillary trapped residual by waterflooding can remove some of residual organic liquid whenever the capillary number exceeds the critical value: $N_c > N_c^c$ (see Figure 9-9). All of it will be removed when $N_c > N_c^{c*}$. Figures 9-38a and 9-38b are plots of water phase hydraulic gradient, J, necessary to initiate mobilization in a soil of intrinsic permeability, k. The curves are taken from Wilson and Conrad (1984), who based them on the sandstone N_c^c capillary number correlation of Figure 9-6, and the sandstone value of the critical capillary number, $N_c^{c*} = 2 \times 10^{-5}$. Various organic-water interfacial tensions, σ, are shown.

For example, PCE has a density of 1.63 g/cm, greater than that of water, and is likely to sink in the saturated zone. It has an interfacial tension of 47.5 dyne/cm. In a fine gravel, with $k = 10^{-5}$ cm², Wilson and Conrad (1984) estimated that a gradient of $J = 0.1$ is necessary to start some of the blobs moving. This is a steep but not unreasonable gradient. In a medium sand with $k = 10^{-7}$ cm², the necessary gradient is a very steep $J = 10$. Figure 9-39 is their plot of percentage residual organic liquid recovered as a function of gradient and soil permeability, for an interfacial tension of 10 dyne/cm. The top curve there and in Figure 9-38a is the 100% recovery curve for the same organic liquid. Other organic liquids can be examined by simply multiplying these results by $\sigma/10$. For the fine gravel example, which required a gradient of only 0.1 to begin to mobilize PCE blobs, Wilson and Conrad (1984) estimated that the gradient must be increased to 47.5 times as large, or $J = 4.75$, in order to "get it all". Such a large gradient is improbable at a remediation site, but is not uncommon in a laboratory experiment. In the medium sand (where k is 100 times smaller) it would take a gradient of $J = 100 \times 4.75 = 475$ to remove all of the residual PCE, clearly an impossible feat at a remediation site.

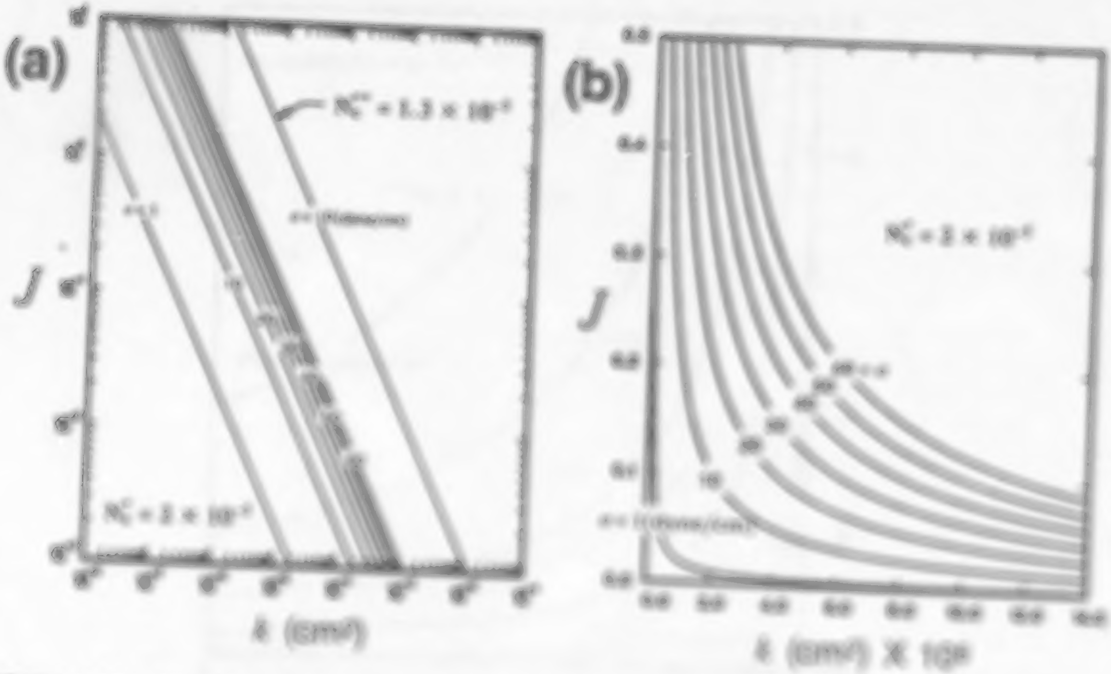

FIGURE 9.08. Hydraulic gradients required to initiate blob mobilization in porous media of various permeabilities, for organic liquids of various interfacial tensions. A critical capillary number of $N_c^* = 2 \times 10^{-5}$ was used. Plot (a) uses a log-log scale, while (b) is plotted using linear coordinates. The upper curve in (a) represents the gradient necessary for complete removal of all organic liquid with an interfacial tension of 10 dynes/cm. Constructed from sandstone data presented in Figure 9.8. From Wilson and Conrad (1984).

Even these predictions are optimistic. We've found that the critical capillary number for two sandy soils is forty to a hundred times higher than the sandstone values used in these figures and calculations. If we take the lower value of forty, then it would take a gradient of $J = 40 \times 0.1 = 4$, just to begin to mobilize the PCE from the fine gravel, and a gradient of [illegible] to "get it all". Clearly, it is not practical to mobilize residual organic liquid in the saturated zone using hydraulic means.

In summary, residual organic liquid is easier to mobilize for lower interfacial tensions, higher permeability soils, and in the lab. It's harder to mobilize for higher interfacial tensions, lower permeabilities, and in the field where there are severe practical constraints on the hydraulic gradient. Although it may be possible, intentionally or by accident, to mobilize some of the residual, it is difficult to get it all.

Implications for remediation using surfactants and [illegible]:

The only practical way to improve mobilization of the residual will be to lower the interfacial tension using surfactants. Surfactants may already be present at a contamination site, either as part of the disposed waste or spilled fuel, or as a by-product of biological growth. Surfactants can also be injected, although there is some difficulty getting the injected surfactant to actually make contact with the resid-

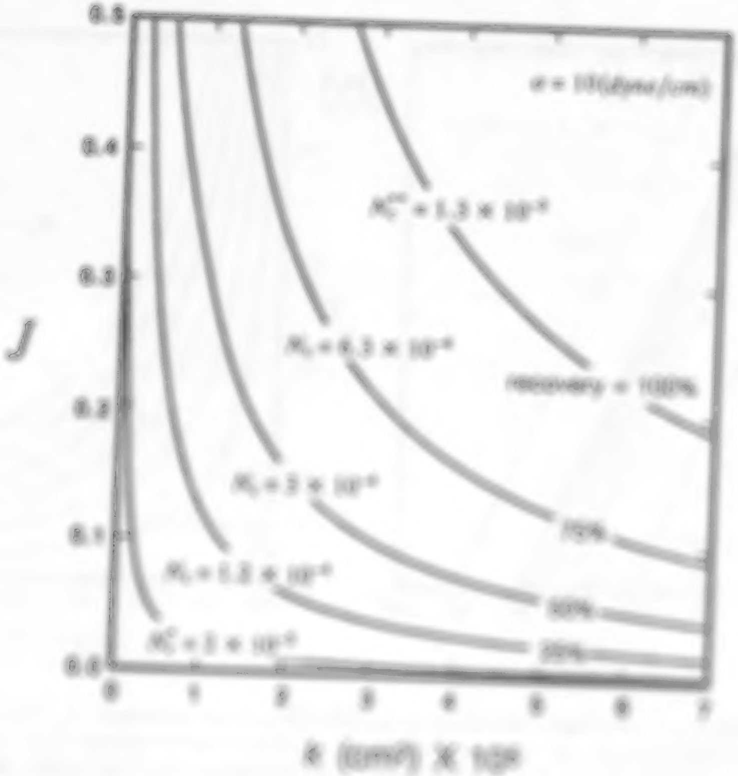

FIGURE 9.29. Recovery of residual saturation as a function of permeability and hydraulic gradient for an interfacial tension of 10 dynes/cm. Based on sandstone data. From Wilson and Conrad (1984).

Finally, the biological community can be stimulated to consume some of the dissolved organic, producing more bio-surfactant as a by-product.

Even if surfactants reduce the interfacial tension a factor of ten or more, we cannot expect dramatically increased mobilization. We believe that, in the saturated zone, surfactant concentrations have to be high enough to emulsify the organic liquid, in order for them to have a significant impact.

Implications for improving predictions of transport and fate --

Accurate measures of relative permeabilities at reduced residual saturations will be important in reliably predicting pollutant movement. As the organic phase dissolves, its saturation becomes reduced and the permeability to water increases. Increases in permeability result in either increased water flow under constant head boundary conditions, or increased residence time under constant flux conditions. In either case, an accelerated rate of dissolution is the ultimate result. Having good estimates of the relative permeabilities may be as important as good estimates of the mass transfer coefficients for predicting pollutant migration.

ORGANIC LIQUID MOVEMENT AND CAPILLARY TRAPPING IN A HETEROGENEOUS POROUS MEDIA

No soil is truly homogeneous. Soils exhibit spatially variable properties that are a result of their original deposition and subsequent diagenesis. The importance of this variability on the flow of fluids and the transport of contaminants has only recently been accepted by most groundwater hydrologists. Gelhar (1986), Sudicky (personal communication, 1988) and Dagan (1986) have reviewed the literature on this topic. Conspicuously absent from these reviews is any discussion of multiphase flow, other than water percolation in a soil with air at a uniform pressure. This is the so-called Richard's equation approach to two phase flow. Following this approach Yeh et al. (1985a,b,c), Mantoglou and Gelhar (1987), and Ababou et al (1988) have developed geostatistical theoretical and computer simulation models that demonstrate the importance of soil stratification on moisture movement in the vadose zone. At high capillary pressures the finer textured layers and lenses of soil absorb water through capillary forces, while the coarse layers remain relatively dry and impervious. The net result is a hypothesis that the anisotropy of water permeability is a function of saturation. At low water saturations the fine material is more permeable to water than the coarse material, and water has a preference for horizontal flow along the beds due to capillary forces. At high saturations the coarse material has the greater water permeability, and gravity forces tend to cause vertical flow. This hypothesis has been verified in the field and the laboratory by Stephens and Heermann, 1988; Mattson et al., 1988; McCord et al., 1988a,b; and others. A similar observation was made by Schwille (1988), using a hydrocarbon as the wetting phase.

Petroleum reservoir engineers have largely ignored spatial variability, although this has started to change. The 1989 SPE Reservoir Simulation Conference had several sessions devoted to this topic, which reservoir engineers refer to as "reservoir heterogeneity" (Lake and Carroll, 1986; also Mohanty et al., 1989; Ewing et al., 1989). Most of the petroleum related work is focused on miscible displacement, involving the advection and dispersion of chemical components in a single non-homogeneous fluid phase. Earlier, Chatzis et al. (1983) briefly examined the effect of reservoir heterogeneity on immiscible displacement, at the pore network level, using heterogeneous glass bead packs. They observed that during water floods the spatial variation of capillary properties can lead to large scale by-passing of oil-filled, coarse bead zones. This observation is consistent with the vadose zone water infiltration studies showing air by-passed in the coarse lenses and layers.

We hypothesized that the spatial variation or heterogeneity of soil properties has a dominant effect on the movement and capillary trapping of organic liquids. We tested this hypothesis using the visualization of two phase flow in micromodels, representing three different types of spatial variability. The behavior of these displacements was compared with homogeneous displacements. The first type of heterogeneity concerned the boundary of a fine material with a coarse material. [illegible]

[illegible]

[illegible]

[illegible]

[illegible]

[illegible]

[illegible]

[illegible]

[illegible]

[illegible]

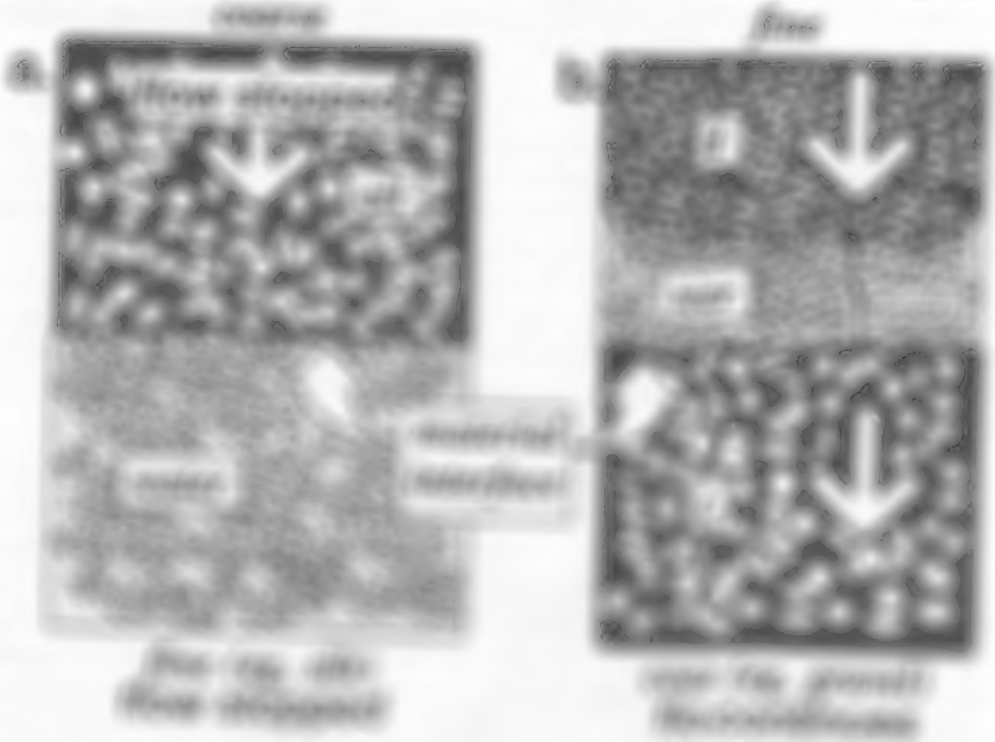
coarse
fine
a.
b.
flow stopped
material interface

[illegible]

[illegible]

[illegible]

[illegible]

[illegible]

[illegible]

[illegible]

[illegible]

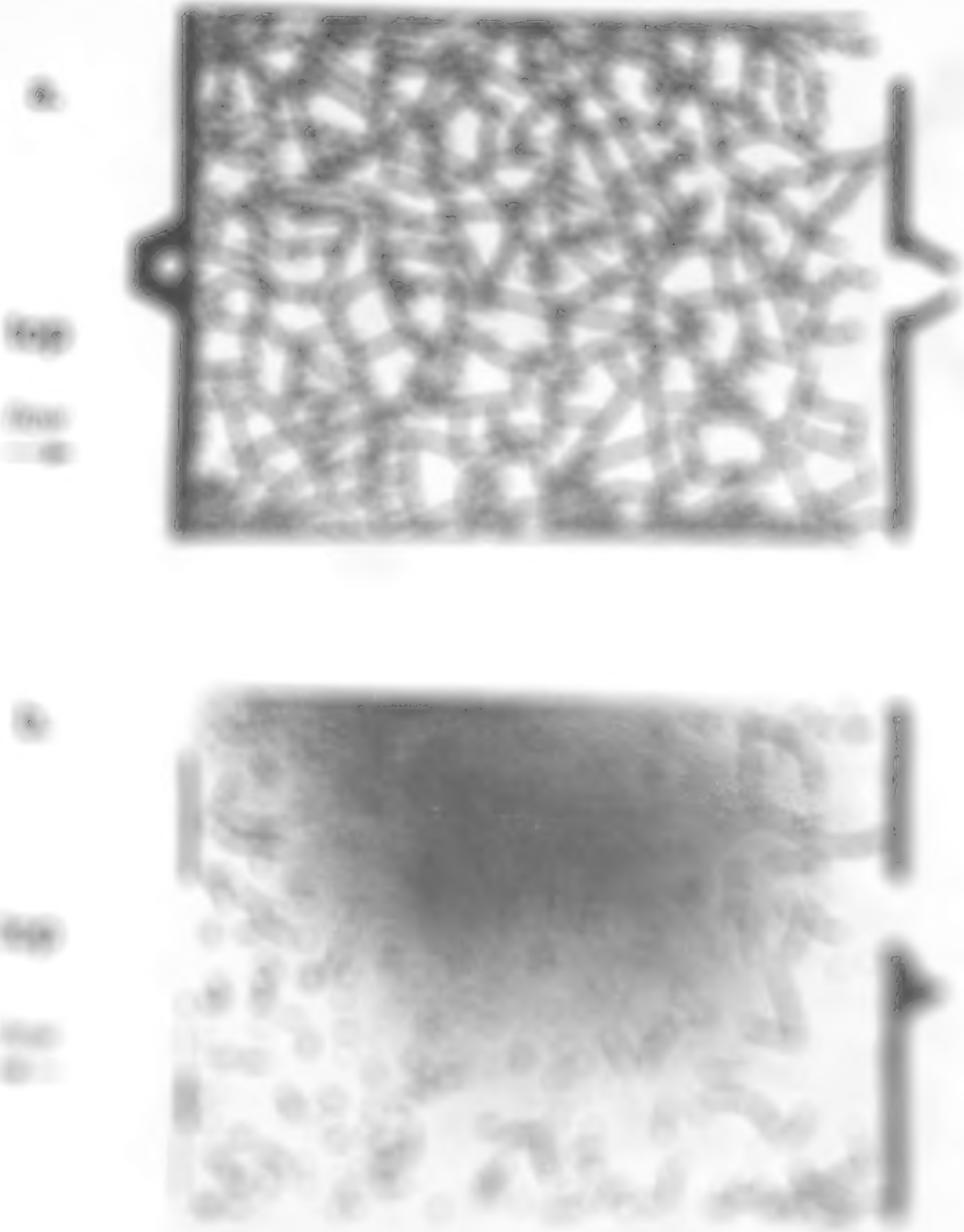
a.
b.

[illegible]

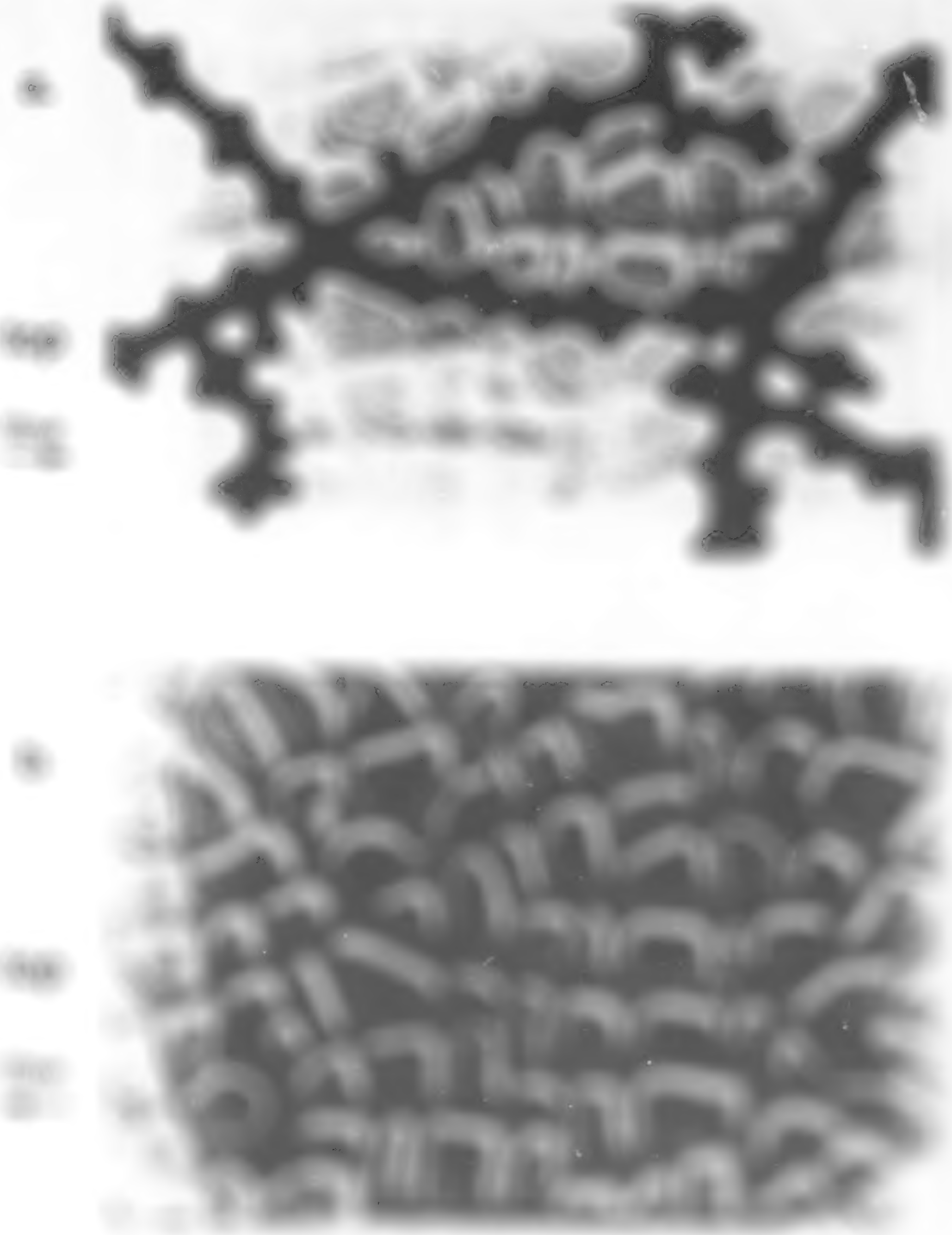

[illegible]

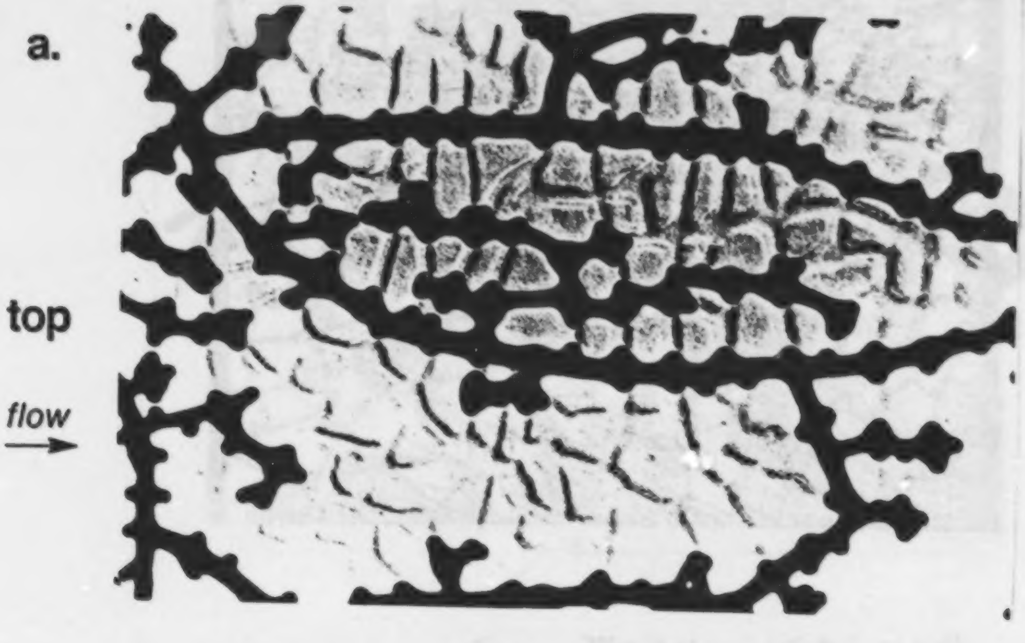

FIGURE 9-43. Aggregated model detail from Figure 9–11, showing conditions following the displacement of the water by Soltrol (a. upper photo), and at residual non–wetting phase saturation (b. lower photo). The area is located near the top of the model, just to the right of the centerline.

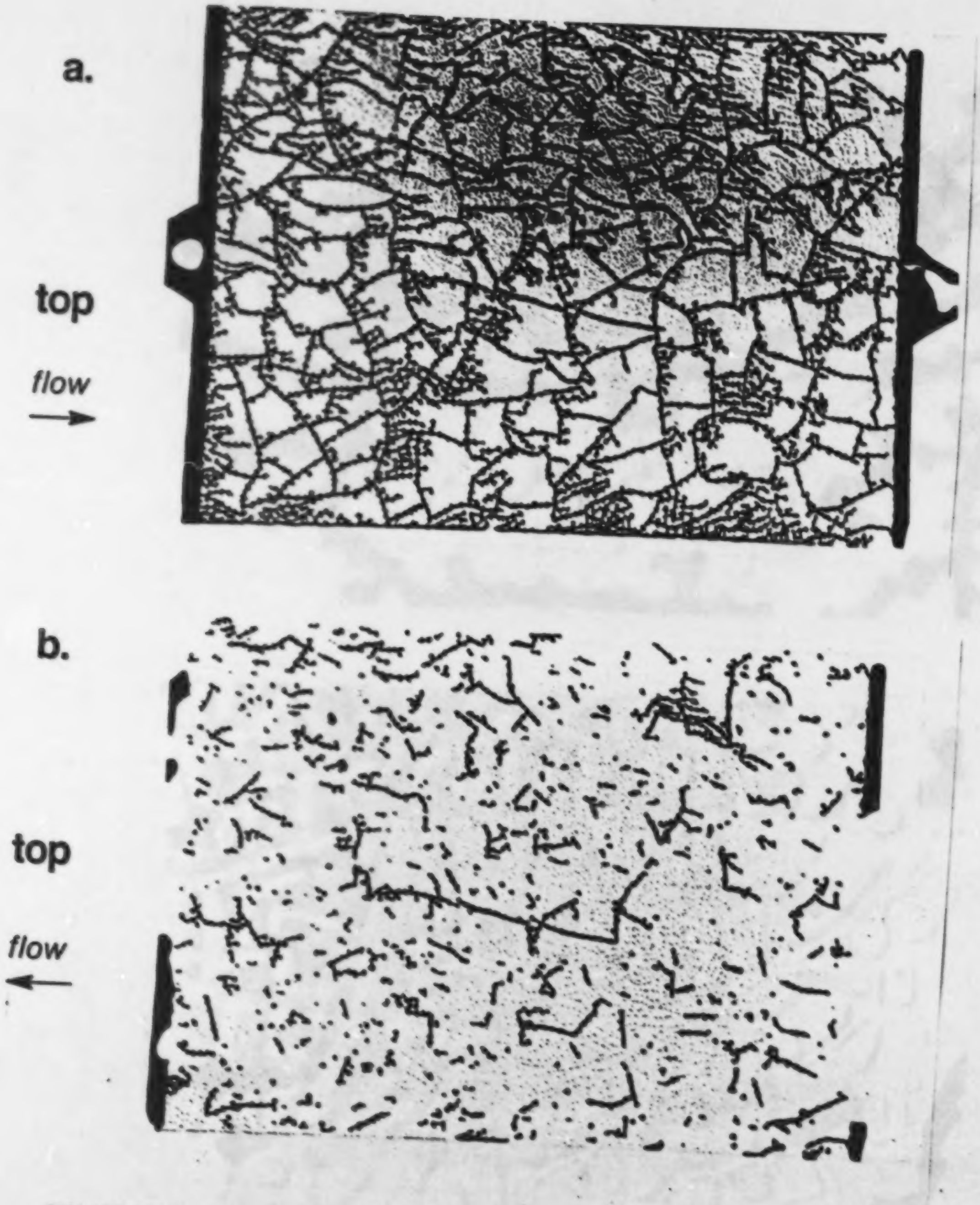

FIGURE 9-44. Aggregated model. In the upper photo (a) Soltrol displaced water from the left (the top of the model) to the right (the bottom of the model), at 1.5 ml/min yielding a residual (irreducible) wetting phase saturation. In the lower photo (b) Soltrol was displaced by water from the right (the bottom of the model) to the left (the top), also at 1.5 ml/min, yielding a residual non-wetting residual saturation. Soltrol was dyed red and appears dark grey; the water was not dyed. The photos record steady state flow conditions at the end of the displacements.

experiment led to a slightly higher residual, with more trapping within the aggregates. When the organic liquid advanced into the model at a 'fast' rate it was able to penetrate into a portion of the some of the aggregates. Later, during the water flood, some of this organic was left behind, even though the water flood occurred under high flow rate conditions with significant viscous forces. The low flow rate water flood led to slightly lower residual organic saturations, not because it was more efficient, but because there was less organic to be removed. In the field the 'slow' rate of organic liquid advance might correspond, for example, to a slow leak from an underground storage tank, while the 'fast' rate might be associated with a spill from a tanker accident.

Implications for spill migration rates and travel distances —

In New England groundwater consultants commonly distinguish between gasoline leaking from underground tanks in unconsolidated, glacial deposits, and leaks in ledge or bedrock. In the unconsolidated deposits anecdotal evidence suggests that the much of the gasoline is trapped by capillary forces, with very limited and slow migration of the liquid gasoline. The gasoline tends to appear in nearby brooks dissolved in the groundwater discharge. In crystalline rock terrain the gasoline moves quickly and far, with observable liquid gasoline discharges to nearby brooks. The aggregated micromodel appears to provide a good analogue to the fractured bedrock situation.

Implications for aquifer remediation —

Two-phase flow experiments conducted in an aggregated micromodel demonstrate that the saturation and spatial distribution of organic liquid found behind an advancing front of free product depends on the combined effects of soil heterogeneity and capillarity. The amount of organic liquid that is ultimately trapped within a unit volume of aquifer is strongly dependent on how much organic liquid was originally emplaced within that volume.

Spilled organics can be expected to move quickly through aquifers which have interconnected macropores or fractures. The organic phase travels preferentially through large pores and fractures by-passing smaller pores in the matrix of these dual porosity systems. The residual saturations left behind following the recovery of free product tend to be comparatively low, but can be expected to extend over a much larger portion of the aquifer.

In this aggregated micromodel, most of the residual organic liquid was trapped as by-passed strings in the macropores. For field sites involving aggregated or cracked soils, or fractured rock, the implications are that it will be difficult to hydraulically remove all of the organic liquid from the cracks and fractures. Since real fractures tend to be planar features, rather than the simple linear cracks shown in this micromodel, multiphase flow in the field is considerably more complex than in laboratory micromodel experiments (see, e.g., the videotape on multiphase flow in a single fracture by Wilson *et al.*, 1988).

Multiphase Movement in a Heterogeneous Aquifer Containing Lenses and Stringers

Stringers or lenses of coarse porous material embedded in a matrix of fine porous material represent a type of spatial heterogeneity found in clastic sedimentary deposits. For example, gravel bars are often buried in fluvial deposits. The bars are the lenses, and the surrounding sand and silt is the matrix. Figure 8-13 is an illustration of the micromodel pattern used to represent this type of variability. The pore network was identical to the homogeneous model (Figure 8-1), but the pores in the coarse zones were enlarged in size. The coarse lenses were also simulated in short glass and TFE columns filled with Sevilleta soil, yielding both pore casts of the trapping in a heterogeneously packed sand column, and quantitative measurements of altered trapping. A new theoretical model is presented that explains the observed behavior.

Drainage of water by organic liquid–

Soltrol drained a water-filled, horizontally-held micromodel containing a number of coarse lenses. The lenses were oriented parallel to the flow direction. The Soltrol injection was relatively slow, at 0.096 ml/min. Figure 9-45 illustrates the process.A videotape is also available (Conrad *et al.*, 1989, see Appendix B). During the experiment, the front of Soltrol advanced in the finer pore matrix until it encountered a lens, then slowed while most of the incoming organic liquid preferentially traveled through that lens. Capillary forces resisting Soltrol entry were lower in the larger pores of the lens (see top photo, Figure 9-45a). When the lens was full, the front in the fine pores picked up speed again until another lens was encountered. If the front encountered more than one lens at a time it fed both of them until the one was full, and then fed only the second. The front in the fine pore matrix always advanced from the rear. Although a full lens might serve as a source for a new front in the fine pores, movement always proceeded slower than movement of the front through fine pores further behind. Due to the presence of the discontinuous lenses, progress of the advancement was very unsteady, with the fine matrix front decelerating and accelerating as lenses were encountered. This unsteady flow is a macroscopic analogy to the Haines' jumps seen on a pore level during the advancement (Haines' jumps on a pore scale are graphically recorded on the videotape by Mason *et al.*,1988). Favorable mobility (a more viscous fluid displacing a less viscous one) played a stabilizing role in this displacement. The final steady state fluid distribution is shown in the bottom photo, in Figure 9-45b. The distribution did not change when the Soltrol flow was cut off. Wetting phase residual (irreducible) saturation is found in both the coarse and fine pore regions. Because of the role of the lenses in the advancement, there are zones of fine material, located between closely spaced coarse lenses, where the water was largely by-passed, leaving a large residual wetting phase saturation. We also ran models with coarse lenses that extended across the length of the model. The fine regions were almost entirely by-passed, similar in behavior to the aggregated model.

The horizontal experiment was repeated in the same heterogeneous model but at a faster flow rate of 1 ml/min. As above, the front of organic liquid advanced in the finer-pore matrix until it encountered a lens, then slowed. Even though there was a slight difference in the way the model filled with organic liquid, it did not make much difference in the residual water saturations behind the front in each model. The only difference was that at the faster rate, there was less of a capillary end effect.

Implications for spill migration rates and travel distances —

Organic liquid selectively travels through the coarser portions of heterogeneous aquifers. Lenses of coarse material embedded in a matrix of fine material (e.g. gravel in sand; sand in silt) will influence the rate and direction of movement of an organic liquid, and create a 'fingering' or 'dispersion' of the

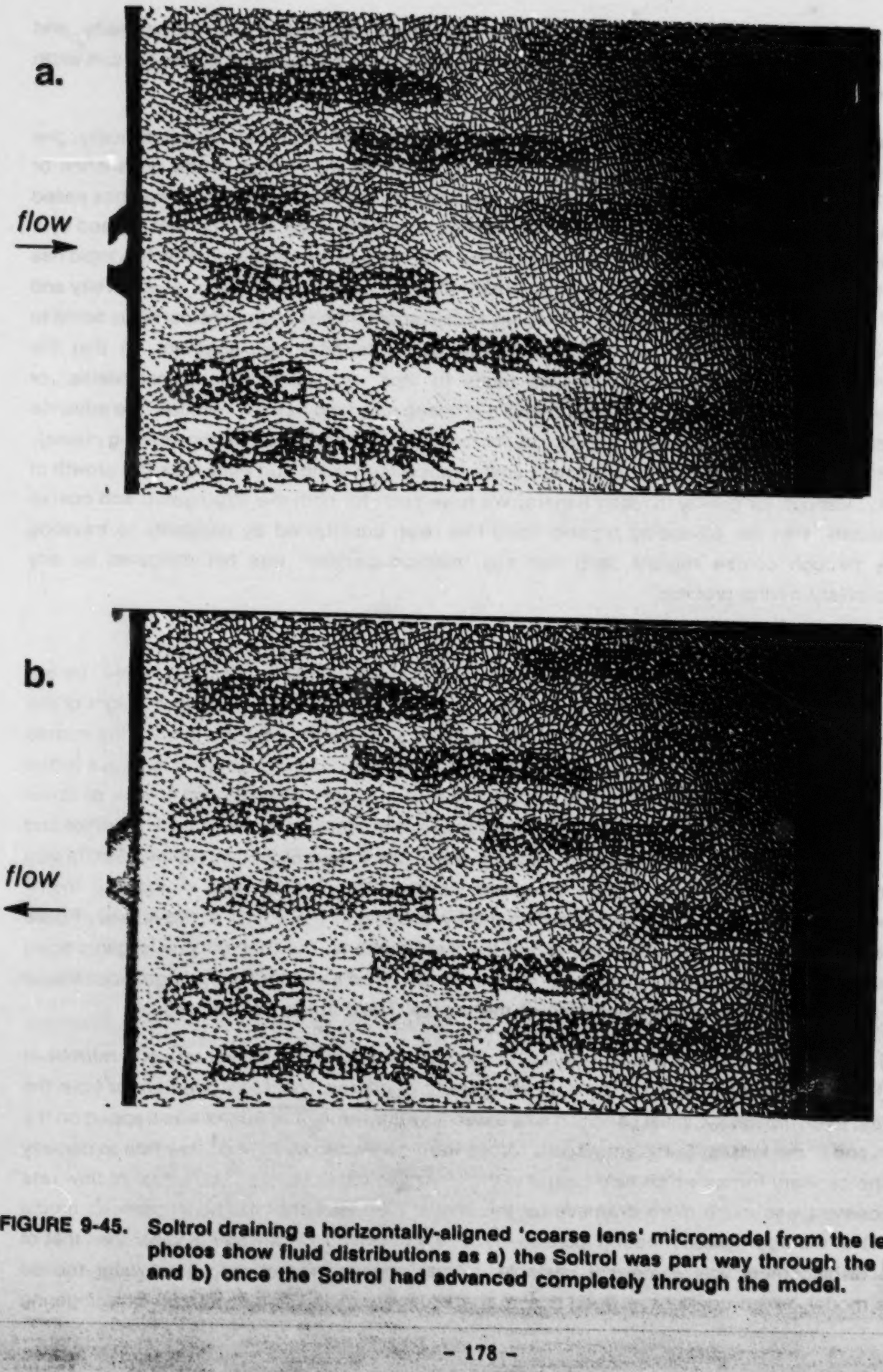

FIGURE 9-45. **Soltrol draining a horizontally-aligned 'coarse lens' micromodel from the left. The photos show fluid distributions as a) the Soltrol was part way through the model, and b) once the Soltrol had advanced completely through the model.**

location of the immiscible displacement front. The front will 'finger' because of the heterogeneity, and the competition between viscous and capillary forces. This fingering is a function of the length and width of the lenses, and their pore size contrast with the matrix.

For media with continuously varying properties, such as we often represent geostatistically, the parameter equivalent to the lens length is the correlation length,or the range of the covariance or variogram. There is a current controversy over when 'fingering' due to heterogeneity, sometimes called 'macrodispersion', dominates over fingering due to viscous or density instabilities that are caused by a contrast in viscosity or density across the immiscible interface. Most of the recent work on this topic has focused on miscible displacement (Araktingi *et al.*, 1988; Moissis, *et al.*, 1989; Ewing, *et al.;* Welty and Gelhar, 1987,1989). The effect of capillarity in immiscible displacement has been considered by some to be similar to local hydrodynamic dispersion operating during miscible displacement, in that the transverse mixing caused by either processes tends to limit viscous or gravity instabilities, or 'macrodispersion' induced by heterogeneities. While this notion may hold true for imibition (the advance of a wetting phase), the opposite appears to be true for drainage (the advance of a non-wetting phase). During any drainage process capillarity effectively limits transverse mixing and enhances the growth of heterogeneity, viscous, or gravity induced fingers. We have seen for both the aggregated and coarse lens micromodels, that the advancing organic liquid has been constrained by capillarity to traveling preferentially through coarse regions, and that this 'macrodispersion' was not mitigated by any transverse capillary mixing process.

Water flooding–

Figure 9-46a shows the fluid distributions at the end of a displacement of the Soltrol by water, for the model depicted in Figure 9-45. The water was injected at a rate of 0.096 ml/min (from the right of the photo). The water front moved in the fine pore matrix, splitting as it migrated around each of the coarse lenses filled with organic liquid. At this slow rate, capillary forces dominated over viscous forces to the extent that water was preferentially imbibed into the fine pore matrix even though it was of lower permeability. When the wetting front reached the downstream end of a lens it closed back together and trapped the non-wetting fluid in the lens via by-passing. Very little, if any, of the non-wetting Soltrol was displaced from the coarse lenses. Typical pore-level capillary trapping of blobs in the fine matrix occurred, but it was of much smaller in scale than the by-passing of the Soltrol in the lenses. Figure 9-46a shows the equilibrium condition at the end of the displacement. The total residual organic liquid saturation was significantly higher for this heterogeneous model, than it was for the homogeneous model (Figure 9-11b), due to large-scale by-passing of the organic liquid in the coarse lenses.

Figure 9-46b shows the model after Soltrol had been displaced by water at a fast rate of 1 ml/min. In contrast to the slow rate displacement, a significant amount of organic liquid has been swept from the coarse lenses, even though the initial condition was essentially the same. The Soltrol was trapped on the downstream end of the lenses. Sufficient viscous forces were generated by the fast flow rate to partially overcome the capillary forces which held Soltrol in the lenses at the slow rate. The effect of flow rate upon displacement was much more dramatic for this model than for either the homogeneous model (Figure 9-11) or the aggregated model (Figure 9-41). Since the viscosity of water is lower than that of Soltrol, this displacement was somewhat unstable. Some fingering was observed as water moved through the model, which could have been due to the instability or the heterogeneity. The fingering

Reproduced from
best available copy.

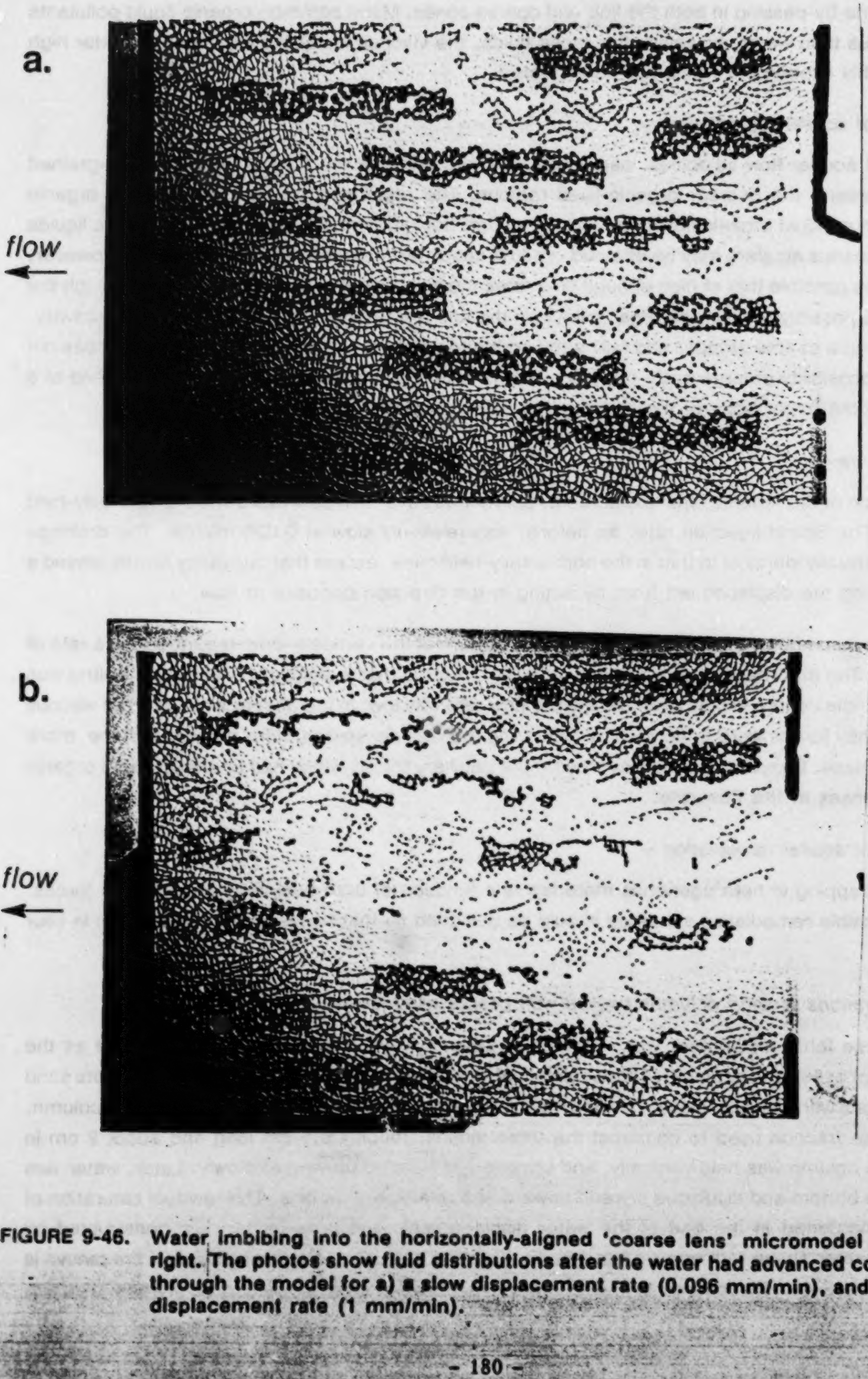

FIGURE 9-46. **Water imbibing into the horizontally-aligned 'coarse lens' micromodel from the right. The photos show fluid distributions after the water had advanced completely through the model for a) a slow displacement rate (0.096 mm/min), and b) a fast displacement rate (1 mm/min).**

resulted in some by-passing in both the fine and coarse zones. Many common organic liquid pollutants are less viscous than water, however. For these fluids, the viscous instability experienced under high flow rates in this experiment would not be expected.

Implications for aquifer remediation —

At typical aquifer flow velocities, capillary forces can relegate the flow of water to finer-grained regions, by-passing the coarser organic-filled regions. The result can be poor recovery of organic liquids, as high residual organic liquid saturations are left behind. Increased recovery of organic liquids from heterogeneous aquifers may be attained in some cases by increasing the pumping rate. However, it appears to be possible that at high enough flow rates the water would preferentially move through the coarse lenses, possibly by-passing organic liquid in the fine matrix and again leading to poor recovery. Finally, sampling a coarse stringer and failing to find it effectively saturated with organic liquid does not eliminate the possibility of large scale trapping. The sample may be taken from the upstream end of a stringer, while the major body of trapped organic is found toward the downstream end.

Buoyancy Effects–

In a variation of the 'coarse lens' experiment, Soltrol was advanced downward into the vertically-held micromodel. The Soltrol injection rate, as before, was relatively slow at 0.096 ml/min. The drainage process was virtually identical to that in the horizontally-held case, except that buoyancy forces played a role in stabilizing the displacement front by acting in the direction opposite to flow.

Water was then imbibed into the model from the bottom of the vertically-oriented model, at a rate of 0.096 ml/min. The end result is depicted in Figure 9-47. Notice that a significant amount of Soltrol was displaced from the coarse lenses even though the flow rate was low. In the absence of sufficient viscous forces, buoyancy forces were generated by displacing the less dense Soltrol from below with the more dense water phase. Buoyancy partially overcome the capillary forces which had previously held organic liquid in the lenses at this flow rate.

Implications for aquifer remediation —

Capillary trapping in heterogeneous materials is a function of both buoyancy and viscous forces. Whenever possible remediation schemes should be designed so that buoyancy forces operate in your favor.

Residual saturations in short columns packed with coarse sand lenses–

This 'coarse lens' experiment was repeated in several short TFE columns using styrene as the organic liquid phase (see Section 7). Three cylindrical lenses were created by splitting the Sevilleta sand into two fractions with a size 50 sieve. The fine fraction was used to pack the major portion of the column, with the coarse fraction used to construct the three lenses, roughly 3.5 cm long and about 2 cm in diameter. The column was held vertically, and styrene was flooded downward slowly. Later, water was injected at the bottom and displaced styrene upward at a relatively slow rate. The residual saturation of styrene was hardened at the end of the water displacement, and pore casts were constructed by replacing the water phase with epoxy. A longitudinal section of the column through one of the lenses is shown in Figure 9-48. The coarse lenses contained a much greater saturation of styrene than the

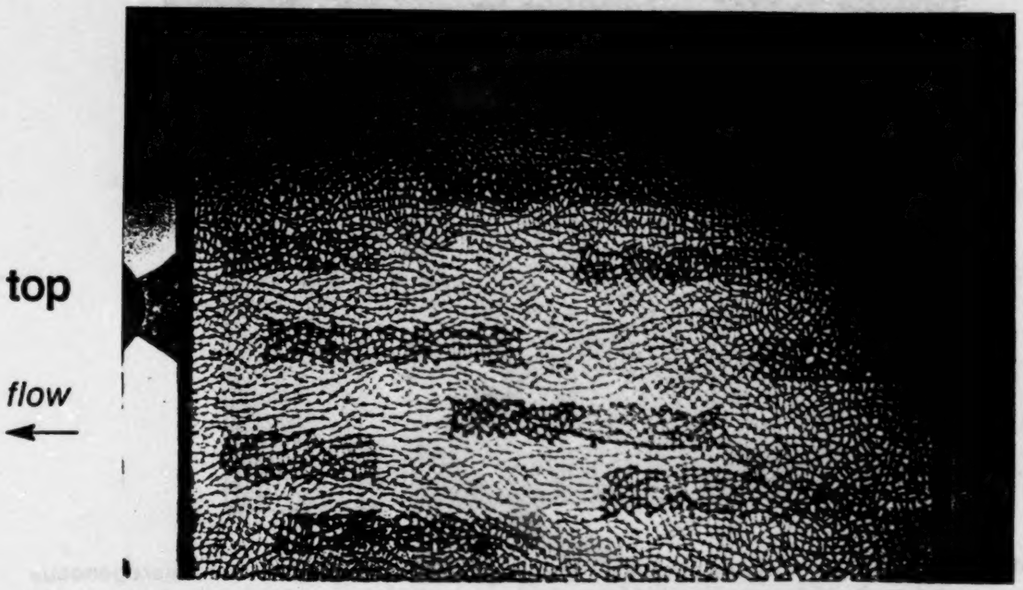

FIGURE 9-47. **Water imbibing into the vertical 'coarse lens' micromodel from the right (the bottom of the model). The photos show fluid distributions after the water had advanced completely through the model.**

surrounding fine matrix, validating the micromodel results. The residual saturation trapped in the fine matrix was observed to be approximately the same as that observed in the earlier homogeneous experiments. Even though this column was oriented vertically, buoyancy forces were small and had little effect on the results. The greater density of styrene, along with much smaller pore sizes in the sand pack, resulted in a much smaller ratio of buoyancy forces to capillary forces than was encountered in the vertically-oriented micromodel.

Another experimental trial was conducted in a similar column, but this time the column was oriented horizontally during the organic displacement step, and the displacement was conducted at a much faster rate. A longitudinal section of this column through a lens is shown in Figure 9-49. Notice that some organic liquid was displaced from the coarse lenses, again corroborating the results from the corresponding micromodel experiment. By-passed styrene still remained in the down-gradient end of the stringer, but the residual saturation in the up-gradient end was reduced to small disconnected blobs similar to that found in the matrix of finer pores.

Two vertical glass short column experiments were also run with coarse lenses, and quantitative measurements were made of final Soltrol residual saturation. The columns were packed with three lenses, similar to the heterogeneous pore cast experiments. The quantitative results are given in Table 9-14.The observed 'bulk' maximum and 'bulk' residual Soltrol saturations represent volumetric

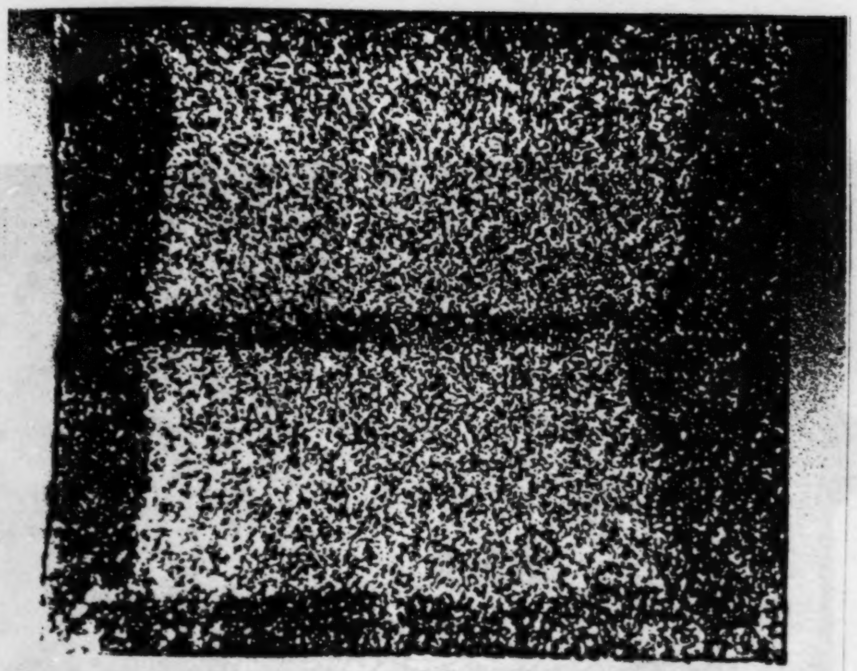

FIGURE 9-48. Photograph of residual organic liquid saturation (shaded light) in a heterogeneous sand pack. Water was flooded from right to left at a low rate. Notice the high organic liquid saturation in the coarse lenses. The core is 5 cm long.

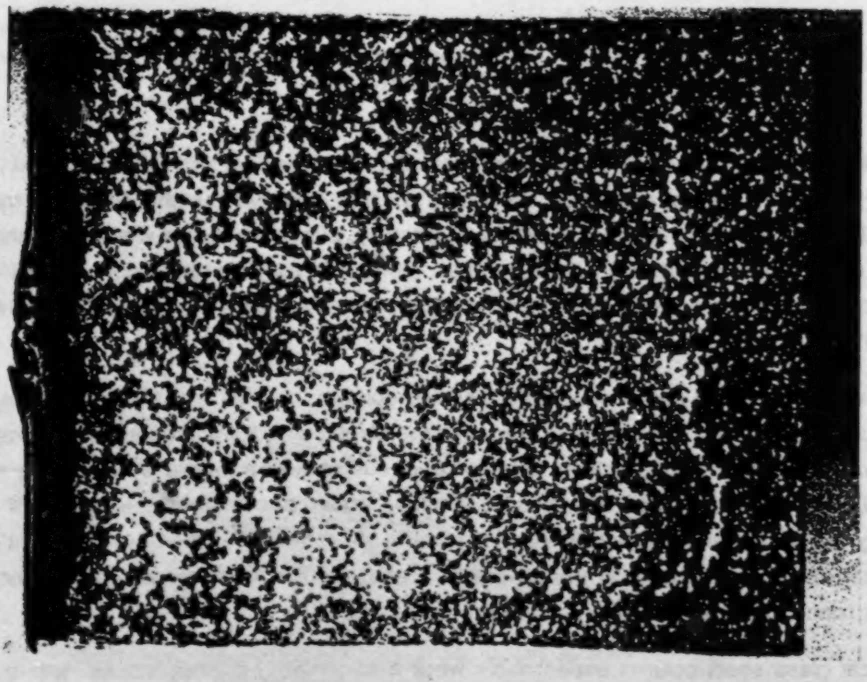

FIGURE 9-49. Photograph of residual organic liquid saturation (shaded light) in another heterogeneous sand pack. Water was flooded from right to left. A high rate of flow produced sufficient force to displace some organic liquid from the coarse lenses. This core is 5.8 cm long.

sample	porosity * (%)	volumetric percent coarse/fine	bulk maximum organic liquid saturation * (%)	bulk residual organic liquid saturation * (%)
1	38.2 ± 0.4	29 / 71	85.1 ± 2.5	31.0 ± 1.4
2	37.6 ± 0.4	31 / 69	85.4 ± 2.4	31.2 ± 1.5

* measured value ± propagated error

TABLE 9-14. Measurements of bulk residual organic saturations in two heterogeneous packings of the Sevilleta sand. The sand was divided into a coarse and a fine fraction, and the coarse fraction was packed into the column as cylindrical lenses within a matrix of the fine fraction.

averages over the entire column pore space. The observed 'bulk' maximum Soltrol saturation is consistent with that observed in the homogeneously packed Sevilleta soil columns. If both the coarse and fine zones had the same maximum organic saturation, and if no water imbibed into the coarse lenses during the upward water displacement, then the residual Soltrol saturation in the lenses should not have changed from this value of roughly 85%. In the fine matrix surrounding the lenses the Soltrol saturation was presumably reduced to no less than 15%, the S_{or} values reported for packings of uniform glass beads (Morrow *et al.*, 1988). Dry packing of these columns could have avoided any micro-layering, such as we have suggested is responsible for the higher S_{or} values in the more common wet packed columns. Accounting for the relative volume of each soil fraction in the heterogeneous columns, an estimate for the expected bulk residual Soltrol saturation can be made. If one assumes that little to no drainage of styrene occurred in the stringers, the measured 'bulk' residual saturation can be compared with a theoretical value:

$$\begin{aligned}
&\textit{estimated bulk residual saturation}\\
&\quad = (\textit{normalized lense volume}) \times S_o + (\textit{normalized matrix volume}) \times S_{or}\\
&\quad = 0.3 \times 0.85 + 0.7 \times 0.15\\
&\quad = 0.36
\end{aligned}$$

Had the typical wet packed Sevilleta sand value of 27% been used for the matrix residual, instead of 15%, then this estimate would have been higher. The actual bulk residual Soltrol saturation in the heterogeneous columns was only 31%, greater than the 27% found in the homogeneous columns, but also lower than the lowest 'expected' value of 36%. Perhaps the coarse lenses actually occupied less volume than calculated. It is also likely that some mixing occurred between the coarse lenses and the fine matrix when the packing forms used to make the lenses were removed from the column, thereby reducing the effective volume of the coarse lenses.

These quantitative results are somewhat inconclusive. On one hand, residual saturations were increased by the presence of coarse lenses in agreement with both the micromodel and pore cast results, but the observed residual saturations were less than the theoretically predicted value.

Mechanisms For Trapping via By-passing In Heterogeneous Porous Media

The basic mechanism for capillary trapping via large scale by-passing has been recently recognized in both the petroleum and hydrologic literature, as we reviewed earlier in the introduction to these experiments on heterogeneity. The displacing wetting fluid migrates around pockets, or lenses, of the larger or coarser pores, which are preferentially occupied by the non-wetting fluid. Although this basic mechanism is recognized, there appears to be no literature that discusses the incomplete displacement of non-wetting fluid from finite sized lenses, as observed here for the larger viscous and gravity force displacements.

To better understand the mechanisms, consider a simple conceptual model of the aquifer with porous lenses of intrinsic permeability k_2 embedded in a matrix of permeability k_1, as illustrated in Figure 9-50. The pore space of this binary media is initially filled by fluid B, one of two immiscible fluid phases. The other fluid is designated fluid A. Fluid A is injected at a known flow rate $\bar{q}$ from the left, and displaces fluid B from the pore space. There may also be an initial pore level residual saturation of fluid A. The pore space may be strongly wet by either of the two fluids, or it may be neutrally wet. For example, Soltrol would be represented by fluid A, as it advanced into a glass micromodel saturated with water, fluid B. When water displaced Soltrol, fluid A would be the water and fluid B the Soltrol. The capillary properties of the matrix and lenses are assumed to be correlated with their permeability. The spatial pattern and efficiency of the displacement depends on the spatial statistics of the lenses (size, shape, frequency), wetting, permeabilities, capillary properties, and the flow rate.

For this simple mathematical analysis a greatly simplified geometrical and fluid mechanical conceptual model is adopted, as shown in Figure 9-51. The lenses are assumed to be roughly rectangular in shape, with length l and width w. Over the cross-section taken normal to the flow, relative areas of each flow zone can be calculated. The relative area of the lenses is a_2, while the relative area of the matrix is a_1, such that:

$$a_1 + a_2 = 1.0 \qquad (9\text{-}14)$$

When the front hits the lenses the total flux will be divided into flow around the lenses, q_1, over the area a_1, and flow through the lenses, q_2, over area a_2. The net flux $\bar{q}$ is related to the individual fluxes by:

$$\bar{q} = a_1 q_1 + a_2 q_2 \qquad (9\text{-}15)$$

Note that if the total cross-sectional flow area is A, then the flow areas of k_1 and k_2, are A_1 and A_2, respectively. That is $A = A_1 + A_2 = (a_1 A + a_2 A)$, and the total flux over area A is given by $\bar{q} A = q_1 A_1 + q_2 A_2$. Flux is conserved and compressibility is ignored.

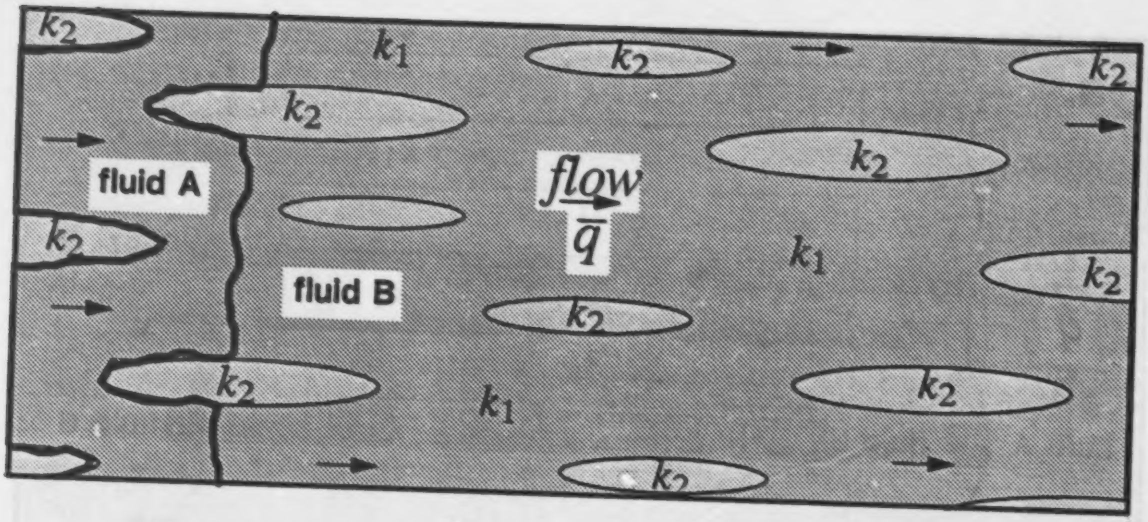

FIGURE 9-50 **Random lenses of permeability k_2 in a matrix of permeability k_1.**

The model is base on the premise that displacement occurs as a sharp front. On each side of the front only one of the two fluids is at greater than residual saturation. To the right this would be fluid B, while to the left it would be fluid A. Then the flux rates are given by Darcy's law, which for flux in area a_i (i = 1,2) is:

$$q_i = \frac{k_i k_r}{\mu} \frac{\nabla p_i}{l} \tag{9-16}$$

where q_i is the flux over the solution domain, l , in material i, which has intrinsic permeability k_i . The relative permeability for each fluid is k_r , and the viscous pressure drop is Δp_{μ_i} (as distinguished from the total pressure drop, Δp, or the capillary pressure, p_c). For the sake of simplicity, several assumptions are made.

- uniform viscosity, the same in both fluids ($\mu_A = \mu_B$) — this assumption is easily relaxed for a more sophisticated analysis;
- uniform relative permeability, within each the fluid ($eg., k_{rA} = constant$);
- each fluid has the same relative permeability($k_{rA} = k_{rB}$) — this assumption is also easily relaxed for a more sophisticated analysis;
- pressure in each material of the domain is uniformly varying in the direction of flow— ie, constant pressure gradient— except for a pressure jump at the immiscible front caused by capillary forces;
- pressure at each end of the domain is constant and fixed; there is a known total pressure drop from one end of the domain to the other (ie, $\Delta p = \Delta p_1 = \Delta p_2$);

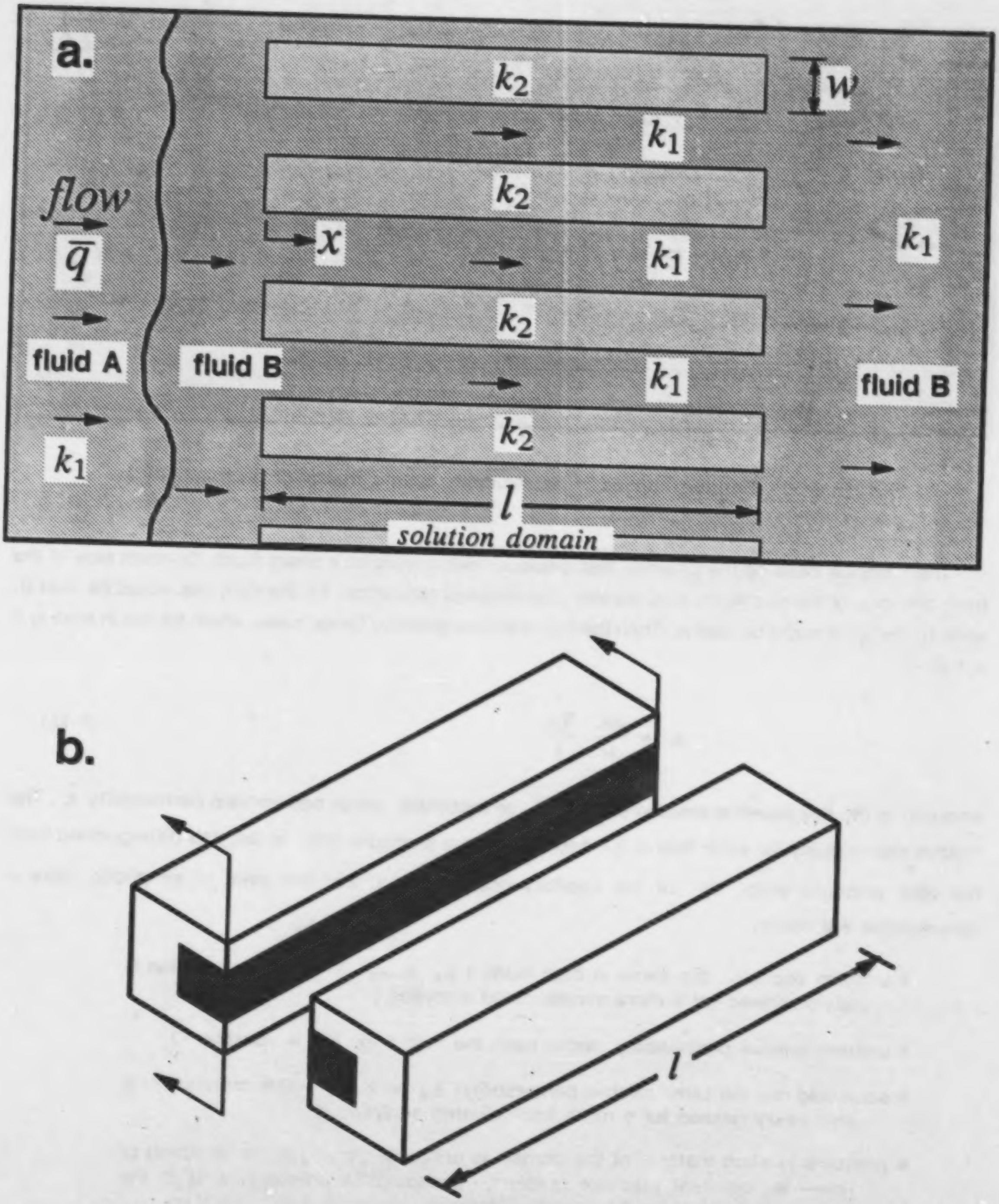
a.
k2
w
k1
flow
q̄
x
k1
k2
fluid A
fluid B
fluid B
k1
l
solution domain
b.
l

FIGURE 9-51 Uniform, parallel lenses of permeability k_2 in a matrix of permeability k_1: a) side view of several lenses, and b) cut-away view of one lense.

- there is no longitudinal smearing of the front by capillary forces — ie, the front is sharp; and
- there is no transverse smearing of the front by capillary forces in the vicinity of the lenses; this assumption is very accurate except for the case of very high flow rates where fluid A is the wetting fluid.

From these assumptions it follows that, within each material, the pressure gradient across the domain will be constant except for a pressure jump at the immiscible front caused by capillary forces, as sketched in Figure 9-52.

For the case that we are interested in a wetting fluid displaces a non-wetting fluid, and the lenses with permeability k_2 represent the coarse material. In this case the pressure profiles in each material look something like that shown in Figure 9-53. Note that the total pressure drop across the domain must be the same for both materials (ie, $\Delta p_1 = \Delta p_2$), from which it follows that:

$$\Delta p_{\mu_1} - p_{c_1} = \Delta p_{\mu_2} - p_{c_2} \tag{9-17}$$

By rearranging (9-17) in terms of Δp_{μ_1}, substituting the result into (9-16), and solving in terms of q_1, we get:

$$q_1 = \frac{k_1 k_r \,(\Delta p_{\mu_2} + p_{c_1} - p_{c_2})}{\mu\, l} \tag{9-18}$$

Now, solving (9-16) in terms of Δp_{μ_2} and substituting the result into (9-18):

$$q_1 = \frac{k_1 k_r}{\mu l}\left(\frac{q_2 \mu l}{k_2 k_r} + p_{c_1} - p_{c_2}\right) \tag{9-19}$$

By rearranging (9-15) in terms of q_2, substituting the result into (9-19) and solving for q_1 we get the flow rate in the matrix:

$$q_1 = \frac{\frac{q_2\mu l}{k_2 k_r a_2} + p_{c_1} - p_{c_2}}{a_1 \mu l\left(\frac{1}{k_1 k_r a_1} + \frac{1}{k_2 k_r a_2}\right)} \tag{9-20}$$

And, by analogy, we can find the flow rate in the lenses:

$$q_2 = \frac{\frac{q_1\mu l}{k_1 k_r a_1} + p_{c_2} - p_{c_1}}{a_2 \mu l\left(\frac{1}{k_2 k_r a_2} + \frac{1}{k_1 k_r a_1}\right)} \tag{9-21}$$

Within each material, the capillary pressures can be related to the permeabilities in a gross sense by way of the Kozeny-Carman equation (Carman, 1937). First, let's note that for a single pore or capillary:

$$p_{c_i} = \frac{2\sigma \cos\theta}{r_i} \tag{9-22}$$

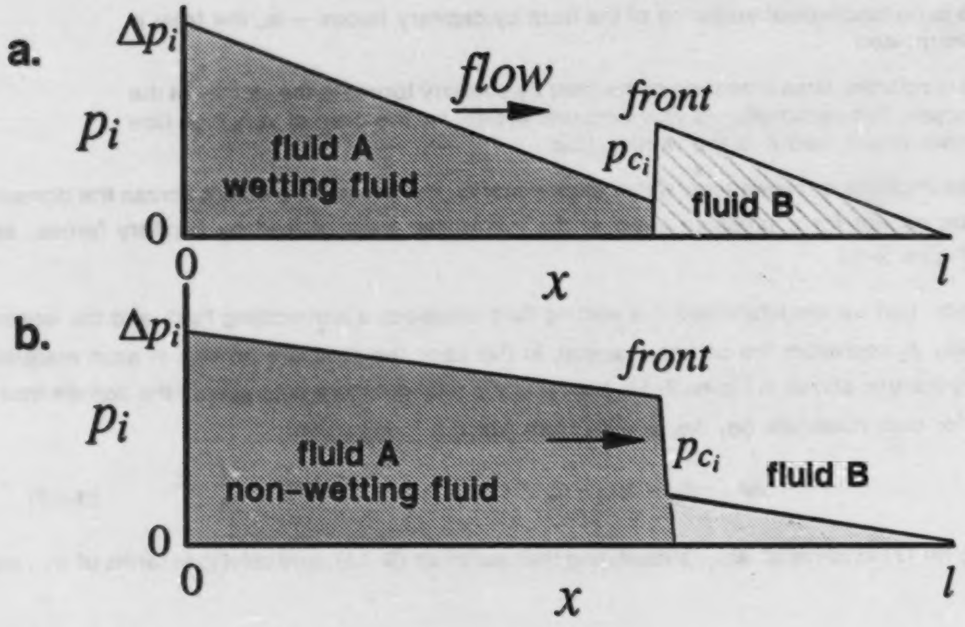
a.
Δp_i
p_i
flow
front
fluid A
wetting fluid
p_{c_i}
fluid B
0
0
x
l
b.
Δp_i
p_i
front
fluid A
non-wetting fluid
p_{c_i}
fluid B
0
0
x
l

FIGURE 9-52 Pressure profiles in soil *i* for fluids A and B, with fluid A as a) the wetting fluid, and b) the non-wetting fluid. *i* =1,2 coarse or fine.

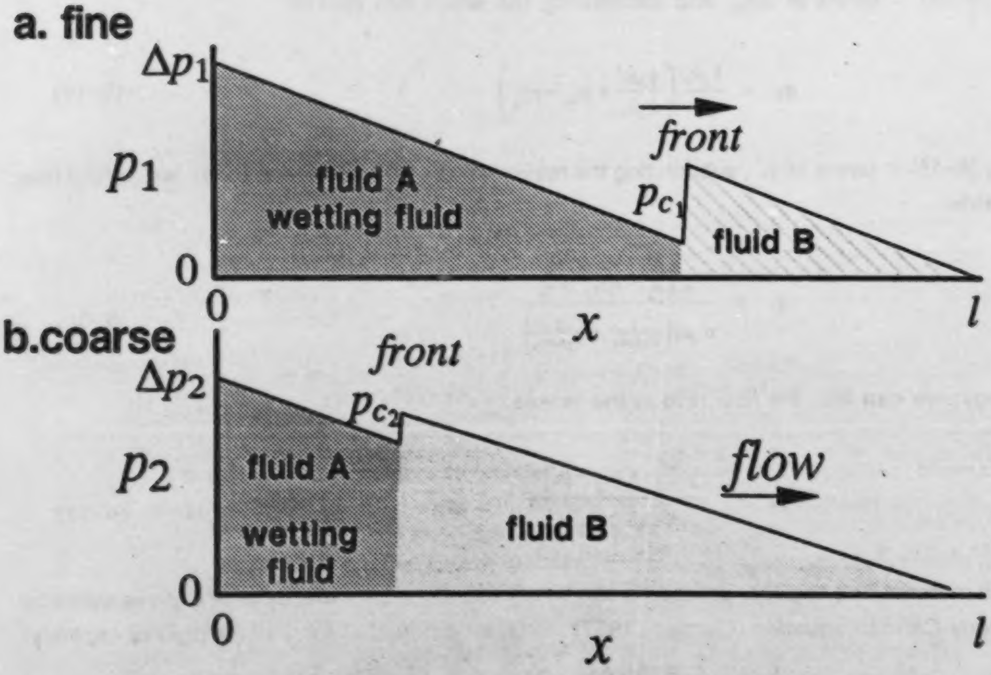
a. fine
Δp_1
p_1
front
fluid A
wetting fluid
p_{c_1}
fluid B
0
0
x
l
b.coarse
Δp_2
p_2
front
p_{c_2}
fluid A
wetting fluid
fluid B
flow
0
0
x
l

FIGURE 9-53. Pressure profiles for fluids A and B, with fluid A as the wetting fluid, for a) the fine matrix and b) the more coarse lense.

where r_i is the radius of the capillary. By the Kozeny-Carman equation, $R_i \approx 18\sqrt{k_i}$ for random packings of equal spheres (where R_i is the sphere radius). If media of well-sorted spheres is assumed where r is of the same order as R:

$$p_{c_i} = \frac{2\sigma\cos\theta}{r_i} = \frac{2\sigma\cos\theta}{R_i} = \frac{\sigma\cos\theta}{9\sqrt{k_i}} \qquad (9\text{–}23)$$

Finally, by substituting this relation into equations (9–20) and (9–21) and by merging these equations into ratio form we get:

$$\frac{q_2}{q_1} = \frac{\frac{\bar{q}\mu l}{k_1 k_r} + \frac{a_1\sigma\cos\theta}{9}\left(\frac{1}{\sqrt{k_2}} - \frac{1}{\sqrt{k_1}}\right)}{\frac{\bar{q}\mu l}{k_2 k_r} - \frac{a_2\sigma\cos\theta}{9}\left(\frac{1}{\sqrt{k_1}} - \frac{1}{\sqrt{k_2}}\right)} \qquad (9\text{–}24)$$

When $\frac{q_2}{q_1} > 0$, water will flow into the coarse lenses displacing organic liquid.

To find the critical flux, $\bar{q}^*$, needed to initiate the flow of wetting fluid into the non-wetting fluid filled coarse lenses, equation (9–24) is set equal to zero and solved in terms of $\bar{q}$:

$$\bar{q}^* = \frac{\sigma\cos\theta\ k_1 k_r (1 - a_2)}{9\mu l}\left(\frac{1}{\sqrt{k_1}} - \frac{1}{\sqrt{k_2}}\right) \qquad (9\text{–}25)$$

This is really an effective critical capillary number, necessary to begin to reduce the macroscopic residual non-wetting phase saturation caused by the heterogeneity:

$$N_c^* = \frac{\bar{q}_c^*\mu}{\sigma} = \frac{\cos\theta\ k_r}{9l}\sqrt{k_1}\ (1 - a_2) \qquad (9\text{–}26)$$

From equation (9–25), one can see that the critical flux needed to initiate displacement of non-wetting organic liquid from coarse lenses is inversely proportional to the length of the lense, l, and the relative area occupied by the lenses, a_2, but is directly proportional to the capillary force, $\sigma\cos\theta$.

Figure 9–54 shows the relationship between the critical flux and the permeabilities. When $k_1 = k_2$, the system is homogeneous and the critical flux is zero. Displacement occurs at the same rate in both materials. When the lenses are composed of coarser material, k_2 is larger than k_1, and it takes the critical flux to initiate displacement of non-wetting fluid from the lenses. For very coarse lenses, and large

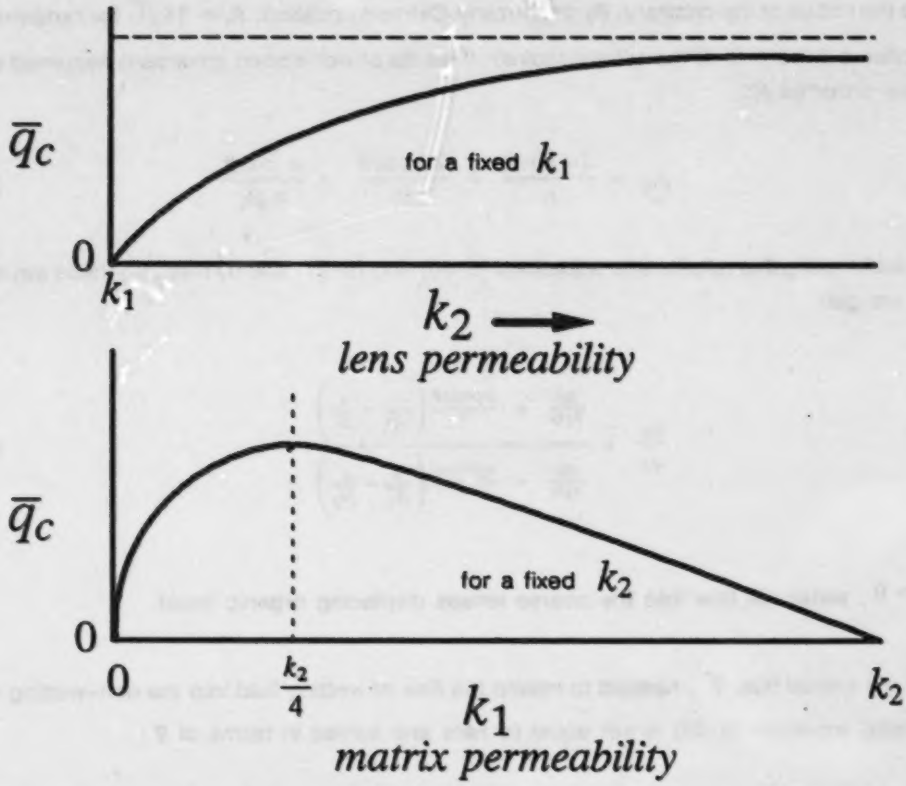

FIGURE 9-54. Critical flow rates needed to displace organic liquid from coarse lenses as a function of permeability in the coarse lens (top), and in the fine matrix (bottom).

values of k_2, this critical flux increases toward an asymptotic value that depends on the permeability of the matrix:

$$\bar{q}_c^{*} = \frac{\sigma \cos\theta \sqrt{k_1}\, k_r (1 - a_2)}{9 \mu l} \quad ; \textit{for large } k_2 \tag{9-27}$$

or, expressed as the critical capillary number necessary to begin to reduce the macroscopic residual non-wetting phase saturation caused by the heterogeneity:

$$N_c^{*} = \frac{\bar{q}_c^{*} \mu}{\sigma} = \frac{\cos\theta \; k_r}{9 l} \sqrt{k_1} \; (1 - a_2) \quad ; \textit{for large } k_2 \tag{9-28}$$

Note that this critical effective capillary number is zero if the contact angle is near to 90°.

The fine matrix permeability, k_1, can vary between zero and k_2. Toward either of these end points, the critical flux approaches zero, in one instance as k_1 becomes impermeable, and in the other instance as the system approaches homogeneity. In between these extremes the critical flux reaches a maximum at $k_1 = k_2/4$, in which displacing organic liquid from the coarse becomes most difficult (see Figure 9-54).

For flux rates exceeding the critical value, non-wetting fluid is displaced from each coarse lense, starting at the upstream end, and proceeding through the lense. When the fine matrix wetting front reaches the downstream end of the lense, the wetting fluid front coming around each side is presumed to join, isolating the remaining non-wetting fluid that has not yet been displaced from the coarse lense. This non-wetting fluid is trapped on the downstream end of the lense. The proportion of the lense not swept by water is described by equation 9-24:

$$\textit{Proportion of lense left unswept} = \frac{q_2}{q_1} \tag{9-29}$$

The critical flux rate necessary to displace all of the non-wetting fluid from the lens, except for pore scale trapping, is found by setting equation 9-24 to one. The result can be expressed as an effective critical capillary number for complete sweeping of the lenses:

$$N_c^{**} = \frac{\overline{q}_c^{**} \mu}{\sigma} = \frac{\cos\theta \;\; k_r}{9l} \frac{\sqrt{k_1 k_2}}{(\sqrt{k_1} + \sqrt{k_2})} \tag{9-30}$$

This critical number is independent of the relative areas of lenses and matrix. If the lenses are very coarse (k_2 very large), this critical number approaches an asymptote,

$$N_c^{**} = \frac{\cos\theta \;\; k_r}{9l} \sqrt{k_2} \qquad ; \textit{for large } k_2 \tag{9-31}$$

This model qualitatively explains most of the results seen in the experiments. In effect, the capillary trapping of residual non-wetting phase in the lenses is analogous to the by-passing mechanism on the pore level. If the capillary number is sufficiently high, less non-wetting fluid is originally trapped, and perhaps most or even all of the large scale by-passing can be avoided. However, this model does not explore the issue of mobilizing the large scale by-passed residual once it is cut off from its neighbors. Presumably, the situation may be similar to attempting to mobilize pore scale singlets in a glass bead pack. Recall that in that case it was much easier to avoid trapping in the first place, than to subsequently mobilize the blobs (Morrow *et al.*, 1988).

We have not attempted to quantitatively validate the simple heterogeneous media trapping model presented here. The experiments were conducted before the theory was developed, and were not designed to collect all of the necessary quantitative information. The actual experiments involved lenses of varied length and a somewhat random pattern. We strongly recommend further model development with appropriate experimental validation. The model and experiments should test a variety of geometrical heterogeneity patterns and material property contrasts. We especially recommend examining the case of fine lenses imbedded in a matrix of coarser material.

Implications for modelling multiphase flow–

The simple mathematical model developed here suggests that it is feasible to develop effective properties, or equivalent homogeneous models of behavior in heterogeneous materials. The simulation codes into which these equivalent homogeneous properties are inserted may not be conventional codes. They will need to account for the partial de-saturation of lenses, and the effect that has on effective relative permeabilities and saturations. For example, the effective permeabilities and residual saturations will certainly depend on the rate and direction of flow. We believe that this is a typical consequence of dealing with effective properties in non-linear systems. Certainly Yeh *et al.* (1985a,b,c), Mantoglou and Gelhar (1987), and McCord *et al.* (1988a,b) encountered the same issue in their work on the Richard's equation approach to water flow in the vadose zone.

Discussion of Multiphase Movement and Capillary Trapping in Heterogeneous Media

The experimental results and simple mathematical model confirm our hypothesis that the spatial variation or heterogeneity of soil properties has a dominant effect on the movement and capillary trapping of organic liquids. The impact of this issue on movement and trapping far exceeds that of the influence of organic liquid composition or local soil texture.

SECTION 10

VADOSE ZONE RESULTS AND DISCUSSION

Figure 10-1 depicts the portion of the aquifer that includes residual saturation in the vadose zone, above the capillary fringe, where an organic liquid shares pore space with both gas and water. Whether an organic liquid is more (left) or less (right) dense than water, it leaves behind a trail of capillary trapped residual in the vadose zone as it moves downward toward the capillary fringe. This movement is much more complex and diverse than in the saturated zone, especially on a pore scale, primarily because of the presence of the gas phase. A dropping or fluctuating water table can further complicate the situation.

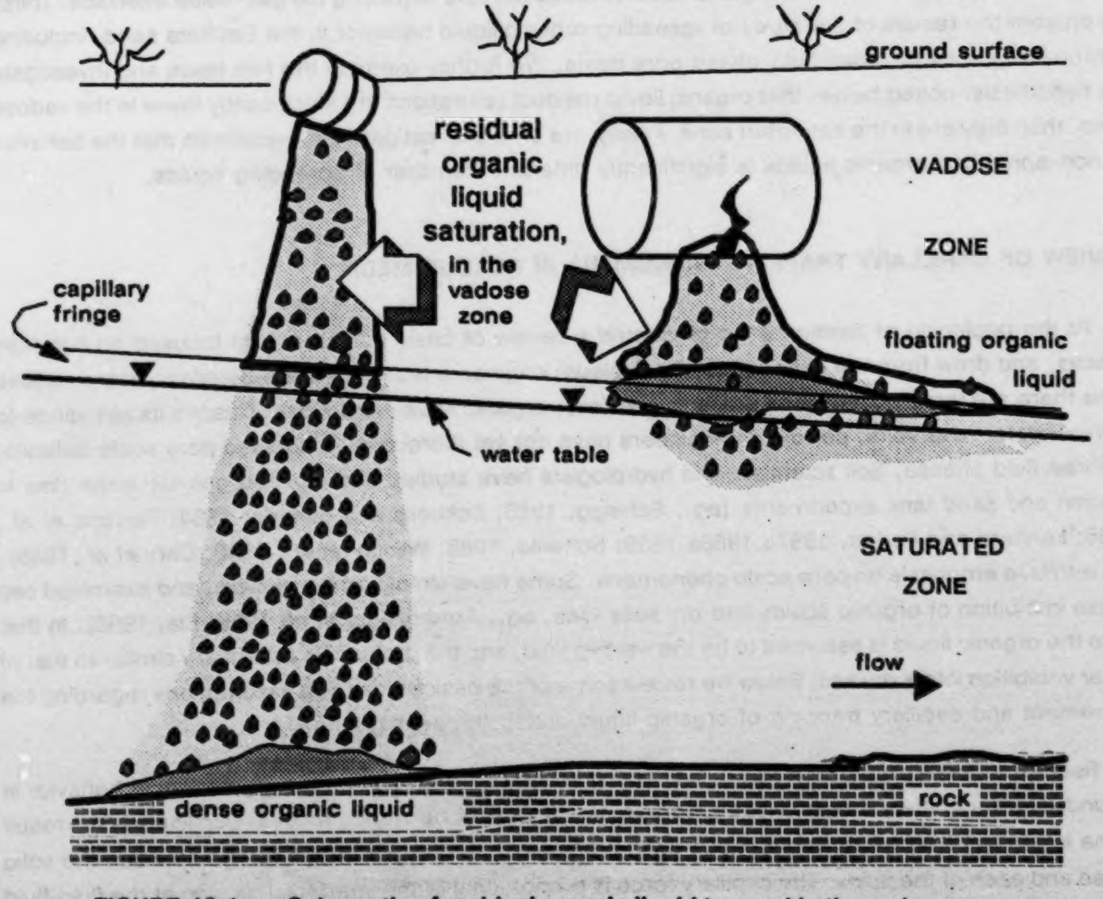
ground surface
residual organic liquid saturation, in the vadose zone
VADOSE ZONE
capillary fringe
floating organic liquid
water table
SATURATED ZONE
flow
dense organic liquid
rock

FIGURE 10-1. Schematic of residual organic liquid trapped in the vadose zone.

This section on organic liquid movement and capillary trapping in the saturated zone contains four main parts:

- $\bullet_1$ review of basic concepts and assumptions,
- $\bullet_2$ flow visualization of three-phase displacement and capillary trapping in a micromodel,
- $\bullet_3$ capillary trapping and organic liquid residual saturation in an unconsolidated soil: the Sevilleta sand,
- $\bullet_4$ micromodel visualization of three-phase capillary trapping of a non-spreading organic liquid.

The first part is a brief review of three-phase flow concepts and assumptions. It describes some of what we know about organic liquid behavior in the vadose zone. Second is a description of three-phase displacement and capillary trapping as observed in a homogeneous micromodel. It visually demonstrates some of the important behavior issues for so-called 'spreading' organic liquids. We examine the hypothesis that the organic liquid spreads out as a film along the gas-water interface. Third, we present the results of our study of spreading organic liquid behavior in the Sevilleta sand, including photomicrographs of three-fluid-phase pore casts. We further examine the film issue and investigate the hypothesis, posed below, that organic liquid residual saturations are significantly lower in the vadose zone, than they are in the saturated zone. Finally, we briefly investigate the hypothesis that the behavior of non-spreading organic liquids is significantly different than that of spreading liquids.

REVIEW OF CAPILLARY TRAPPING PHENOMENA IN POROUS MEDIA

At the beginning of Section 9 we presented a review of basic concepts that focused on two fluid phases, and drew from the experience of petroleum engineers with pore scale behavior. In the vadose zone there are three fluid phases present: gas (air), organic liquid, and water. Despite its relevance to gas-oil-water reservoirs, petroleum engineers have not yet thoroughly addressed pore scale behavior of three fluid phases. Soil scientists and hydrologists have studied three-phase gas-oil-water flow in column and sand tank experiments (eg., Schiegg, 1980; Eckberg and Sunada, 1884; Ferrand *et al.*, 1986; Lenhard and Parker, 1987a,1988a,1989; Schwille, 1988; Wilson *et al.*, 1988; Cary *et al.*,1989), but with little emphasis on pore scale phenomena. Some have simplified the system, and examined two phase imbibition of organic liquids into dry soils (see, eg., Ammozegar *et al*, 1986; Kia, 1988). In that case the organic liquid is assumed to be the wetting fluid, and the problem is essentially similar to that of water imbibition into a dry soil. Below we review some of the basic issues and assumptions regarding the movement and capillary trapping of organic liquid during three-phase flow.

Recall that there are three major forces acting in both oil recovery, and in organic liquid behavior in groundwaters: **capillary forces**, **viscous forces**, and **gravity** or **buoyancy forces**. Capillarity is the result of the interplay of cohesive forces within each fluid phase, and the adhesive forces between the solid phase and each of the fluids. The capillary force is proportional to the interfacial tension at the fluid-fluid interface and the strength of fluid wetting to the solid surface, and inversely proportional to the pore size.

Viscous or dynamic forces within a phase are proportional to the media permeability, the fluid phase relative permeability, and the fluid phase pressure gradient. Buoyancy is a gravitational force proportional to the density difference between the fluids.

The additional third phase in the vadose zone is the gas phase. Gas has a much lower density than either of the two other fluids, so that gravity (buoyancy) forces play a more significant role here than in the saturated zone. Gas is almost always the non-wetting phase in the vadose zone, so that it takes the role that the organic liquid usually takes in the saturated zone.

Many organic liquids appear to be of intermediate wettability in typical aquifer materials; that is, non-wetting relative to water, but wetting relative to gas. The organic phase, depending on whether it encounters gas or water, can then display either wetting or non-wetting behavior, or both. Many organic liquids also have low internal cohesion and will spread, presumably forming a film between the water phase, which because of capillarity preferentially occupies the smallest pores, and the gas phase, which preferentially fills the largest pores.

This film should interconnect the pockets of organic liquid, which even at residual saturation should be largely continuous. This is the usual assumption in mathematical models (see, eg, the model of Parker and Lenhard, 1987; Parker et al, 1987; Lenhard and Parker, 1987a, 1988, 1989). Because the residual organic liquid is interconnected by films the term *capillary trapped* may be misleading. With some exceptions described below, the organic liquid is not actually trapped in isolated blobs. This vadose zone residual saturation has been referred to by other researchers as the organic phase 'retention' for a soil.

The propensity to spread can be measured by the 'spreading coefficient' (eg, Adamson, 1982):

$$\Sigma = \sigma_{aw} - (\sigma_{ow} + \sigma_{ao}) \qquad (10\text{-}1)$$

where:
Σ = spreading coefficient
σ_{aw} = air (gas) - water interfacial tension (*the surface tension,* γ)
σ_{ow} = organic liquid - water interfacial tension
σ_{ao} = air (gas) - organic liquid interfacial tension

Intermediate wetting organic liquids that tend to spread as a film have a positive spreading coefficient, Σ. In this case the surface tension between the gas and water, σ_{aw}, exceeds the sum of the interfacial tensions between the organic liquid and the two other fluids, σ_{ow} & σ_{ao}. Figure 10-2 depicts the force balance. Most of our experimental work focused on spreading organic liquids.

Despite the presence of the intermediate wetting phase organic liquid film, it is realistic to hypothesize that there are portions of the pore space where there would be no continuous non-wetting gas phase. Here the intermediate wetting phase would act like a non-wetting phase, and become trapped by capillary forces in the same way we discussed in Section 9. Discontinuous blobs of organic liquid should tend to occur in these portions.

Some organic liquids have more internal cohesion, as measured by a negative spreading coefficient, Σ (eg, halogenated hydrocarbons such as carbon tetrachloride and PCE). In this case the

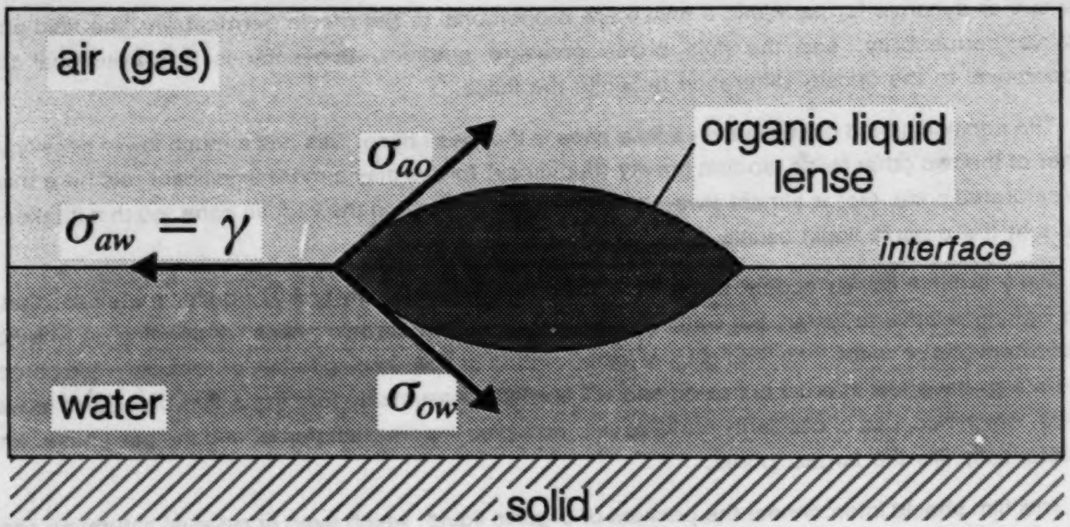

FIGURE 10-2. **Diagram of spreading potential for a drop of organic liquid floating on the air (gas)-water interface (after Adamson, 1982, and others). The water is wetting, the air is non-wetting, and the organic liquid is intermediate wetting.**

sum of the interfacial tensions between the organic liquid and the two other fluids, σ_{ow} & σ_{ao}, exceeds the surface tension between the gas and water, σ_{aw} (see Figure 10-2). These organic liquids will not spread as films. On a flat water surface (the water-gas interface) non-spreading liquids tend to coalesce into lenses that float on the surface (much as depicted in Figure 10-2). When the water-gas interface is within a porous media we don't know what behavior to expect.

In the previous section (Section 9) we introduced micromodel experiments which suggested that the wetting phase residual saturation may depend on non-wetting phase flow rate. This suggestion was amplified by the work of Amulfule and Handy (1982), Dullien *et al.* (1986), and Chatzis *et al.* (1988), which we discussed on page 161. In effect, any increase in either viscous forces, as represented by flow rate, or buoyancy forces can cause a change in the wetting phase residual saturation. The process is illustrated in Figure 10-3, in which residual saturations are plotted as a function of the ratio of viscous plus buoyancy forces, to capillary forces, $(F_v + F_b)/F_c$ (ie., capillary plus Bond numbers). A typical non-wetting phase residual saturation mobilization curve is also illustrated. This represents water displacing organic liquid in the saturated zone, such as we described in Section 9 (see, eg, Figures 9-9 & 9-10). There is a critical value of $(F_v + F_b)/F_c$ for the non-wetting residual, S_{or}, below which viscous and buoyancy forces are small compared to capillary forces, and the non-wetting phase residual saturation is at a maximum value of S_{or}^*. In contrast, the wetting phase residual saturation is a smooth function of $(F_v + F_b)/F_c$ (Wilson *et al.*, 1988; Handy, 1988, personal communication). There is no critical combination of forces necessary to begin reducing wetting phase residual, because the wetting phase is interconnected by films, and can always drain.

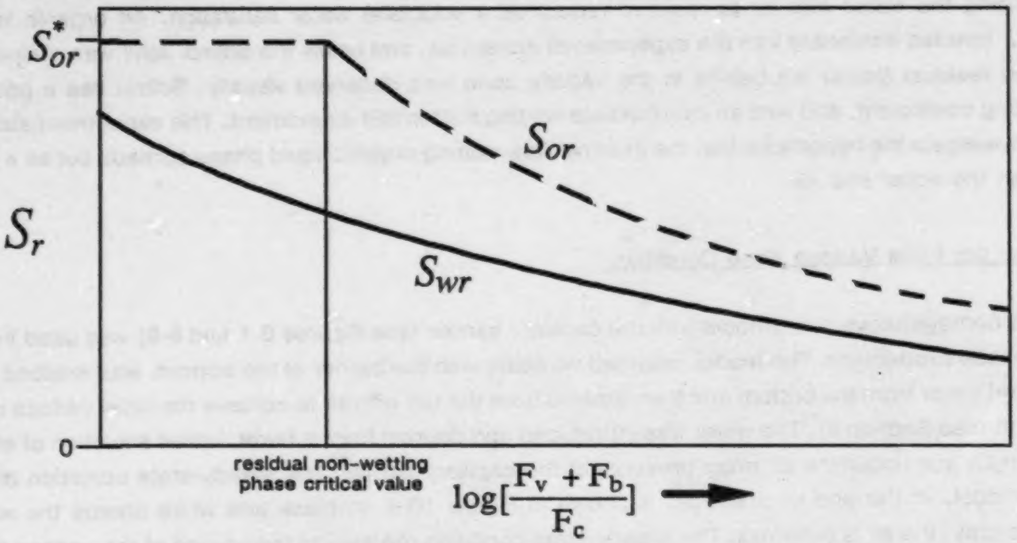

FIGURE 10-3. A conceptual plot of residual saturation for the wetting fluid (solid line) and th non-wetting fluid (dashed line), as a function of the ratio of the sum of viscous an buoyancy forces, to capillary forces.

In the vadose zone, when the organic liquid spreads as a intermediate wetting phase film, we can expect somewhat similar behavior. That is, because the residual organic liquid saturation is largely interconnected, it should be a smooth function of the force ratio $(F_v + F_b)/F_c$. Buoyancy forces are proportional to the organic liquid's density contrast with gas. Higher density organic liquids will result in greater (negative) buoyancy forces, and smaller residual organic liquid saturations. Significant gas phase flows will increase the viscous forces and also reduce residual organic film saturation. Although such velocities may not normally be expected in the vadose zone, they may be common in vacuum extraction and other similar *in situ* volatilization approaches to remediation.

We hypothesize that the organic liquid residual saturation in the vadose zone is smaller than it is in the saturated zone. The presence of gas as the non-wetting phase, filling the pore bodies, is the main basis for this hypothesis. There is also a propensity for greater buoyancy forces, because of the density contrast with gas. Conversely, in the saturated zone, the combined buoyancy and viscous forces are not usually great enough to overcome the capillary forces and the residual saturation is at its maximum.

MICROMODEL FLOW VISUALIZATION OF THREE PHASE DISPLACEMENT AND CAPILLARY TRAPPING

Micromodel flow visualization techniques in homogeneous media illustrate the scenario of a large slug of organic liquid percolating vertically downward into the vadose zone. Later, it's drained by air as it continues downward on its migration toward the water table. This scenario was simulated by first saturating a water-wet etched glass micromodel with water. Then, a vadose zone condition was created by draining the water with air to residual (so-called irreducible) water saturation. An organic liquid, Soltrol, invaded downward into the experimental apparatus, and finally the Soltrol itself was drained by air. The residual Soltrol left behind in the vadose zone was observed visually. Soltrol has a positive spreading coefficient, and was an intermediate wetting fluid in this experiment. This experiment allowed us to investigate the hypothesis that the intermediate wetting organic liquid phase spreads out as a film, between the water and air.

Creating the Initial Vadose Zone Condition

The homogeneous micromodel with the capillary barrier (see Figures 8-1 and 8-9) was used in this three-phase experiment. The model, oriented vertically with the barrier at the bottom, was imbibed with blue dyed water from the bottom and then drained from the top with air to achieve the initial vadose zone condition (see Section 8). The water was introduced and drained from a buret, under a suction of about 15 cm H_2O, just under the air entry pressure of the capillary barrier. The steady-state condition of the entire model, at the end of drainage, is shown in Figure 10-4. In black and white photos the water appears gray; the air is colorless. This steady-state condition represents the portion of the vadose zone well above the capillary fringe (see Figure 10-1), where water saturation is near its so-called irreducible value. The water fills some of the pore throats, an occasional by-passed pore body, and forms a film around the air-filled pores. Because the model had fairly large pores and a relatively uniform pore size distribution, not much suction was needed to achieve a fairly complete drainage. Unlike the results obtained from the micromodels used in the saturated zone experiments, the presence of the capillary barrier at the bottom of the model prevented a capillary end effect. (Capillary end effect was discussed in Section 9, for the case of Soltrol advancing into the same model without a capillary barrier under water-saturated conditions.) This photograph can be compared to Figures 9-11a and 9-34a. Here air was the non-wetting phase; there it was Soltrol.

Organic Liquid Invasion

In the next step red dyed Soltrol invaded downward into the drained micromodel at a relatively slow rate of 0.096 ml/min. Air and perhaps some water was pushed ahead of the Soltrol, which primarily advanced by displacing air, in bulk, from the interconnected air-filled pore bodies and pore throats. The Soltrol largely bypassed water that had previously been 'trapped' in pore throats. At the bottom of the model sufficient pressure was achieved to exceed the air entry pressure of the capillary barrier, thus allowing air to escape.

During this displacement, some pockets of organic liquid were developed ahead of the main front of advancing organic liquid. At first glance, we were puzzled as to where this fluid had come from, but closer examination revealed that it had traveled through thin films of organic phase formed between the air and water phase. Figure 10-5, a photograph take from a videotape of an earlier experiment, illustrates this process (Mason et al, 1989; a similar videotape is available for viewing, see Appendix B). The blue water and red Soltrol dyes were deeper in color in this experiment. In black and white the Soltrol

Reproduced from
best available copy.

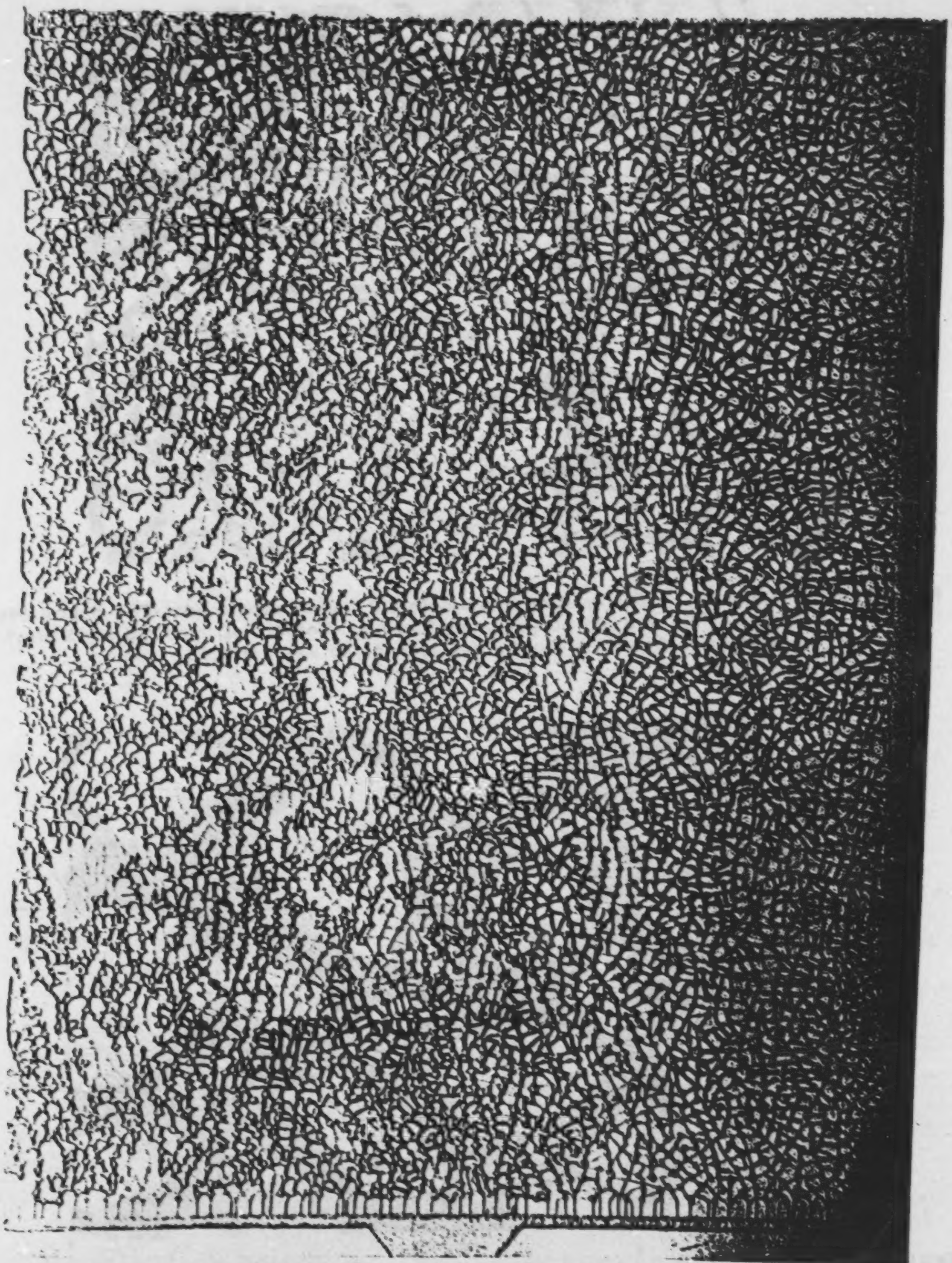

FIGURE 10–4. Initial vadose zone condition, with water drained by air to residual (irreducible) water saturation. The water was dyed blue (light grey), and the air was not dyed.

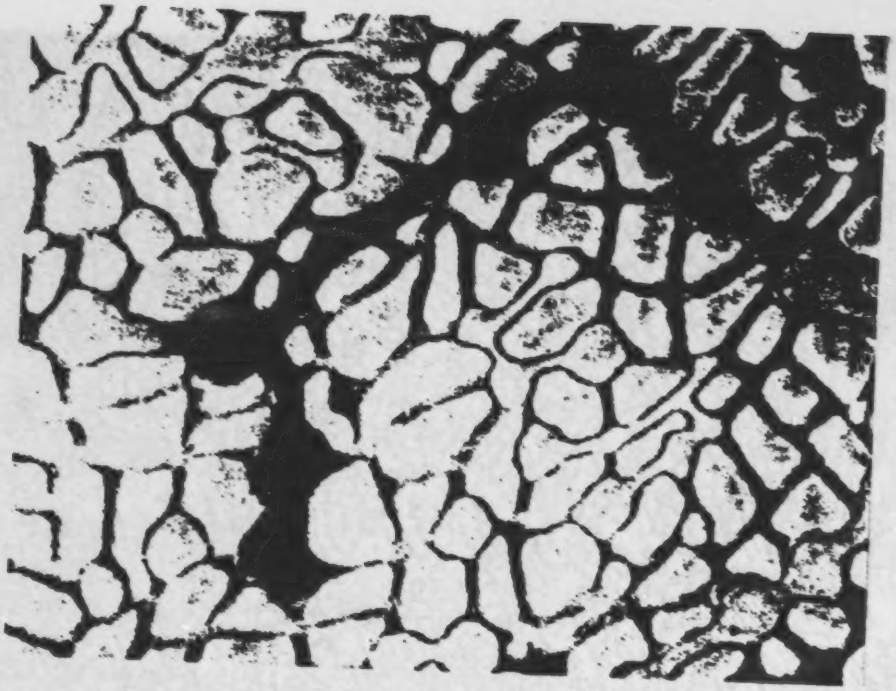

FIGURE 10-5. Detail of Soltrol invasion into a different vadose zone model. The Soltrol was advancing by filling pores and by film flow. Soltrol was dyed red (dark grey), water was dyed blue (light grey), and the air was not dyed.

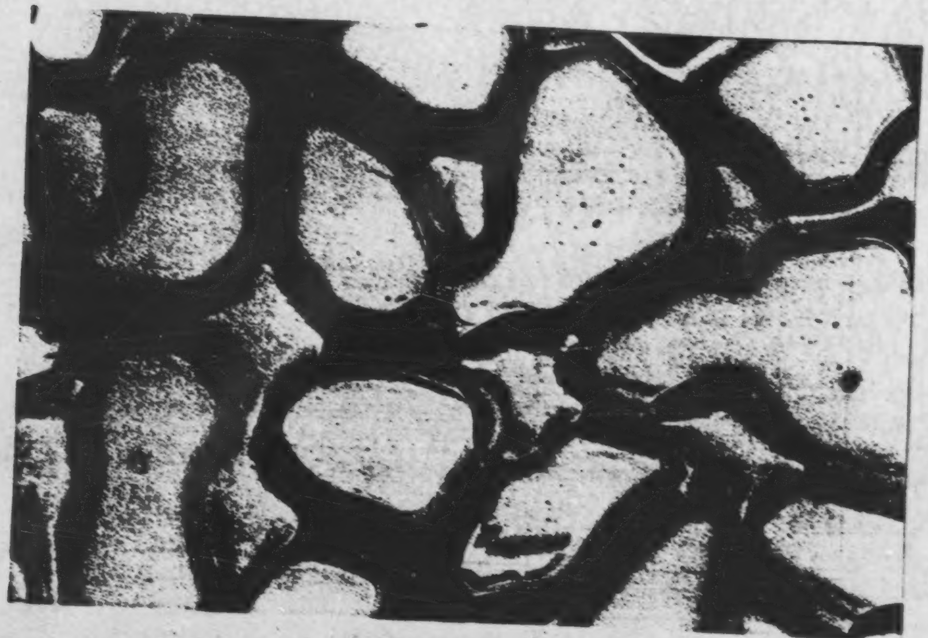

FIGURE 10-6. Detail of steady state conditions after the Soltrol invasion into the vadose zone model. Soltrol was dyed red (dark grey), water was dyed blue (light grey), and the air was not dyed.

appears as a very dark grey, and the water is a lighter grey. The initial water saturation was also greater than the irreducible value. A finger of Soltrol, filling the pores, penetrates the frame from the top. In the Soltrol-filled pore moving off to the left, the Soltrol attached to the water coated walls as a film, with air filling the center of the pore. Soltrol was flowing in this film, which leaves the frame and then re-enters just below. Soltrol then moved off toward the bottom of the frame as film flow. To the right center of the frame is a film bridging an air-filled pore body between two Soltrol-filled pore throats. Rapid advancement of Soltrol through film flow is apparently a form of preferential flow.

The steady-state condition for the entire model, at the end of the organic liquid invasion, is shown in Figure 10-7. A more detailed photo is shown in Figure 10-6. In black and white the Soltrol appears as a dark gray and the water appears as a lighter gray. Notice in the detailed photo that the Soltrol filled many pore throats and formed a film between the air and the water. This film penetrated somewhat into the water-filled pore throats, almost 'smiling' at the observer. In short water-filled pore throats the 'smiles' from each end almost touched, and the water phase pendular ring was clearly visible. Water was also present as a wetting phase film between the Soltrol and the solid surface. Figure 8-8 is an SEM photomicrograph of a typical eye-shaped micromodel pore cross-section. The wetting phase 'film' actually occupied the wedges on either side of the pore. The saturation and distribution of the water phase remained almost entirely unchanged when compared to the initial vadose zone condition.

The steady state condition depicted in Figure 10-7 can be compared to the two phase flow experiments. The non-wetting air phase was trapped in isolated bubbles or blobs, similar to those seen for the saturated zone organic phase (as shown in Figures 9-11b, 9-12b, 9-13b, 9-15, and 9-16). Here air was the non-wetting trapped phase; there it was Soltrol. Because of the presence of air in the vadose zone (in addition to organic liquid and water), the maximum organic liquid saturation achieved was not as great as in the saturated-zone case.

Drainage of Organic Liquid by Air

In the final step of the experiment, Soltrol was drained from the model by air, representing the continued percolation of the organic phase downward toward the water table. The Soltrol was drained from the model under a small applied suction. This suction is believed to have been insufficient to completely drain the organic phase to its lowest possible saturation, but because Soltrol has a much lower surface tension than water, higher applied suctions would have resulted in air breaking through the capillary barrier. We refer to the resulting Soltrol saturation as 'residual saturation'.

The final distribution of fluids within the entire model is shown in Figure 10-9, while the close-up photos in Figure 10-8 illustrate the more complex nature of organic liquids left behind in the vadose zone. Comparing Figure 10-9 to Figure 9-11b we note that the amount of organic phase retained in the vadose zone was much less than the residual saturation left behind in the saturated zone, as we expected. The distribution of fluids is also much more complex. The micromodel photographs in Figure 10-10 further illustrate these points. The lower photo shows residual saturation obtained under two-phase conditions in a small section of a micromodel, representing saturated zone conditions. The upper photo shows residual saturation in the identical portion of the same micromodel under three-phase conditions, representing vadose zone conditions.

Reproduced from best available copy.

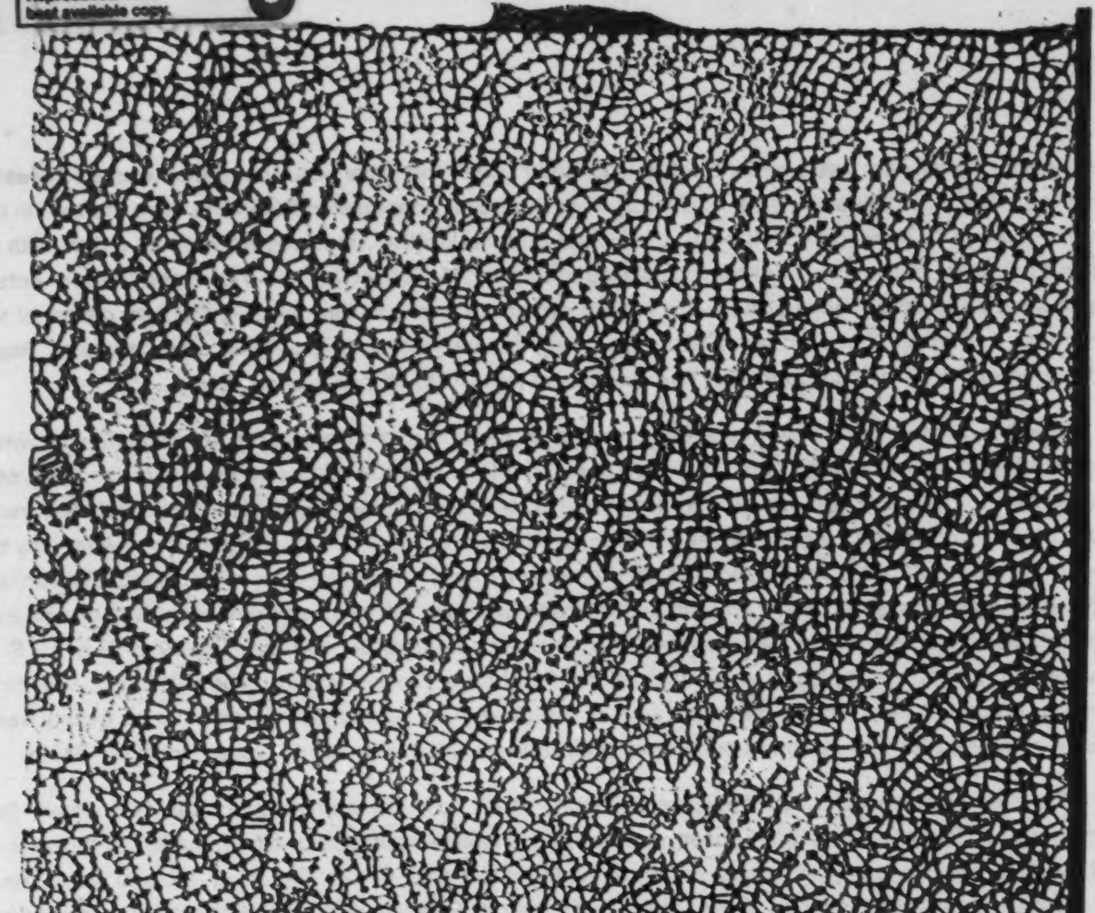

FIGURE 10-7. Steady state conditions after the Soltrol invasion into the vadose zone model. Soltrol was dyed red (dark grey), water was dyed blue (light grey), and the air was not dyed.

Inspection of Figures 10-8 and 10-9 reveals that residual organic liquid is distributed in several different ways in the vadose zone. In particularly dry portions of the pore space, it is found in pore throats, as pendular rings, in small pore bodies (see lower right portion of Figure 10-8), and as a film between the air and water phases. The film helps fill the wedges of the pore cross-section (see Figure 8-8) and penetrates as 'smiles' into the water-filled pore throats, surrounding water-filled pendular rings. This film can be quite thin, as shown in Figure 10-11, taken from another micromodel. Sometimes organic liquid was trapped, similar to the two-phase case, as blobs within the water phase. We found that this kind of trapping is more likely to occur when the initial water content is relatively high or when infiltrating water follows the organic liquid (eg, rainfall infiltration following a spill event). Occasionally we saw a gas bubble trapped inside one of these organic liquid blobs. However, due to its intermediate wetting properties and its tendency to spread, organic liquid in the vadose zone is most commonly retained in between the water and air phases.

In contrast to organic liquid blobs trapped in the saturated zone, the residual organic phase in the vadose zone remains more or less continuous, interconnected by the ubiquitous films (with the exception of any organic liquid that might have been trapped as blobs entirely within the water phase). We refer to this organic liquid as 'residual' and 'trapped', but these terms must be used with care. As we discussed in reference to Figure 10-3, the intermediate wetting phase saturation is a continuous function of applied viscous and gravity forces; it can always be reduced further, albeit slowly.

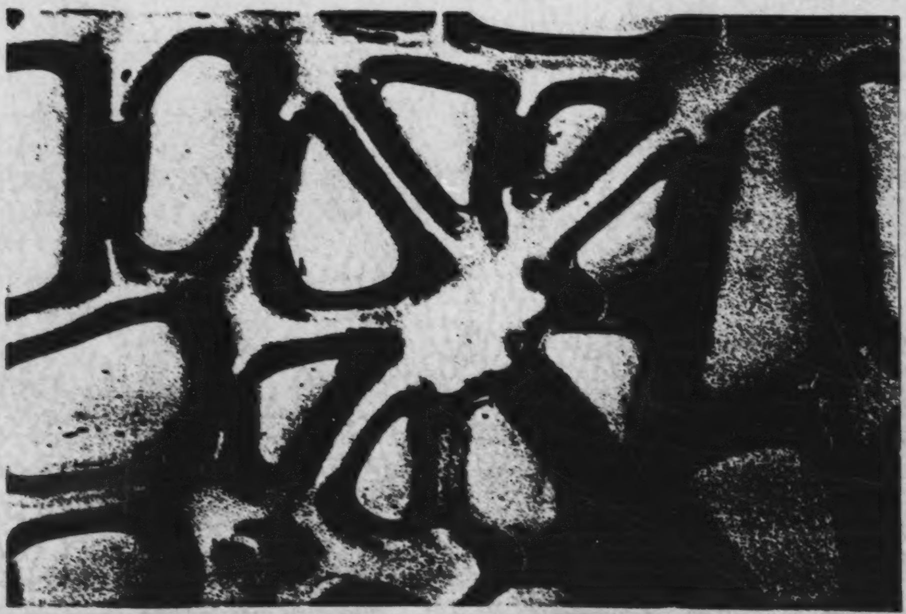

FIGURE 10-8. Detail of steady state conditions after the Soltrol has been drained by air from the vadose zone model. Soltrol was dyed red (dark grey), water was dyed blue (light grey), and the air was not dyed.

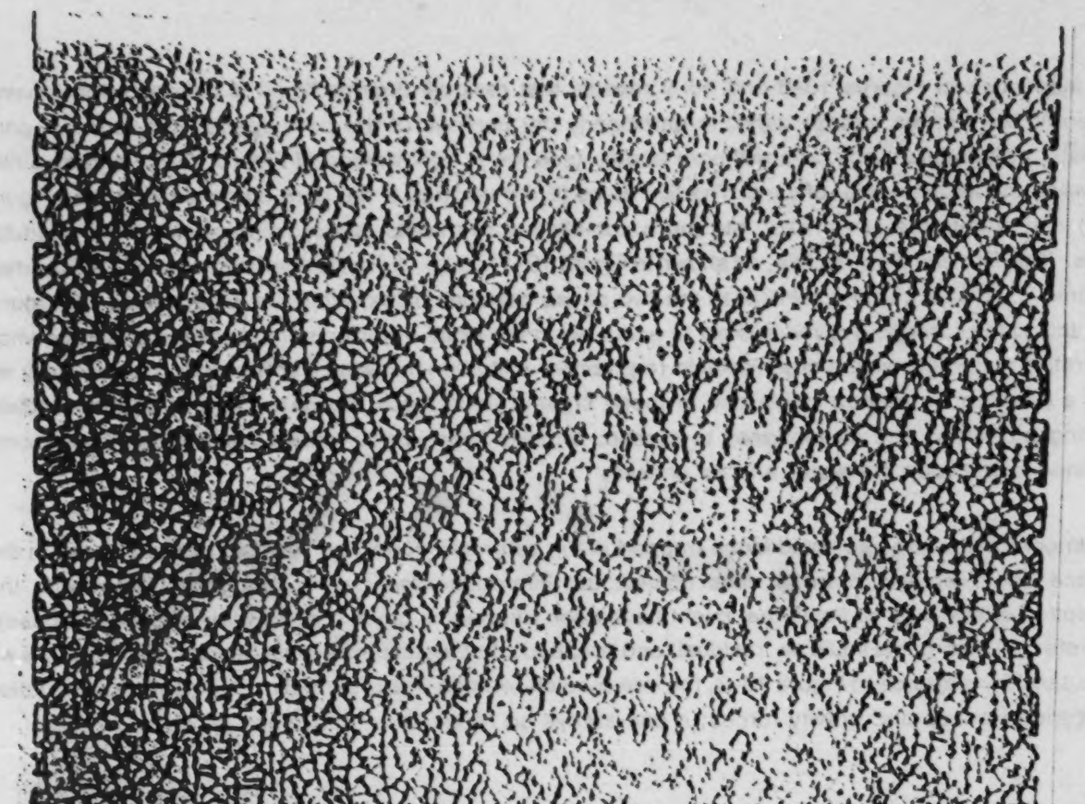

FIGURE 10–9. Steady state conditions after the Soltrol has been drained by air from the vadose zone model. Soltrol was dyed red (dark grey), water was dyed blue (light grey), and the air was not dyed.

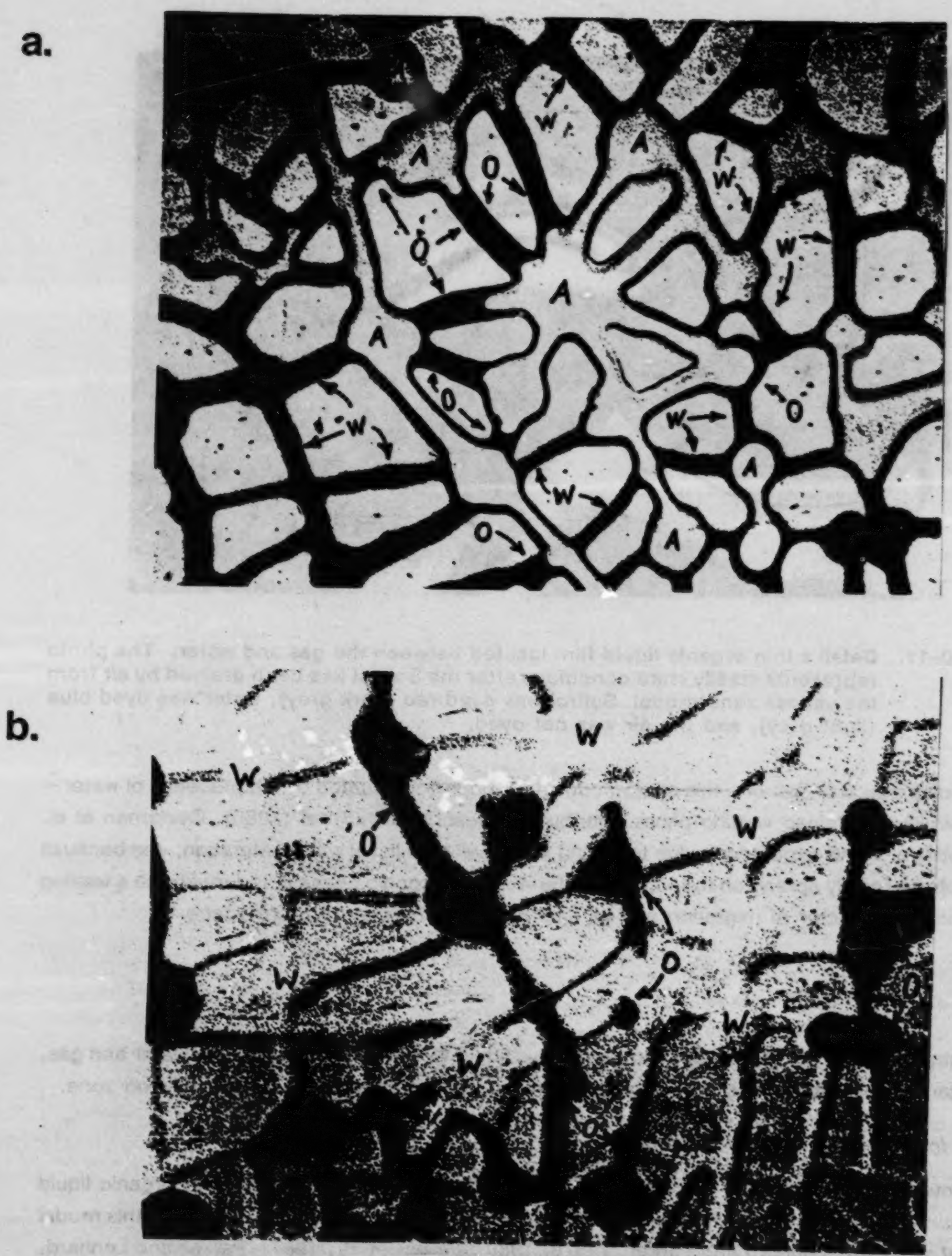
a.
W
A
O
A
W
O
W
A
A
O
W
W
O
W
A
O
A
b.
W
W
O
W
O
W
O
W
W
O

FIGURE 10–10. **Steady state conditions in a micromodel after a) Soltrol has been drained by air from a vadose zone model, and b) Soltrol has been displaced by water in a saturated zone model.. Soltrol was dyed red (dark grey), water was dyed blue (light grey), and the air was not dyed.**

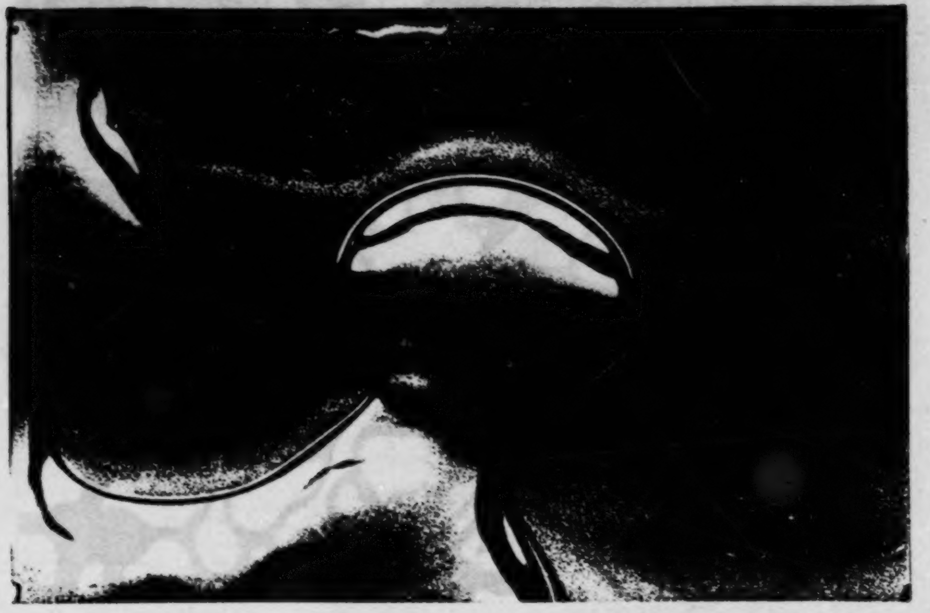

FIGURE 10-11. Detail a thin organic liquid film located between the gas and water. The photo represents steady state conditions after the Soltrol has been drained by air from the vadose zone model. Soltrol was dyed red (dark grey), water was dyed blue (light grey), and the air was not dyed.

The final distribution of Soltrol in this micromodel — although complicated by the presence of water — was not dissimilar to drained wetting phase distributions described by Hillel (1980), Gvirtzman et al. (1987) and others. In this experiment, due to having a relatively low initial water saturation, and because the organic phase readily spread on the water/air interface, the organic phase acted much like a wetting phase both in its character of migration and its final distribution within the pore space.

Discussion

Our results support the hypotheses that the organic liquid forms a film between the water and gas, and that organic liquid saturations are much lower in the vadose zone than in the saturated zone.

Implications for modelling multi-phase flow –

Most continuum mathematical models of organic liquid migration assume that the organic liquid phase is continuous and forms a layer between the water and air phases (for one example of this model see Parker *et al.*, 1987; Lenhard and Parker, 1987a, 1989 ; Parker et al., 1987; Parker and Lenhard, 1987). Within the context of this experiment that assumption appears valid.

Mathematical percolation network models of multi-phase flow (eg, Soll and Celia, 1988) often assume that only one phase can occupy a given pore body or pore throat at any given time, and neglect films and film flow. In our experiments we have commonly observed two and three phases simultaneously occupying a single pore, and we've seen that film flow can play an important role in the movement of organic liquids. The wetting and intermediate-wetting phases remain self-connected through the films, which maintain a continuity for drainage or imbibition that cannot be captured using a traditional percolation network approach. Future versions of these network models should explore this issue.

Implications for phase partitioning–

As discussed earlier in the saturated zone section, the pore-scale distribution of the organic phase influences the partitioning of organic liquid components. Because the organic phase is almost always less wetting than water but more wetting than air, it remains in direct contact with both the air and water allowing for both solubilization into the water phase and especially volatilization into the air phase. The formation of thin organic liquid films between the water and air increases the surface area of the organic phase, enhancing the propensity for inter-phase partitioning of organic components. Soil venting of organics in the vadose zone has become an attractive remediation strategy because volatile organics partition easily to the air phase. The thin film in Figure 10-11 provides a good example of the large organic/air and organic/water interfaces generated by the organic phase's tendency to spread. However, the films are not of uniform thickness. They interconnect organic liquid filled 'smiles' and pore throats. In a multicomponent organic liquid, mass transfer rates could be limited by the diffusion of the more volatile components to the interface, from the 'smiles' and pore throats. The potential rate of transfer would then be distributed non-uniformly along the gas-organic liquid interface.

CAPILLARY TRAPPING AND RESIDUAL SATURATION IN AN UNCONSOLIDATED SOIL:

the SEVILLETA SAND

We carried out three-phase flow experiments on an unconsolidated natural soil, the Sevilleta sand, using air, water, and Soltrol for the fluids (see Section 4). The Sevilleta sand was strongly water-wet, and Soltrol was the intermediate wetting fluid. We made quantitative measurements of Soltrol residual (see Section 5), for conditions representing the vadose zone well above the capillary fringe (see Figure 10-1), where water saturation is near its so-called irreducible value. In other experiments we used styrene as the organic phase, which we hardened in place and photographed (see Section 7). Through these two sets of experiments we further examined the film issue and investigated the hypothesis that organic liquid residual saturations are significantly lower in the vadose zone, than they are in the saturated zone. Finally, we measured residual Soltrol saturations for conditions representing the vadose zone just above the capillary fringe.

Quantitative Measurements Of Residual Saturation In Three-phase Soil Columns

Quantitative measurements of residual Soltrol saturation were made in short soil columns, as described in Section 5. Ten trials of the column experiments were successfully completed, representing vadose zone conditions far above the water table. Briefly, in each experiment an initially water saturated soil column was first drained with air under an applied suction to create an initial 'vadose zone' condition.

After the water saturation stabilized, an organic phase was flooded into the column, simulating the infiltration of organic pollutants through the vadose zone. After the fluid saturations had equilibrated, the organic liquid was drained under an applied suction. Once the column re-equilibrated, the residual organic liquid saturation was measured.

We believe that the residual organic liquid saturation left behind in the vadose zone may be a function of saturation history. In our column studies, we chose one simple but realistic saturation history to directly compare residual organic liquids found trapped in the saturated zone to those found in the vadose zone. Owing to the saturation history dependence of residual saturation, the following operational definition for residual saturation in the vadose zone was used:

> *vadose zone residual saturation* — The organic liquid saturation obtained by injecting organic liquid into a water- and air-filled porous medium — in which water is already at its irreducible water saturation — until the fluid saturations stabilize, followed by drainage of the organic liquid with air until the organic liquid becomes immobile and can be reduced no further.

A summary of the quantitative vadose zone results is presented in Table 10-1. In the first step of each experiment, an initially water-saturated column was drained to create unsaturated conditions. The column was drained under sufficient suction to reach the asymptotic portion of the capillary retention curve where the sand was almost completely drained and the water saturation became relatively insensitive to changes in capillary pressure. Water saturations in this region of the retention curve approached the so-called irreducible water saturation, S_{wi} . The water saturation established in this drainage step remained constant throughout the duration of the experiment. The air saturation after this initial drainage step was: 100% – S_{wi} . The average water saturation over the ten experimental trials was 19.8%, thus the average air saturation was 80.2%.

Next, Soltrol was injected into the column simulating the movement of organic liquid percolating through the vadose zone toward the water table. Soltrol displaced only air from the column. Again, because the water saturation was so low (at or near its 'irreducible' saturation), the water was essentially immobile and none was displaced from the column. At the conclusion of this step the Soltrol had reached its maximum saturation (listed in Table 10-1). The maximum organic saturation reached in these vadose zone experiments was significantly lower than the maximum saturation reached in the saturated zone column experiments (66.0% versus 85.1% on average) due to to the presence of a third phase — that is, entrapped air occupied pore space that otherwise would have been occupied by Soltrol in a two-phase or saturated zone system (see Figure 10-6).

The residual or entrapped air saturation at the conclusion of the Soltrol injection was calculated as: 100% – S_o – S_w . The mean residual air saturation over the ten vadose zone experimental trials was 14.2%. Two-phase organic/air and water/air retention curves yield somewhat similar residual air saturations (less than 20%; see Appendix C: Figures C-10, C-12 & C-13 and Table C-1). Since the water saturation was unchanging in the vadose zone experiments, it might be reasonable to think of organic liquid displacing air as being analogous to the final displacement step of the saturated zone experiments where water displaced organic liquid leaving behind a residual saturation — in each case a more wetting fluid displaced a less wetting one and some entrapped non-wetting phase was left behind.

However, the entrapped air saturation in the three-phase experiments was found to be only about one half the residual organic saturation of the saturated zone experiments (14.2% versus 27.1%). Some of the air may have dissolved into the displacing organic phase, but more likely the displacement was more efficient for some reason. Perhaps, due to the very low viscosity of the air phase, the air was less likely to become by-passed. One could think of this phenomena as the effect of an extremely favorable mobility ratio operating on a pore scale. The presence of an intermediate wetting fluid, Soltrol, with a lower interfacial tension to air, could also have played a role (see Table 10-2). However, we saw similar results in all two-phase experiments using air as the non-wetting phase (Appendix C). Perhaps the greater Bond number of the displacement was sufficiently high to permit a greater efficiency. The low density of air leads to a greater density difference (see Table 10-2) and greater gravity forces. However, these forces were acting upward, whereas the displacement in the vadose zone experiment was horizontal (see Figure 5-6). At any rate, it appears that residual air saturations, created under two and three-phase flow conditions were consistently smaller than residual organic liquid saturations created under two-phase flow conditions.

In the final step of the three-phase experiment, organic liquid was drained from the column and replaced by air. Sufficient suction was applied to reduce the organic liquid saturation as low as possible

Trial	Suction * (± 1 cm)	Temperature Range (°C)	Water Saturation (%)	Maximum Organic Liquid Saturation (%)	Residual Organic Liquid Saturation (%)
1	60	4.0	18.1 ± 1.9	62.1 ± 1.6	8.3 ± 0.4
2	68	3.6	19.8 ± 1.9	65.5 ± 1.8	12.0 ± 0.5
3	59	5.0	22.8 ± 2.3	63.9 ± 2.1	9.7 ± 0.6
4	61	4.3	21.6 ± 2.1	78.3 ± 2.2	11.3 ± 0.5
5	66	2.3	18.5 ± 2.1	64.5 ± 1.9	7.7 ± 0.4
6	71	4.3	20.3 ± 2.2	66.2 ± 2.0	7.9 ± 0.5
7	70	2.1	23.2 ± 2.2	56.9 ± 1.8	12.2 ± 0.6
8	69	1.9	18.3 ± 2.4	65.2 ± 2.1	7.1 ± 0.4
9	71	2.6	19.8 ± 3.7	66.1 ± 3.2	9.1 ± 0.7
10	75	2.0	15.8 ± 2.4	71.4 ± 2.2	5.5 ± 0.4
Avg.	–	–	19.8	66.0	9.1
σ_{n-1}	–	–	2.3	5.6	2.2

* cm of water were used during water drainage, cm of Soltrol were used during organic liquid drainage.

TABLE 10-1. Results from the vadose zone column experiments. Soltrol-130 was used as the organic liquid and Sevilleta sand served as the soil.

Zone	fluid pair	density difference (g/cm3)	Interfacial tension (dyne/cm)
Vadose	Soltrol-air	0.75	19.2
Saturated	Soltrol-water	0.25	48.7

TABLE 10-2. Relative density differences and interfacial tensions in the vadose zone an saturated zone.

by purely hydraulic means. **The average measurement of residual organic liquid saturation in the vadose zone was found to be 9.1 ± 2.2% — less than one third of the value measured in the saturated zone (see Table 10-1).**

The Soltrol residual for these three-phase experiments were not significantly different from the minimum organic saturations obtained from air/organic drainage curves (compare with results in Appendix C). These findings are somewhat inconsistent with those of other researchers, who generally use the term 'organic retention'. Eckberg (1983) reported slightly higher organic retentions in two-phase (organic/air) systems than for three-phase (water/organic/air) systems. Convery (1979) reported two-phase retentions to be between 10% and 25% higher, while Hoag and Marley (1986) reported retentions between 20% and 30% higher. However, these researchers measured average saturations over the length of long soil columns, in which the fluid saturations were not uniform. The actual relationship depends on the soil and the fluid-fluid interfacial tensions.

Photomicrographs of Three-phase Pore Casts

Thin section photomicrographs of three-phase pore casts constructed from Sevilleta soil columns are shown in Figures 10-12 to 10-14. These pore casts were constructed following the procedures and techniques described in Section 7. Styrene was the wetting phase in these casts, while epoxies represented the intermediate and non-wetting phases. The styrene was dyed red and appears grey or even black in black-and-white photos. The intermediate phase appears white or light grey, while the non-wetting phase was dyed blue and appears dark grey. Because these fluids were applied and hardened sequentially their distribution within the pore space only simulates three-phase conditions in the vadose zone. The wetting phase simulated water, the intermediate wetting phase simulated the organic liquid, and the non-wetting phase simulated the soil gas. These photomicrographs should be compared to the micromodel results, particularly Figure 10-8. The observed behavior was similar.

Figure 10-12 shows a pore body filled with non-wetting fluid. The intermediate wetting phase forms a thick film between this pore body and the adjacent pore throat, which is filled with the wetting phase.

Reproduced from
best available copy.

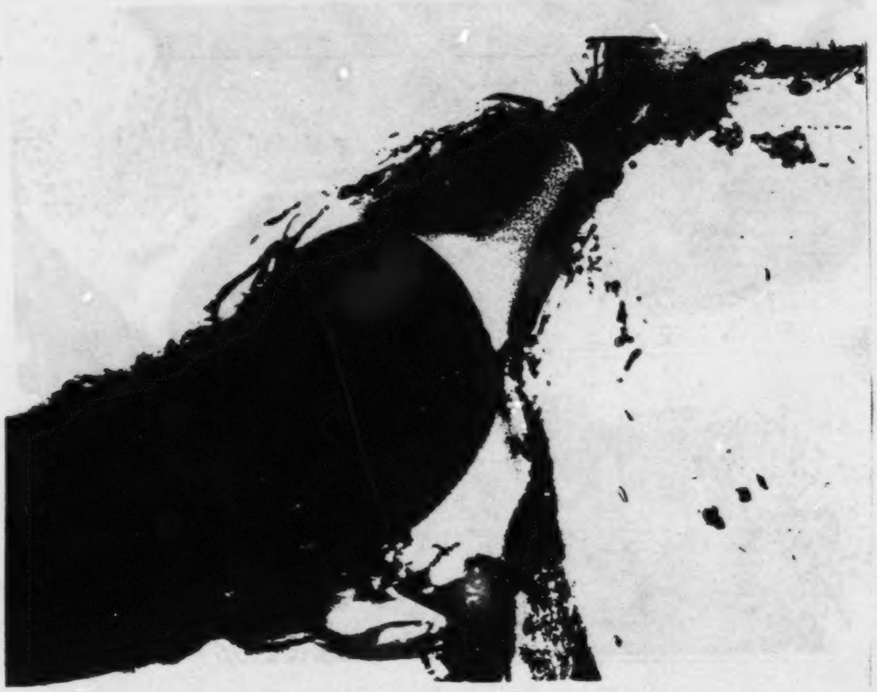

FIGURE 10-12. A photomicrograph of a pore cast thin section from the simulated three-phase system in the Sevilleta sand. The middle of the photo depicts a pore body filled with non-wetting phase (blue or dark grey). Above it is thick 'film' of intermediate wetting phase (white or light grey), that is 'smiling' into a pore throat. The pore throat is otherwise filled with wetting fluid (red or light grey). Shown at 100X magnification.

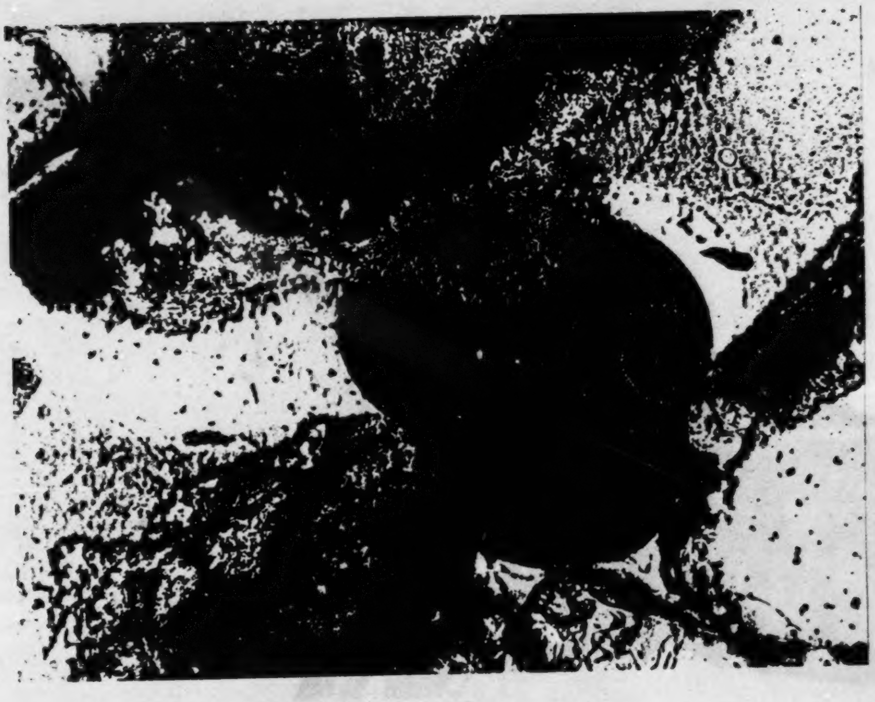

FIGURE 10–13. A photomicrograph of a pore cast thin section from the simulated three-phase system in the Sevilleta sand. The middle of the photo depicts a pore body filled with non-wetting phase (blue or dark grey). It is surrounded by an intermediate wetting film (white or light grey), that is 'smiling' into the pore throat on the right, and filling most of the pore throat to the left. Shown at 100X magnification.

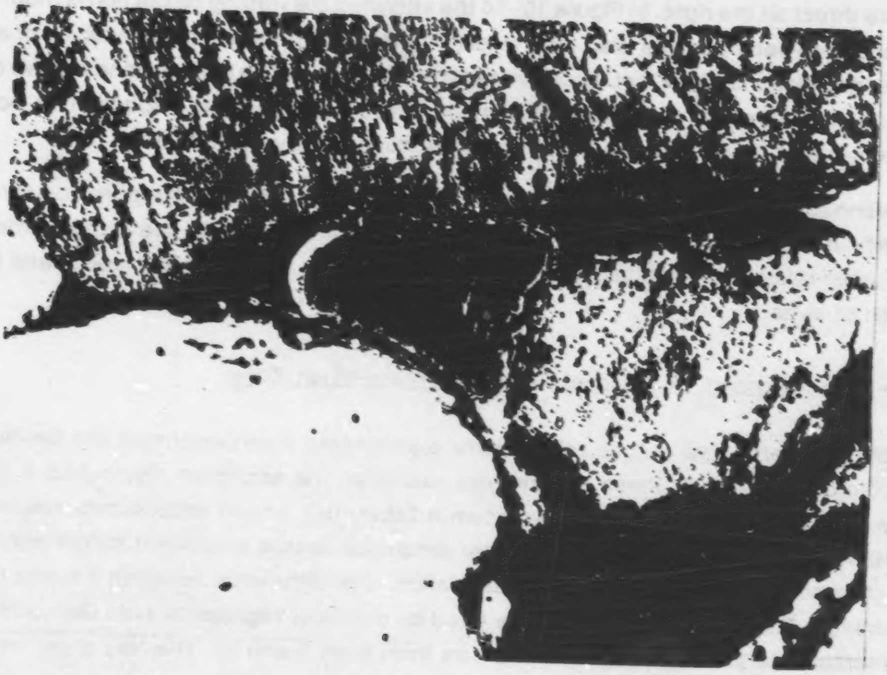

FIGURE 10–14. **A photomicrograph of a pore cast thin section from the simulated three-phase system in the Sevilleta sand. The middle of the photo depicts a small pore body filled with non-wetting phase (blue or dark grey). It is surrounded by an intermediate wetting film (white or light grey), that is 'smiling' into the pore throats on the right, left and below. The pore throats are filled with the wetting fluid (red or black in this photo). Shown at 100X magnification.**

The relative wetting of the phases can be deduced by the interfacial curvatures and the interface contact angles with the surrounding grains. In this location the intermediate wetting phase film is very thick as it 'smiles' into the pore throat. These so-called 'smiles' represent a thick film of intermediate wetting fluid 'coating' a wetting phase pendular ring.

Figure 10-13 shows another pore body filled with non-wetting fluid. The intermediate wetting phase occupies most of the pore throat on the left and forms a thick film between this pore body and the adjacent pore throat on the right. In Figure 10-14 the intermediate wetting phase film is much thinner, as it surround the non-wetting phase filled pore throat. In these two photos the non-wetting phase appears to be isolated and discontinuous, but this impression is misleading. The thin sections are two dimensional sections through a three-dimensional soil sample. Stereo microscopic inspection of pore cast fat sections insured that these non-wetting zones were continuously connected.

The wetting and intermediate wetting films along the grain boundary of the pore body are not visible at the magnification shown in the micrographs. Indeed, they are difficult to see at higher magnifications because of grain roughness, thin section preparation limitations, small film thickness, and the leaching and diffusion of dyes.

Quantitative Measurements Of Residual Saturation In Transition Zone

Six additional quantitative vadose zone column experiments were performed with Sevilleta sand and Soltrol, as the organic liquid. These experiments examined the saturation distribution in the transition zone above the capillary fringe. Results are shown in Table 10-3, and all vadose zone results are plotted in Figure 10-15. The left curve shows the water saturation versus equivalent height above the water table; the right curve shows the total liquid saturation. The difference between the two curves is the Soltrol saturation. The saturation curves were fitted by nonlinear regression (van Genutchten, 1980) to the experimental data points(excluding the results from trials 5 and 6). The 'dry zone' marked on the graph represents conditions far above the vadose zone.

For the Sevilleta soil, the difference between the two curves remains relatively constant, for distances more than 30 cm above the water table. In the transition zone below 30 cm the curves diverge as the organic liquid saturation increases. Unlike the 'dry zone' experiments discussed above, the initial water saturations in these transition zone experiments were higher, and some water was displaced along with air as organic liquid moved through the columns. Particularly for experimental trials intended to simulate conditions beneath 40 cm above the water table, the initial water saturations were quite high and a significant amount of that water was displaced as organic liquid was injected into the columns. In a natural system, this type of displacement is to be expected as organic liquid approaches the water table. If sufficient organic liquid reaches the water table, the water table may be depressed by the weight of the organic phase as it forms a lens on the water (see, eg, right side of Figure 10-1). In time however, as the organic lens spreads laterally, the water table will rebound and water (since it is the most wetting phase) will re-imbibe back into the pore space above the water table displacing some organic liquid. Our experimental technique did not allow the water to re-imbibe into the soil. Under low suctions corresponding to the region in and just above the capillary fringe, this flaw in our experimental technique lead to lower than reasonable final water saturations and higher than reasonable Soltrol saturations. Final

trial	suction * (cm)	Final Fluid Saturations (%)		
		Air	Water	Organic Liquid
1	50	57.1 ± 4.0	32.4 ± 2.5	10.5 ± 2.5
2	48	69.2 ± 2.3	26.2 ± 1.9	4.6 ± 0.4
3	41	50.4 ± 3.0	40.1 ± 1.9	9.5 ± 1.1
4	32	47.5 ± 4.0	31.0 ± 2.2	21.5 ± 1.7
5	22	50.9 ± 4.9	26.6 ± 2.8	22.4 ± 2.2
6	19	4.4 ± 7.8	15.8 ± 3.6	79.8 ± 4.2

* cm of water were used during water drainage, cm of Soltrol were used during organic liquid drainage.

TABLE 10-3. Results from vadose zone column experiments performed to examine the saturation distributions in the transition zone between the saturated zone and the vadose zone. The media was Sevilleta sand and the organic liquid was Soltrol. Results from experimental trials 5 and 6 are suspect for reasons discussed in the text.

'equilibrium' water saturations below 30% were measured from the two trials nearest the capillary fringe (trials 5 and 6). A Soltrol saturation of nearly 80% was measured in trial 6, the experiment conducted with the lowest suction. We believe these results are not indicative of conditions found in natural systems and serve as examples of the limitations of the experimental technique in the low suction range above the capillary fringe.

The largest change in forces acting on the organic liquid occurs in the transition zone above the capillary fringe. Unfortunately, the procedure used in these experiments proved to be inappropriate for measuring fluid saturations in this region. This low suction range is important, particularly for organic liquids lighter than water, because it is the region in which these organic liquids spread laterally, forming a lens on the water table (see Figure 10-1).

Discussion

Our quantitative results support the hypothesis that residual organic liquid saturations are much lower in the vadose zone than in the saturated zone. Vadose zone column experiments using the Sevilleta soil yielded an average value for residual Soltrol saturation (9.1%), approximately one-third as large as the saturated zone residual Soltrol saturation (27.1%). The thin section photomicrographs validate the probable presence of organic liquid films at the gas-water interface, and support our micromodel observation that the distribution of fluids in the vadose zone is more complex than the distribution found in the saturated zone.

As discussed earlier, we believe that the presence of a third and non-wetting phase, air, along with the continuity of the films during drainage and increased buoyancy forces, helps account for the lower

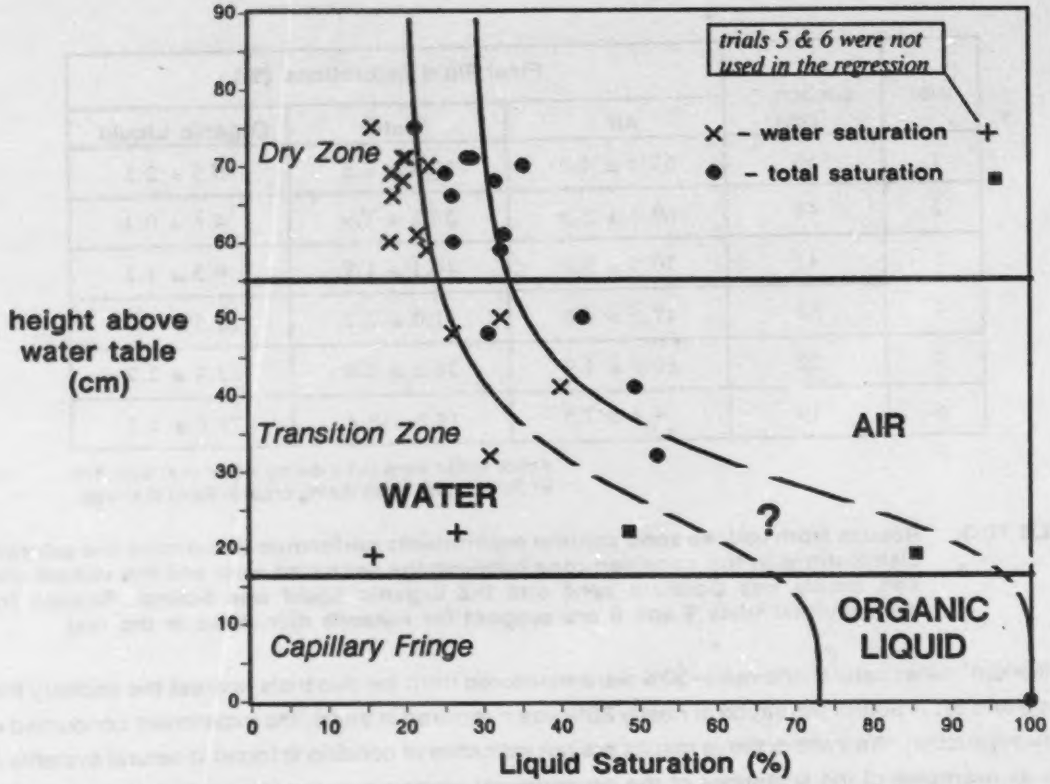

FIGURE 10-15. **Inferred distribution of fluids in the vadose zone for the Sevilleta sand, usin Soltrol-130 as the organic liquid in individual short column experiments. The dr zone data is taken from Table 10-1, while the transition zone data is taken fro Table 10-3. Results from experimental trials 5 and 6 are suspect for reason discussed in the text.**

residual saturation in the vadose zone. Referring back to saturation-force diagram in Figure 10-3, the residual saturation decreases as the ratio, $(F_v + F_b)/F_c$, is increased. Most organic pollutants immiscible with water have a much greater buoyancy force in the vadose zone (larger F_b), due to the large fluid density difference with air. We've also noticed that the interfacial tension between air and organic in the vadose zone is also usually smaller than the tension between the organic liquid and water in the saturated zone (smaller F_c). For example, Soltrol-130, the organic liquid used in the micromodel experiments and column studies, has three times the buoyancy forces and 2.5 times less capillary forces in the vadose zone than in the saturated zone (see Table 10-2). Under equivalent conditions (i.e., same soil and packing), the ratio of forces, $(F_v + F_b)/F_c$, will be a much larger in the vadose zone compared to the saturated zone.

Implications for aquifer contamination –

The capacity for 'storing', retaining or trapping organic liquids is much smaller in the vadose zone than it is in the saturated zone. For organic liquids less dense than water (right side of Figure 10-1) this may be a misleading observation. After all, these 'floaters' can sweep through a large volume of the vadose zone, between the surface and the water table, but can only sweep through that portion of the saturated zone near the water table.

Implications for modeling multi-phase flow –

Models like that of Parker and Lenhard (1987) assume that three-phase capillary pressure/saturation relationships can be approximated by two two-phase relationships. This assumption, first proposed by Leverett in the early 1940's, maintains that water saturations in a three-phase system are a function of the two-phase water/organic retention curve, while the total fluid saturations (water + organic) are functions of the organic/gas curve. Implicitly, this assumption does not allow water/gas interfaces to exist. Indeed, in our flow visualization experiments we see comparatively few water/gas interfaces. So for the majority of common organic pollutants which tend to spread between the air and water phases in the vadose zone, approximation of three-phase capillary pressure/saturation relationships using two two-phase retention curves seems to be an appropriate assumption to invoke. It preserves the physics and surface chemistry of the three-phase flow system in addition to being computationally advantageous.

Implications for phase partitioning –

The rate of mass transfer from the organic liquid phase to the gas phase depends on the interfacial surface area. In reviewing the micromodel results, we hypothesized that this rate of transfer can be limited by diffusion within a multi-component organic liquid. The photomicrographs presented in Figures 10-12 to 10-14 suggest that this film can be very thin. The rate of diffusion would be limited by the film thickness and tortuosity, and the geometry of its connection to larger pockets of organic liquid.

Implications for biotransformation –

Microorganisms tend to adhere to pore walls. There are a number of different environments that organisms might colonize in the vadose zone. Some of these are revealed in the micromodel (Figure 10-8) and pore cast (Figures 10-12 through 10-15) photomicrographs. There are largely air filled pores, with a ready access to oxygen, but with only a very thin double film of water and organic liquid. At residual saturation these films would have a very limited ability to resupply needed nutrients. The environment of water filled pore throats and pendular rings may be controlled by the lack of oxygen. The film of organic liquid should suppress oxygen transfer to the water phase. We speculate that transient changes in fluid saturations would improve the environmental conditions for aerobic bacteria.

Other implications for aquifer remediation – the surfactant effect

Biosurfactants are a by-product of biological activity, especially for organisms that attach at the organic liquid-water interface. We hypothesize that these natural surfactants could change interfacial tensions enough to reduce organic liquid saturations by drainage (see Figure 10-3).

MICROMODEL VISUALIZATION OF CAPILLARY TRAPPING OF A NON-SPREADING ORGANIC LIQUID

On a flat water surface (water-air interface) a non-spreading organic liquid coalesces into a lens, like that depicted in Figure 10-2. We hypothesized that this coalescence would interrupt the tendency of the organic liquid to spread out as a film in the vadose zone, leading to a different behavior than we had observed for Soltrol. To investigate this hypothesis we repeated the vadose zone micromodel experiment using PCE, a non-spreading organic liquid. The results were recorded on videotape (Mason *et al.*, 1989). The photos shown below were taken from that tape, and have a lower than desired resolution. The PCE was not dyed, as the dyes reversed the spreading coefficient. The experiment looks essentially the same in both color and black-and-white. Black-and-white photos are shown here.

The major result of this experiment is shown in Figures 10-16 and 10-17. The left side of Figure 10-16 shows an air-filled pore body. The air extends down into an air-filled pore throat. Above the pore body and to its upper left are PCE-filled pore throats. A PCE 'smile' extents into the pore throat on the right and abuts a pendular ring of water. There is no PCE on the other side of this pendular ring, which directly contacts another air-filled pore body. Direct your attention to the PCE that surrounds the air-filled pore body on the left. The PCE film extends downward along the side of the air pocket, and then stops. Figure 10-17 is a close up of this truncated film. It comes to an abrupt end that could clearly be seen through the stereo microscope, especially under different lighting conditions. Figure 10-18 is a photograph taken from the Soltrol experiments, and reproduced with similar black-and-white shading. The Soltrol film shows no similar tendency to truncate.

In the PCE experiment notice the golf-ball dimples on the air-filled pore body. These 'dimples' do not appear in the Soltrol experiment. They represent small lenses of PCE 'floating' on the air-water interface within the pore (see, eg, Figure 10-2). These lenses would not occur if the PCE completely surrounded the air-filled pore body. Recall the typical eye-shape of micromodel pores displayed in Figure 8-8. The smallest dimension is from the 'floor' to the 'roof' of the pore. We infer that the PCE film truncates somewhere along the floor and roof. Beyond that point the PCE has coalesced into small lenses along the air-water interface. In the Soltrol experiment the stereo microscope revealed that the Soltrol layer completely surrounded the air.

Our hypothesis was correct: a non-spreading fluid has a different behavior in the vadose zone. Although it may fill or 'smile' into some pore throats, and may form or coat pendular rings, it does not spread out as a film. The organic liquid coalesces into lenses and pockets. Large portions of the pore space does not have a layer of organic liquid between the air and the water.

Implications for aquifer contamination -

We have not quantitatively investigated the amount of residual saturation expected for non-spreading organic liquids in vadose zone soils, but we can speculate. Halogenated hydrocarbons such as carbon tetrachloride and PCE are non-spreading. They are also much denser than water (see left side of Figure 10-1). Greater density means a greater (negative) buoyancy force, and a lower residual saturation (see Figure 10-3). The micromodel experiments indicate that non-spreading organic liquids may have a greater tendency to by-pass portions of the pore space , leading to lower residual saturations (consider the lack of PCE in right-hand air-filled pore in Figure 10-16). The experiments also indicated the absence of an interconnecting film, leading to a lower residual saturation. In summary, we hypothesize that non-spreading organic liquids have lower residual saturations in the vadose zone, than do spreading organic liquids. (see Lenhard and Parker, 1987b)

Reproduced from
best available copy.

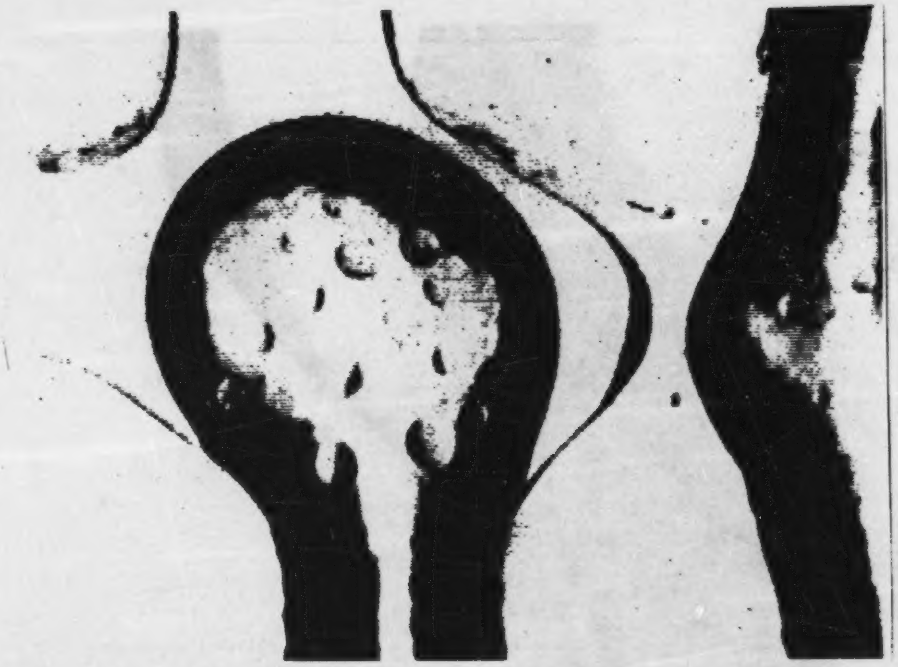

FIGURE 10-16. A photomicrograph of non-spreading PCE in a micromodel.

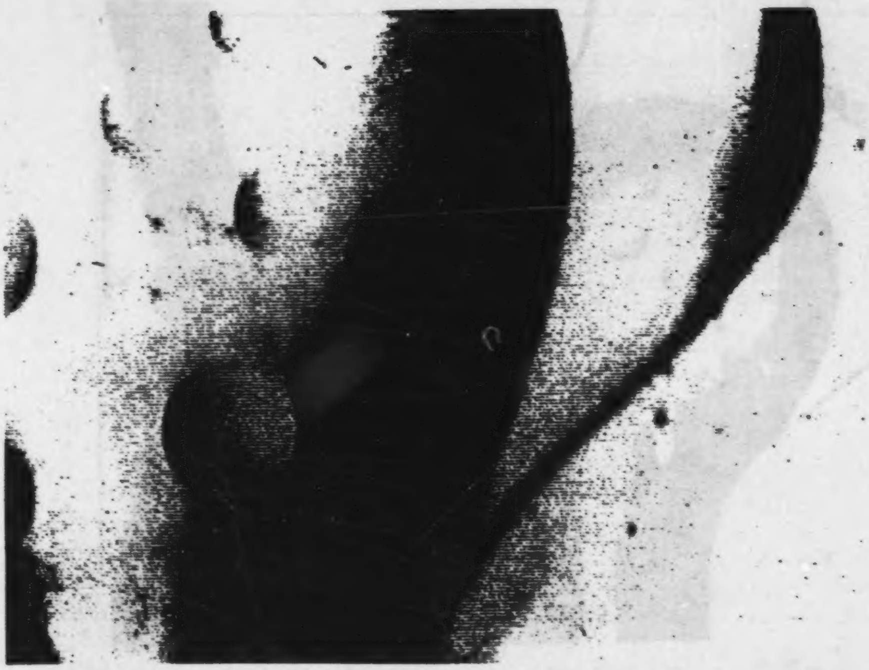

FIGURE 10-17. A photomicrograph of non-spreading PCE in a micromodel. This is a close-up to the photo shown in Figure 10-16.

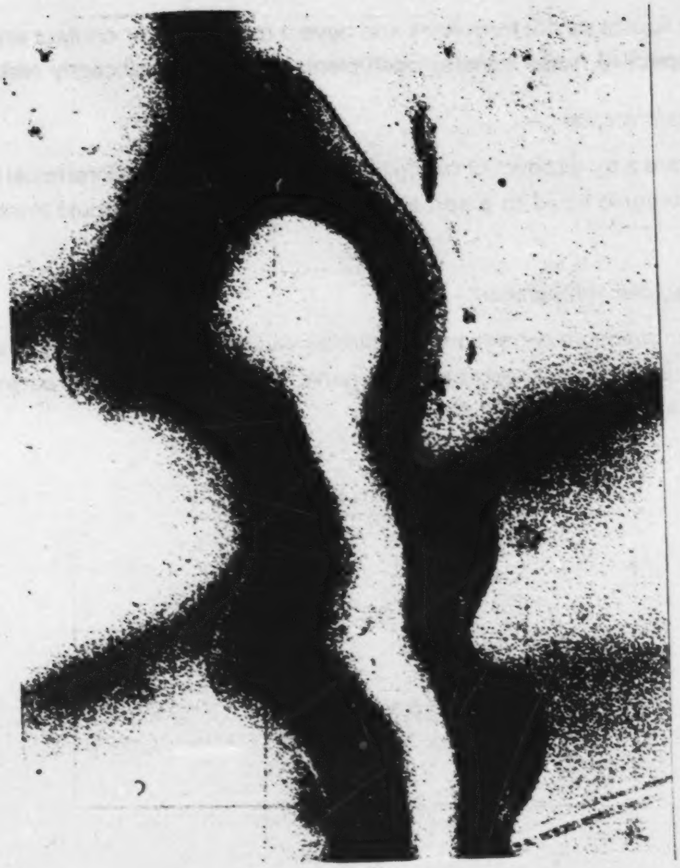

FIGURE 10-18. A photomicrograph of Soltrol in a micromodel. The geometry is similar to that depicted for PCE in Figure 10-16.

Implications for modeling multi-phase flow -

Parker and Lenhard's (1987) model effectively assumes a zero or neutral spreading coefficient (see Lenhard and Parker, 1987b). This somewhat contradicts their other assumption that the organic liquid always forms a layer between the water and air. In any case, it is not clear whether or not this model can handle the significantly different physics associated with a non-spreading organic liquid.

Implications for phase partitioning -

Coalescing organic liquids do not form films and have a much smaller contact area with the gas and water phases. The respective mass transfer coefficients must be significantly reduced.

Implications for biotransformation -

Biosurfactants that are a by-product of biological activity could change interfacial tensions enough to alter a non-spreading organic liquid to a spreading organic liquid. This should improve mass transfer coefficients.

Other implications for aquifer remediation -

Induced volatilization, vacuum extraction, and similar vadose zone remediation schemes may be a much less effective strategy for non-spreading organic liquids, than for spreading organic liquids, because of reduced mass transfer coefficients.

REFERENCES

Ababou, R., L. W. Gelhar, and D. McLaughlin. 1988. Three-dimensional flow in random porous media. Ralph M. Parsons Laboratory, Tech. Rpt. 318, Massachusetts Institute of Technology Department of Civil Engineering. 833pp.

Abriola, L. M., and G. F. Pinder. 1985a. A multiphase approach to the modeling of porous media contaminated by organic compounds 1. Equation development. Water Resources Research, vol.21, no.1, pp.11-8.

Abriola, L. M. , and G. F. Pinder. 1985b. A multiphase approach to the modeling of porous media contaminated by organic compounds 2. Numerical Simulation. Water Resources Research, vol.21, no.1, pp.19-26.

Adamson, A. W. 1982. *Physical Chemistry of Surfaces*, 4th edition. Wiley, New York.

Albertson, M., G. Baldauf, F. Birk, Th. Dracos, A. Golwer, H. Horauf, W. Kab, P. Muntzer, G. Ruddig4er, H.O. Schiegg, F. Schweisfurth, F. Schwille, H. Tangermann, H.G. Van Waegeningh, P. Werner, L. Zilliox, and L. Zwitting. 1986. *Evaluation and treatment of cases of oil damage with regard to groundwater protection*, part 1, Scientific fundamental principles for understanding the behavior of oil in the ground. LTwS-Nr. 20, Federal Office of the Environment, West Germay, english translation available from Batelle Pacific Northwest Laboratory.

Amaufule J. O., and L. L. Handy. 1982. The effect of interfacial tensions on relative oil/water permeabilities of consolidated porous media. SPE Journal, vol.22, no.3, pp.371-381.

ASTM. 1986. *Annual Book of ASTM Standards*. American Society for Testing and Materials, Philadelphia, PA.

Amott, E. 1959. Observations relating to the wettability of porous rock. AIME Transactions, vol.216, pp.156-62.

Amoozegar, A., A.W. Warrick, and W.H. Fuller. 1986. Movement of selected organic liquids into dry soils. Hazardous Waste & Hazardous Materials, vol.3, no.1, pp.29-41.

Anderson, W. G. 1986a. Wettability literature survey — part 1: rock-oil-brine interactions and the effects of core handling on wettability. Journal of Petroleum Technology, vol.38, no.10, pp.1125-49.

Anderson, W. G. 1986b. Wettability literature survey — part 2: wettability measurement. Journal of Petroleum Technology, vol. 38, no.11, pp.1246-62.

Anderson, W. G. 1987a. Wettability literature survey — part 4: the effects of wettability on capillary pressure. Journal of Petroleum Technology, vol. 39, no.10, pp.1283-1300.

Anderson, W. G. 1987b. Wettability literature survey — part 5: the effects of wettability on relative permeability. Journal of Petroleum Technology, vol. 39, no.11, pp.1453-68.

Anderson, W. G. 1988. Wettability literature survey — part 6: the effects of wettability on water flooding. Journal of Petroleum Technology, vol. 39, no.12, pp.1605–22.

Araktingi, U.G., D.C.Brock, and F.M.Orr. 1988. Viscous fingering in heterogeneous porous media. presented at Fall 1888 Amer. Geophys. Union Meeting. Abstract in *EOS*, Transactions, American Geophysical Union, vol.69, no.44, pp.1204-5.

Baehr, A. L. 1987. Selective transport of hydrocarbons in the unsaturated zone due too aqueous and vapor phase partitioning. Water Resources Research, vol.23, no.10, pp.1926-1938.

Baehr, A. L., and M. Y. Corapcioglu. 1984. A predictive model for pollution from gasoline in soils and ground water. in proceedings of *Petroleum Hydrocarbons and Organic Chemicals in Ground Water*, NWWA, Houston, TX, pp.144-56.

Baehr, A. L., and M. Y. Corapcioglu. 1987. A compositional multiphase model for groundwater contamination by petroleum products 2. numerical solution. Water Resources Research, vol.23, no.1, pp.201-13.

Bitton, G. and K. C. Marsell. (eds.) 1979. *Adsorption of microorganisms to surfaces*, Wiley, New York.

Bobek, J. E., C. C. Mattax, and M. O. Denekas. 1958. Reservoir rock wettability — its significance and evaluation. Trans. AIME, vol.213, pp.155-60.

Bouchard, D.C., R.M. Powell and D.A. Clark. 1987. Alkylammonium cation effects on aquifer material sorptivity, Agronomy Abstracts, vol.79, no.166.

Bowman, R.S., M.E.Essington, and G.A.O'Conner. 1981. Soil sorption of nickel: influence of solution composition. SSSAJ, v.45, no.5, pp.680-5.

Boyd, S.A., M.M. Mortland and C.T. Chiou. 1987. Organo–clays as sorbents for organic contaminants, Agronomy Abstracts, vol.79, no.166.

Boyer, R. F., ed. 1970. Styrene Polymer, in *Encyclopedia of Polymer Science and Technology*, Bikales, N. M., ed., vol.13, Interscience Publishers, New York, pp.128-447.

Brown, C. E., and E. L. Neustadter. 1980. The wettability of oil/water/silica systems with reference to oil recovery. Journal of Canadian Petroleum Technology, vol.19, no.3, pp.100-10.

Burmaster, D. E., and R. H. Harris. 1982. Groundwater contamination: an emerging threat. Technology Revue, vol.84, no.7, pp.50-62.

Burris, D. R., and W. A. MacIntyre. 1986. Solution of hydrocarbons in a hydrocarbon-water system with changing phase compositon due to evaporation. Environmental Science and Technology, vol.20, no.3, pp.296-299.

Callahan, M. A., and others. 1979. *Water- Related Fate of 129 Priority Pollutants* (2 volumes). EPA Office of Water Planning and Standards (WH-553), Washington, D.C., EPA-440/4-79-029(a and b).

Carman, P. C. 1937. Fluid flow through granular beds. Transactions: Institute of Chemical Engineers (London), vol.15, pp.150-66.

Cary, J. W., J. F. McBride, and C. S. Simmons. 1989. Observation of water and oil infiltration into soil: some simulation challenges. Water Resources Research, vol.25, no.1, pp.73-80.

Chaffee, W. T., and R. A. Weimar. 1983. Remedial programs for ground-water supplies contaminated by gasoline. in proceedings of Third National Symposium on *Aquifer Restoration and Ground-Water Monitoring*, National Water Well Association, pp.39-46.

Chatzis, I. 1982. Photofabrication technique of two1-dimensional glass micromodels. PRRC report no. 82-12, New Mexico Institute of Mining and Technology, Socorro, NM.

Chatzis, I., and N. R. Morrow. 1981. Correlation of capillary number relationships for sandstones. paper SPE 10114, presented at 1981 SPE Annual Technical Conference and Exhibition, San Antonio, TX.

Chatzis, I., and N. R. Morrow. 1984. Correlation of capillary number relationships for sandstone. SPE Journal, vol.24, no.5, pp.355-562.

Chatzis, I., and F. A. L. Dullien. 1983. Dynamic immiscible displacement mechanisms in pore doublets: theory versus experiment. Journal of Colloid and Interface Science, vol.91, no.1, pp.199-222.

Chatzis, I., N. R. Morrow, and H. T. Lim. 1983. Magnitude and detailed structure of residual oil saturation. SPE Journal, vol.23, no.2, pp.311-25.

Chatzis, I., M. S. Kuntamukkula, and N. R. Morrow. 1984. Blob-size distribution as a function of capillary number in sandstones. paper SPE 13213, presented at 1984 SPE Annual Technical Conference and Exhibition, Houston, TX.

Chatzis, I., M. S. Kuntamukkula, and N. R. Morrow. 1988. Effect of capillary number on the microstructure of residual oil in strongly water-wet sandstones. SPE Reservoir Engineering, vol.3, no.3, pp.902-912.

Chilingar, G. V., and T. F. Yen. 1983. Some notes of wettability and relative permeability of carbonate reservoir rocks. Energy Sources, vol.7, no.1, pp.67-75.

Chiou, C.T., V.H.Freed, D.W. Schmedding and R. L. Kohnert. 1977. Partition coefficient and bioaccumulation of selected organic chemicals. Environmental Science and Technology, vol.11, no.5, pp.475-8.

Conrad, S. H., J. L. Wilson, W. R. Mason, and W. Peplinski. 1989. Observing the transport and fate of petroleum hydrocarbons in soils and in ground water using flow visualization techniques, in Proceedings, Symposium on *Environmental Concerns in the Petroleum Industry*, American Association of Petroleum Engineers, Palm Springs, CA, May 10, 1989.

Convery, M. P. 1979. The Behavior and Movement of Petroleum Products in Unconsolidated Surficial Deposits. M.S. Thesis, University of Minnesota.

Corapcioglu, M. Y., and A. L. Baehr. 1987. A compositional multiphase model for groundwater contamination by petroleum products 1. theoretical considerations. Water Resources Research, vol.23, no.1, pp.191-200.

Craig, F. F. 1971. *Reservoir Engineering Aspects of Waterflooding.* SPE Monograph Series, no.3, Dallas, TX.

Dagan, G. 1985. Stochastic modeling of groundwater flow by unconditional and conditional probabilities: the inverse problem. Water Resources Research, vol.21, no.1, pp.65-72.

Dagan, G. 1986. Statistical theory of groundwater flow and transport: pore to laboratory, laboratory to formation, and formation to regional scale. Water Resources Research, vol.22, no.9, pp.120S-34S.

Davis, J. A., and S. C. Jones. 1968. Displacement mechanisms of miscellar solutions. Jour. Pet. Tech., Dec. 1968, pp.1415-28.

Dean, J. A. (ed.). 1979. *Lange's Handbook of Chemistry* (12th edition). McGraw-Hill, New York.

Denekas, M. O., C. C. Mattax, and G. T. Davis. 1959. Effect of crude oil components on rock wettability. Journal of Petroleum Technology, Nov., pp.330-3.

de Pastrovich, T.L., Y.Baradat, R.Barthel, A. Chiarelli, and D.R. Fussell. 1979. *Protection of Groundwater from Oil Pollution.* Report 3/79, CONCAWE, Den Haag, the Netherlands.

Donahue, D. J., and F. E. Bartell. 1952. The boundary tension at water — organic liquid interfaces. Journal of Physical Chemistry, vol.56, p.480.

Donaldson, E. C., R. D. Thomas, and P. B. Lorenz. 1969. Wettability determination and its effects on recovery efficiency. SPE Journal, vol.9, no.1, pp.13-20.

Dreisbach, R. R. 1955-1961. *Properties of Chemical Compounds* (3 volumes). American Chemical Society, Washington, D.C.

Dullien, F. A. L., F. S. Y. Lai, and I. F. MacDonald. 1986. Hydraulic continuity of residual wetting phase in porous media. J. Coll. Sci., vol.109, no.1, pp.201-18.

Eames, V. 1981. Influence of Water Saturation on Oil Retention Under Field and Laboratory Conditions. University of Minnesota M.S. Thesis.

Eastman Kodak Company. 1975. Decorating Glass Using Kodak Photosensitive Resists. Kodak Publication No. P-245, 4 pp.

Eastman Kodak Company. 1979. Photofabrication Methods with Kodak Photoresists. Kodak Publication No. G-184, 32 pp.

Eckberg, D. K., and D. K. Sunada. 1984. Nonsteady three-phase immiscible fluid distribution in porous media. Water Resources Research, vol.20, no.12, pp.1891-7.

EPA. 1979. Waste alert. EPA Journal, vol.5, no.2, p.12.

EPA. 1980. Proposed Groundwater Protection Strategy. Office of Drinking Water, Washington, D.C.

EPA. 1982. Massive voluntary cleanup to help with hazardous waste removal. EPA Journal, vol.9, no.5, pp.24-5.

EPA. 1983. Hazardous Waste Site Descriptions: National Priority List — Final Rule. Office of Solid Waste and Emergency Response (WH-5624), Washington, D.C., HW-8.1.

Epstein, S. S., L. O. Brown, and C. Pope. 1982. *Hazardous Waste in America*. Sierra Club Books, San Francisco, CA, 593pp.

Ewing, R. E., T. F. Russel, and L. C. Young. 1989. An anisotropic coarse-grid dispersion model of heterogeneity and viscous fingering in five-spot miscible displacement that matches experiments and fine-grid models, in proceeedings of Tenth Annual SPE Symposium on Reservoir Simulation, February 6-8, Houston, TX, pp.447-465.

Faust, C. R. 1985. Transport of immiscible fluids within and below the unsaturated zone: a numerical model. Water Resources Research, vol.21, no.4, pp.587-596.

Feenstra, S., and J. Coburn. 1986. Subsurface contamination from spills of denser than water chlorinated solvents. Bull. Calif. Water Poll. Control Assoc. vol.23, no.4, pp.26-34.

Felsenthal, M. 1979. A statistical study of core waterflood parameters. Journal of Petroleum Technology, vol.31, no.10, pp.1303-4.

Ferrand, L. A., P. C. D. Milly, and G. F. Pinder. 1986. Dual-gamma attenuation for the determination of porous medium saturation with respect to three fluids. Water Resources Research, vol.22, no.12, pp.1657-1663.

Fowkes, F. M. 1967. Attractive forces at solid-liquid interfaces, in *Wetting*. Society of Chemical Industry, London, pp.3-31.

Gaudin, A.M., A.F. Witt, and T.G. Decker. 1963. Contact angle hysteresis — principles and application of measurement methods. Trans. AIME, vol.226, pp.107-12.

Gelhar, L. W. 1986. Stochastic subsurface hydrology from theory to applications. Water Resources Research, vol.22, no.9, pp.135S-145S.

Girifalco, L. A., and R. J. Good. 1957. A theory for the estimation of surface and interfacial energies, I: derivation and application to interfacial tension. Journal of Physical Chemistry, vol.61, p.904.

Gvirtzman, H., M. Magaritz, E. Klein, and A. Nader. 1987. A scanning electron microscopy study of water in soil. Transport In Porous Media, no.2, pp.83-93.

Hillel, D. 1980. *Fundamentals of Soil Physics*. Academic Press, New York, NY, 413p.

Hornof, V. and N. R. Morrow. 1988. Flow Visualiztion of the effects of interfacial tension on displacement, SPE Reservoir Engineering, vol.3, no.1, pp.251-56.

Jercinovic, D. E. 1984. Petroleum-Product Contamination of Soil and Water in New Mexico. Ground Water/Hazardous Waste Bureau, New Mexico Environmental Improvement Division, EID/GWH-84/4.

Jones, S.C. and W.O.Roszelle. 1978. Graphical techniques for determining relative permeability from displacement experiments. Journal of Petroleum Technology, May, pp.807-17.

Kia, S.F. 1988. Modeling of the retention of organic contaminants in porous media of uniform spherical partricles. Water Research, vol.22, no.10, pp.1301-9.

Kobayashi, H., and B. E. Rittmann. 1982. Microbial removal of hazardous organic compounds. Environmental Science and Technology, vol.16, no.3, pp.170A-183A.

Kuppusamy, T., J. Sheng, J. C. Parker, and R. J. Lenhard. 1987. Finite element analysis of multiphase immiscible flow through soils. Water Resources Research, vol.23, pp.625-31.

Kyte, J. R., R. J. Stanclift Jr., S. C. Stephan Jr., and L. A. Rapoport. 1956. Mechanism of water flooding in the presence of free gas. Trans. AIME, vol.207, pp.215-21.

Lake, L. W., and H. B. Carroll, Jr. - eds. 1986. *Reservoir Characterization*. Harcourt Brace Jovanovich, Publishers, Orlando, FL., 659pp.

Lam, K. 1979. Three-phase gravity drainage. unpublished report, Petroleum Recovery Research Center, New Mexico Tech, Socorro, NM.

Lenhard, R. J., and J. C. Parker. 1987a. A model for hysteretic constitutive relations governing multiphase flow, 2. permeability - saturation relations. Water Resources Research, vol.23, pp.2197-96.

Lenhard, R. J., and J. C. Parker. 1987b. Measurement and prediction of saturation - pressure relationships in three phase porous media systems. Journal of Contaminant Hydrology, vol.1, pp.407-24.

Lenhard, R. J., and J. C. Parker. 1988a. Experimental validation of the theory for extending two phase saturation-pressure relations to three phase systems for onotonic drainage paths. Water Resources Research, vol.24, pp.373-80.

Lenhard, R. J., and J. C. Parker. 1988b. Estimation of oil volumes in soils from observed fluid levels in monitoring wells. presented at Fall 1888 Amer. Geophys. Union Meeting. Abstract in *EOS*, Transactions, American Geophysical Union, vol.69, no.44, pp.1212-1213.

Lenhard, R. J., and J. C. Parker. 1989. A model for hysteretic constitutive relations governing multiphase flow, 3. refinements and numerical simulations. Water Resources Research, vol.25, pp.1727-36.

Lenhard, R. J., J. H. Dane, and J. C. Parker. 1988. Measurement and simulation of one-dimensional transient three-phase flow for monotonic liquid drainage. Water Resources Research, vol.24, pp.853-63.

Lyman, W. J., W. F. Reehl, and D. H. Rosenblatt (eds.). 1982. *Handbook of Chemical Property Estimation Methods*. McGraw-Hill, New York.

Mantoglou, A., and L. W. Gelhar. 1987. Stochastic modeling of large-scale transient unsaturated flow in stratified soils. Water Resources Research, vol.23, no.1, pp.57-68.

Marsell, K.C. (ed.) 1985. *Microbial adhesion and aggregation*, Springer–Verlag, KG, Berlin.

Mason, W. R., S. H. Conrad, and J. L. Wilson. 1988. Micromodel study of organic liquid advance into a soil. presented at Spring 1988 Amer. Geophys. Union Meeting. Abstract in *EOS*,Transactions, American Geophysical Union, vol.69, no.16, pp.370.

Mason, W.M., W. Peplinski, J.L. Wilson and S.H. Conrad. 1989. Pore level flow visualizaion of three phase fluid flow. presented at Spring 1989 Amer. Geophys. Union Meeting, Abstract in EOS,Transactions, American Geophysical Union vol. 70.

Mattax, C. C., and J. R. Kyte. 1961. Ever see a water flood? Oil and Gas Jour., Oct.16, 1961, pp.115-128.

Mattson, E. D., A. M. Parsons, D. B. Stephens, K. Black, and K. Flanigan. 1988. Field simulation of waste impoundment seepage in the vadose zone, in proceedings of *FOCUS on Southwestern Ground Water Issues Conference*, March 23-25, National Water Well Association, Dublin, OH.

Maugh II, T. H. 1979. Toxic waste disposal a growing problem. Science, vol.204, pp.819-23.

McCarty, P.L., M. Reinhard, and B. E. Rittmann. 1981. Trace organics in groundwater. Environmental Science and Technology, vol.15, no.1, pp.40-51.

McCord, J. T., D. B. Stephens, J. L. Wilson. 1988a. Field-scale variably saturated flow and transport in a sloping uniform porous media: field experiments and numerical simulations, in proceedings of International Workshop on *Validation of Flow and Transport Models for the Unsaturated Zone*. May 23-26, Ruidoso, NM, New Mexico State University.

McCord, J. T., D. B. Stephens, and J. L. Wilson. 1988b. Field-scale variably saturated flow and transport: the roles of hysteresis and state-dependent anisotropy, in proceedings of NATO Advanced Study Institute on *Recent Advances in Modeling Hydrologic Systems*, July 9-22, Sintra, Portugal.

McKee, J. E., F. B. Laverty, and R. H. Hertel. 1972. Gasoline in groundwater. Journal of the Water Pollution Control Federation, vol.44, no.2, pp.293-302.

McKellar, M., and N. C. Wardlaw. 1988. A Method of Viewing "Water" and "Oil" Distribution in Native-State and Restored-State Reservoir Core. AAPG Bulletin, V. 72, No. 6, pp. 765-771.

Melrose, J. C., and C. F. Brandner. 1974. Role of capillary forces in determining microscopic displacement efficiency for oil recovery by waterflooding. Journal of Canadian Petroleum Technology, vol.13, no.4, pp.54-62.

Mohanty, K. K., H. T. Davis, and L. E. Scriven. 1980. Physics of oil entrapment in water-wet rock. paper SPE 9406, presented at 1980 SPE Annual Technical Conference and Exhibition, Dallas, TX.

Moissis, D. E., C. A. Miller, and M. F. Wheeler. 1989. Simulation of miscible viscous fingering using a modified method of characteristics: effects of gravity and heterogeneity, in proceedings of Tenth Annual SPE Symposium on Reservoir Simulation, February 6-8, Houston, TX, pp.431-446.

Moore, T. F., and R. L. Slobod. 1956. The effect of viscosity and capillarity on the displacement of oil by water. Producers Monthly, vol.20, pp.20-30.

Morrow, N.R. 1970. Physics and thermodynamics of capillary action in porous media. Industrial Engineering Chem., vol.62, no.6, pp.32-56.

Morrow, N. R. 1979. Interplay of capillary, viscous and buoyancy forces in the mobilization of residual oil. Journal of Canadian Petroleum Geology, vol.18, no.3, pp.35-46.

Morrow, N. R. 1984. Measurement and Correlation of Conditions for Entrapment and Mobilization of Residual Oil. Report NMERDI 2-70-3304, New Mexico Energy Research and Development Institute, Santa Fe, NM.

Morrow, N. R., P. J. Cram, and F. G. McCaffery. 1973. Displacement studies in dolomite with wettability control by octanoic acid. SPE Journal, vol.13, pp.221-32.

Morrow, N. R., and B. Songkran. 1981. Effect of trapping and buoyancy forces on non-wetting phase trapping in porous media. in *Surface Phenomena in Enhanced Oil Recovery*, D.O.Shah (ed.), Plenum Publishing Corporation.

Morrow, N. R., and I. Chatzis. 1982. Measurement and Correlation of Conditions for Entrapment and Mobilization of Residual Oil. Report DOE/BC/10310-20, Department of Energy.

Morrow, N. R., H. T. Lim, and J. S. Ward. 1986. Effect of crude-oil-induced wettability changes on oil recovery. SPE Formation Evaluation, vol.1, no.1, pp.89-103.

Morrow, N. R., I. Chatzis, and J. J. Taber. 1988. Entrapment and mobilization of residual oil in bead packs. SPE Reservoir Engineering, vol.3, no.3, pp.927-934.

Mortland, M.M., S. Shaobaio and S.A. Boyd. 1986. Clay-organic complexes as adsorbents for phenol and chlorophenols, Clays & Clay Minerals, vol.34, no.5, 581-5.

Ng, K. M., H. T. Davis, and L. E. Scriven. 1978. Visualization of blob mechanics in flow through porous media. Chemical Engineering Science, vol.33, pp.1009-17.

Parker, J. C., R. J. Lenhard and T. Kuppusamy. 1987. A parametric model for constitutive properties governing multiphase flow in porous media. Water Resources Research, vol.23, pp.618-24.

Parker, J. C., and R. J. Lenhard. 1987. A model for hysteretic constitutive relations governing multiphase flow, 1. saturation - pressure relations. Water Resources Research, vol.23, no.12, pp.2187-96.

Pathak, P., H. T. Davis, and L. E. Scriven. 1982. Dependence of residual non-wetting liquid on pore topology. paper SPE 11016, presented at 1982 SPE Annual Technical Conference and Exhibition, New Orleans.

Pfannkuch, H. O. 1984. Determination of the contaminant source strength from mass exchange processes at the petroleum-ground-water interface in shallow aquifer systems. in proceedings of *Fourth National Symposium on Aquifer Restoration and Groundwater Monitoring*, NWWA, Columbus, OH.

Pinder, G. F., and L. M. Abriola. 1986. On the simulation of nonaqueous phase compounds in the subsurface. Water Resources Research, vol.22, no.9, pp.109s-19s.

Powers, S.E., Y. M. Chen, L. M. Abriola, and W. J. Weber. 1988. The significance of non-equilibrium effects on interphase partitioning of organic contaminants in multiphase systems [abst.]. Eos, Transactions, American Geophysical Union, vol.69, no.44, p.1201.

Pringle, J.H. and M. Fletcher. 1983. Influence of substratum wettability on attachment of freshwater baceria to soil surfaces, Applied Environmental Microbiology, vol.45, no.3, 811-7.

Roberts, J. R., J. A. Cherry, and F. W. Schwartz. 1982. A case study of a chemical spill: polychlorinated biphenyls (PCBs) 1. history, distribution, and surface translocation. Water Resources Research, vol.18, no.3, pp.523-34.

Roberts, P. V., M. Reinhard, and A. J. Valocchi. 1982. Movement of organic contaminants in groundwater: implications for water supply. Journal of the American Water Works Association, vol.74, pp.408-13.

Salathiel, R. A. 1973. Oil recovery by surface film drainage in mixed-wettability rocks. Journal of Petroleum Technology, vol.25, pp.1216-24.

Schiegg, H.O. 1980. Fundamentals, setups, and results of laboratory experiments on oil propagation in aquifers. VAX-Mitteilung no. 43, Versuchsanstalt für Wasserbau, Hydrologie und Glaziologie, ZTH, Zurich, english translation available from Batelle Pacific Northwest Laboratory.

Schiegg, H.O. and J.F. McBride. 1987. Laboratory setup to study two-dimensional multiphase flow in porous media. in proceedings of *Petroleum Hydrocarbons and Organic Chemicals in Ground Water*, NWWA, Houston, TX, pp. 371-95.

Schwille, F. 1967. Petroleum contamination of the subsoil — a hydrological problem. in *The Joint Problems of the Oil and Water Industries* (P.Hepple — ed.), Elsevier, Amsterdam, pp.23-53.

Schwille, F. 1981. Groundwater pollution in porous media by fluids immiscible with water. in *Quality of Groundwater* (W. van Duijvenbooden et al. — eds.), Elsevier, Amsterdam, pp.451-63.

Schwille, F. 1984. Migration of organic fluids immiscible with water in the unsaturated zone. in *Pollutants in Porous Media: The Unsaturated Zone Between Soil Surface and Groundwater* (B. Yaron, G. Dagan, and T. Goldschmid — eds.), Springer-Verlag, New York, pp.27-48.

Schwille, F. 1988. *Dense Chlorinated Solvents in Porous and Fractured Media*. Lewis Publishers, Chelsea, MI. 146pp.

Sharma, M. M., and R. W. Wunderlich. 1985. The alteration of rock properties due to interactions with drilling fluid components. paper SPE 14302 presented at 1985 SPE Annual Technical Conference and Exhibition, Las Vegas.

Soll,W.E. and M.A.Celia. 1988. A pore-scale model of three-phase immiscible fluid flow. presented at Fall 1988 Amer. Geophys. Union Meeting. Abstract in *EOS*,Transactions, American Geophysical Union, vol.69, no.44, pp.1189-90.

Stephens, D. B., and S. Heermann. 1988. Dependence of anisotropy on saturation in a stratified sand. Water Resources Research, vol.24, no.5, pp.770-778.

Taber, J. J. 1969. Dynamic and static forces required to remove a discontinuous oil phase from porous media containing both oil and water. SPE Journal, vol.2, pp.3-12.

Taber, J. J. 1981. Research on enhanced oil recovery: past, present, and future. in *Surface Phenomena in Enhanced Oil Recovery* (D.O.Shah ed.), Plenum, New York, pp.13-52.

Treiber, L. E., D. L. Archer, and W. W. Owens. 1972. A laboratory evaluation of the wettability of fifty oil producing reservoirs. SPE Journal, vol.12, pp.531-40.

Tuck, D.M., P.R. Jaffe, D.A. Crerar, and R.T. Mueller. 1988. Enhancing recovery of immobile residual non-wetting hydrocarbons form the unsaturated zone using surfactant solutions. in proceedings of *Petroleum Hydrocarbons and Organic Chemicals in Ground Water*, NWWA, Houston, TX, pp.457-78.

van Dam, J. 1967. The migration of hydrocarbons in water-bearing stratum. in: *The Joint Problems of the Oil and Water Industries* (P.Hepple — ed.), Elsevier, Amsterdam, pp.55-88.

van Genuchten, M. Th. 1980. A closed-form equation for predicting the hydraulic conductivity of unsaturated soils. Soil Sci. Soc. Amer. J., vol.44, pp. 892-8.

van Loosdrecht, M.C.M., J. Lyklema, W. Norde, G. Schraa, and A.J.B. Zehnder. 1987a. The role of bacterial cell wall hydrophobicity in adhesion, Applied Environmental Microbiology, vol.53, no.8,pp.1893-7.

van Loosdrecht, M.C.M., J. Lyklema, W. Norde, G. Schraa, and A.J.B. Zehnder. 1987a. Electrophoretic mobility and hydrophobicity as a measure to predict the initial steps of bacterial adhesion, Applied Environmental Microbiology, vol.53, no.8,pp.1898-901.

Villaume, J. F. 1985. Investigations at sites contaminated with dense non-aqueous phase liquids. Groundwater Monitoring Review, vol.5, no.2, pp.60-74.

Vomocil, J. A. 1965. Porosity. in *Methods of Soil Analysis*, Part 1, C. A. Black (Ed.), American Society of Agronomy, Madison, WI, pp.299-314.

Wardlaw, N. C. 1982. The effect of geometry, wettability, viscosity, and interfacial tension on trapping in single pore-throat pairs. Journal of Canadian Petroleum Technology, vol.21, no.3, pp.21-7.

Wardlaw, N. C., and R. P. Taylor. 1976. Mercury capillary pressure curves and the interpretation of pore structure and capillary behavior in reservoir rocks. Bulletin of Canadian Petroleum Geology, vol.24, no.2, pp.225-262.

Weast, R. C. (ed.). 1981. *Handbook of Chemistry and Physics*. CRC Press, Boca Raton, Fla.

Welty, C. 1989. Stochastic analysis of viscosity and density variability on macrodispersion in heterogeneous porous media. Ph. D. thesis, Dept. of Civil Engr., Mass. Inst. of Tech., Cambridge, Ma.

Welty, C. and L.W. Gelhar, 1987. Stochastic analysis of the effects of viscosity variability on macrodispersion in heterogeneous porous media. presented at Fall 1987 Amer. Geophys. Union Meeting. Abstract in *EOS*,Transactions, American Geophysical Union, vol.68, no.44, pp.1189-90.

Welty, C. and L.W. Gelhar, 1989. Stochastic analysis of the effects of density variability on macrodispersion in heterogeneous porous media. presented at Spring 1989 Amer. Geophys. Union Meeting. Abstract in *EOS*, Transactions, American Geophysical Union, vol.70, no.15, pp.340.

Williams, D. E., and D. G. Wilder. 1971. Gasoline pollution of a ground-water reservoir — a case history. Ground Water, vol.9, no.6, pp.50-4.

Wilson, J. L. 1984. Double-cell hydraulic containment of pollutant plumes. in proceedings of Fourth National Symposium on *Aquifer Restoration and Groundwater Monitoring*, NWWA, Columbus, OH.

Wilson, J. L. 1988. The role of wetting in environmental problems. in proceedings of Conference on *Fundamental Research Needs in Environmental Engineering*, Assoc. Environ. Engr. Professors, Washington, DC.

Wilson, J. L., and S. H. Conrad. 1984. Is physical displacement of residual hydrocarbons a realistic possibility in aquifer restoration? in proceedings of *Petroleum Hydrocarbons and Organic Chemicals in Ground Water*, NWWA, Houston, TX, pp.274-98.

Wilson, J. L., S. H. Conrad, E. Hagan, W.R. Mason, and W. Peplinski. 1988. The pore level spatial distribution and saturation of organic liquids in porous media. in proceedings of *Petroleum Hydrocarbons and Organic Chemicals in Ground Water*, NWWA, Houston, TX, pp.107-133.

Wilson, J.L., W. Cox and W.M. Mason. 1988. Flow visualization of two-phase flow in a fracture. videotape presented at Spring 1988 Amer. Geophys. Union Meeting, Abstract in *EOS*, vol. 69, no. 16, p.353.

Yadav, G. D., F. A. L. Dullien, I. Chatzis, and I. F. Macdonald. 1987. Microscopic Distribution of Wetting and Nonwetting Phases in Sandstones During Immiscible Displacements. SPE Reservoir Engineering, vol. 2, may, pp. 137-147.

Yeh, T.-C. Jim, L. W. Gelhar, A. L. Gutjahr. 1985a. Stochastic analysis of unsaturated flow in heterogeneous soils, 1, statistically isotropic medium. Water Resources Research, vol.21, no.4, pp.447-456.

Yeh, T.-C. Jim, L. W. Gelhar, A. L. Gutjahr. 1985b. Stochastic analysis of unsaturated flow in heterogeneous soils, 2, statistically anisotropic media with variable α. Water Resources Research, vol.21, no.4, pp.457-464.

Yeh, T.-C. Jim, L. W. Gelhar, A. L. Gutjahr. 1985c. Stochastic analysis of unsaturated flow in heterogeneous soils, 3, observations and applications. Water Resources Research, vol.21, no.4, pp.465-472.

APPENDIX A:

QUANTITATIVE TWO-PHASE RESIDUAL SATURATION RESULTS, WITH STYRENE AS THE ORGANIC PHASE

The pore and blob cast experiments described in Section 7 produced quantitative results, as well as results pertaining to flow visualization. Unfortunately, the experimental methods made these quantitative results too inaccurate to be included with the main body of two-phase residual saturation data presented in Section 9. There were several reasons for the inaccuracies, as reviewed in Section 7.

Perhaps the largest source of error in the styrene experiments was the mass of the TFE column itself. Another factor contributing to the lower accuracy in the results was the density of the styrene. In comparison to Soltrol-130, styrene is the denser — 0.90 versus 0.75 g/cm^3. The column was weighed, during the gravimetric determinations of saturation, on the high capacity Mettler PM 11 balance, which has an accuracy of only 0.1 grams. As a result of these problems the styrene experiments had saturation errors of ±6-8%, while the short-column experiments had errors of only ±2-3%. When we considered that 6-8% was sometimes up to 50% of the residual saturation measurement, it seemed prudent to consider these less accurate results separately.

Another reason for excluding the styrene data from the other quantitative data was that the residual saturations obtained were consistently lower than those obtained with the short-columns. In Section 7 we hypothesize that time constraints, put on the experiment by styrene's ever increasing viscosity, did not allow enough time for the column to come to equilibrium. The wettability of the column walls was also found to affect the amount of time required to reach an equilibrium during the organic liquid flood, and may have influenced the residual styrene saturations.

EXPERIMENTAL RESULTS

The first column in the Table A-1 describes the experimental column, and the experimental run performed in it. There were three TFE columns constructed, two of which are represented here. For example, experiment 0-6 was the sixth experiment performed in TFE column 0, and experiment 2-1 was the first experiment performed in column 2. Column 1 was used exclusively for three-phase experiments, which were non-quantitative, so it is not represented in this table. Porosity values in column 2, maximum organic liquid saturations, S_o , in column 3, and residual organic saturations, S_{or} , in column 4, were calculated as described in Section 7.

Experiments 0-1 through 0-4 and 2-1 were homogeneous two-phase runs using the Sevilleta soil and styrene. The S_{or} data set has an average value of 0.16 and a standard deviation of 0.04. In comparison to the glass short column results (see Section 9), they are uniformly lower.

In experiment 0-6, Soltrol-130 was flooded into, and drained out of, a TFE column following procedures dictated by the viscosity related time constraints of the styrene procedure. The residual

Column	Porosity (%)	S_o	S_{or}
0-1 homogeneous	32.3	0.710 ± .091	0.170 ± .065
0-2 homogeneous	33.5	0.667 ± .087	0.108 ± .059
0-3 homogeneous	33.5	0.713 ± .094	0.192 ± .065
0-4 homogeneous	31.7	0.722 ± .101	0.157 ± .071
2-1 homogeneous	34.6	0.700 ± .086	0.200 ± .060
0-5 soltrol-130	33.4	0.764 ± .039	0.265 ± .027
0-6 soltrol-130	34.1	0.745 ± .038	0.186 ± .025
2-2 crushed tuff	38.7	0.918 ± .116	0.295 ± .082
0-8 heterogeneous	34.5	0.936 ± .107	0.263 ± .072
2-3 heterogeneous	37.1	0.896 ± .133	0.407 ± .105

TABLE A-1. Two-phase TFE column residual saturation results; styrene was used unless otherwise noted.

saturation obtained matched those commonly found when performing experiments with styrene in the TFE column (19%). In experiment 0-5 Soltrol was again flooded into the TFE column but without time constraints, following the glass short column procedures of Section 5. Since sufficient time was allowed for the system to come to equilibrium, a value of residual saturation was obtained (27%) which closely matched those found when using Soltrol-130 in a glass column. These results suggest that the differences in residual saturation values were related not to differences in fluid characteristics, but to the amount of time the liquid/soil system had in which to equilibrate.

Experiment 2-2 was a homogeneous two-phase run done with a crushed and sieved tuff. This was an attempt to obtain blob casts that would photograph well on black and white film. The black tuff would stand out from the hardened fluid phases. Other methods of creating black and white photographs were successful so these casts were never used.

Experiments 0-8 and 2-3 were heterogeneous two-phase runs using Sevilleta soil split into two fractions, as described in Section 7 of this report. High organic saturations, as seen in these experiments, indicated that the organic liquid displaced the aqueous phase from the larger pores found in the stringers. This was expected, as a non-wetting fluid will move preferentially to larger pores in order to decrease its surface to volume ratio, and therefore decrease the surface energy of the system. So with the larger pores available, more non-wetting liquid can enter the system for a given energy level, or head. The fact that the columns were packed dry may have also contributed to the higher S_o values. The dry soil may have settled and compacted during the water saturation process, creating a large pore at one end of the column. This one 'macro' pore could have filled with styrene and contributed to a high organic saturation.

The S_{or} values presented represent 'bulk' residual saturations in that they are averaged over the whole heterogeneous column. Observations of the core, after it had been cut on a rock saw indicate however, that most of the residual styrene was trapped in the coarse stringers. A lesser amount, approximately the same as that observed in the earlier homogeneous experiments (16%), was trapped in the finer matrix. The measured 'bulk' residual saturation can be compared with a theoretical value (see Section 9):

Estimated bulk residual styrene saturation =

$$= (\textit{normalized lens volume}) \times S_o + (\textit{normalized matrix volume}) \times S_{or}$$

$$= (0.40 \times 0.90) + (0.60 \times 0.16) = (0.36 + 0.09) = 0.45 = 45\%$$

Column 2-3's value of residual saturation, 41%, comes close to the theoretical value, while column 0-8 is nowhere near the predicted value. This suggests that by-pass trapping may not totally exclude water from the coarse stringers (refer to Section 9).

The differing S_{or} values of experiments 0-8 and 2-3 are explained by the flow rate of the water flood. Experiment 0-8 was flooded with water as described in Section 7 of the report. That is to say, it was flooded exactly as if it were a homogeneous two-phase experiment. The residual saturation value, 26%, reflects the relatively larger volume of styrene trapped in the coarser sand stringers. Column experiment 2-3, in contrast, was water-flooded at a much lower rate, approximately 1 ml/minute. This flow rate was controlled by pushing water through the column with a syringe pump. The low flow rate led to a situation where almost 45% of the styrene in the column was bypassed and trapped. In this case, the combination of viscous and buoyancy forces were not strong enough to overcome the capillary forces holding the styrene in place. Although some $CaCl_2$ did flow through the stringers, the majority of the stringer's pore space remained filled with styrene. For photographs of the styrene filled stringers, see Section 9 of this report.

APPENDIX B

VIDEOTAPES OF MICROMODEL EXPERIMENTS

Videotapes of the micromodel experiments described in Sections 9 and 10 are available on VHS format tapes. They are treated as Open File Reports, Hydrology Progam, Department of Geoscience, New Mexico Institute of Mining and Technology, Socorro, New Mexico 87801. The following videotapes are currently (1990) available:

- **Wilson, J.L., W. Cox and W.M. Mason.** 1988. Flow visualization of two-phase flow in a fracture. videotape presented at Spring 1988 Amer. Geophys. Union Meeting, Abstract in *EOS*, vol. 69, no. 16, p.353; order as Hydrology Open File Report 88-1.
- **Mason, W.M., S.H. Conrad and J.L. Wilson.** 1988. Micromodel study of organic liquid advance in a soil. poster & videotape presented at Spring 1988 Amer. Geophys. Union Meeting, Abstract in EOS, vol. 69, no. 16, p.370, 1988; order as Hydrology Open File Report 88-2.
- **Mason, W.M., W. Peplinski, J.L. Wilson and S.H. Conrad.** 1989. Pore level flow visualizaion of three phase fluid flow. talk & videotape presented at Spring 1989 Amer. Geophys. Union Meeting, Abstract in EOS, vol. 70, no. 15; order as Hydrology Open File Report 89-6.
- **S.H. Conrad, W.M. Mason and J.L. Wilson.** 1989. Two phase immiscible displacement in a heterogeneous porous media. Order as Hydrology Open File Report 89-7.

The tapes were originally recorded on Beta II format tape, and subsequently edited for distribution. The VHS tapes are copies of Beta masters, and are several generations old. They are not of broadcast quality.

There is a nominal charge for the tapes, to cover media and reproduction expenses. Please contact the Hydrology Secretary at 505-835-5308 or 5307 for the current charge.

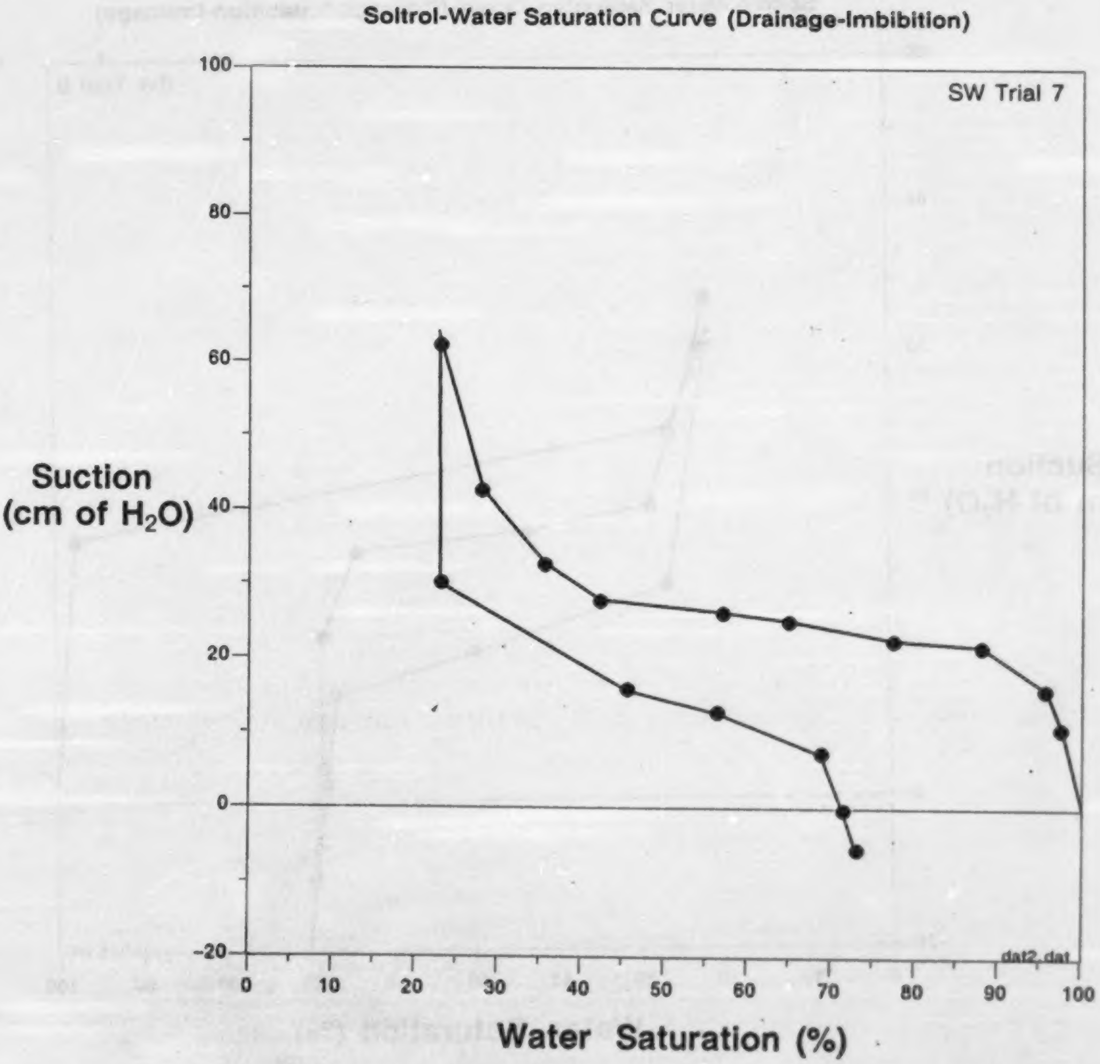

FIGURE C-1. Soltrol-water saturation curve for SW trial 7.

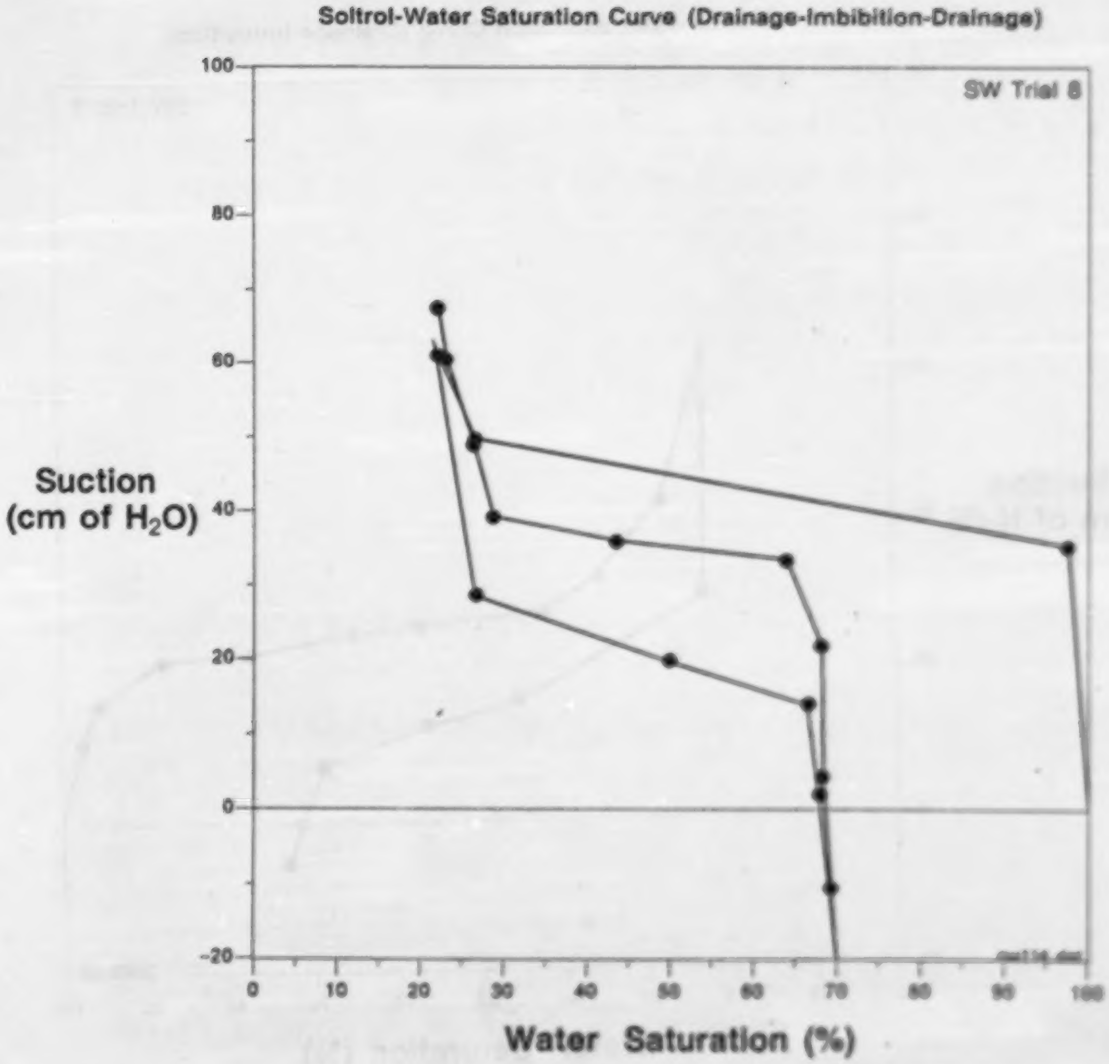

FIGURE C-2. Soltrol-water saturation curve for SW trial 8.

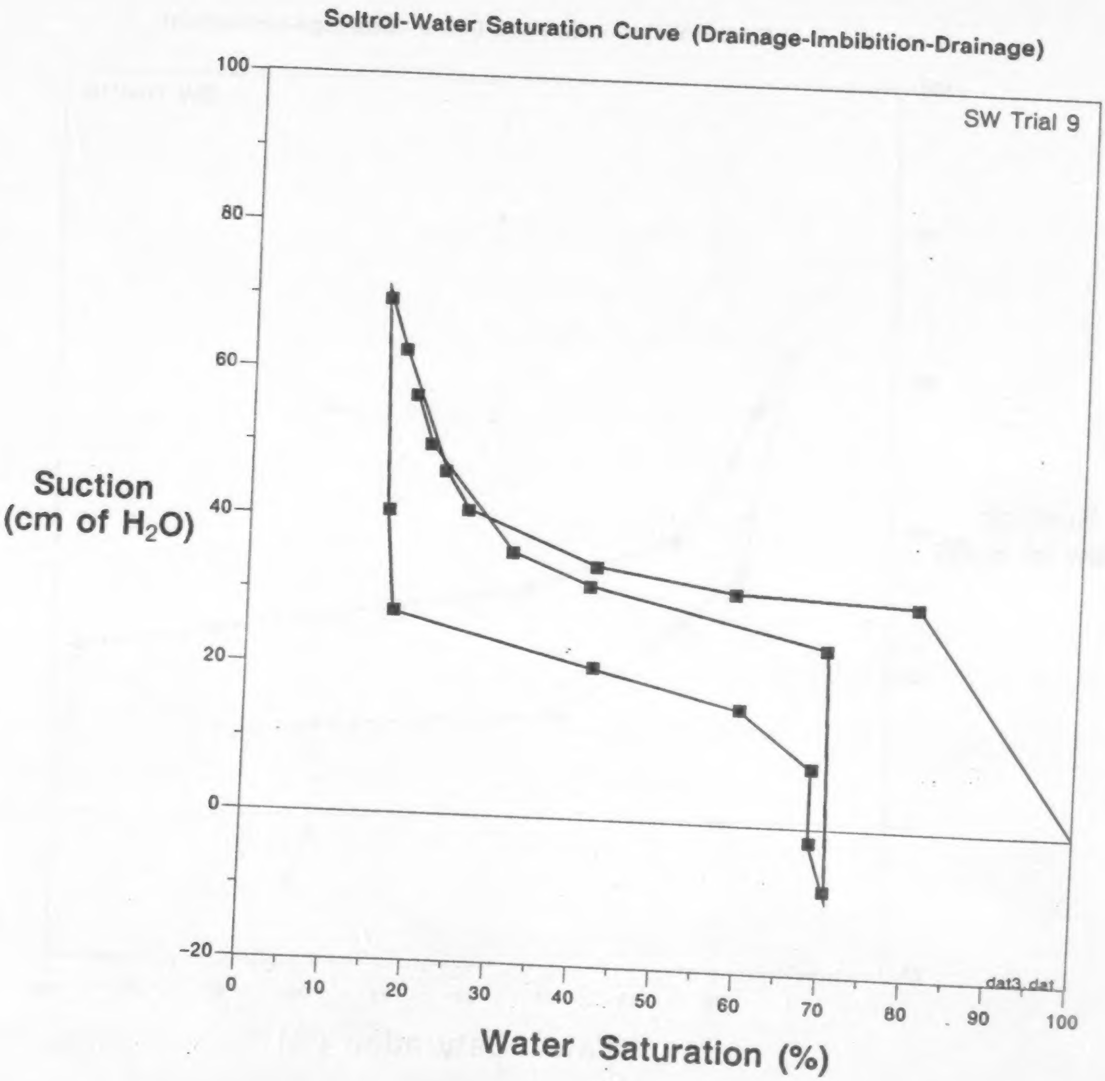

FIGURE C-3. Soltrol-water saturation curve for SW trial 9.

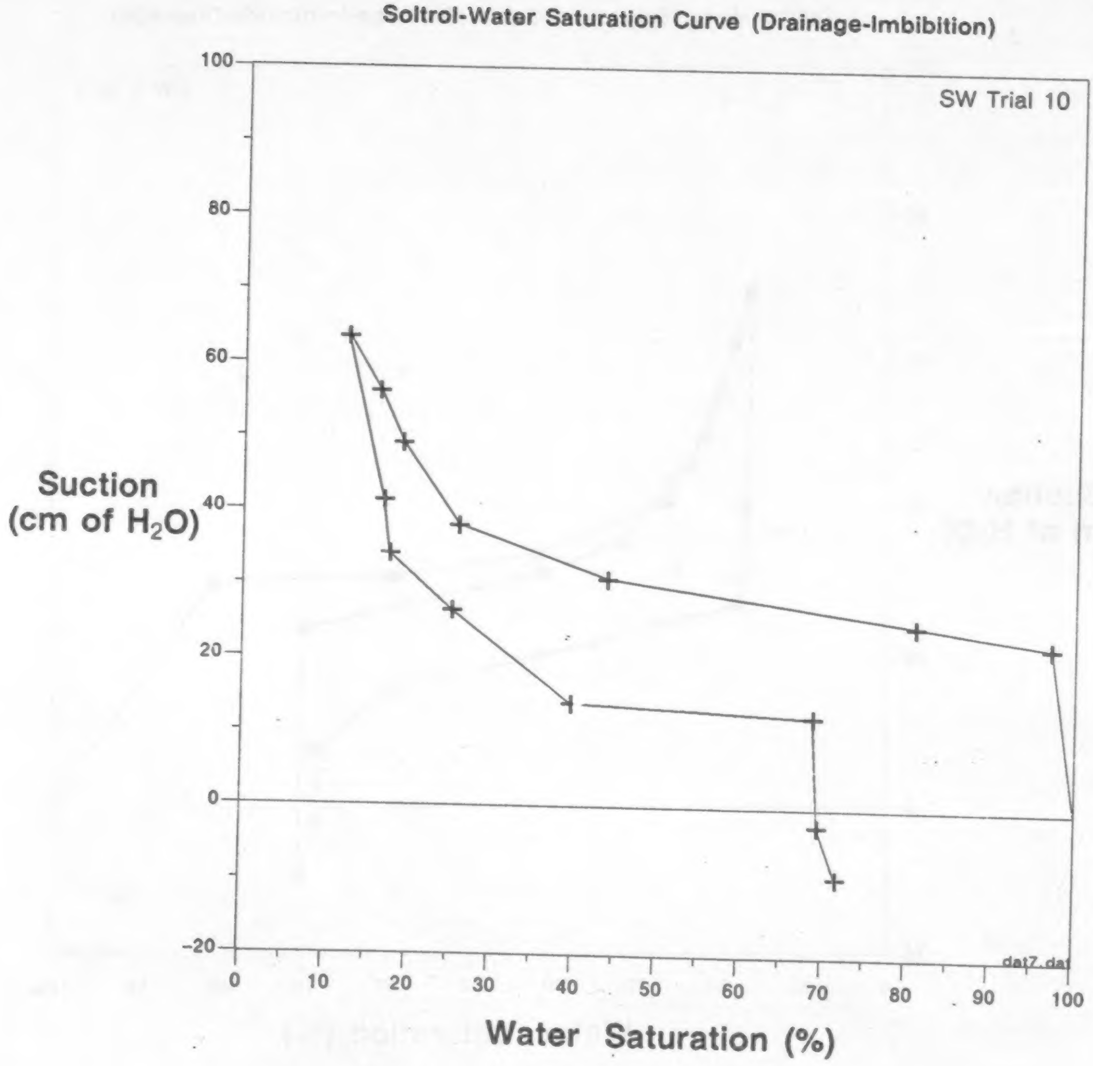

FIGURE C-4. Soltrol-water saturation curve for SW trial 10.

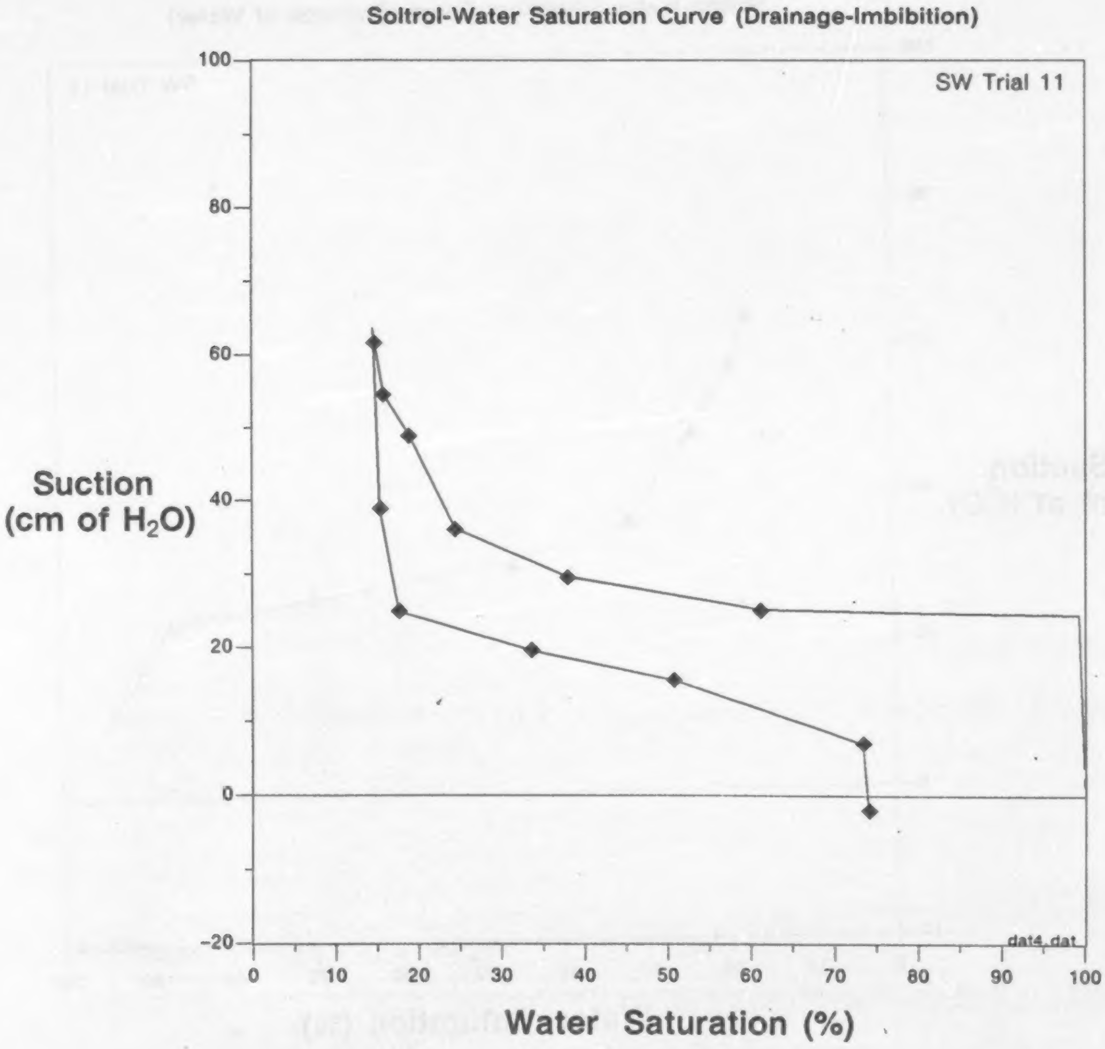

FIGURE C-5. Soltrol-water saturation curve for SW trial 11.

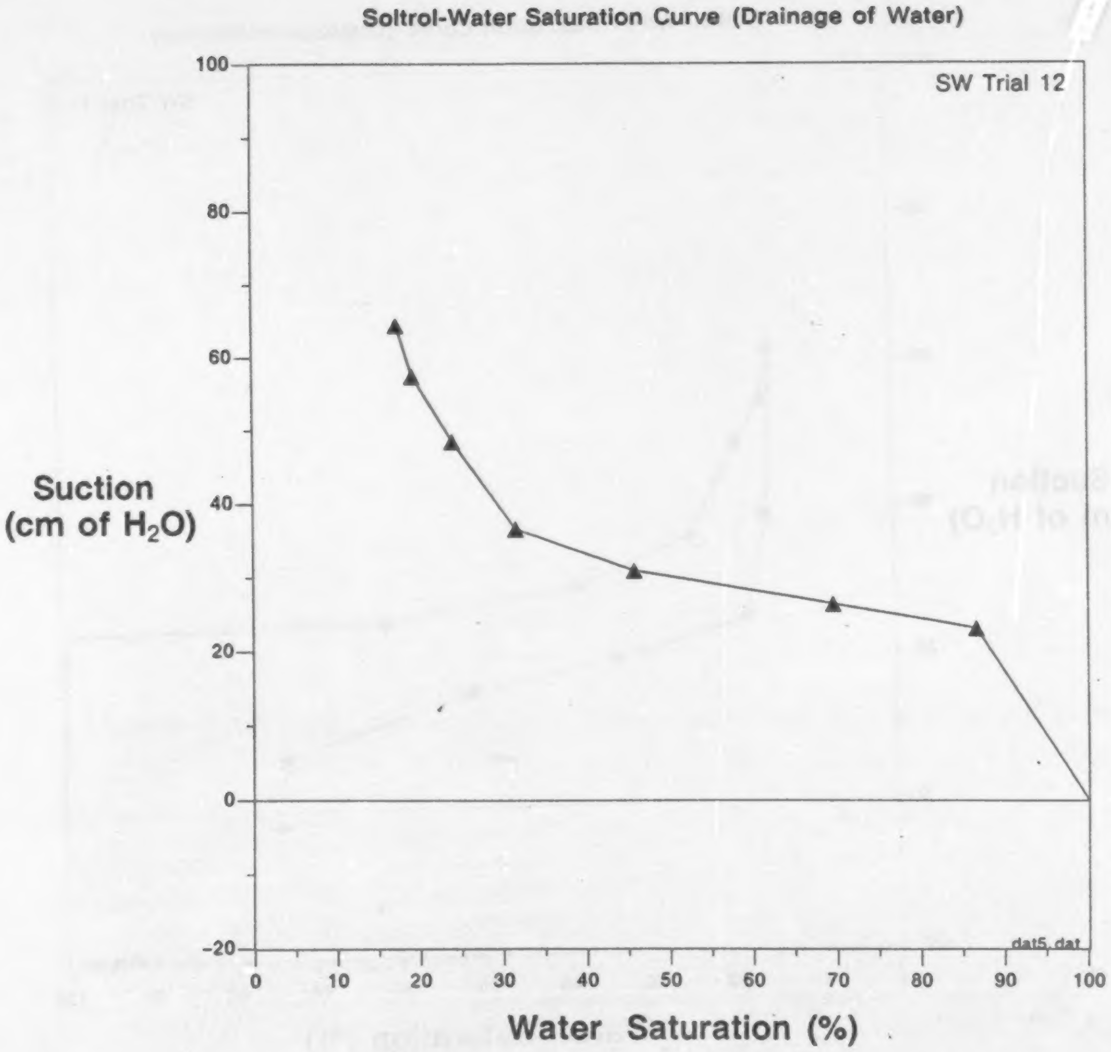

FIGURE C-6. Soltrol-water saturation curve for SW trial 12.

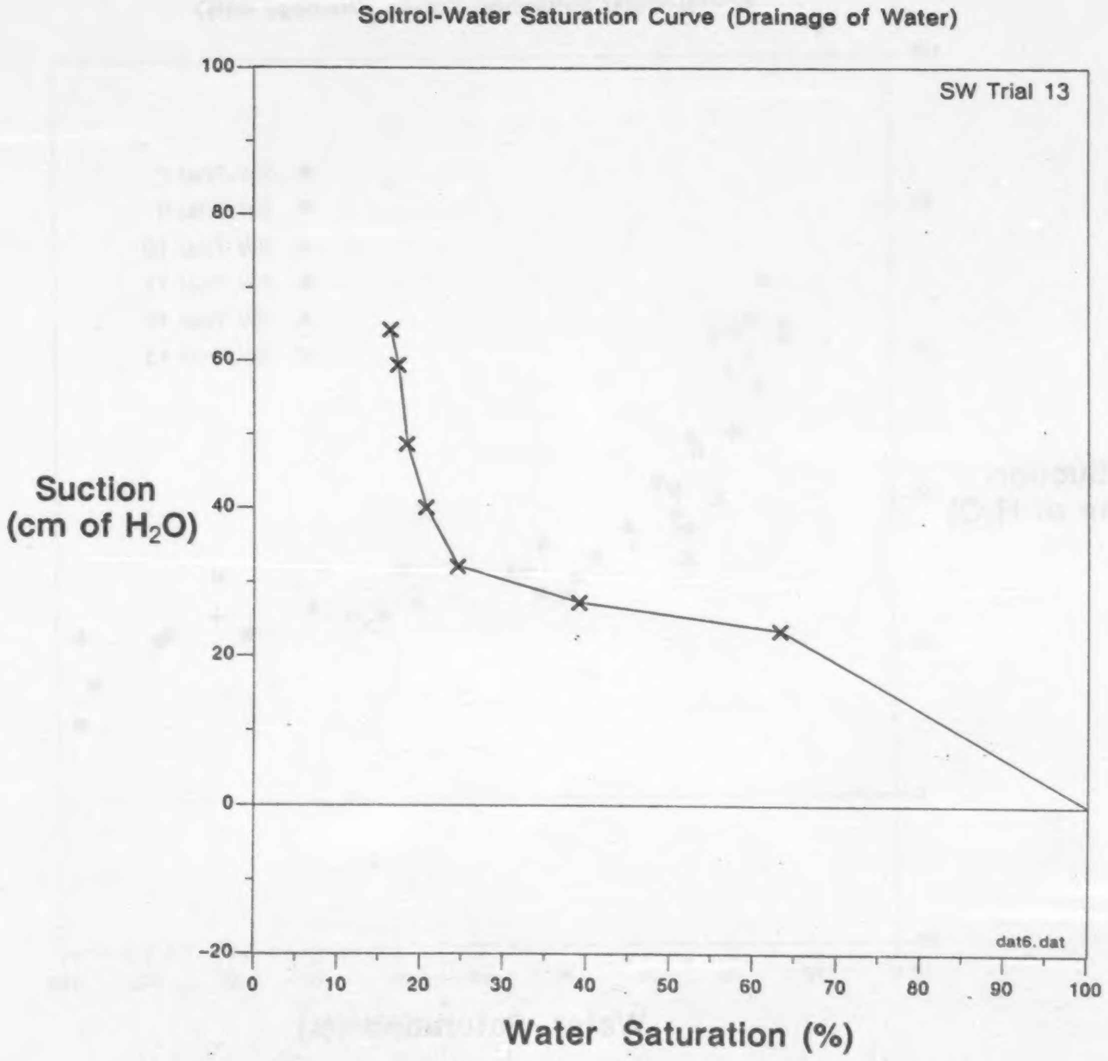

FIGURE C-7. Soltrol-water saturation curve for SW trial 13.

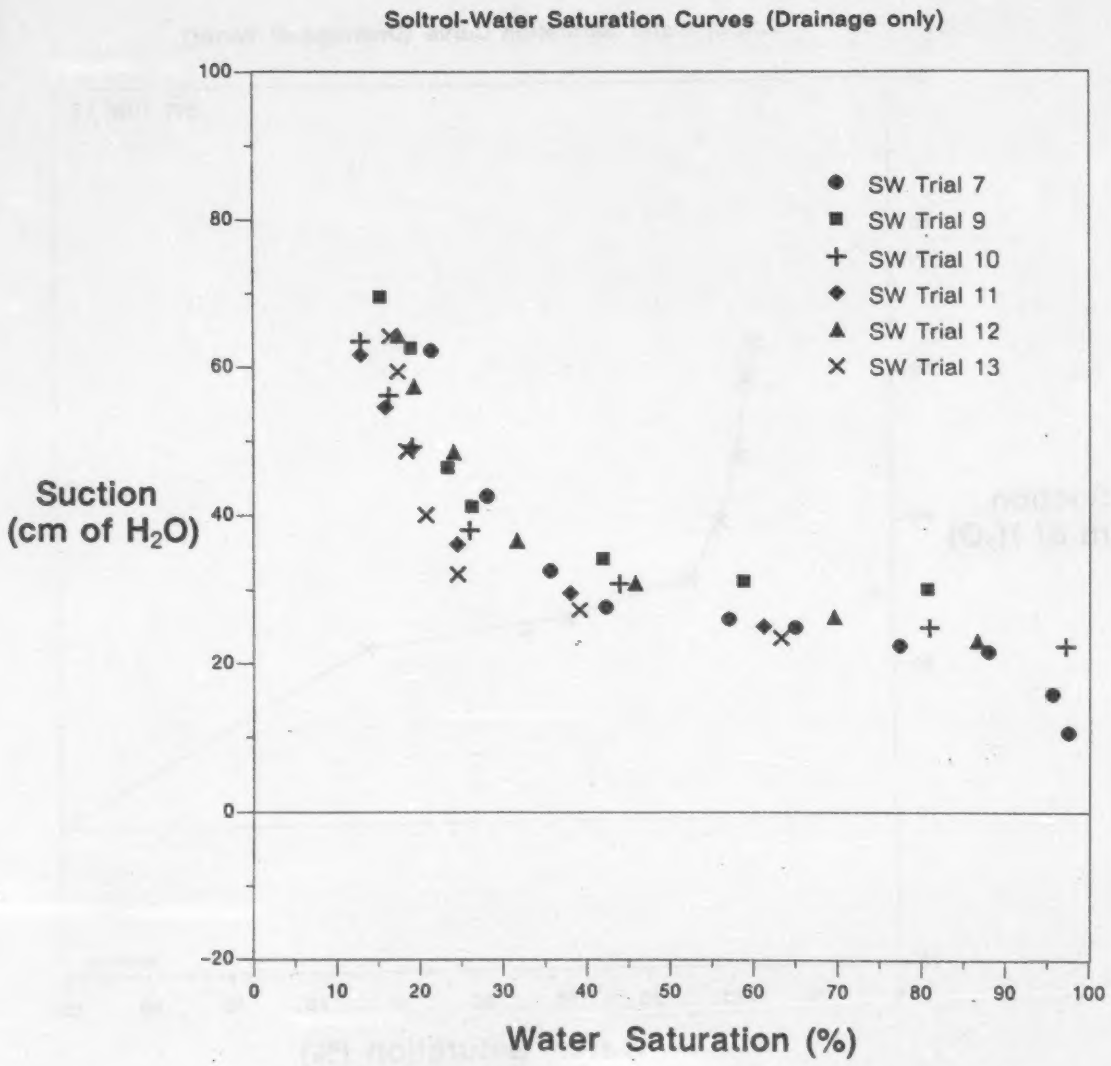

FIGURE C-8. Soltrol-water primary drainage curves for SW trials 7-13, minus trial 8.

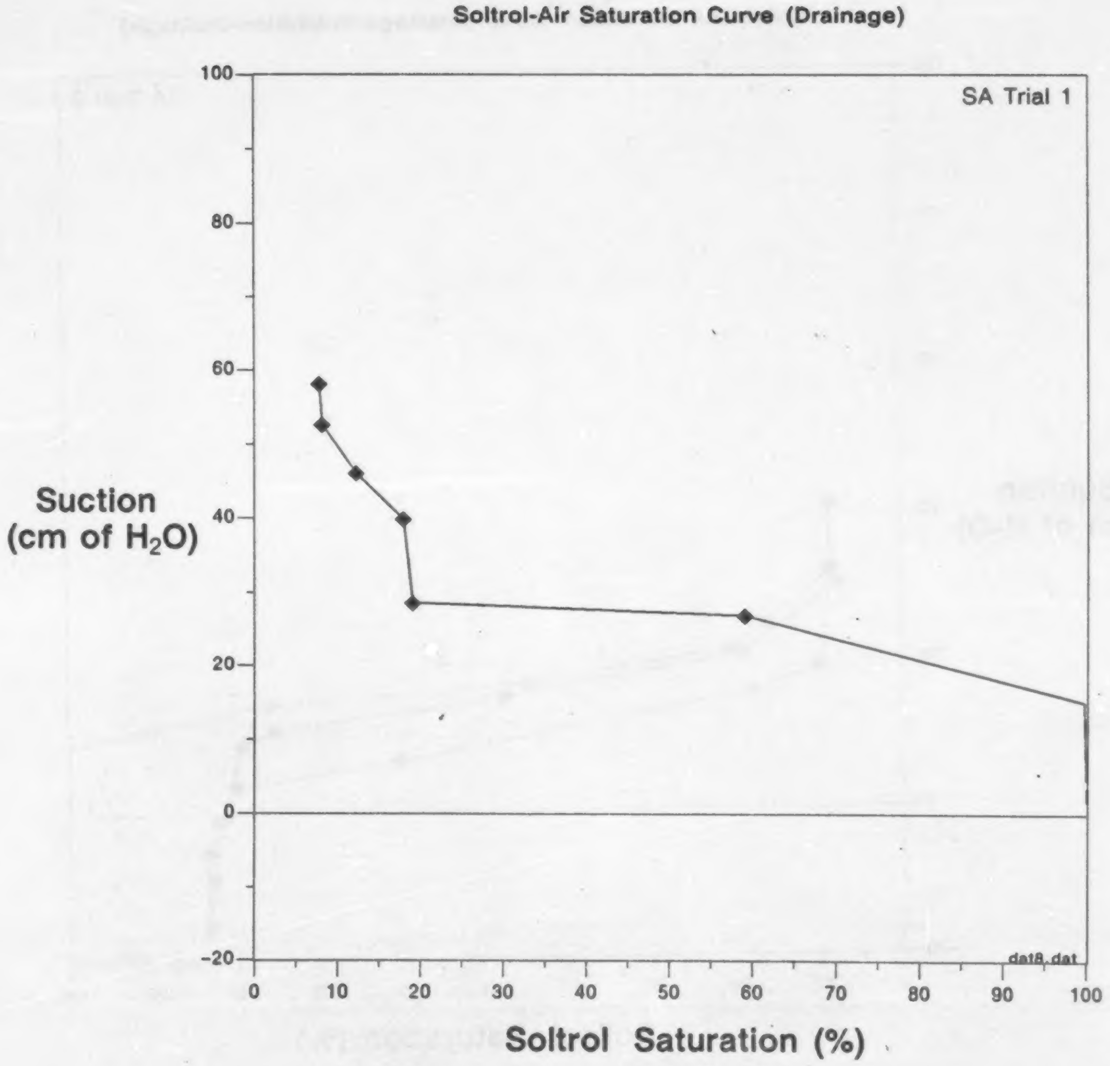

FIGURE C-9. Soltrol-air saturation curve for SA trial 1.

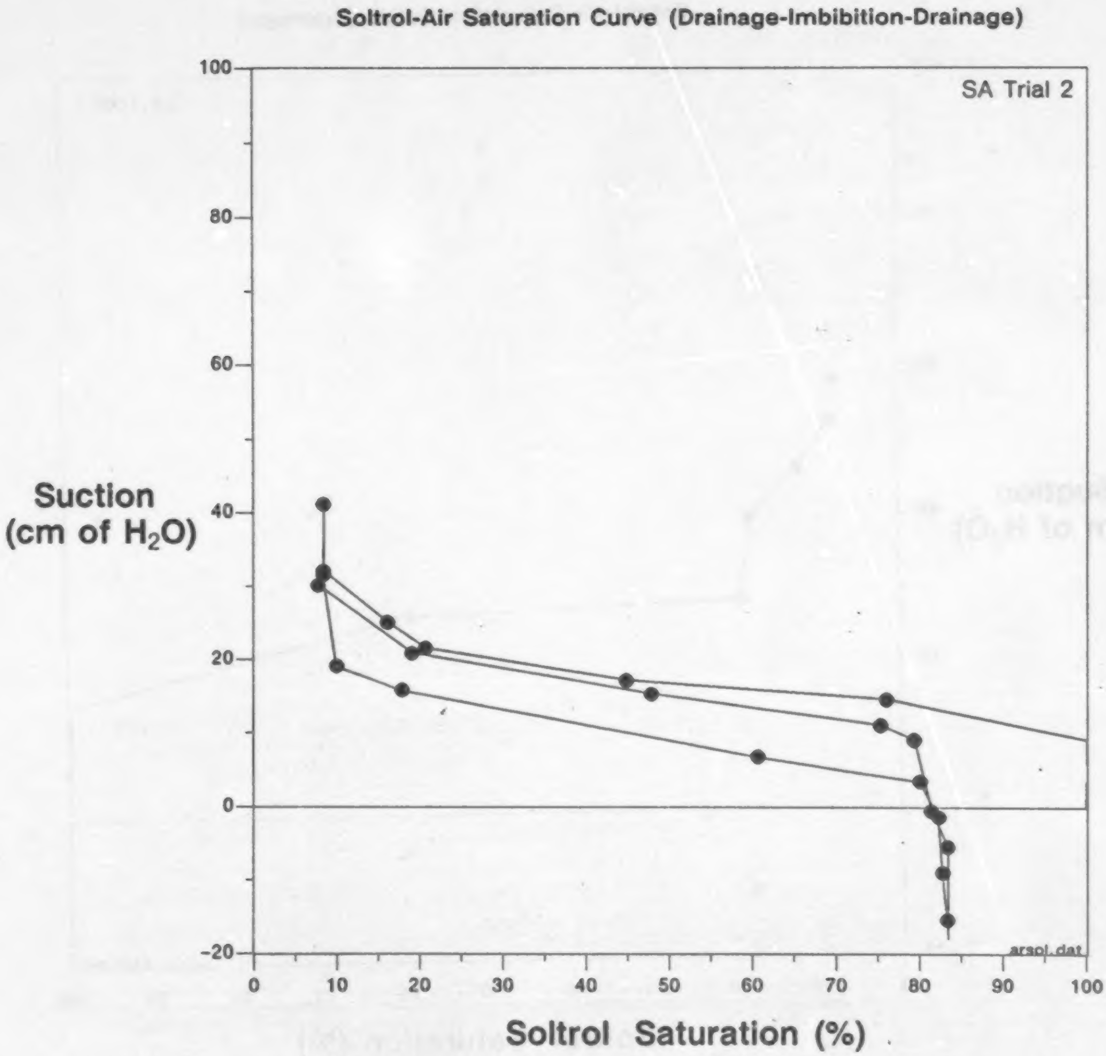

FIGURE C-10. Soltrol-air saturation curve for SA trial 2.

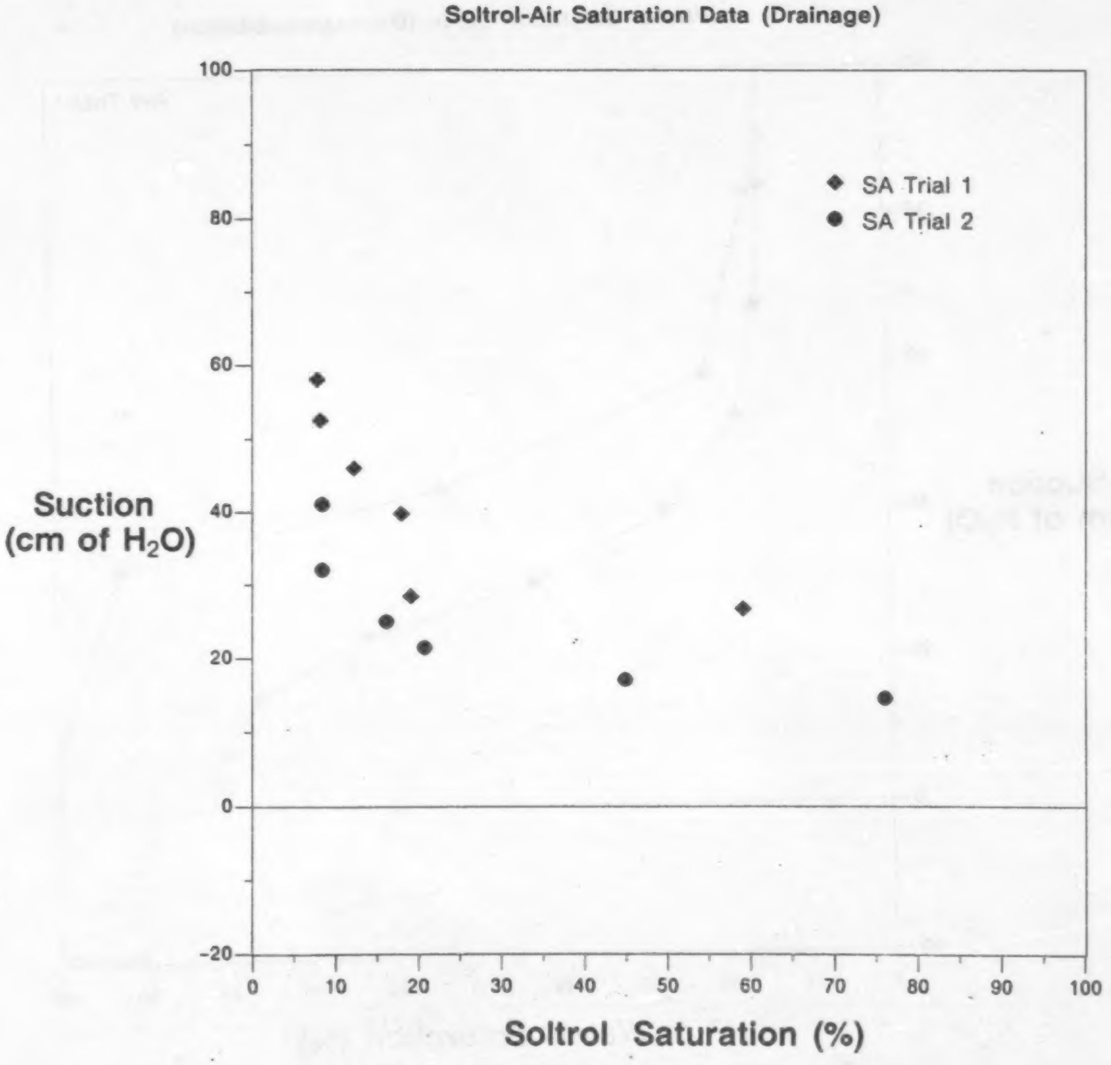

FIGURE C-11. Comparison of Soltrol-air primary drainage curves for SA trials 1 & 2.

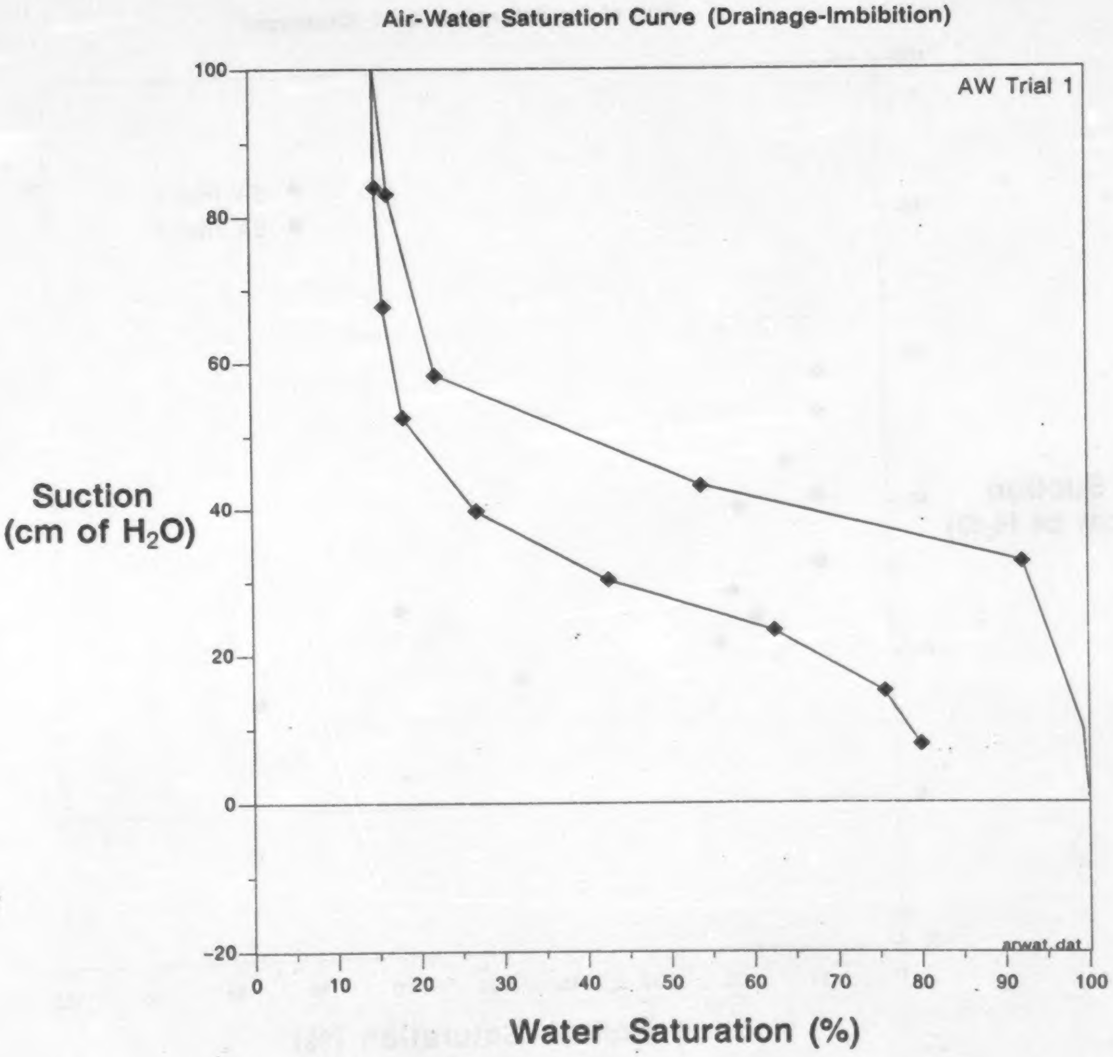

FIGURE C-12. Air-water saturation curve for AW trial 1.

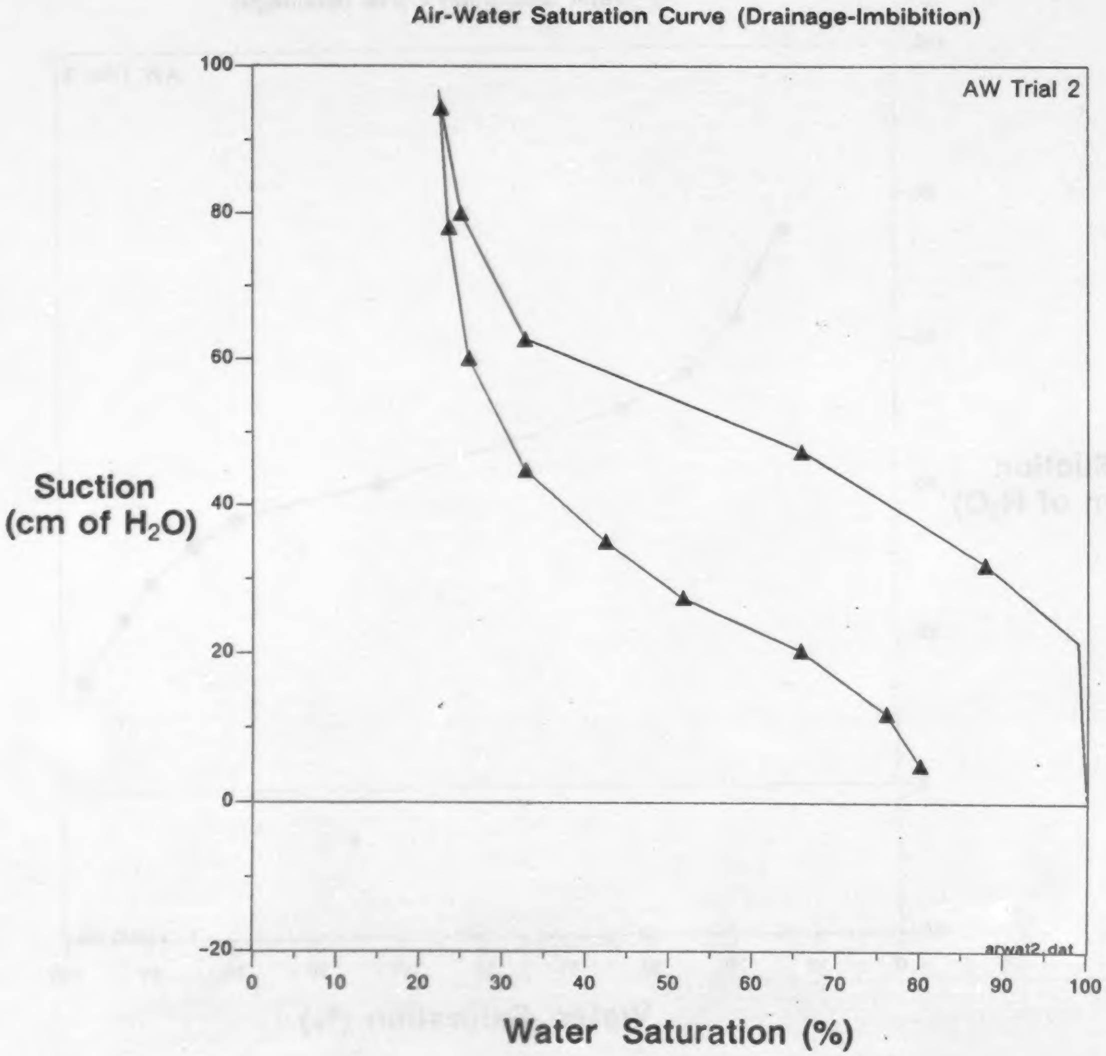

FIGURE C-13. Air-water saturation curve for AW trial 2.

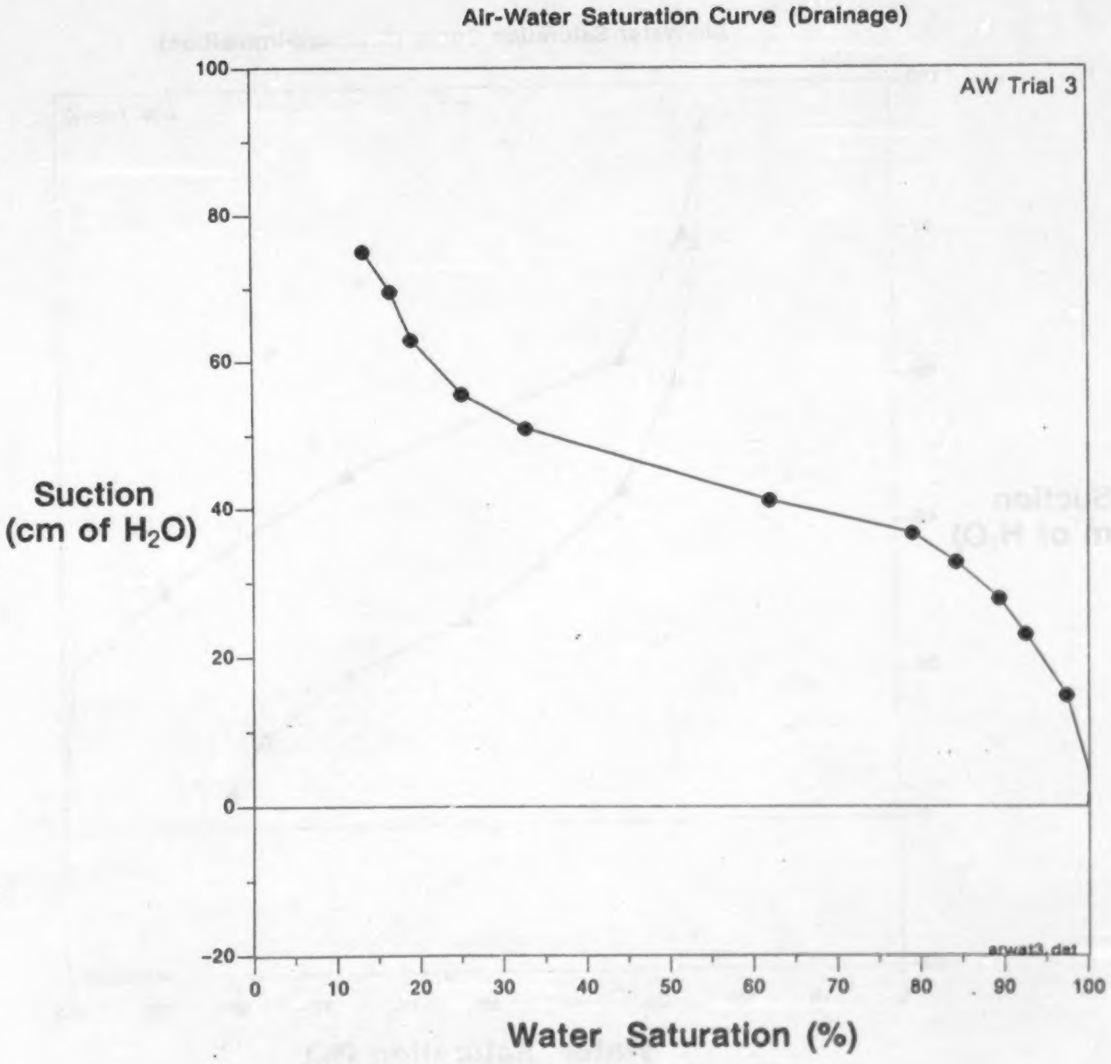

FIGURE C-14. Air-water saturation curve for AW trial 3.

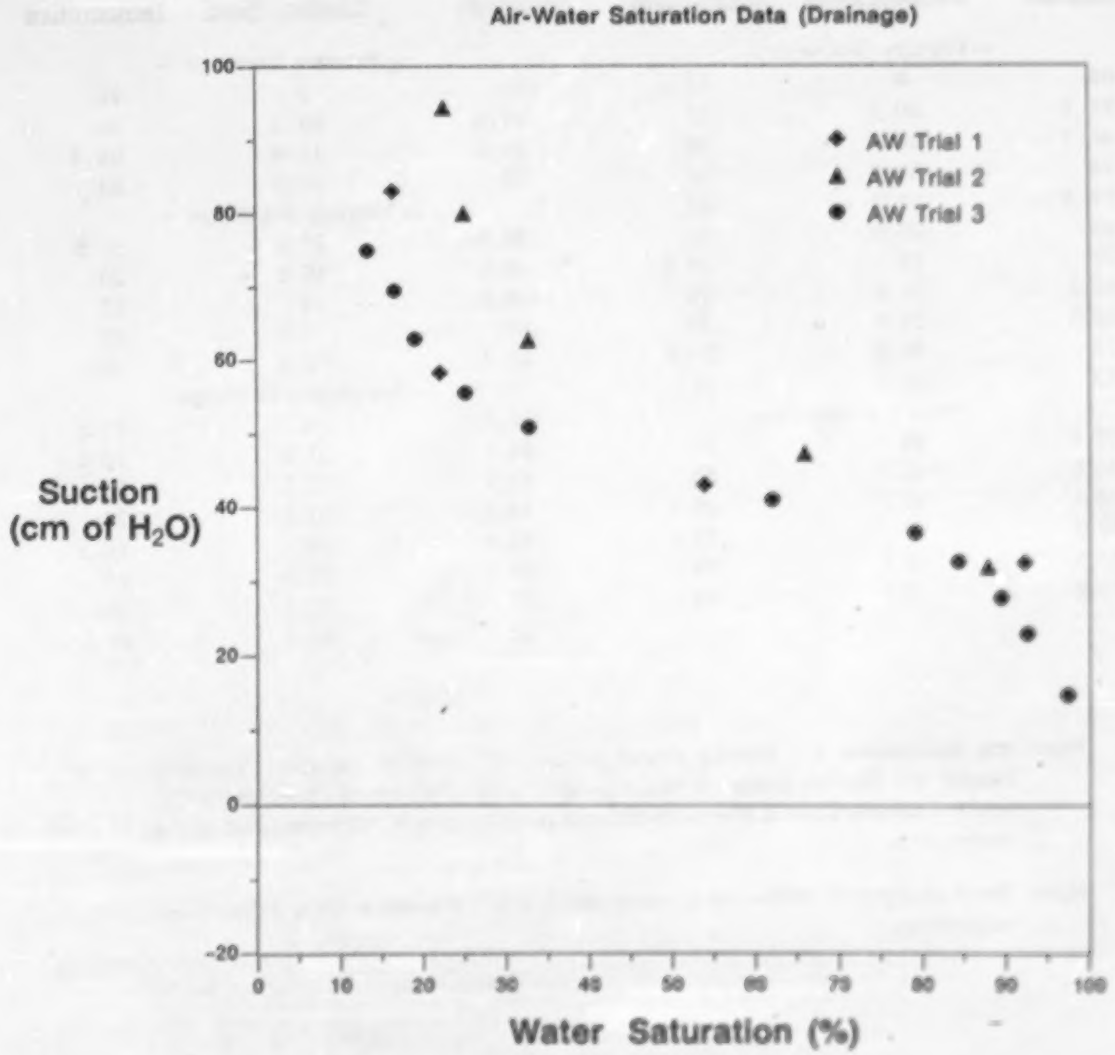

FIGURE C-15. Comparison of air-water primary drainage curves for SA trials 1 through 3.

TABLE C-1. **Numerical values of measured saturations, pressures, and temperatures.** (continued on next four pages)

SW Trial 7

Saturation	Capillary Head	Temperature
	— Primary Drainage —	
100	0	26.5
97.6	10.5	26
95.7	15.7	25
88	21.5	24
77.5	22.3	23
65	24.8	24
57	26	24.5
42.3	27.6	25
35.6	32.5	27
28	42.5	28.5
23	62.1	31
	— Primary Imbibition —	
23.1	30	31
45.6	15.7	31
56.4	12.7	28.5
68.9	7.2	18.5
71.6	-0.4	19
73.2	-5.7	20

SW Trial 8

Saturation	Capillary Head	Temperature
	— Primary Drainage —	
100	0	23
97.6	33.1	24
26.5	49.6	24.5
22	60.9	24
	— Primary Imbibition —	
25.7	28.6	24.5
49.9	19.8	23
66.6	14	27
69	1.9	28
69.3	-10.6	28
	— Secondary Drainage —	
68.3	4.3	21.5
68.1	21.6	20.5
63.9	33.3	20
43.5	35.6	20
28.7	39.1	18.3
26.3	29.8	20
23	60.4	23
22	67.4	21.5

Note: the saturations are wetting phase saturations given in percent; 'capillary heads' are capillary pressure heads given in equivalent cm of water (at 20°C); and the temperature is the room/cabinet temperature in °C, measured at the same time.

Note: The S designates Soltrol, W is water and A is air. Therefore SA is a Soltrol-air experiment.

TABLE C-1. **Numerical values of measured saturations, pressures, and temperatures.** (continued)

SW Trial 9

Saturation	Capillary Head	Temperature
	— Primary Drainage —	
100	0	24
80.8	30	24.5
58.8	31.1	25.5
41.9	34.1	24
26.2	41.1	24.5
23.3	46.3	20
18	62.5	24
16	69.5	24.5
	— Primary Imbibition —	
16.6	40.8	25.5
17.6	27.3	23
41.9	20.5	27
59.8	15.6	28
68.7	8	22
68.7	-2	22.5
70.6	-8.6	21.5
	— Secondary Drainage —	
70	24	20.5
41.2	31.4	20
31.7	35.6	20
21.4	49.8	18
19.5	56.4	20
15.7	66.5	20.5

SW Trial 10

Saturation	Capillary Head	Temperature
	— Primary Drainage —	
100	0	23
97.2	22.2	23.2
81	24.8	20.5
43.9	30.8	21.5
25.9	38	20.5
19	49.1	21.8
16.2	56.1	21.3
12.3	63.4	21.8
	— Primary Imbibition —	
16.8	41.3	21.8
17.6	34.1	20.8
25.2	26.4	23
39.7	13.9	20
68.8	12.4	22
69.5	-2.4	22.5
71.8	-9.3	19.5

TABLE C-1. **Numerical values of measured saturations, pressures, and temperatures.** (continued)

SW Trial 11

Saturation	Capillary Head	Temperature
	— Primary Drainage —	
100	0	23.2
99.3	24.3	21.6
61.2	25	20.5
38	29.5	21.5
24.4	36.1	20.5
18.9	48.8	21.8
15.8	54.5	21.3
14.7	61.6	21.7
	— Primary Imbibition —	
15.4	38.9	21.8
17.7	24.9	20.8
33.6	19.6	23
50.8	15.6	20
73.5	7	22
74.2	-2.1	22.5

SW Trial 12

Saturation	Capillary Head	Temperature
	— Primary Drainage —	
100	0	24.5
86.7	23	24.5
69.6	26.3	26.8
45.8	30.9	25.8
31.6	36.5	26.4
24	48.4	24.8
19.2	57.3	27.6
17.3	64.3	25.6

SW Trial 13

Saturation	Capillary Head	Temperature
	— Primary Drainage —	
100	0	24.5
63.3	23.4	26.8
39.1	27.2	25.8
24.5	32	26.4
20.7	40	24.8
18.4	48.5	27.6
17.3	59.3	25.6
16.4	64.1	28.2

SA Trial 1

Saturation	Capillary Head	Temperature
	— Primary Drainage —	
100	0	23
99.7	15	21.5
59	26.8	22.4
19	28.5	22.8
17.9	39.8	22
12.2	46	22
8.1	52.5	22.6
7.8	58	22

TABLE C-1. Numerical values of measured saturations, pressures, and temperatures. (continued)

SA Trial 2

Saturation	Capillary Head	Temperature
	— Primary Drainage —	
100	0	21.3
100	9	21.8
76.1	14.5	21.2
44.9	17	22
20.7	21.5	22.2
16.1	25	22.2
8.4	32	22
8.4	41	22
	— Primary Imbibition —	
8.4	31.5	22
10	19	22
17.9	15.7	22
60.7	6.7	22
80.1	3.4	22
82.3	-1.5	22.6
82.8	-9.1	22
83.4	-15.5	22.5
	— Secondary Drainage —	
83.4	-5.5	22.8
81.4	-0.6	22.9
79.4	9	22.7
75.4	11	23
47.9	15.2	23
19.1	20.8	23.5
7.8	30	22.5

AW Trial 1

Saturation	Capillary Head	Temperature
	— Primary Drainage —	
100	0	26.9
99.3	9.7	23.3
92.2	32.5	25
53.9	43.1	25
22	58.2	24
16.4	83.1	18.4
14.9	99	16.8
	— Primary Imbibition —	
15	84	15.6
15.9	67.6	18.6
18.2	52.5	24.2
26.9	39.7	24.6
42.7	30.2	26.2
62.6	23.2	26.8
75.7	14.9	22.2
80	7.7	21

TABLE C-1. **Numerical values of measured saturations, pressures, and temperatures.** (continued)

AW Trial 2			AW Trial 3		
Saturation	Capillary Head	Temperature	Saturation	Capillary Head	Temperature
	— Primary Drainage —			— Primary Drainage —	
100	0	27	100	0	24.9
99.4	10.2	23.3	100	4.5	24.3
98.9	21.5	24	97.4	14.7	24
87.8	31.9	25	92.6	22.9	25.1
65.9	47.3	25	89.4	27.7	24.6
32.7	62.7	18.4	84.3	32.6	24
25	80	16.8	79.1	36.5	27
22.6	94.4	15.6	62	41	24.6
	— Primary Imbibition —		32.8	50.8	24.4
23.6	78.1	18.6	25.1	55.5	24.4
26	60.1	24.2	19.1	62.8	26.1
32.8	44.8	24.6	16.6	69.5	26
42.4	35.1	26.2	13.4	75	22.9
51.7	27.5	26.8			
65.8	20.4	22.2			
76.1	11.9	21			
80.1	5	20			

APPENDIX D

RAW DATA FROM THE SHORT COLUMN EXPERIMENTS

This appendix contains the Lotus 1-2-3 worksheets for the short glass column, quantitative experiments described in Section 5. The results are summarized and discussed in Sections 9 and 10.

Reproduced from
best available copy.

```
                          TWO-PHASE COREFLOOD DATA

INPUT DATA
                                                       |----FLUIDS----|  |--------------DENSITIES (g/cc)---------------|  |-----COLUMN MASS (g)------|
trial #  in box?   from:       to:        soil         organic  aqueous   organic   +/-   aqueous   +/-   particle   +/-    empty   +/-    w/H2O   +/-  soil mass (g)  +/-
///////////////////////////////////////////////////////////////////////////////////////////////////////////////////////////////////////////////////////////////////.
   1      no     21-Jan-87  04-Feb-87  sevilleta   soltrol  CaCl2    0.753   0.001   1.000   0.002    2.65    0.01   861.70  0.03   957.55  0.02     167.31     0.04
   2      no     17-Jan-87  05-Feb-87  sevilleta   soltrol  CaCl2    0.753   0.001   1.000   0.002    2.65    0.01   904.13  0.03  1022.70  0.02     198.12     0.04
   3      no     16-Feb-87  01-Mar-87  sevilleta   soltrol  CaCl2    0.753   0.001   1.000   0.002    2.65    0.01   881.07  0.03   996.88  0.02     201.38     0.04
   4      no     16-Feb-87  02-Mar-87  sevilleta   soltrol  CaCl2    0.753   0.001   1.000   0.002    2.65    0.01   886.11  0.03   981.41  0.02     165.74     0.04
   5      no     21-Feb-87  03-Mar-87  sevilleta   soltrol  CaCl2    0.753   0.001   1.000   0.002    2.65    0.01   905.92  0.03   999.43  0.02     164.18     0.04
   6      no     04-Mar-87  19-Mar-87  sevilleta   soltrol  CaCl2    0.753   0.001   1.000   0.002    2.65    0.01   877.31  0.03   991.88  0.02     197.10     0.04
   7      no     04-Apr-87  21-Apr-87  sevilleta   soltrol  CaCl2    0.753   0.001   1.000   0.002    2.65    0.01   909.10  0.03  1006.61  0.02     156.90     1.00
   8      no     02-May-87  05-Jun-87  sevilleta   soltrol  CaCl2    0.753   0.001   1.000   0.002    2.65    0.01   877.74  0.03   996.25  0.02     202.78     0.04
   9      no     09-May-87  07-Jun-87  sevilleta   soltrol  CaCl2    0.753   0.001   1.000   0.002    2.65    0.01   910.37  0.03  1000.93  0.02     154.58     0.04
  10      no     18-May-87  18-Jun-87  sevilleta   soltrol  CaCl2    0.753   0.001   1.000   0.002    2.65    0.01   896.32  0.03   981.24  0.02     144.49     0.04
  11      no     20-May-87  17-Jun-87  sevilleta   soltrol  CaCl2    0.753   0.001   1.000   0.002    2.65    0.01   877.17  0.03   962.53  0.02     147.30     0.04
  12      no     17-Jun-87  20-Jul-87  sevilleta   soltrol  CaCl2    0.753   0.001   1.000   0.002    2.65    0.01   880.86  0.03   973.24  0.02     159.68     0.04
  13      no     17-Jun-87  20-Jul-87  sevilleta   soltrol  CaCl2    0.753   0.001   1.000   0.002    2.65    0.01   881.01  0.03   997.21  0.02     202.17     0.04
  14      yes    16-Dec-87  22-Jan-88  sevilleta   soltrol  CaCl2    0.753   0.001   1.000   0.002    2.65    0.01   884.00  0.03   975.60  0.02     155.89     0.04
  15      yes    08-Dec-87  30-Jan-88  sevilleta   soltrol  CaCl2    0.753   0.001   1.000   0.002    2.65    0.01   881.04  0.03   974.90  0.02     160.78     0.04
  16      yes    09-Dec-87  02-Feb-88  sevilleta   soltrol  CaCl2    0.753   0.001   1.000   0.002    2.65    0.01   889.76  0.03   982.70  0.02     156.55     0.04
  17      yes    16-Dec-87  07-Feb-88  sevilleta   soltrol  CaCl2    0.753   0.001   1.000   0.002    2.65    0.01   928.73  0.03  1044.87  0.02     201.41     0.04
  18      yes    18-Jan-88  27-Feb-88  sevilleta   soltrol  CaCl2    0.753   0.001   1.000   0.002    2.65    0.01   862.89  0.03   955.94  0.02     160.86     0.04
  19      yes    19-Jan-88  06-Mar-88  sevilleta   soltrol  CaCl2    0.753   0.001   1.000   0.002    2.65    0.01   885.42  0.03   968.61  0.02     143.92     0.04
  20      yes    16-Apr-88  06-Jun-88  sevilleta   soltrol  CaCl2    0.753   0.001   1.000   0.002    2.65    0.01   898.80  0.03   983.10  0.02     147.85     0.04
  21      yes    11-May-88  06-Jun-88  sevilleta   soltrol  CaCl2    0.753   0.001   1.000   0.002    2.65    0.01   898.82  0.03   991.48  0.02     162.52     0.04
  22      yes    18-May-88  08-Jun-88  sevilleta   soltrol  CaCl2    0.753   0.001   1.000   0.002    2.65    0.01   890.08  0.03   985.30  0.02     165.84     0.04

          |-------------------------------TO FIND CORE VOLUME----------------------------------|
          glue mass         glue dens.        filter vol.      groove vol.       shy of mk           |-----------EXPERIMENTAL MASSES (g)-----------|   |--TEMP (C)--
trial #      (g)     +/-      (g/cc)   +/-       (cc)   +/-       (cc)   +/-        (cm)    +/-     at start   +/-    at Swi    +/-    at Sor    +/-     low   high
///////////////////////////////////////////////////////////////////////////////////////////////////////////////////////////////////////////////////////////////////.
   1    |    0.49   0.03      1.84   0.03      0.34   0.02      0.45   0.05       1.40   0.10   1069.73   0.03  1062.99   0.03  1067.40   0.03    23.0   24.0
   2    |    0.70   0.03      1.84   0.03      0.34   0.02      0.45   0.05       0.70   0.10   1151.88   0.03  1143.16   0.03  1148.41   0.03    22.0   27.0
   3    |    0.37   0.03      1.10   0.02      0.34   0.02      0.44   0.05       1.20   0.10   1130.79   0.03  1123.30   0.03  1128.41   0.03    24.0   25.0
   4    |    0.56   0.03      1.84   0.03      0.34   0.02      0.43   0.03       0.80   0.10   1094.56   0.03  1087.74   0.03  1092.33   0.03    23.0   24.0
   5    |    0.38   0.03      1.10   0.02      0.34   0.02      0.57   0.03       1.30   0.10   1107.35   0.03  1100.29   0.03  1104.71   0.03    23.0   24.0
   6    |    0.38   0.03      1.10   0.02      0.34   0.02      0.44   0.03       1.30   0.10   1122.45   0.03  1114.32   0.03  1119.25   0.03    26.0   27.0
   7    |    0.61   0.03      1.10   0.02      0.34   0.02      0.57   0.03       1.00   0.10   1105.76   0.03  1098.53   0.03  1103.77   0.03    20.0   24.0
   8    |    0.34   0.03      1.10   0.02      0.68   0.04      0.44   0.03       0.15   0.05   1130.90   0.03  1122.87   0.03  1127.20   0.03    21.0   24.5
   9    |    0.45   0.03      1.10   0.02      0.68   0.04      0.57   0.03       0.30   0.10   1103.18   0.03  1096.73   0.03  1100.95   0.03    22.0   24.5
  10    |    0.38   0.03      1.10   0.02      0.68   0.04      0.80   0.03       0.10   0.01   1080.73   0.03  1074.58   0.03  1078.72   0.03    21.5   24.0
  11    |    0.37   0.03      1.10   0.02      0.68   0.04      0.68   0.03       1.40   0.10   1063.07   0.03  1056.90   0.03  1061.16   0.03    21.7   23.3
  12    |    0.41   0.03      1.10   0.02      0.68   0.04      0.50   0.03       1.50   0.10   1080.46   0.03  1074.10   0.03  1078.59   0.03    21.5   23.5
  13    |    0.50   0.03      1.10   0.02      0.68   0.04      0.44   0.03       1.40   0.10   1130.77   0.03  1122.76   0.03  1128.55   0.03    22.5   23.5
  14    |    0.38   0.03      1.10   0.02      0.68   0.04      0.44   0.03       0.10   0.01   1078.48   0.03  1071.72   0.03  1076.31   0.03    22.5   23.3
  15    |    0.45   0.03      1.10   0.02      0.68   0.04      0.49   0.03       1.80   0.25   1082.69   0.03  1076.07   0.03  1080.75   0.03    22.7   25.0
  16    |    0.44   0.03      1.10   0.02      0.68   0.04      0.68   0.03      -1.60   0.25   1090.26   0.03  1083.41   0.03  1088.05   0.03    22.6   25.0
  17    |    0.37   0.03      1.10   0.02      0.68   0.04      0.57   0.03       0.10   0.01   1080.40   0.03  1072.41   0.03  1077.98   0.03    22.6   23.0
  18    |    0.38   0.03      1.10   0.02      0.68   0.04      0.44   0.03       1.20   0.15   1064.87   0.03  1058.23   0.03  1062.77   0.03    23.4   23.5
  19    |    0.33   0.03      1.10   0.02      0.68   0.04      0.52   0.03       1.80   0.20   1068.21   0.03  1062.24   0.03  1066.18   0.03    23.4   24.0
  20         0.48   0.03      1.10   0.02      0.68   0.04      0.52   0.03       0.90   0.15   1084.63   0.03  1078.69   0.03  1082.77   0.03    23.0   24.0
  21         0.38   0.03      1.10   0.02      0.68   0.04      0.51   0.03       1.20   0.15   1102.20   0.03  1095.99   0.03  1100.36   0.03    23.0   24.0
  22         0.49   0.03      1.10   0.02      0.68   0.04      0.50   0.03       0.10   0.01   1098.10   0.03  1091.65   0.03  1096.08   0.03    23.1   24.2

COLUMN VOLUME                                                                   ORGANIC LIQUID SATURATIONS                  EXTRAS

          total vol.           void vol.                            b.dens.                                                             temp.range
trial #      (cc)     +/-        (cc)    +/-   porosity    +/-      (g/cc)    +/-         maximum    +/-    residual    +/-      time(days)      (C)
////////////////////////////////////////////////////////////////////////////////////////////////////////////////////////////////////////////////////
   1         95.39   0.41       32.24   0.66    0.338    0.006      1.754   0.008          0.846   0.035     0.293    0.017          14         [illegible]
   2        117.69   0.45       42.93   0.75    0.365    0.005      1.683   0.007          0.822   0.030     0.325    0.015          19         [illegible]
   3        115.20   0.46       39.13   0.76    0.340    0.005      1.750   0.007          0.775   0.031     0.246    0.014          13         [illegible]
   4         94.50   0.39       32.21   0.64    0.341    0.005      1.747   0.008          0.857   0.035     0.293    0.017          14         [illegible]
   5         92.80   0.41       30.85   0.66    0.332    0.006      1.769   0.008          0.927   0.039     0.347    0.020          10         [illegible]
   6        114.07   0.46       39.63   0.75    0.348    0.005      1.729   0.007          0.841   0.032     0.327    0.016          35         [illegible]
   7         97.47   0.41       37.26   1.02    0.386    0.009      1.626   0.017          0.786   0.037     0.316    0.015          38         [illegible]
   8        117.05   0.42       40.55   0.72    0.346    0.005      1.732   0.007          0.802   0.030     0.370    0.017          38         [illegible]
   9         89.16   0.38       30.85   0.62    0.346    0.005      1.733   0.005          0.847   0.035     0.293    0.017          29         [illegible]
  10         92.30   0.37       31.46   0.59    0.341    0.005      1.743   0.007          0.875   0.036     0.286    0.018          33         [illegible]
  11         84.30   0.42       28.71   0.65    0.341    0.006      1.747   0.009          0.870   0.039     0.269    0.018          30         [illegible]
  12         91.44   0.44       31.18   0.68    0.341    0.006      1.746   0.009          0.826   0.036     0.243    0.016          38         1.3
  13        114.14   0.49       38.85   0.79    0.337    0.005      1.756   0.008          0.835   0.033     0.231    0.014          38         2.8
  14         90.20   0.34       31.45   0.58    0.349    0.005      1.726   0.007          0.870   0.034     0.279    0.016          37         2.3
  15         92.86   0.37       31.47   0.76    0.342    0.006      1.745   0.010          0.858   0.039     0.250    0.017          43         0.8
  16         90.55   0.37       31.43   0.75    0.347    0.006      1.730   0.010          0.882   0.039     0.285    0.018          55         0.4
  17        114.60   0.39       38.59   0.70    0.337    0.005      1.758   0.006          0.838   0.032     0.254    0.014          48         0.3
  18         92.06   0.41       31.39   0.69    0.341    0.006      1.747   0.009          0.856   0.037     0.271    0.017          29         0.4
  19         85.45   0.46       28.12   0.70    0.341    0.006      1.746   0.011          0.860   0.040     0.292    0.019          37         0.9
  20         93.05   0.42       27.24   0.65    0.328    0.006      1.781   0.010          0.883   0.041     0.276    0.019          51         [illegible]
  21         92.92   0.43       30.29   0.70    0.331    0.006      1.774   0.009          0.830   0.037     0.246    0.017          26         [illegible]
  22         93.64   0.35       31.06   0.61    0.332    0.005      1.771   0.007          0.841   0.034     0.266    0.016          21         1.1
```

```
                                   ===========================
                                   TWO-PHASE COREFLOOD DATA
INPUT DATA                         ===========================

trial #  in box?  from:      to:        soil       |----FLUIDS----|  |-------------DENSITIES (g/cc)----------------|   |-----COLUMN MASS (g)------|
                                                   organic  aqueous  organic   +/-   aqueous   +/-   particle   +/-    empty    +/-   w/H2O    +/-  soil mass (g)  +/-
//////////////////////////////////////////////////////////////////////////////////////////////////////////////////////////////////////////////////////////////////
   1     yes     26-Aug-88  14-Sep-88  sevilleta  gasoline  CaCl2    0.730   0.010   1.000   0.002    2.65     0.01   896.29   0.03   988.72   0.03    156.18   0.0
   2     yes     26-Aug-88  19-Sep-88  sevilleta  gasoline  CaCl2    0.730   0.010   1.000   0.002    2.65     0.01   884.34   0.03   974.28   0.03    156.13   0.0
   3     yes     26-Aug-88  11-Oct-88  sevilleta  gasoline  CaCl2    0.730   0.010   1.000   0.002    2.65     0.01   859.33   0.03   942.80   0.03    146.42   0.0
   4     yes     10-Sep-88  18-Nov-88  sevilleta  gasoline  CaCl2    0.730   0.010   1.000   0.002    2.65     0.01   898.01   0.03   986.93   0.03    157.85   0.0
   5     yes     07-Sep-88  19-Nov-88  sevilleta  gasoline  CaCl2    0.730   0.010   1.000   0.002    2.65     0.01   916.44   0.03  1003.79   0.03    151.18   0.0


      |------------------------------TO FIND CORE VOLUME-----------------------------------|
trial  glue mass         glue dens          filter vol          groove vol          shy of mk             |-----------EXPERIMENTAL MASSES (g)-----------|   |--TEMP (C)--|
           (g)    +/-      (g/cc)    +/-       (cc)     +/-        (cc)     +/-        (cm)      +/-    at start   +/-    at Swi    +/-    at Sor    +/-     low   high
//////////////////////////////////////////////////////////////////////////////////////////////////////////////////////////////////////////////////////////////////////
  1        0.32   0.03      1.10     0.03      0.74     0.04       0.88     0.06      -2.20      0.20   1092.86   0.03   1086.62   0.03   1090.63   0.03    22.8   23.7
  2        0.34   0.03      1.10     0.03      0.74     0.04       0.68     0.05      -0.15      0.05   1079.58   0.04   1073.21   0.03   1077.27   0.03    22.8   23.7
  3        0.38   0.03      1.10     0.03      0.74     0.04       0.49     0.04       0.10      0.01   1040.80   0.03   1034.80   0.03   1038.56   0.03    22.6   23.8
  4        0.38   0.03      1.10     0.03      0.74     0.04       0.51     0.04       0.30      0.10   1095.62   0.03   1089.21   0.03   1093.58   0.03    22.6   23.8
  5        0.30   0.03      1.10     0.03      0.74     0.04       0.57     0.04       0.40      0.10   1106.29   0.03   1099.98   0.03   1104.07   0.03    22.2   23.8


COLUMN VOLUME
                                                                                      ORGANIC LIQUID SATURATIONS
trial #      total vol          void vol                                                                                       EXTRAS
                (cc)    +/-        (cc)    +/-   porosity   +/-     b.dens     +/-      maximum    +/-    residual    +/-
                                                                    (g/cc)                                                     time(days)   temp.range
                                                                                                                                               (C)
//////////////////////////////////////////////////////////////////////////////////////////////////////////////////////////////////////////////////////////////////
  1            89.61   0.51       30.67   0.78    0.342    0.007    1.743    0.011      0.754    0.060    0.269    0.026         19           0.9
  2            88.04   0.39       29.12   0.63    0.331    0.006    1.773    0.008      0.810    0.062    0.294    0.028         24           0.9
  3            81.93   0.34       26.67   0.57    0.326    0.006    1.787    0.008      0.833    0.063    0.311    0.029         46           1.2
  4            81.44   0.40       25.98   0.64    0.319    0.006    1.805    0.009      0.852    0.065    0.271    0.026         69           1.2
  5            85.75   0.41       28.70   0.64    0.335    0.006    1.763    0.009      0.814    0.062    0.286    0.027         73           1.6
```

TWO-PHASE COREFLOOD DATA

```
INPUT DATA

trial #  in box?   from:      to:        soil       |----FLUIDS----|  |------------DENSITIES (g/cc)----------------|  |-----COLUMN MASS (g)------|
                                                    organic aqueous   organic  +/-   aqueous  +/-   particle  +/-    empty   +/-   w/H2O   +/-  soil mass (g)  +/-
   1        no   19-May-88  03-Jun-88  sevilleta   xylene   CaCl2    0.860   0.010  1.000   0.002    2.65   0.01    905.22  0.03  998.58  0.05     159.78     0.04
   2        no   10-Jun-88  24-Jul-88  sevilleta   xylene   CaCl2    0.860   0.010  1.000   0.002    2.65   0.01    888.29  0.03  972.10  0.03     143.15     0.04
   3        no   15-Jul-88  16-Aug-88  sevilleta   xylene   CaCl2    0.860   0.010  1.000   0.002    2.65   0.01    891.18  0.03  973.71  0.02     144.08     0.04
   4        no   20-Jul-88  17-Aug-88  sevilleta   xylene   CaCl2    0.860   0.010  1.000   0.002    2.65   0.01    880.96  0.03  972.74  0.02     161.78     0.04
   5        no   23-Jul-88  18-Aug-88  sevilleta   xylene   CaCl2    0.860   0.010  1.000   0.002    2.65   0.01    897.83  0.03  988.69  0.05     156.27     0.04
   6        no   09-Aug-88  06-Sep-88  sevilleta   xylene   CaCl2    0.860   0.010  1.000   0.002    2.65   0.01    900.86  0.03  990.94  0.03     155.48     0.04


         |-------------------------------------TO FIND CORE VOLUME-------------------------------------|  |-----------EXPERIMENTAL MASSES (g)-----------|  |--TEMP (C)--|
trial #  glue mass          glue dens,          filter vol        groove vol.        shy of mk             at start   +/-   at Swi   +/-   at Sor   +/-      low   high
           (g)      +/-      (g/cc)     +/-       (cc)    +/-       (cc)     +/-       (cm)      +/-
   1       0.38    0.03       1.10     0.03       0.68   0.04       0.57    0.03      -0.70     0.10       1105.64  0.03  1102.90  0.03  1104.58  0.03     22.0   24.0
   2       0.38    0.03       1.10     0.03       0.34   0.02       0.54    0.04      -2.50     0.10       1067.97  0.03  1064.90  0.06  1066.98  0.06     22.0   27.0
   3       0.38    0.03       1.04     0.03       0.68   0.04       0.47    0.03      -0.50     0.10       1069.45  0.03  1066.65  0.03  1068.66  0.03     22.5   24.0
   4       0.47    0.03       1.04     0.03       0.68   0.04       0.71    0.03       1.50     0.10       1079.39  0.03  1076.16  0.03  1078.56  0.03     22.3   23.4
   5       0.32    0.03       1.04     0.03       0.68   0.04       0.53    0.03       0.10     0.01       1092.49  0.03  1089.16  0.03  1091.36  0.03     22.4   25.0
   6       0.30    0.03       1.10     0.03       0.68   0.04       0.51    0.04       0.10     0.01       1094.24  0.03  1090.94  0.03  1093.32  0.03     22.6   23.2


COLUMN VOLUME                                                                          ORGANIC LIQUID SATURATIONS                      EXTRAS

trial #  total vol,         void vol,                                b.dens,
           (cc)     +/-       (cc)    +/-   porosity   +/-           (g/cc)    +/-     maximum   +/-    residual   +/-           time(days)   temp.range
                                                                                                                                                  (C)
   1       91.45   0.44      31.17   0.69     0.341   0.006           1.747   0.009     0.628   0.081    0.243   0.040              15            1
   2       81.56   0.47      27.55   0.69     0.338   0.006           1.755   0.011     0.796   0.111    0.257   0.052              44            5
   3       80.90   0.38      26.53   0.60     0.328   0.006           1.781   0.009     0.754   0.098    0.213   0.039              32           1.5
   4       90.57   0.45      29.52   0.69     0.326   0.006           1.786   0.009     0.782   0.100    0.201   0.036              28           1.1
   5       89.38   0.38      30.41   0.62     0.340   0.005           1.748   0.008     0.782   0.097    0.265   0.042              36           2.6
   6       88.66   0.36      29.99   0.60     0.338   0.005           1.754   0.008     0.786   0.097    0.219   0.037              28           0.6
```

TWO-PHASE COREFLOOD DATA

INPUT DATA

trial #	in box?	from:	to:	soil	FLUIDS		DENSITIES (g/cc)						COLUMN MASS (g)				soil mass (g)	+/-
					organic	aqueous	organic	+/-	aqueous	+/-	particle	+/-	empty	+/-	w/H2O	+/-		
1	yes	11-Feb-89	24-Feb-89	sevilleta	decane	CaCl2	0.727	0.002	1.000	0.002	2.65	0.01	897.29	0.03	988.22	0.03	155.05	0.04
2	yes	11-Feb-89	24-Feb-89	sevilleta	decane	CaCl2	0.727	0.002	1.000	0.002	2.65	0.01	902.32	0.03	985.71	0.03	146.08	0.04
3	yes	11-Feb-89	04-Mar-89	sevilleta	decane	CaCl2	0.727	0.002	1.000	0.002	2.65	0.01	886.90	0.03	978.18	0.03	157.64	0.04
4	yes	15-Feb-89	14-Apr-89	sevilleta	decane	CaCl2	0.727	0.002	1.000	0.002	2.65	0.01	902.49	0.03	991.43	0.03	156.31	0.04
5	yes	17-Feb-89	20-Apr-89	sevilleta	decane	CaCl2	0.727	0.002	1.000	0.002	2.65	0.01	887.93	0.03	981.30	0.03	163.00	0.04

trial #	TO FIND CORE VOLUME										EXPERIMENTAL MASSES (g)						TEMP (C)	
	glue mass (g)	+/-	glue dens. (g/cc)	+/-	filter vol. (cc)	+/-	groove vol. (cc)	+/-	shy of mk (cm)	+/-	at start	+/-	at Swi	+/-	at Sor	+/-	low	high
1	0.60	0.03	1.84	0.25	0.51	0.04	0.77	0.07	0.50	0.10	1093.78	0.03	1087.26	0.03	1091.36	0.03	22.8	23.7
2	0.50	0.03	1.84	0.25	0.51	0.04	0.47	0.04	0.90	0.10	1084.27	0.03	1078.86	0.03	1082.43	0.03	22.8	23.7
3	0.59	0.03	1.84	0.25	0.51	0.04	0.52	0.04	1.20	0.10	1085.30	0.03	1078.64	0.05	1083.18	0.05	22.6	23.8
4	0.41	0.03	1.10	0.03	0.51	0.04	0.51	0.04	-1.30	0.15	1096.30	0.03	1090.00	0.03	1094.27	0.03	22.7	23.9
5	0.38	0.03	1.10	0.03	0.51	0.04	0.68	0.04	1.30	0.15	1091.24	0.03	1084.27	0.03	1089.16	0.03	22.3	23.8

COLUMN VOLUME

trial #	total vol. (cc)	+/-	void vol. (cc)	+/-	porosity	+/-	b.dens. (g/cc)	+/-	ORGANIC LIQUID SATURATIONS				EXTRAS	
									maximum	+/-	residual	+/-	time(days)	temp.range (C)
1	89.53	0.47	31.02	0.71	0.347	0.006	1.732	0.010	0.770	0.036	0.286	0.018	19	0.9
2	82.52	0.44	27.39	0.66	0.332	0.006	1.770	0.010	0.723	0.036	0.246	0.018	24	0.9
3	90.43	0.47	30.95	0.71	0.342	0.006	1.743	0.010	0.788	0.039	0.251	0.019	46	1.2
4	87.00	0.47	28.02	0.71	0.322	0.006	1.797	0.010	0.824	0.041	0.265	0.018	69	1.2
5	92.46	0.49	30.96	0.73	0.335	0.006	1.763	0.010	0.825	0.039	0.246	0.017	73	1.6

```
                                   TWO-PHASE COREFLOOD DATA

INPUT DATA

trial #  in box?   from:       to:        soil      |----FLUIDS----|  |-------------DENSITIES (g/cc)---------------|   |-----COLUMN MASS (g)------|
////////////////////////////////////////////////////organic  aqueous///organic   +/-  aqueous   +/-  particle   +/-////empty   +/-   w/H2O   +/- //soil mass (g)  +/-
[illegible]  yes   21-Jan-87  04-Feb-87  sevilleta    pce     CaCl2     1.620  0.010   1.000  0.002     2.65   0.01   893.05  0.03  982.10  0.02     154.72  0.04
[illegible]  yes   11-Aug-88  02-Sep-88  sevilleta    pce     CaCl2     1.620  0.010   1.000  0.002     2.65   0.01   894.53  0.03  986.00  0.02     160.77  0.04
[illegible]  yes   12-Aug-88  09-Sep-88  sevilleta    pce     CaCl2     1.620  0.010   1.000  0.002     2.65   0.01   898.42  0.03  985.40  0.02     152.02  0.04
[illegible]  yes   18-Aug-88  11-Sep-88  sevilleta    pce     CaCl2     1.620  0.010   1.000  0.002     2.65   0.01   899.13  0.03  988.46  0.02     159.44  0.04
[illegible]  yes   19-Aug-88  12-Sep-88  sevilleta    pce     CaCl2      1.62  0.010   1.000  0.002     2.65   0.01   890.51  0.03  973.29  0.02     145.92  0.04

        |-------------------------------TO FIND CORE VOLUME---------------------------------|
trial #  glue mass         glue dens.           filter vol          groove vol          shy of mk            |-----------EXPERIMENTAL MASSES (g)-----------|  |--TEMP (C)--|
//////////// (g)    +/- ///// (g/cc)   +/- ////// (cc)    +/- //////// (cc)    +/- ///////// (cm)    +/- ///at start   +/-   at Swi   +/-   at Sor   +/- ////low   high///
   [illegible] [illegible]  0.03     1.04   0.03       0.40   0.02        0.50   0.03        0.60   0.10    1086.58  0.03  1092.58  0.03  1090.37  0.03    23.0  24.2
   [illegible] [illegible]  0.03     1.04   0.03       0.74   0.04        0.52   0.05        0.10   0.01    1093.40  0.03  1106.00  0.03  1098.38  0.03    23.0  23.8
   [illegible] [illegible]  0.03     1.04   0.03       0.74   0.04        0.55   0.05        0.50   0.10    1087.81  0.03  1102.70  0.03  1092.31  0.03    21.[illegible]  23.[illegible]
   [illegible] [illegible]  0.03     1.04   0.03       0.74   0.04        0.47   0.04        2.20   0.10    1097.19  0.03  1111.19  0.03  1101.82  0.03    22.0  23.[illegible]
   [illegible]    0.36      0.03     1.04   0.03       0.74   0.04        0.71   0.06        1.00   0.10    1069.63  0.03  1083.74  0.03  1074.35  0.03    22.4  23.7

COLUMN VOLUME
                                                                                          ORGANIC LIQUID SATURATIONS
trial #    total vol            void vol                               b.dens                                                         EXTRAS
///////////// (cc)    +/- //////// (cc)    +/- ////porosity    +/- //// (g/cc)    +/- ////////maximum   +/-   residual   +/- //////////time(days)  temp.range
                                                                                                                                                     (C)
   [illegible]  [illegible]  0.39     26.57  0.67     0.327  0.006     1.757  0.008        0.726  0.035     0.206  0.012          14          1.2
   [illegible]  [illegible]  0.37     27.19  0.67     0.335  0.006     1.789  0.008        0.696  0.031     0.275  0.014          13          0.8
   [illegible]  [illegible]  0.42     26.25  0.68     0.328  0.006     1.777  0.009        0.852  0.039     0.257  0.014          18          1.7
   [illegible]  [illegible]  0.48     26.47  0.72     0.322  0.006     1.797  0.010        0.790  0.039     0.261  0.015          23          0.8
   [illegible]    81.40      0.44     26.34  0.66     0.324  0.006     1.793  0.010        0.864  0.042     0.289  0.017          24          1.3
```

TWO-PHASE COREFLOOD DATA

INPUT DATA

trial #	in box?	from:	to:	soil	FLUIDS organic	FLUIDS aqueous	DENSITIES (g/cc) organic	+/-	aqueous	+/-	particle	+/-	COLUMN MASS (g) empty	+/-	w/H2O	+/-	soil mass (g)	+/-
1	yes	10-Apr-89	30-Apr-89	traverse	soltrol	CaCl2	0.753	0.010	1.000	0.002	2.65	0.01	902.45	0.03	994.48	0.03	156.60	0.04
2	yes	20-Apr-89	02-May-89	traverse	soltrol	CaCl2	0.753	0.010	1.000	0.002	2.65	0.01	899.28	0.03	989.19	0.03	154.85	0.04
3	yes	22-Apr-89	03-May-89	traverse	soltrol	CaCl2	0.753	0.010	1.000	0.002	2.65	0.01	891.15	0.03	976.60	0.03	144.39	0.04
4	yes	23-Apr-89	04-May-89	traverse	soltrol	CaCl2	0.753	0.010	1.000	0.002	2.65	0.01	889.03	0.03	972.41	0.03	138.37	0.04
5	yes	24-Apr-89	04-May-89	traverse	soltrol	CaCl2	0.753	0.010	1.000	0.002	2.65	0.01	901.73	0.03	991.33	0.03	154.64	0.04

trial #	TO FIND CORE VOLUME glue mass (g)	+/-	glue dens. (g/cc)	+/-	filter vol. (cc)	+/-	groove vol. (cc)	+/-	sby of mk (cm)	+/-	EXPERIMENTAL MASSES (g) at start	+/-	at Swi	+/-	at Sor	+/-	TEMP (C) low	high
1	0.41	0.03	1.10	0.03	0.68	0.04	0.53	0.04	?	0.10	1100.70	0.03	?	0.03	?	0.03	22.0	23.8
2	0.44	0.03	1.10	0.03	0.51	0.04	0.52	0.04	1.50	0.10	1093.63	0.03	1087.18	0.06	1092.34	0.06	23.2	23.9
3	0.44	0.03	1.10	0.03	0.51	0.04	0.51	0.04	1.80	0.10	1073.88	0.03	1067.57	0.03	1072.70	0.03	22.0	23.9
4	0.72	0.06	1.10	0.03	0.72	0.06	0.47	0.04	0.10	0.01	1065.55	0.03	1059.27	0.03	1064.15	0.03	22.3	23.4
5	0.70	0.06	1.10	0.03	0.74	0.04	0.50	0.03	1.20	0.10	1094.31	0.03	1087.82	0.03	1092.95	0.03	22.9	24.0

COLUMN VOLUME | ORGANIC LIQUID SATURATIONS | EXTRAS

trial #	total vol. (cc)	+/-	void vol. (cc)	+/-	porosity	+/-	b.dens. (g/cc)	+/-	maximum	+/-	residual	+/-	time(days)	temp.range (C)
1	ERR	ERR	ERR	ERR	ERR	ERR	ERR	ERR	ERR	ERR	ERR	ERR	15	1.8
2	89.11	0.46	30.68	0.70	0.344	0.006	1.738	0.009	0.851	0.073	0.170	0.024	44	0.7
3	84.68	0.47	30.19	0.69	0.357	0.006	1.705	0.010	0.846	0.068	0.158	0.019	32	1.9
4	81.59	0.41	29.37	0.62	0.360	0.006	1.696	0.009	0.866	0.069	0.193	0.022	28	1.1
5	88.23	0.47	29.87	0.71	0.339	0.006	1.753	0.010	0.880	0.072	0.184	0.021	36	1.1